

**BIOMIMETIC STRATEGIES FOR
ELECTROPHORETIC DEPOSITION OF
POLYMERS AND COMPOSITES**

**BIOMIMETIC STRATEGIES FOR
ELECTROPHORETIC DEPOSITION OF
POLYMERS AND COMPOSITES**

BY

QINFU ZHAO, B.Eng., M.Eng.

A Thesis Submitted to the School of Graduate Studies in Partial Fulfilment
of the Requirements for the Degree Doctor of Philosophy

McMaster University © Copyright by Qinfu Zhao, November 2022

McMaster University DOCTOR OF PHILOSOPHY (2022) Hamilton, Ontario

(Materials Science and Engineering)

TITLE: Biomimetic Strategies for Electrophoretic Deposition of Polymers and
Composites

AUTHOR: Qinfu Zhao

M.Eng. in Applied Science (University of Quebec at Chicoutimi)

B.Eng. in Materials Science and Engineering (University of Science and Technology
Beijing)

SUPERVISORS: Prof. Igor Zhitomirsky & Prof. Stephen C. Veldhuis

Faculty of Engineering, McMaster University, Hamilton, Ontario, Canada

NUMBER OF PAGES: xxii, 218

Abstract

The global market for fluoropolymers, including polytetrafluoroethylene (PTFE), polyvinylidene fluoride (PVDF), and poly(vinylidene fluoride-co-hexafluoropropylene) (PVDF-HFP), is growing rapidly due to their copious applications in the construction, automotive, medical, chemical, and electrical industries. Fluoropolymers owe their popularity partly to their excellent chemical and thermal stability and useful mechanical, piezoelectric, and ferroelectric properties. They are made into films or coatings that are used for corrosion protection or surface property enhancement. Electrophoretic deposition (EPD) has generated increasing interest in manufacturing advanced films for various applications due to its low cost, versatility, simple apparatus, and good film quality compared with other deposition techniques like dip coating, spin coating, electrospinning, or spray coating. Moreover, EPD facilitates uniform deposition on the substrates of complex shapes at a high deposition rate.

The aim of this research is to develop novel biomimetic strategies for fabricating polymer films and their composite films with multifunctional particles through EPD. This method involves the electrophoresis of charged particles in a stable colloidal suspension towards an electrode, forming deposition. Fluoropolymers, however, are electrically neutral and chemically inert, and their EPD presents difficulties. Therefore, successful EPD depends on understanding how to modify the surface of polymer particles using advanced biosurfactants to impart charge and form a well dispersed, stable colloidal suspension.

One strategy is to leverage the unique dispersing power of bile acids and salts as biosurfactants for EPD of PTFE and PVDF films and composite films. When doing so, it was found that the amphiphilic structure of bile salts such as sodium deoxycholate (DChNa) facilitated adsorption on the chemically inert, hydrophobic surfaces of PTFE, diamond, and carbon dots. In this strategy, DChNa acted as a charging, dispersing, film-forming agent for the co-deposition of PTFE composite films from an aqueous suspension. Water insoluble bile acids (BAs) were found to be biosurfactants for the EPD of PTFE and PVDF from organic solvents, in which lithocholic acid (LCA) was used as a co-dispersant for the fabrication of composite PTFE-diamond coatings and PTFE coatings provided corrosion protection for stainless steel in 3% NaCl solutions. The dispersing performance of four other bile acids, chenodeoxycholic acid (CDCA), deoxycholic acid (DCA), ursodeoxycholic acid (UDCA), and cholic acid (ChA), was analyzed and compared with LCA on the deposition performance of PVDF. It was found that the PVDF deposition yield obtained using different BAs increased in the order of $LCA < CDCA < DCA < UDCA < ChA$. This was attributed to the difference in number, position, and orientation of OH groups in the structures of the BAs.

Another biomimetic strategy for the EPD of polymers and composites was inspired by the strong adsorption of mussel protein on rock surfaces in sea water. Catecholate-type molecules, caffeic acid (CA) and catechol violet (CV), were found to be biosurfactants for dispersing, charging, and depositing PVDF films and composites. Analyses of the deposition yield data, the chemical structure of the CA and CV, and the microstructure and

composition of the films suggested that the aromatic rings on the CA and CV had hydrophobic interactions with the PVDF particles and that the phenolic groups formed bidentate chelating or bridging bonding to inorganic particle surfaces. The study demonstrated the feasibility of co-depositing PVDF with nanoparticles of TiO_2 , MnO_2 , and NiFe_2O_4 . CA was also used for preparing PVDF-HFP particles and as a co-dispersant for the co-deposition of PVDF-HFP with NiFe_2O_4 and CuFe_2O_4 nanoparticles in order to make composite films that combine the ferrimagnetic properties of spinel ferrites with the multifunctional properties of ferroelectric polymers.

Acknowledgements

More than four years later, I still clearly remember how excited I was the moment Dr. Igor Zhitomirsky and Dr. Stephen C. Veldhuis accepted my application to be a PhD candidate in the electrochemical field as an applicant with a background in aluminium alloy solidification. The valuable opportunity they offered reoriented my entire life toward a better and brighter path. I am extremely grateful for their immense knowledge and plentiful experience. Without their continuous support and patient supervision during my studies, this research would not be possible. I am also very thankful to Dr. Oleg Rubel, whose insightful comments and suggestions were extraordinarily valuable, for being my committee member.

Furthermore, I would like to thank all the technicians I worked with for their technical support on my research. I would also like to express thanks to my colleagues from Dr. Zhitomirsky's group for a cherished time spent together in the lab. I also appreciate all the other colleagues, friends, staff, and professors from McMaster University, especially from the Department of Materials Science and Engineering, for their assistance and guidance and for being part of my PhD journey.

Finally, I would like to extend my sincere thanks to my parents, wife, daughter, and whole family for their infinite love. Their tremendous understanding and encouragement over the past few years gave me the strength and power to accomplish this research.

Table of Contents

Abstract	iii
Acknowledgements	vi
Table of Contents	vii
List of Figures and Tables	xi
List of Abbreviations and Symbols	xviii
Declaration of Academic Achievements	xxi
Chapter 1 Thesis Organization	1
Chapter 2 Introduction	6
2.1 Background	6
2.2 References	10
Chapter 3 Literature Review	13
3.1 Fundamental Aspects of EPD	13
3.1.1 Suspension stabilization mechanisms in EPD	14
3.1.2 Particle charging mechanisms for EPD	21
3.1.3 Deposition mechanisms in EPD	23
3.1.4 Kinetics of EPD	27
3.1.5 Advantages and applications of EPD	31
3.2 Materials Sciences Aspects of EPD	32
3.2.1 Particles and molecules	32
3.2.2 Solvents	35
3.2.3 Binders	38
3.3 Biosurfactants for EPD	39
3.3.1 Bile acids and bile salts	40
3.3.2 Catecholates, gallates, and salicylates	45
3.3.3 Other natural surfactants	51
3.4 Challenges in EPD	52

3.4.1	Polymers	52
3.4.2	Carbon materials	54
3.4.3	Composite materials.....	56
3.5	Objectives.....	57
3.6	References	58
Chapter 4	DChNa for EPD of Composite Coatings	72
4.1	Abstract	72
4.2	Introduction	73
4.3	Experimental Procedures.....	75
4.4	Results and Discussion.....	77
4.5	Conclusions	89
4.6	Acknowledgements	90
4.7	Supplementary Data	90
4.8	References	92
Chapter 5	LCA for PTFE Composites.....	99
5.1	Abstract	99
5.2	Introduction	100
5.3	Experimental Procedures.....	101
5.4	Results and Discussion.....	101
5.5	Conclusions	106
5.6	Acknowledgements	106
5.7	References	106
Chapter 6	Influence of Bile Acids on EPD of PVDF Composites	109
6.1	Abstract	109
6.2	Introduction	110
6.3	Experimental Procedures.....	113
6.4	Results and Discussion.....	114
6.5	Conclusions	127
6.6	Acknowledgments	127

6.7	References	128
Chapter 7 Versatile Strategies for EPD of PVDF Nanocomposites		133
7.1	Abstract	133
7.2	Introduction	134
7.3	Experimental Procedures.....	137
7.3.1	Materials	137
7.3.2	Film deposition	138
7.3.3	Characterization	138
7.4	Results and Discussion.....	139
7.5	Conclusions	150
7.6	Acknowledgments	151
7.7	Supplementary Data	152
7.8	References	153
Chapter 8 EPD of PVDF-HFP-NiFe₂O₄ Composites		157
8.1	Abstract	157
8.2	Introduction	158
8.3	Experimental Procedures.....	162
8.4	Results and Discussion.....	164
8.5	Conclusions	178
8.6	Acknowledgements	179
8.7	Supplementary Data	179
8.8	References	181
Chapter 9 EPD of PVDF-HFP-CuFe₂O₄ Composites		190
9.1	Abstract	190
9.2	Introduction	191
9.3	Experimental Procedures.....	194
9.4	Results and Discussion.....	197
9.5	Conclusions	207
9.6	Acknowledgments	208

9.7	References	208
Chapter 10	Conclusions and Future Works	215

List of Figures and Tables

Figure 3.1 Schematic illustration of anodic EPD process. Reprinted from [2] with permission from Elsevier.	14
Figure 3.2 (a) Electrostatic stabilization and (b) steric stabilization illustrations. Reprinted from [4] with permission from Elsevier.....	15
Figure 3.3 Schematic illustration of electric double layer. Reprinted from [7] with permission from Elsevier.	17
Figure 3.4 The potential energy between two particles in a colloidal suspension as a function of the intermolecular distance. Reprinted from [7] with permission from Elsevier.	18
Figure 3.5 Lyosphere distortion and thinning mechanism during EPD process. Reprinted from [30] with permission from Elsevier.....	25
Figure 3.6 Schematic illustrations of chitosan solubility transition and deposition mechanism. Reprinted from [13] with permission from Elsevier.....	35
Figure 3.7 Chemical structures, molecular formula, and theoretical mass of bile acids. Reprinted with permission from [109] . Copyright {2019} American Chemical Society.	41
Figure 3.8 Formation of (a) primary and (b) secondary micelles of BAs/BSs molecules. Reprinted from [108] with permission from John Wiley and Sons.	43
Figure 3.9 Schematic illustration of dispersion of CNT via unzipping mechanism in which white dots represent bile acid molecules. Reprinted from [25] with permission from Elsevier.	44
Figure 3.10 Chemical structures of various catecholic molecules.....	46
Figure 3.11 Schematic illustrations of adsorption mechanisms of caffeic acid on inorganic particles: (a) bidentate chelating bonding, (b) inner sphere bidentate bridging bonding, (c) outer sphere bidentate bridging bonding, and (d) carboxylic group bonding [50].	48
Figure 3.12 Chemical structures of gallic acid.	49
Figure 3.13 Chemical structures of salicylate-type molecules.	50

Figure 3.14 Salicylate bonding: (a) bidentate chelating bonding, (b) inner sphere bidentate bridging bonding, and (c) outer sphere bidentate bridging bonding [50].	51
Figure 3.15 Chemical structures of citric acid and oxalic acid.	52
Figure 4.1 Chemical structure of DChNa.	77
Figure 4.2 SEM images of films, prepared from 1 g·L ⁻¹ DChNa solutions, containing 5 g·L ⁻¹ PTFE at a deposition voltage of 50 V.	79
Figure 4.3 FTIR spectra of (a) as-received PTFE and (b) deposit, prepared from 1 g·L ⁻¹ DChNa solutions, containing 5 g·L ⁻¹ PTFE at a deposition voltage of 50 V.	80
Figure 4.4 SEM images at different magnifications of films, prepared from 1 g·L ⁻¹ DChNa solutions, containing 5 g·L ⁻¹ PTFE at a deposition voltage of 50 V and annealed at 350 °C for 1 hour.	80
Figure 4.5 Tafel plots for stainless steel: (a) uncoated and (b) coated from 1 g·L ⁻¹ DChNa solutions, containing 5 g·L ⁻¹ PTFE at a deposition voltage of 50 V during 5 min and annealed at 350 °C for 1 hour.	81
Figure 4.6 Bode plots of impedance data for stainless steel (a) uncoated and (b) coated from 1 g·L ⁻¹ DChNa solutions, containing 5 g·L ⁻¹ PTFE at a deposition voltage of 50 V during 5 min and annealed at 350 °C for 1 hour.	83
Figure 4.7 SEM images of films, deposited from solutions, containing 0.5 g·L ⁻¹ CDs and 0.5 g·L ⁻¹ DChNa at a cell voltage of 15 V.	83
Figure 4.8 FTIR spectra of (a) as received DChNa, (b) deposit, prepared from 0.5 g·L ⁻¹ DChNa solution, (c) as-prepared CDs, (d) deposit, prepared from a solution, containing 0.5 g·L ⁻¹ CDs and 0.5 g·L ⁻¹ DChNa.	85
Figure 4.9 SEM images of films, prepared from 2 g·L ⁻¹ DChNa solutions, containing 4 g·L ⁻¹ diamond at a deposition voltage of 7 V.	86
Figure 4.10 SEM image of a PPy film, prepared from 0.1 M Py solution containing 0.01 M Tiron at a deposition voltage of 7 V.	88
Figure 4.11 SEM images for PPy-diamond films, prepared from 0.1 M Py solution, containing 0.01 M Tiron, 1 g·L ⁻¹ diamond and 0.5 g·L ⁻¹ DChNa at a cell voltage of 7 V.	88

Figure S4.1 Cross section of annealed PTFE film, prepared from 1 g·L ⁻¹ DChNa solution, containing 5 g·L ⁻¹ PTFE at a cell voltage of 50 V and deposition time of 5 min.	90
Figure S4.2 Equivalent circuit of PTFE coating: R _S -solution resistance, R _{pore} -resistance of electrolyte in pores, R _{CT} -charge transfer resistance, CPE1 and CPE2 constant phase elements, describing coating capacitance and double layer capacitance at the electrode interface formed by penetrating electrolyte.	91
Figure S4.3 Nyquist plot of AC impedance for PTFE coating.	91
Table S4.1 Zeta potentials of materials.....	91
Table S4.2 Conductivities of suspensions	91
Figure 5.1 (A) Chemical structure of LCA and (B) FTIR data of (a) as-received PTFE and (b) PTFE deposit, prepared from 5 g·L ⁻¹ PTFE suspension, containing 1 g·L ⁻¹ LCA. ..	102
Figure 5.2 SEM images of films: (A) PTFE, as-deposited; (B) PTFE, annealed at 350 °C, prepared from 5 g·L ⁻¹ PTFE suspension, containing 1 g·L ⁻¹ LCA; (C) as-deposited diamond from 5 g·L ⁻¹ diamond suspension, containing 1 g·L ⁻¹ LCA; (D) as-deposited PTFE-diamond composite, prepared from a suspension, containing 5 g·L ⁻¹ PTFE, 5 g·L ⁻¹ diamond and 1 g·L ⁻¹ LCA.	103
Figure 5.3 Tafel dependences for steel: (a) uncoated and (b) coated from 5 g·L ⁻¹ PTFE suspension, containing 1 g·L ⁻¹ LCA and annealed at 350 °C for 1 h.....	104
Figure 5.4 EIS Bode plots for steel (A) absolute value of impedance Z versus frequency, (B) phase angle versus frequency for (a) uncoated and (b) coated from 5 g·L ⁻¹ PTFE suspension, containing 1 g·L ⁻¹ LCA and annealed at 350 °C for 1 h.....	105
Figure 6.1 Chemical structures of BAs.	115
Figure 6.2 Deposit mass of PVDF films deposited using various BAs as surfactants from 10 g·L ⁻¹ PVDF suspensions in ethanol solutions, containing 1 g·L ⁻¹ BAs at a deposition voltage of 50 V and deposition time of 5 min.	116

Figure 6.3 Deposit mass versus (A) deposition voltage at a deposition time of 5 min and (B) deposition time at a deposition voltage of 50 V for 10 g·L ⁻¹ PVDF suspensions in ethanol, containing dissolved (a) 1 g·L ⁻¹ LCA and (b) 1 g·L ⁻¹ ChA.	119
Figure 6.4 SEM images of (A1-A5) as deposited and (B1-B5) annealed films, prepared from 10 g·L ⁻¹ PVDF suspensions in ethanol, containing dissolved (A1, B1) 1 g·L ⁻¹ LCA, (A2, B2) 1 g·L ⁻¹ CDCA and (A3, B3) 1 g·L ⁻¹ DCA, (A4, B4) 1 g·L ⁻¹ UDCA and (A5, B5) 1 g·L ⁻¹ ChA.	120
Figure 6.5 Tafel plots for uncoated 304 type stainless steel and coated from 10 g·L ⁻¹ PVDF suspensions containing different BAs at deposition voltage of 50 V and deposition time of 5 min and annealed at 200 °C for 1 hour.	122
Figure 6.6 EIS Bode plots for uncoated 304 type stainless steel and coated from 10 g·L ⁻¹ PVDF suspensions containing different BAs at deposition voltage of 50 V and deposition time of 5 min and annealed at 200 °C for 1 hour.	122
Figure 6.7 SEM images of (A1-A4) as-deposited and (B1-B4) annealed films at (A1, B1, A3, B3) low magnification and (A2, B2, A4, B4) high magnifications for deposition from 10 g·L ⁻¹ PVDF suspensions, containing (A1, A2, B1, B2) 1 g·L ⁻¹ diamond and (A3, A4, B3, B4) 5 g·L ⁻¹ diamond and 1 g·L ⁻¹ ChA for deposition voltage of 50 V.	125
Figure 6.8 SEM images of (A1-A4) as-deposited and (B1-B4) annealed films at (A1, B1, A3, B3) low magnification and (A2, B2, A4, B4) high magnifications for deposition from 10 g·L ⁻¹ PVDF suspensions, containing (A1, A2, B1, B2) 1 g·L ⁻¹ silica and (A3, A4, B3, B4) 5 g·L ⁻¹ silica and 1 g·L ⁻¹ ChA for deposition voltage of 50 V.	127
Figure 7.1 Chemical structures of dispersants.	140
Figure 7.2 (A) Deposit mass versus PVDF concentration for suspensions, containing 0.2 g·L ⁻¹ CA (0.2CA), 0.5 g·L ⁻¹ CA (0.5CA), 0.2 g·L ⁻¹ CV (0.2CV), 0.5 g·L ⁻¹ CV (0.5 CV) at a deposition voltage of 50 V and a deposition time of 5 min and (B) deposit mass versus deposition voltage for suspensions containing 0.2 g·L ⁻¹ CA and 5 g·L ⁻¹ PVDF (0.2CA5P); 0.5 g·L ⁻¹ CA and 10 g·L ⁻¹ PVDF (0.5CA10P); 0.2 g·L ⁻¹ CV and 5 g·L ⁻¹ PVDF (0.2CV5P); and 0.5 g·L ⁻¹ CV and 10 g·L ⁻¹ PVDF (0.5CV10P) for deposition time of 5 min.	142
Figure 7.3 SEM images of films at different magnifications prepared from suspensions containing 10 g·L ⁻¹ PVDF with (A, C) 0.5 g·L ⁻¹ CA or (B, D) 0.5 g·L ⁻¹ CV at a deposition voltage of 50 V for 5 min; (A, B) as-deposited and (C, D) annealed at 200 °C.	144

Figure 7.4 FTIR spectra of (a) as-received PVDF and (b, c) as-deposited PVDF, prepared from 0.5 g·L ⁻¹ (b) CA or (c) CV solution containing 10 g·L ⁻¹ PVDF at a deposition voltage of 50 V during 5 min.....	145
Figure 7.5 Tafel plots for stainless steel (a) uncoated and (b, c) coated from 0.5 g·L ⁻¹ (b) CA or (c) CV solutions, containing 10 g·L ⁻¹ PVDF at a deposition voltage of 50 V during 5 min and annealed at 200 °C for 1 hour.	146
Figure 7.6 (A) Absolute impedance and (B) Phase versus frequency impedance data for stainless steel (a) uncoated and (b, c) coated from 0.5 g·L ⁻¹ (b) CA or (c) CV solutions, containing 10 g·L ⁻¹ PVDF at a deposition voltage of 50 V during 5 min and annealed at 200 °C for 1 hour.	146
Figure 7.7 SEM images of films, prepared from 5 g·L ⁻¹ PVDF solutions, containing (A, D) 1 g·L ⁻¹ CA and 1 g·L ⁻¹ MnO ₂ , (B, E) 1 g·L ⁻¹ CV and 1 g·L ⁻¹ TiO ₂ , (C, F) 1 g·L ⁻¹ CV and 1 g·L ⁻¹ NiFe ₂ O ₄ at a deposition voltage of 50 V and (D, E, F) annealed at 200 °C for 1 hour.	148
Figure 7.8 X-ray diffraction pattern of films (a) pure PVDF, (b) PVDF and TiO ₂ , (c) PVDF and MnO ₂ , and (d) PVDF and NiFe ₂ O ₄ (peaks corresponding to ♦ JCPDS file 00-061-1403, ● JCPDS file 00-064-0863, ■ JCPDS file 04-003-0648, ▼ JCPDS file 00-054-0964). EPD conditions are similar to Figure 7.7.	149
Figure 7.9 Magnetization versus magnetic field for (a) as received NiFe ₂ O ₄ nanoparticles and (b) PVDF-NiFe ₂ O ₄ composites prepared from 5 g·L ⁻¹ PVDF solutions containing 1 g·L ⁻¹ CV and 1 g·L ⁻¹ NiFe ₂ O ₄ at a deposition voltage of 50 V.	150
Figure S7.1 TEM images of as received PVDF particles.	152
Figure S7.2 SEM images of annealed composite films.	152
Figure 8.1 Chemical structures of (A) CA and (B) ChA.	161
Figure 8.2 TEM images at different magnifications of PVDF-HFP particles.	165
Figure 8.3 SEM images for PVDF-HFP films prepared using (A-C) CA at 50 V and (D-F) ChA at 100 V: (A, B, D, E) film surfaces at different magnifications, (C, F) cross sections, arrows show film thickness.....	167

Figure 8.4 Tafel plots of (a) uncoated and (b, c) coated stainless steel. The coatings were prepared from PVDF-HFP suspensions at optimized deposition conditions: (b) CA at 50 V (c) ChA at 100 V and deposition time of 5 min.....	168
Figure 8.5 EIS data of (a) uncoated and (b, c) coated stainless steel. The coatings were prepared from PVDF-HFP suspensions at optimized deposition conditions using (b) CA at 50 V (c) ChA at 100 V and deposition time of 5 min.....	169
Figure 8.6 XRD patterns of (a) as-received NiFe ₂ O ₄ , and deposits obtained from 5 g·L ⁻¹ PVDF-HFP suspensions, containing 1 g·L ⁻¹ CA with (b) 5 g·L ⁻¹ NiFe ₂ O ₄ (c) 45 g·L ⁻¹ NiFe ₂ O ₄ at 20 V and deposition time of 5 min (♦ peaks corresponding to JCPDS file 54-0964)	170
Figure 8.7 FTIR spectra of (a) as-received NiFe ₂ O ₄ , (b) PVDF-HFP deposit, prepared from 5 g·L ⁻¹ PVDF-HFP suspension, containing 1 g·L ⁻¹ CA at 50 V and deposition time of 5 min and (c) PVDF-HFP-NiFe ₂ O ₄ deposit, prepared from 5 g·L ⁻¹ PVDF-HFP and 5 g·L ⁻¹ NiFe ₂ O ₄ suspension, containing 1 g·L ⁻¹ CA at 20 V and deposition time of 5 min.....	171
Figure 8.8 (A) TGA and (B) DTA data for deposits prepared from 5 g·L ⁻¹ PVDF-HFP suspensions, containing 1 g·L ⁻¹ CA with (a) 5 and (b) 45 g·L ⁻¹ NiFe ₂ O ₄ at 20 V and deposition time of 5 min.	173
Figure 8.9 SEM images for films prepared at a deposition voltage of 20 V and deposition time of 5 min from 5 g·L ⁻¹ PVDF-HFP suspensions, containing 1 g·L ⁻¹ CA with (A-C) 5 and (D-F) 45 g·L ⁻¹ NiFe ₂ O ₄ : (A, B, D, E) surfaces at different magnifications, (C, F) cross sections, arrows show film thickness.....	175
Figure 8.10 Deposit mass versus (A) deposition time at a deposition voltage of 20 V and (B) voltage at a deposition time of 5 min for films prepared from 5 g·L ⁻¹ PVDF-HFP suspensions, containing 1 g·L ⁻¹ CA with 5 g·L ⁻¹ NiFe ₂ O ₄	176
Figure 8.11 Magnetization versus magnetic field for (a) as-received NiFe ₂ O ₄ and composite deposits prepared from 5 g·L ⁻¹ PVDF-HFP suspensions, containing 1 g·L ⁻¹ CA and (b) 45 and (c) 5 g·L ⁻¹ NiFe ₂ O ₄ at 20 V and deposition time of 5 min.	176
Figure S8.1 (A) Tafel plot and (B, C) Bode plot of complex impedance for coated stainless steel. The coating was prepared from PVDF-HFP suspensions using (b) CA at 50 V and deposition time of 2 min.	179
Figure S8.2 (A) Tafel plot and (B, C) Bode plot of complex impedance for coated stainless steel. The coating was prepared from PVDF-HFP suspensions using (b) ChA at 100 V and deposition time of 2 min.	179

Figure S8.3 Electron microscopy data for deposits prepared from 5 g·L ⁻¹ PVDF-HFP suspensions, containing 1 g·L ⁻¹ CA with (a-c) 5 and (d-f) 45 g·L ⁻¹ NiFe ₂ O ₄ at 20 V and deposition time of 5 min: (a, d) SEM and (b, c, e, f) corresponding EDX.	180
Figure S8.4 Electron microscopy data for deposits prepared from 5 g·L ⁻¹ PVDF-HFP suspensions, containing 1 g·L ⁻¹ CA with (a-c) 5 and (d-f) 45 g·L ⁻¹ NiFe ₂ O ₄ at 20 V and deposition time of 5 min: (a, d) Cross-sectional SEM and (b, c, e, f) corresponding EDX.	181
Figure 9.1 Magnetization versus magnetic field for as-received CuFe ₂ O ₄	197
Figure 9.2 (A) CVs at sweep rates of (a) 5, (b) 10 and (c) 20 mV s ⁻¹ and (B) capacitance, calculated from CV data versus scan rate for CuFe ₂ O ₄ electrodes.	198
Figure 9.3 (A) Nyquist plot, (B,C) frequency dependences of (B) C _s ' and (C) C _s '' for CuFe ₂ O ₄	199
Figure 9.4 TEM image of PVDF-HFP particles.	200
Figure 9.5 SEM images at different magnifications for (A, B) PVDF-HFP and (C, D) PVDF-HFP-CuFe ₂ O ₄ films prepared by EPD.	201
Figure 9.6 (A) Chemical structure of CA, (B, C) CA adsorption on particle surface by bidentate (A) bridging or (C) chelating bonding, involving metal atoms M=Cu or Fe on the surface.	202
Figure 9.7 X-ray diffraction patterns of (a) as-received CuFe ₂ O ₄ and (b) PVDF-HFP-CuFe ₂ O ₄ deposit prepared by EPD (● peaks, corresponding to JCPDS file 04-006-6233 of CuFe ₂ O ₄).	203
Figure 9.8 FTIR spectra of (a) as-received CuFe ₂ O ₄ , (b) deposited PVDF-HFP film and (c) deposited PVDF-HFP-CuFe ₂ O ₄ composite film.	204
Figure 9.9 (a) TGA and (b) DTA data for PVDF-HFP-CuFe ₂ O ₄ composite deposit.	205
Figure 9.10 (A) Magnetization versus magnetic field at 300 K and (B) ZFC and FC magnetization data for PVDF-HFP-CuFe ₂ O ₄ composite.	206

List of Abbreviations and Symbols

Abbr.	Full Description	Abbr.	Full Description
AC	Alternating Current	HA	Hydroxyapatite
ATR	Attenuated Total Reflectance	HFP	Hexafluoropropylene
BAs	Bile Acids	IEP	Isoelectric Point
BSs	Bile Salts	LCA	Lithocholic Acid
CA	Caffeic Acid	MEK	Methyl Ethyl Ketone
CD	Carbon Dots	MWCNT	Multiwalled CNT
CDCA	Chenodeoxycholic Acid	NMP	N-Methyl-2-Pyrrolidone
ChA	Cholic Acid	PAA	Poly(Acrylic Acid)
CHIT	Chitosan	PAH	Poly(Allylamine Hydrochloride)
CMC	Critical Micelle Concentration	PAMPS	Poly(2-Acrylamido-2-Methyl-1-Propanesulfonic Acid)
CNT	Carbon Nanotubes	PDDA	Poly(Diallyl Dimethylammonium Chloride)

CPE	Constant Phase Elements	PEI	Poly(Ethylene Imine)
CV	Catechol Violet	Ppy	Polypyrrole
CVD	Chemical Vapor Deposition	PTFE	Polytetrafluoroethylene
DBA23	2,3-Dihydroxybenzoic Acid	PVA	Polyvinyl Alcohol
DBA25	2,5-Dihydroxybenzoic Acid	PVB	Polyvinyl Butyral
DBA26	2,6-Dihydroxybenzoic Acid	PVDF	Polyvinylidene Fluoride
DC	Direct Current	PVDF-HFP	Poly(Vinylidene Fluoride- <i>Co</i> -Hexafluoropropylene)
DCA/ DChH	Deoxycholic Acid	PVF	Polyvinyl Fluoride
DChNa	Sodium Deoxycholate	QDs	Quantum Dots
DHB	3,4-Dihydroxybenzoic Acid	rGO	Reduced Graphene Oxide
DHC	3,4-Dihydroxyhydrocinnamic Acid	SA	Salicylic Acid
DHP	3,4-Dihydroxyphenylacetic Acid	SCE	Saturated Calomel Electrode
DMA	Dimethylacetamide	SEM	Scanning Electron Microscopy
DMF	Dimethylformamide	SSA	5-Sulfosacrylic Acid

DMSO	Dimethyl Sulfoxide	SWCNT	Single Wall CNT
DOPA	L-3,4-Dihydroxyphenylalanine	TBA	2,3,4-Trihydroxybenzoic Acid
DTA	Differential Thermal Analysis	TEM	Transmission Electron Microscopy
EDX	Energy-Dispersive X-Ray Spectroscopy	TFE	Tetrafluoroethylene
EIS	Electrochemical Impedance Spectroscopy	TGA	Thermogravimetric Analysis
EPD	Electrophoretic Deposition	UDCA	Ursodeoxycholic Acid
FEP	Fluorinated Ethylene-Propylene	VF	Vinyl Fluoride
FTIR	Fourier Transform Infrared Spectroscopy	VF2	Vinylidene Fluoride
GA	Gallic Acid	XRD	X-Ray Diffraction
GO	Graphene Oxide	YSZ	Yttria-Stabilized Zirconia
GRM	Graphene Related Materials		

Declaration of Academic Achievements

I, Qinfu Zhao, declare that this thesis is my own work and was written to fulfill the requirements for a PhD degree in the Department of Materials Science and Engineering at McMaster University. All of the experiments were conducted from September 2018 to September 2022 and adhered to the research policy and procedures from McMaster University. This dissertation contains six published, peer-reviewed journal papers in which I am the first author and the main contributor under the supervision of Dr. Zhitomirsky. To the best of my knowledge, the contents of this thesis do not infringe on anyone else's copyright and have not been submitted or published previously or anywhere else for the award of any other academic degree or diploma.

The six first-authored, peer-reviewed journal papers are the following:

1. **Q. Zhao**, X. Liu, S. Veldhuis, I. Zhitomirsky, "Sodium deoxycholate as a versatile dispersing and coating-forming agent: A new facet of electrophoretic deposition technology," *Colloids and Surfaces A: Physicochemical and Engineering Aspects*, vol. 588, p. 124382, 2020.
2. **Q. Zhao**, X. Liu, and I. Zhitomirsky, "Electrophoretic deposition of materials using lithocholic acid as a dispersant," *Materials Letters*, vol. 275, p. 128129, 2020.
3. **Q. Zhao**, S. Veldhuis, R. Mathews, and I. Zhitomirsky, "Influence of chemical structure of bile acid dispersants on electrophoretic deposition of poly (vinylidene

- fluoride) and composites,” *Colloids and Surfaces A: Physicochemical and Engineering Aspects*, vol. 627, p. 127181, 2021.
4. **Q. Zhao**, X. Liu, S. Veldhuis, and I. Zhitomirsky, “Versatile Strategy for Electrophoretic Deposition of Polyvinylidene Fluoride-Metal Oxide Nanocomposites,” *Materials*, vol. 14, no. 24, p. 7902, 2021.
 5. **Q. Zhao** and I. Zhitomirsky, “Biomimetic strategy for electrophoretic deposition of composite ferroelectric poly (vinylidene, fluoride-co-hexafluoropropylene)-ferrimagnetic NiFe_2O_4 films,” *Colloids and Surfaces A: Physicochemical and Engineering Aspects*, p. 129743, 2022.
 6. **Q. Zhao**, X. Liu, S. Veldhuis, and I. Zhitomirsky, “Colloidal processing of ferroelectric poly(vinylidene fluoride-co-hexafluoropropylene) – ferrimagnetic pseudocapacitive CuFe_2O_4 composite films,” *Colloid Polymer Science*, 300, 1197–1204 (2022).

Chapter 1 Thesis Organization

Following the regulations of McMaster University, this research project is presented in a sandwich thesis format, containing six coherent, peer-reviewed, scholarly works between an introductory chapter outlining the general background and objectives and a final conclusive chapter describing the engineering and scientific achievements of the research.

A summary of the contents in each chapter is provided below:

Chapter 2 is an introductory chapter which outlines the research theme, relevant background, and general research objectives.

Chapter 3 is a comprehensive literature review chapter which covers the fundamental mechanisms, kinetics, and material science aspects of electrophoretic deposition. The advantages and wide-ranging applications of EPD as a film-forming technique are reviewed thoroughly. An overview of the significance of using natural surfactants as dispersing, charging, and film-forming agents in biomimetic EPD strategies and challenges encountered in the EPD of composite materials is outlined.

Chapter 4 is the first published, peer-reviewed article, “*Sodium deoxycholate as a versatile dispersing and coating-forming agent: A new facet of electrophoretic deposition technology*” in the journal *Colloids and Surfaces A: Physicochemical and Engineering Aspects*. This paper investigates the feasibility of EPD of chemically inert materials such as PTFE, diamond, and carbon dots using DChNa as a charged dispersant and coating-

forming agent. It was found that adding DChNa improved the stability of the PTFE suspension due to its amphiphilic structure and allowed for the EPD of dense and crack-free PTFE films and their composites, which was confirmed by SEM and FTIR analysis. Potentiodynamic and impedance spectroscopy studies revealed the corrosion protection properties of PTFE films deposited by EPD. Finally, a combined EPD and electropolymerization method was developed to successfully fabricate PPy-diamond composite, which opens up potential applications for EPD combined with other electrochemical deposition techniques.

Chapter 5 is the second published, peer-reviewed article, “*Electrophoretic deposition of materials using lithocholic acid as a dispersant*” in the journal *Materials Letters*. In this paper, LCA was found to be an efficient biosurfactant for the dispersion, charging, and EPD of PTFE and diamond composite films in an organic solvent with reduced porosity and a high deposition yield. Tafel and EIS measurements indicated that PTFE films deposited via EPD acted as barriers against electrolyte penetration and provided corrosion protection to stainless steel in 3% NaCl solutions.

Chapter 6 is the third published, peer-reviewed article, “*Influence of chemical structure of bile acid dispersants on electrophoretic deposition of poly(vinylidene fluoride) and composites*” in the journal *Colloids and Surfaces A: Physicochemical and Engineering Aspects*. This paper was founded on and a continuation of the work presented in the previous chapter. In this study, five bile acids, LCA, CDCA, DCA, UDCA, and ChA, were selected as anionic biosurfactants for the EPD of PVDF films from organic solvents, and

their performance compared. It was found that the dispersion efficiency of PVDF particles changed when using different BAs, ordered from lowest to highest $LCA < CDCA < DCA < UDCA < ChA$, depending on the number, position, and orientation of OH groups in the BA's structure. Fabricated PVDF films provided corrosion protection as demonstrated by the plotted Tafel and Bode curves. ChA was discovered to be a co-dispersant that allowed for the co-deposition of PVDF-diamond and PVDF-silica composite films whose compositions could be easily controlled. Employing ChA in this way was a promising strategy for making films with enhanced thermal conductivity, piezoelectric, pyroelectric, and mechanical properties.

Chapter 7 is the fourth published, peer-reviewed article, "*Versatile Strategy for Electrophoretic Deposition of Polyvinylidene Fluoride-Metal Oxide Nanocomposites*" in the journal *Materials*. The goal of this work was to make nanocomposites using EPD, combining the functional properties of PVDF and advanced inorganic nanoparticles. Inspired by the natural phenomenon of the strong adsorption of mussels to rock surfaces in the ocean, caffeic acid (CA) and catechol violet (CV) were used as co-dispersants to successfully deposit PVDF composite with TiO_2 , MnO_2 , and $NiFe_2O_4$ nanoparticles. An EPD kinetic investigation and SEM, FTIR, and XRD characterizations suggested that the co-dispersion properties of CA or CV were related to the hydrophobic interactions of their aromatic rings with PVDF particles and the catechol bonding of their phenolic groups to metal atoms on the surfaces of inorganic particles. The co-dispersing ability of CA and CV enabled the co-deposition of organic-inorganic nanocomposites which had combined

functional properties such as corrosion protection, piezoelectric properties, and superparamagnetic properties, among others.

Chapter 8 is the fifth published, peer-reviewed article, “*Biomimetic strategy for electrophoretic deposition of composite ferroelectric poly(vinylidene, fluoride-co-hexafluoropropylene) – ferrimagnetic NiFe₂O₄ films*” in the journal *Colloids and Surfaces A: Physicochemical and Engineering Aspects*. This article described for the first time the creation of composite films containing a ferroelectric PVDF-HFP polymer with ferrimagnetic NiFe₂O₄ nanoparticles via EPD, which was based on the feasibility of fabrication, surface modification, and EPD of PVDF-HFP particles and NiFe₂O₄ nanoparticles using catechol-type caffeic acid (CA) as a co-dispersant. SEM revealed relatively dense, continuous, and crack-free morphology of PVDF-HFP films possessing corrosion protection properties, which was confirmed by potentiodynamic testing. The NiFe₂O₄ content and magnetic properties of the composites can be altered by varying the EPD bath composition.

Chapter 9 is the sixth published, peer-reviewed article, “*Colloidal processing of ferroelectric poly(vinylidene fluoride-co-hexafluoropropylene) – ferrimagnetic pseudocapacitive CuFe₂O₄ composite films*” in the journal *Colloid Polymer Science*. This paper details the creation of a composite film containing ferrimagnetic CuFe₂O₄ and ferroelectric PVDF-HFP using EPD with CA, which facilitated both the fabrication of micrometer-sized PVDF-HFP particles from bulk beads and the dispersal of CuFe₂O₄ nanoparticles. Electrochemical studies revealed the advanced pseudocapacitive properties

of CuFe_2O_4 in a negative potential range, which is promising for energy storage device applications. The incorporation of CuFe_2O_4 into PVDF-HFP imparted a greater dielectric constant and ferrimagnetic properties to the composites, and by adjusting the EPD parameters, the composition and functional properties of such composites could be easily tuned and controlled.

Chapter 10 is a concluding chapter which summarizes the overall implications of the current research studies as well as offers suggestions for future works.

Chapter 2 Introduction

2.1 Background

Fluoropolymers are polymers that contain the organic element carbon (C) and the reactive element fluorine (F) and have carbon-carbon bonds as their backbone and carbon-fluorine bonds as their pendant groups [1]. Fluorine develops extremely strong bonds with the other component elements, including carbon, because of the high electronegativity of them all. Fluoropolymers owe most of their unique properties to the fluorine-carbon bond having a bond energy of 490 kJ/mol, which is significantly higher than the C-H bond of 420 kJ/mol. One of the most important properties is that the high stability of the C-F bond in a fluoropolymer grants it superior stability inertness in aggressive environments. The substitution of fluorine for hydrogen in organic compounds also triggers greater thermal stability, reduced flammability, a lower surface energy, less friction, and excellent non-stick, electrical, and optical properties [2]. Commonly used fluoropolymers consist of polytetrafluoroethylene (PTFE), polyvinylidene fluoride (PVDF), polyvinyl fluoride (PVF), fluorinated ethylene-propylene (FEP), and others polymerized from their monomers of tetrafluoroethylene (TFE), vinylidene fluoride (VF₂), vinyl fluoride (VF), hexafluoropropylene (HFP), ethylene, and five others [3].

According to public reports, the global fluoropolymer market for 2022 is anticipated to be \$9 billion, and the market value is projected to grow at a compound annual growth rate of

6.7% until 2028 [4]. The vigorous growth of the fluoropolymer market has been driven by the material's expanding applications in the construction, automotive, medical, chemical, electrical, and electronics industries, which is attributed to its chemical and thermal stability, non-toxicity, and excellent mechanical properties. The popularity of using advanced functional polymers to manufacture various components for electronic devices such as smartphones and computers also contributes to the growth of the fluoropolymer industry during the reported period. The sudden outbreak of COVID-19 only briefly impacted production of fluoropolymer materials due to public health measures and restriction policies. The industry quickly returned to a profitable scale of operation as demand exploded for medical products, such as personal protective equipment and tubing, due to the biocompatibility, dielectric properties, and lubricity of these polymers.

PTFE, the most famous fluoropolymer, which is also commercially known by its brand name, Teflon, has been widely applied for years since it was accidentally discovered by Dr. Roy J. Plunkett at DuPont industry in 1938 [5]. Extremely strong, continuous, uniform C-F bonds around a C-C backbone impart PTFE with its superior chemical resistance and thermal stability. PTFE's inert characteristics make it an advanced coating material for use in biomedical implants and stents, pharmaceuticals, automotives, electrical insulation, non-stick cookware, mechanical lubrication, and corrosion protection [5-7].

PVDF is renowned for having the greatest piezoelectric effect of all the polymers because of the high electronegativity of fluorine atoms compared to carbon and hydrogen atoms. PVDF presents four different crystalline phases, α (or form II), β (form I), γ (form III), and

δ (form IV), of which α , β , and γ are the most investigated and the β -phase has the highest dipole moment per unit lattice [8]. This strong dipole moment induces piezoelectric, ferroelectric, and pyroelectric effects which make PVDF a potential candidate for sensor and transducer applications. The excellent chemical and mechanical properties of PVDF also contribute to its applications as full cell separators, membranes, and corrosion protection coatings [9, 10]. PVDF-HFP is a copolymer of PVDF with lower crystallinity, higher solubility, higher hydrophobicity, and better mechanical strength due to the incorporation of HFP groups with enhanced fluorine content [11]. PVDF-HFP shows promise for battery separators, oil-water separation, distillation membranes, and magnetoelectric devices [12].

Depending on the application, fluoropolymers are used in the form of coatings and films, sheets, tubes, additives, or other mediums, among which coatings and films account for a major portion of the market share. Typical film deposition techniques consist of dip coating, spin coating, electrospinning, spray coating, and electrophoretic deposition (EPD) [12]. EPD is a well-established film forming technique carried out in a two-electrode cell where charged particles that have been dispersed in a stable colloidal suspension move toward and deposit onto the oppositely charged electrode, propelled by the applied electric field [13]. EPD is favoured among film deposition methods due to its excellent film quality, inexpensiveness, simple apparatus, and versatility [13, 14]. EPD allows for a wide range of materials, from traditional ceramic powders to advanced polymers, to be made into films a nanometer to several micrometers thick. EPD can produce both homogeneous flat films

and ones in complicated geometries, such as porous microstructures and fibrous or hollow fibers, with controllable composition and thickness.

Particles being properly charged and uniformly dispersed in a stable colloidal suspension is a critical prerequisite for successful EPD. The fluoropolymers mentioned above, PTFE, PVDF, and PVDF-HFP, are electrically neutral and cannot be electrophoretically deposited directly. Suitable charging agents must therefore be introduced to impart to them the proper charge. A stable colloidal suspension can be achieved with electrostatic, steric, and electrosteric stabilization. However, these polymers are famous for their chemical inertness and hydrophobicity, which poses a great challenge for charging and dispersing them by surface modification through the adsorption of chargeable surfactants. Moreover, owing to their substantial chemical resistance, these fluoropolymers are insoluble in most common solvents, and previous studies have shown that they are only soluble in toxic ones. Therefore, discovering environmentally friendly solvents in which to dissolve or suspend them is necessary to extend their biomedical applications. It is also challenging to co-deposit them with other materials that would enhance their properties for multifunctional applications.

Biomimetic strategies are designed approaches to utilizing theory and technology from a biological system to solve technical problems in real industry. It mimics structures, functionalities, processes, and mechanisms from the nature for the purpose of artificially synthesizing similar biocompatible and biodegradable substances. Inspired from bile acids' strong solubilization function to hydrophobic lipids, proteins, dietary fats and oils in human

digestive system, those amphiphilic molecules are utilized as solubilizing, charging, dispersing, and film-forming agents for hydrophobic and chemical inert polymers to fabricating functional composite coatings with high biocompatibility. Another biomimetic strategy is to mimic the strong adsorption of mussel proteins on inorganic surfaces contributed by catecholate-type bonding onto metal atoms for fabrication of composite films containing different type of materials.

Thus, the aim of the present study is to develop novel, biomimetic strategies for making polymer films and composites by EPD that can be used for corrosion protection and biomedical applications. This investigation identifies advanced biosurfactants that can charge and disperse electrically neutral and chemically inert polymer particles in non-toxic solvents in order to achieve successful deposition. The biomimetic strategies employed rely upon using different types of natural biosurfactants with outstanding dispersion power, such as molecules from the catechol and bile acid families. The experimental results of this work demonstrate that various catecholic molecules and bile acid or bile salt molecules make charging and dispersing PTFE, PVDF, and PVDF-HFP particles more efficient and facilitate the EPD of composite films. Relevant adsorption, charging, dispersion, and deposition mechanisms were carefully analyzed, and film composition, microstructure, and properties were thoroughly characterized.

2.2 References

- [1] S. Ebnesajjad, "3 - From Fundamentals to Applications," in *Fluoroplastics (Second Edition)*, S. Ebnesajjad, Ed. Oxford: William Andrew Publishing, 2015, pp. 11-21.

- [2] B. Ameduri and H. Sawada, *Fluorinated Polymers: Applications: Volume 2*. Royal Society of Chemistry, 2016.
- [3] L. W. McKeen, "Chapter 10 - Fluoropolymers," in *Permeability Properties of Plastics and Elastomers (Third Edition)*, L. W. McKeen, Ed. Oxford: William Andrew Publishing, 2012, pp. 195-231.
- [4] "Fluoropolymers Market: Global Market Size, Forecast, Insights, and Competitive Landscape.," Research and Markets.ID: 5642866, June 2022, Available: <https://www.researchandmarkets.com/reports/5642866/fluoropolymers-market-global-market-size>.
- [5] E. Dhanumalayan and G. M. Joshi, "Performance properties and applications of polytetrafluoroethylene (PTFE)—a review," *Advanced Composites and Hybrid Materials*, vol. 1, no. 2, pp. 247-268, 2018.
- [6] Q. Zhao, X. Liu, and I. Zhitomirsky, "Electrophoretic deposition of materials using lithocholic acid as a dispersant," *Materials Letters*, vol. 275, p. 128129, 2020.
- [7] Q. Zhao, X. Liu, S. Veldhuis, I. Zhitomirsky, S. A. Physicochemical, and E. Aspects, "Sodium deoxycholate as a versatile dispersing and coating-forming agent: A new facet of electrophoretic deposition technology," vol. 588, p. 124382, 2020.
- [8] J.-H. Bae and S.-H. Chang, "PVDF-based ferroelectric polymers and dielectric elastomers for sensor and actuator applications: a review," *Functional Composites and Structures*, vol. 1, no. 1, p. 012003, 2019.
- [9] Q. Zhao, S. Veldhuis, R. Mathews, and I. Zhitomirsky, "Influence of chemical structure of bile acid dispersants on electrophoretic deposition of poly (vinylidene fluoride) and composites," *Colloids and Surfaces A: Physicochemical and Engineering Aspects*, vol. 627, p. 127181, 2021.
- [10] Q. Zhao, X. Liu, S. Veldhuis, and I. Zhitomirsky, "Versatile Strategy for Electrophoretic Deposition of Polyvinylidene Fluoride-Metal Oxide Nanocomposites," *Materials*, vol. 14, no. 24, p. 7902, 2021.
- [11] X. Wang, C. Xiao, H. Liu, Q. Huang, and H. Fu, "Fabrication and properties of PVDF and PVDF-HFP microfiltration membranes," *Journal of Applied Polymer Science*, vol. 135, no. 40, p. 46711, 2018.
- [12] Q. Zhao and I. Zhitomirsky, "Biomimetic strategy for electrophoretic deposition of composite ferroelectric poly (vinylidene, fluoride-co-hexafluoropropylene)-

ferrimagnetic NiFe₂O₄ films," *Colloids and Surfaces A: Physicochemical and Engineering Aspects*, p. 129743, 2022.

- [13] P. Amrollahi, J. S. Krasinski, R. Vaidyanathan, L. Tayebi, and D. Vashaee, "Electrophoretic deposition (EPD): Fundamentals and applications from nano-to microscale structures," in *Handbook of nanoelectrochemistry*: Springer, 2016, pp. 561-591.
- [14] N. P. Bansal and A. R. Boccaccini, *Ceramics and composites processing methods*. John Wiley & Sons, 2012.

Chapter 3 Literature Review

3.1 Fundamental Aspects of EPD

Electrophoretic deposition (EPD) is a colloidal process that is widely used for fabricating functional surface coatings. Electrophoresis was first discovered in 1808 by Russian scientist Ruesch when he observed the movement of clay powder in water induced by an electric field. The first patented practical application of EPD was in 1933 when American scientists deposited thoria particles on a platinum substrate for an electron tube. Generally, EPD involves two processes: electrophoresis and deposition. Electrophoresis refers to the migration of properly charged particles in a stable suspension driven by an electric field force toward oppositely charged electrodes. Deposition refers to when a compact, continuous coating forms through colloidal particles accumulating and coagulating on the surface of the electrodes. Depending on which electrode receives the colloidal particles, EPD can be divided into two types: anodic EPD and cathodic EPD [1]. A typical EPD apparatus consists of an external power supply, two electrodes, and a bath in which charged particles are stably suspended, as shown in Figure 3.1.

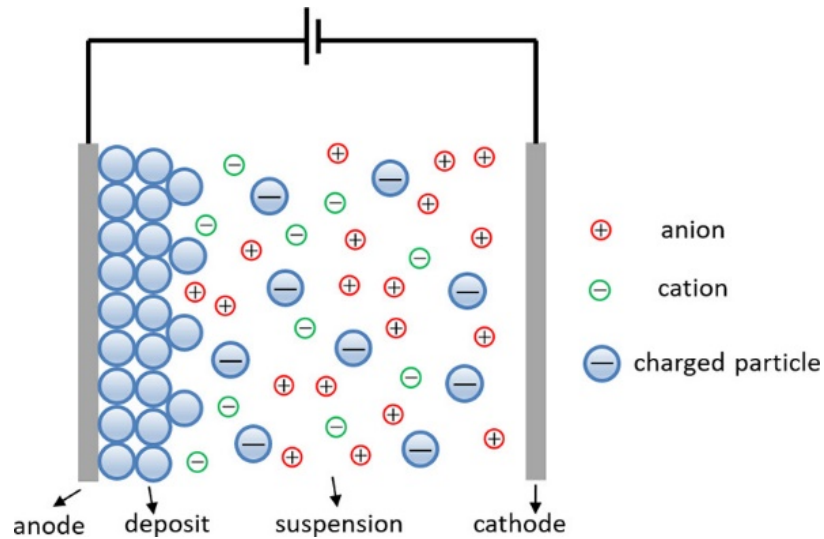


Figure 3.1 Schematic illustration of the anodic EPD process. Reprinted from [2] with permission from Elsevier.

3.1.1 Suspension stabilization mechanisms in EPD

A stable suspension containing charged particles is critical for fabricating high-quality films by EPD. In an unstable suspension, charged particles tend to agglomerate with each other and sedimentate to the bottom of the bath, making the electrophoresis of charged particles very challenging and limiting deposition yield and quality. There are several mechanisms for creating a stable and homogeneous colloidal suspension to achieve successful EPD.

To make a stable colloidal suspension, first the dispersed particles must not be too large, otherwise rapid sedimentation will occur due to the self-gravity of large particles. The typical colloidal size ranges from several nanometers to micrometers [3]. Besides the gravitational force, there are other interacting forces between particles. Attractive van der

Waals forces always exist between the particles, consequently causing unstable suspension. If the attractive forces between particles are large enough, the particles will tend to stick together, forming bulk particle clusters. To prevent particle agglomeration and achieve stable suspension, repulsive force must be introduced to overcome the attractive van der Waals force. The most common ways to create a repulsion interaction are electrostatic stabilization which is when electrostatic charge on the particles produces repulsion, steric stabilization which is when uncharged long polymer chains adsorb onto the particles, and electrosteric stabilization which combines electrostatic and steric repulsion [3]. Electrostatic and steric stabilization mechanisms are schematically illustrated in Figure 3.2.

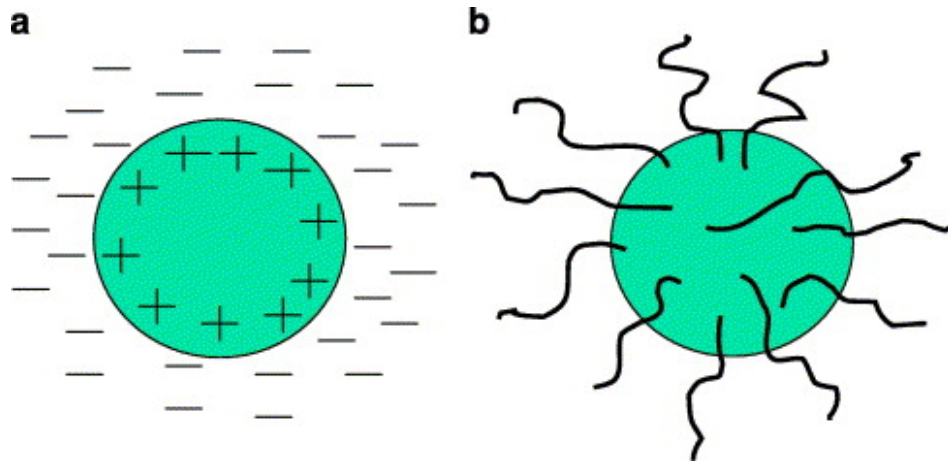


Figure 3.2 (a) Electrostatic stabilization and (b) steric stabilization illustrations. Reprinted from [4] with permission from Elsevier.

3.1.1.1 Electrostatic stabilization

In the case of electrostatic stabilization, the repulsion occurs because of electrostatic charge on the particles. However, this repulsion is not directly produced by charged particles. The

repulsion comes from the interaction of the electrical double layers generated around each charged particle. Provided that a particle in the suspension is positively charged due to the adsorption of positive ions from the solution or the dissociation of ionizable surface groups, negative counterions adsorb onto the positively charged particles and try to neutralize it. Due to thermal motion, the counterions form a round double layer, compacting in the inner layer but spreading out in the solution to form a diffuse layer, as shown in Figure 3.3.

When two particles converge in the colloidal suspension, the electric double layers start to overlap and interactions between them lead to increased repulsion between the particles. If the repulsion force is strong enough to counteract the attractive van de Waals force, the two particles will stop approaching each other any further, thereby establishing a stable colloidal suspension. The classical DLVO theory established by Derjaguin and Landau [5] and Verwey and Overbeek [6] explains this electrostatic stabilization mechanism for colloidal suspensions well.

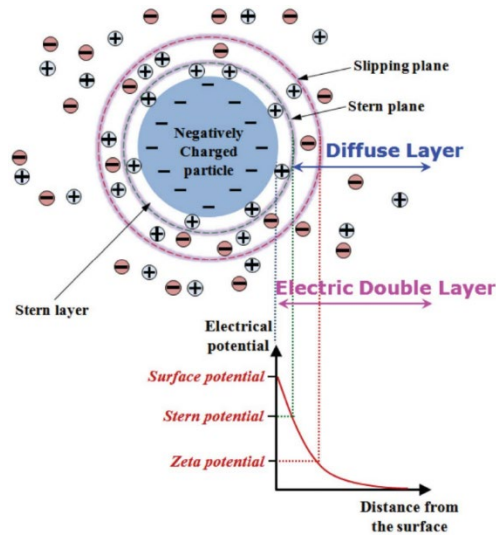


Figure 3.3 Schematic illustration of an electric double layer. Reprinted from [7] with permission from Elsevier.

DLVO theory holds that the stability of a colloidal suspension is governed by the total interparticle forces and potential energies (V_T) that exist between particles, which are summed by the potential energy of the attractive interaction caused by van der Waals force (V_A) and the potential energy of the repulsive interaction due to electric double layer force (V_R).

$$V_T = V_A + V_R \quad (3-1)$$

Figure 3.4 presents the van der Waals attraction (V_A), electric double layer repulsion (V_R), and their combination potentials as a function of the separation distance of two theoretical spherical particles suspended in a colloidal suspension [7]. If the distance between two particles is infinite, both the van der Waals attraction potential and electric double layer repulsion potential are near zero; as the distance shortens, both potentials increase their

value, but in opposite signs. The total potential energy shows a primary minimum at a shorter distance and a secondary minimum located a little farther away, both of which are dominated by the van der Waals attraction potential. Between those two minima, there is an electric double layer dominated maximum potential, which is also known as the repulsive energy barrier.

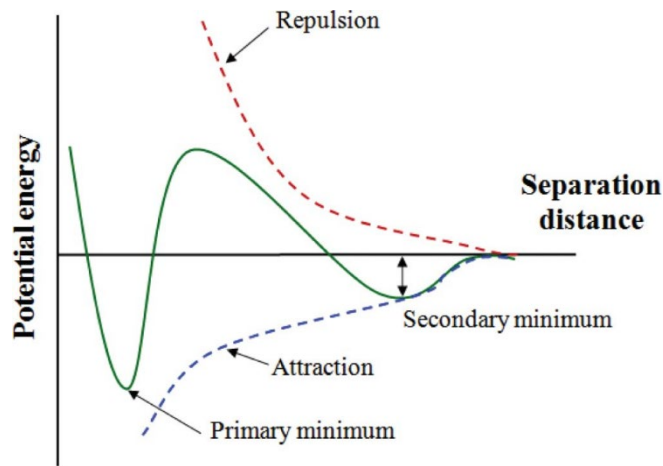


Figure 3.4 The potential energy between two particles in a colloidal suspension as a function of the intermolecular distance. Reprinted from [7] with permission from Elsevier.

If the thermal energy (kT) is smaller than the secondary minimum energy potential when two particles approach each other due to natural Brownian motion to the distance of the secondary minimum, the particles will flocculate together, resulting in the sedimentation of loosely packed particles. However, this flocculation is reversible; redispersion can be achieved by heating the solution to increase the thermal energy or by changing the electrolyte concentration to increase the electric double layer repulsion and thus decrease

the secondary minimum total potential energy. The electric double layer potential depends highly on its double layer thickness, which is determined by the concentration and valence state of the counterions [8]. When the double layer repulsion is weak, the repulsive energy barrier is not high enough compared to the kT and the particles tend to coagulate in the primary minimum area. Coagulation is an irreversible particle aggregation process. Coagulated particles are packed almost in contact, while flocculated particles are held together relatively loosely with greater separation between them. As the double layer repulsion increases, the secondary minimum has the chance to be eliminated. Meanwhile, the thermal energy, kT , of particles is less than that of their repulsion energy barrier, so the particles have very little chance of surpassing that energy barrier to fall into the primary minimum. In this case, a stable colloidal suspension is obtained.

3.1.1.2 Steric stabilization

In steric stabilization, the suspension is stabilized due to the interactions between long chains of polymers that have adsorbed onto the particles' surfaces, and those polymers usually carry no charge. A portion of the polymer chain or functional groups on the polymer adsorbs or anchors onto colloidal particles through either van der Waals attraction or chemical bonding. The remaining part of the polymer chain extends into the solution, offering long-range mixing or osmotic effects and short-range elastic entropic effects or volume restriction to stabilize the colloidal suspension. Aside from the stabilization effect from adsorbed polymers, sometimes the nonadsorbing polymers provide depletion stabilization in the interparticle region, which is a special type of steric stabilization.

Because EPD requires charged particles in order to generate electrophoresis of the particles to the electrode surface, the non-charged steric stabilization method is seldom used for suspension stabilization in EPD, so it is not illustrated in detail here. Steric stabilization can, however, be combined with electrostatic stabilization for successful EPD.

3.1.1.3 Electrosteric stabilization

An electrosteric stabilized suspension is achieved by combining electrostatic repulsion created by an electrical double layer and steric repulsion created by adsorbed polymers. One of the strategies for electrosteric stabilization is applying a polyelectrolyte. Polyelectrolytes are macromolecules that have at least one type of ionizable group that can dissociate to generate charge. Such ionizable groups include amine groups on cationic polyelectrolytes like poly(diallyl dimethylammonium chloride) (PDDA) [9, 10], poly(ethylene imine) (PEI) [11, 12], chitosan (CHIT) [12, 13], and poly(allylamine hydrochloride) (PAH) [10]; carboxylic groups on anionic polyelectrolytes like alginic acid [14, 15] and poly(acrylic acid) (PAA) [16, 17]; sulfonic acid groups on poly(2-acrylamido-2-methyl-1-propanesulfonic acid) (PAMPS) [18] polyelectrolyte, among others.

In suspension, those ionizable groups on polyelectrolytes dissociate to develop electrostatic charges. The generated electrostatic interactions dominate the adsorption of polyelectrolyte onto the particles' surfaces. The dissociation and adsorption of polyelectrolytes is highly dependent on the properties of the particle surface and solvent, such as the particle surface's charge sign, the salt concentration (ionic strength), and the pH of the solvent [19-21]. The

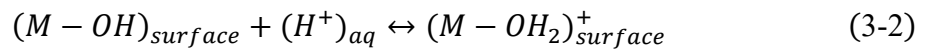
degree of ionization of strong polyelectrolytes is independent from the solution's pH, while the degree of ionization of weak polyelectrolytes is determined by the solution's pH [10]. Solution pH variation can change the polyelectrolyte from fully ionized to completely neutral. In a colloidal suspension with polyelectrolyte, stability results from long-range electrostatic repulsion and short-range steric repulsion.

3.1.2 Particle charging mechanisms for EPD

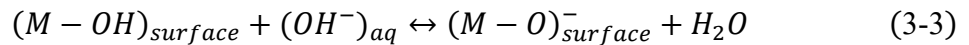
Particle surface charge is critical for both suspension stability and electrophoresis of the particle toward the electrode during EPD. A charged particle can be obtained from either the particle itself via the dissociation or ionization of its functional groups, or the solvent via selective adsorption of ions or ionizable molecules including dispersants, surfactants, charging agents, or polyelectrolytes.

In the self charging mechanism, the ionizable groups on the particles are mainly sulfonate, carboxyl, or amino groups which can protonate or deprotonate to generate charge on the particle's surface. Another special charging mechanism from the particle itself is isomorphic substitution. This is commonly observed in clay minerals [22]. Clay cations are substituted with other lower valence cations, leading to a deficit of positive charges (e.g., Al^{3+} substitution by Mg^{2+}), then smaller exchangeable Na^+ or K^+ ions are adsorbed onto the basal surface of the clay to balance the charge deficit. When dispersed in water, the Na^+ or K^+ ions dissolve, leaving behind negatively charged clay particles.

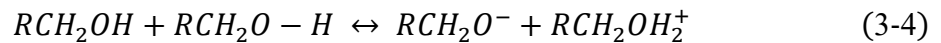
In most cases, particles are charged through the adsorption of ions or additive molecules from the solvent. In an aqueous solvent, the self-ionization of water produces positive hydrogen ions and negative hydroxide ions. Most ceramic particles naturally tend to coordinate with water molecules, forming amphoteric hydroxylic surfaces. The hydroxylic surfaces adsorb either H^+ or OH^- ions to charge the particles depending on the pH of the solution. At a lower pH, H^+ ions adsorb onto hydroxylic surfaces, imparting a positive charge to the particles.



At a higher pH, OH^- ions tend to consume the hydrogen on the hydroxylic sites that are producing water, leaving particles negatively charged.



Non-aqueous solvents, especially ethanol, have analogous ionization behaviour to water. Ionizing pure alcohol produces a protonated alcohol (ROH_2^+) and an alkoxide ion (RO^-) in the following way [23],



Wang et al. successfully deposited alumina particles in ethanol and proposed that the charging mechanism is the adsorption of hydrogen or ethylate ions onto the hydroxylic sites of these particles [24].

Another widely used method of charging particles is using charging additives. This is especially common in the EPD of chemically inert materials. Bile acid salts (BSs) and organic dyes are small-sized biomolecules that can be added to disperse and stabilize carbon nanotube suspensions via the unzipping mechanism, which has been well reviewed by Mustafa S. Ata et al. [25]. BSs adsorb onto CNT through hydrophobic interactions between the hydrophobic convex side of BSs and CNT, dissociating the salt ions from the BSs, offering CNT negative charges. As organic macromolecules, polyelectrolytes are widely used additives for charging colloidal particles. PEI and PDDA can adsorb well onto various materials to charge and stabilize particles for EPD [1].

3.1.3 Deposition mechanisms in EPD

In the EPD process, a stable suspension is a prerequisite for successful deposition, but too much stability disables EPD because the particles need to migrate to and destabilize on the electrode surface to form a high-quality deposit. Several mechanisms have been proposed to explain the deposition phenomenon of how repulsion between the particles deposited on the electrode surface and the incoming particles from bulk suspension is overcome.

In 1940, Hamaker and Verwey [26, 27] first proposed the sedimentation mechanism. They believed that the formation of deposits by EPD was analogous to the sedimentation of particles due to self gravitation. Instead of migrating as sediment to the bottom of the suspension bath, particles overcome the gravitational force under the electric field force, electrophoresed toward the electrode forming deposition. The increasing pressure

introduced by the incoming particles conquers the interparticle repulsion force at the electrode.

In 1954, Koelmans et al. [28] proposed the particle flocculation mechanism that occurs near the electrode due to the reduction of interparticle repulsion. They hypothesized that the concentration of electrolytes near the electrode increases when deposition potential is applied. The increasing electrolyte concentration results in an increase of the ionic strength next to the electrode, and the calculated ionic strength is high enough to trigger flocculation of the suspension. The increased electrolyte concentration also leads to the zeta potential lowering, which is beneficial for particle flocculation.

In 1992, Grillon et al. [29] suggested the particle charge neutralization mechanism, which takes place especially during the initial stage of EPD. Incoming charged particles neutralize the reverse charged electrode and form a deposit. This mechanism holds true for very thin deposits from very dilute suspensions. It was unconvincing when the particle and electrode were isolated by thick deposits or induced, semipermeable membranes.

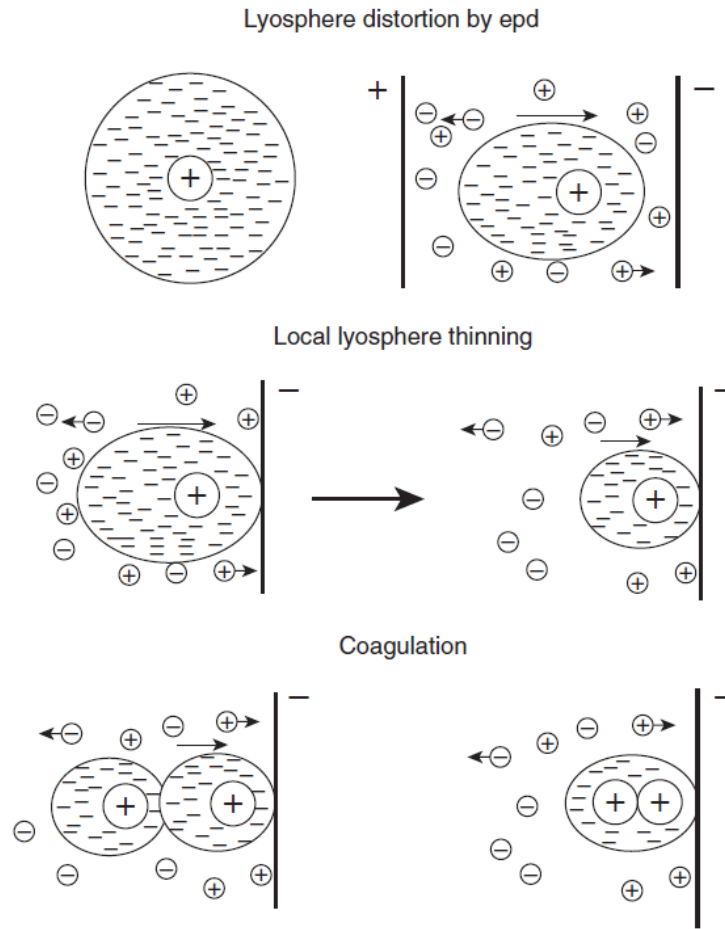


Figure 3.5 Lyosphere distortion and thinning mechanism during EPD. Reprinted from [30] with permission from Elsevier.

In 1996, Sarkar and Nicholson [22] proposed the lyosphere distortion and thinning mechanism during the EPD process, as illustrated in Figure 3.5 [30]. In a colloidal suspension, the charged particle is surrounded by ions from the liquid forming the electrical double layer, which is also termed lyosphere. Under an applied electric field, lyosphere moves toward the electrode, changing its shape from a “perfect” sphere to a distorted sphere with a thinner head and wider tail. Near the electrode, counterions in the wider tail react

with the accompanying cations, resulting in a thinner tail. Incoming particles with a thinner head can get close enough to the thinner tail for the van der Waals attraction force to induce coagulation and deposition.

In 1999, De and Nicholson [31] proposed the pH localization mechanism to explain the formation of deposition, which was experimentally verified by Besra et al. in 2010 using continuous and pulsed DC EPD [32]. The discharge depletion of cations, usually H^+ , near the cathode leads to an increase in the local pH at the cathode/solution interface. Spontaneously, the evolution of oxygen consuming OH^- caused a decrease in the pH at the anode/solution interface. During cathodic EPD of alumina from its aqueous suspension [32], the pH near the electrode shifted toward the isoelectric point (IEP) of the alumina, leading to a spontaneous coagulation. Because the particles carried no charge at the isoelectric point and the electric double layer repulsion vanished, strong van der Waals attraction coagulated the particles, forming deposition.

Beside the mechanisms mentioned above, there are still other hypotheses proposed by other researchers. For example, Koura et al. [33] developed an electrode reaction model to explain the deposition of various oxide particles. In many EPD attempts [34-36], the addition of electrolytes or polyelectrolytes has promoted the formation of adhesive deposition. They act as binder materials which enhance the van der Waals attraction force, inducing particle coagulation or causing bridging flocculation. Each EPD mechanism has its pros and cons. Not a single mechanism can explain every deposition formation during the EPD process because EPD can be applied to an extremely wide range of materials.

3.1.4 Kinetics of EPD

3.1.4.1 Deposit growth kinetics

One distinct advantage of EPD is that it allows for a wide thickness range when making films, which can be easily controlled by adjusting related key parameters. The key parameters that seem to have a significant influence on EPD have been well reviewed by Besra et al. [4] and can be divided into two main categories. The first is suspension parameters, including the colloidal particle size, zeta potential, suspension concentration, stability, conductivity, and dielectric constant; the second is process parameters, which include the deposition time, deposition voltage, deposition current, and conductivity of the substrate, to name a few. Hamaker [26] attempted to establish for the first time correlations between the deposit mass and some of the parameters mentioned above. Hamaker's law (Eq. 3-5) illustrates a linear relationship between deposit mass (m) and electrophoretic mobility (μ), applied electric field strength (E), the surface area of the electrodes (A), deposition time (t), and the suspension's concentration (C).

$$m = \mu E A t C \quad (3-5)$$

As the pioneered fundamental theory for EPD kinetics, Hamaker's law paved the way for the comprehensive development of EPD. Due to limited considerations of realistic conditions such as a continuous decrease in the suspension's concentration due to the consumption of particles, a drop in the potential due to the increasing resistance of the substrate as insulating deposits grow on it, a suspension resistance change during EPD, the

effect of particle movement when they diffuse, a highly concentrated suspension, and the electrical characteristics of the deposit and suspension, many authors have devoted themselves to ameliorating Hamaker's model or establishing new models to interpretate EPD kinetics, the attempts of which have been well summarized by Ferrari and Moreno in their EPD kinetics review paper [37].

Among all the contributions, Sarkar and Nicholson [22] took the variation of particle concentration into consideration and first introduced an efficiency factor, f , based on Hamaker's law,

$$m = m_0 \left(1 - e^{-\frac{t}{\tau}} \right) \quad (3-6)$$

in which m_0 is the starting mass of the particles in a suspension, τ is the characteristic time defined by Sarkar and Nicholson given by Eq. (3-7), and the reciprocal value of τ is defined as the kinetic parameter. Eq. (3-6) has been widely accepted because it is reliable for lengthy depositions and capable of predicting deviations from linearity under constant voltage EPD.

$$\tau = \frac{V}{f\mu AE} \quad (3-7)$$

Whereas V is the volume of suspension which is normally considered constant, f is the induced efficiency factor, ($f \leq 1$ all the time; when all the particles move to the electrode forming deposit, $f = 1$).

Furthermore, considering the resistance variation of suspension during EPD, Ferrari et al. [38] proposed a resistivity model to describe the kinetics by combining Hamaker's initial model [26] and Biesheuvel's modified model [39],

$$m = m_0 \left(1 - \frac{1}{1 + (\rho_{s,0}/\rho_{s,\infty}) \left(e^{\frac{t}{\tau_\infty}} - 1 \right)} \right) \quad (3-8)$$

in which $\rho_{s,0}$ is the initial resistivity of the suspension, $\rho_{s,\infty}$ is the resistivity at infinite time when all the particles have been deposited and the particle content in suspension is 0, and τ_∞ is the characteristic deposition time given by Eq. (3-9),

$$\tau_\infty = \frac{V}{f\mu I\rho_{s,\infty}} \quad (3-9)$$

When $\rho_{s,\infty} = \rho_{s,0}$, meaning that the suspension resistivity variation during EPD is negligible, Eq. (3-8) will reduce to the Sarkar and Nicholson model in Eq. (3-6). If $t \ll \tau_\infty$, this model then turns into Hamaker's law in Eq. (3-5). Therefore, the resistivity model established by Ferrari et al. is a more comprehensive one, which subsumes previous models for EPD kinetics explanation. This model also explains the S-shaped mass versus deposition time curve for long time scale EPD tests.

3.1.4.2 Electrophoretic mobility

Electrophoretic mobility, μ , mentioned above, is a critical parameter in colloidal science and the EPD process which can quantify the migration of charged particles for deposition. It was discovered experimentally that the electrophoretic velocity of suspended particles moving toward the electrode was proportional to the applied electric field strength. Electrophoretic mobility is defined as the ratio of electrophoretic velocity, v , over electric field strength, E ,

$$\mu = \frac{v}{E} \quad (3-10)$$

The relationship between electrophoretic mobility and the zeta potential for rigid spherical particles was established through the Henry equation [39-41],

$$\mu = \frac{2\varepsilon_0\varepsilon_r\zeta}{3\eta} f(\kappa a) \quad (3-11)$$

where ε_0 is the vacuum permittivity, ε_r is the relative permittivity of the solvent medium, ζ is the zeta potential, η is the viscosity of the solvent medium, $1/\kappa$ is the Debye length, a is radius of particle, $f(\kappa a)$ is the Henry's function varying from 1.0 at $\kappa a = 0$ (referred to as the Hückel equation) to 1.5 at $\kappa a = \infty$ (referred to as the Smoluchowski equation) [40, 41].

For “soft particles”, which are hard, spherical particles containing adsorbed polyelectrolytes, an electrophoretic mobility model was proposed by Ohshima [42],

$$\mu = \frac{\rho_{fix}}{\eta\lambda^2} \left[1 + \frac{2}{3} \left(\frac{\lambda}{\kappa} \right)^2 \frac{1 + \frac{\lambda}{2\kappa}}{1 + \frac{\lambda}{\kappa}} \right] \quad (3-12)$$

where ρ_{fix} is the fixed charge density, $\lambda=(\gamma/\eta)^{1/2}$, and γ is the frictional coefficient of the polyelectrolyte.

3.1.5 Advantages and applications of EPD

EPD is a very versatile material processing technique which has wide range of applications in both academia and industry. It can be performed not only under a continuous, direct current (DC) electric field, but also under modulated electric fields such as alternating current (AC) or pulsed direct current [43-45]. Compared to other film forming techniques, EPD has the advantages of an easy operation, simple apparatus, low cost, control over the thickness and morphology of films, and feasibility for use with various material types, like metallics [46, 47], ceramics [1, 48-50], carbons [25, 51-54], polymers [12, 55-57], and biomaterials [58-60] in either nanoscale or macroscale. Moreover, EPD allows for one-step fabrication of composite materials with combined functionalities [13, 61-63]. The main limitations of EPD are that the substrate materials must be electrically conductive, limited thickness of insulating deposits and possibility of unwanted side reactions.

Besides its versatility on types of materials to be deposited, EPD is also famous for its versatile fabrication of films in various shapes. The deposit takes the shape imposed by the substrate electrodes. EPD is capable of processing materials into various complex 3D

morphologies [62, 64, 65] when the substrate geography and particle shape are properly designed. For example, Anné et al. [64] shaped an alumina and zirconia-based femoral ball-head by EPD for biomedical applications. In an investigation by Ma et al. [66], a bioactive porous hydroxyapatite (HA) scaffold and bulk HA scaffold were fabricated by EPD for cell culturing and better tissue penetration and mechanical stability for the implant in the body. Li et al [67] deposited hierarchical, pine needle-shaped MnO_2 -CNT composites onto carbon fiber cloth for potential applications in wearable devices. Zhitomirsky [68] electrophoretically deposited submicron-sized HA powders on individual carbon fibers, carbon fiber bundles and felts. After subsequently burning out the fibrous carbon substrates, hollow HA fibers with various diameters were fabricated.

3.2 Materials Sciences Aspects of EPD

3.2.1 Particles and molecules

EPD involves the electrophoresis of charged particles or molecules in a stable suspension toward the electrode, driven by the applied electric field and deposited on the electrode. The starting materials during the EPD process are typically charged particles or molecules that are well dispersed in a colloidal suspension. EPD was first noticed due to the movement of clay particles in water induced by an electric field, and early patented attempts of EPD deposited thoria particles onto a platinum substrate [4]. Since then, processing various particle materials through EPD has been extensively investigated.

Theoretically, any powdered material can be dispersed in a stable suspension for EPD. Particle size is a critical parameter that has significant impact on EPD. According to the science of colloidal processing, the colloidal size ranges between 1 and 1000 nm [3]. Since a stable colloidal suspension is a prerequisite for successful EPD, this colloidal size range offers a hint of the suitable particle size for EPD. Experimental investigations have also demonstrated good deposition for a variety of larger ceramic and clay particles with sizes up to 20 μm [69]. However, deposition of particles beyond this size range might also be feasible by proper adjudication of other parameters. One of the main problems for the EPD of larger particles is to overcome the strong self-gravity force compelling them to settle down and dispersing them well enough to form a stable suspension suitable for EPD. Electrophoretic deposition of larger particles might also lead to non-uniform deposition, resulting in a thicker foot and thinner head in vertical setups. In these cases, a strong surface charge, efficient dispersant, or thicker electrical double layer are necessary [70].

Particle size greatly impacts suspension stability [71], electrophoretic mobility [72], and crack formation [73]. Sato et al. [73] showed that a smaller particle size contributes to fewer cracks in the films. The deposition rate, particle packing behaviour, deposit density, and the hardness of the sintered coatings were highly related to the particle size, size uniformity, and distribution in Ji et al.'s investigation [74]. Particles with mixed sizes lead to higher density coatings compared to uniform sized particles, and smaller particles lead to harder, sintered coatings [74].

As the EPD technique developed, it stopped being restricted to processing particle materials. Many attempts to deposit molecule materials were carried out using EPD, especially for biomedical macromolecules (also known as biomolecules) [75] and functional polymers, including biopolymers and engineering polymers [12]. Due to its excellent biological properties, chitosan, a polysaccharide molecule, shows promising applications in the biomedical field and food industry [76]. The EPD of chitosan and chitosan-based composite materials has been comprehensively reviewed by Avcu et al. [13]. The deposition mechanism of chitosan relies on its solubility dependence on pH, as illustrated in Figure 3.6 [13]. The amine groups on chitosan tend to protonate out hydrogen ions at a low pH, leaving positively charged chitosan molecules that move to the cathode and deprotonate into an insoluble film on the electrode surface due to a localized pH increase caused by water decomposition.

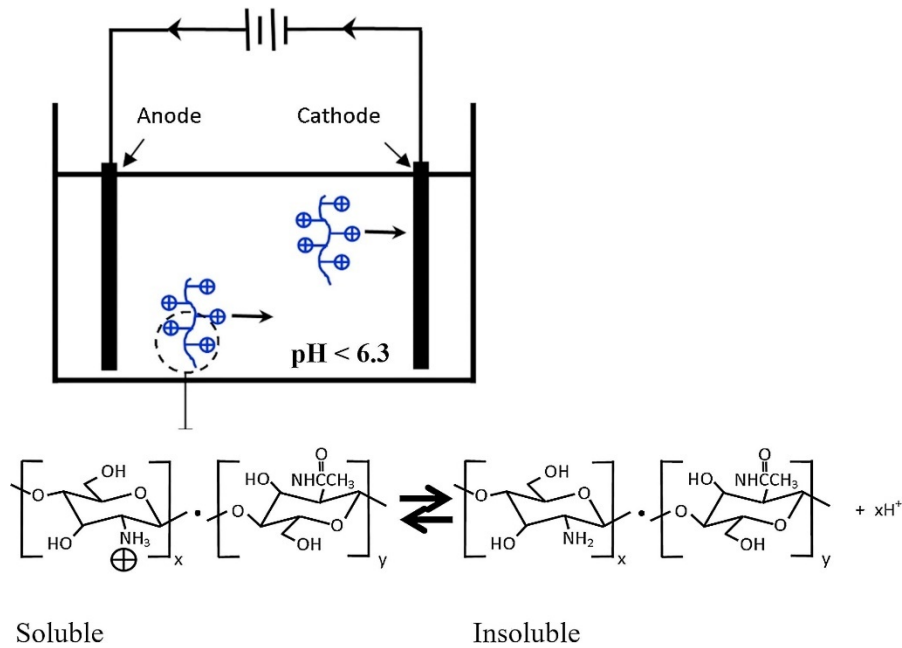


Figure 3.6 Schematic illustrations of the chitosan solubility transition and deposition mechanism. Reprinted from [13] with permission from Elsevier.

Aside from chitosan, the EPD of other polysaccharide molecules, such as alginates [77, 78] and hyaluronic acids [79, 80], is also being widely investigated. The EPD or co-EPD of functional polymers, proteins, and enzymes have been well reviewed by Sikkema et al. [12], Boccaccini et al. [58], and Seuss et al. [75].

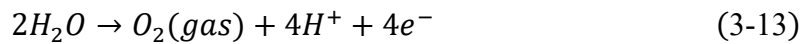
3.2.2 Solvents

Solvents must be carefully selected for specific materials to be deposited because solvents play critical roles in the EPD process. One of the main roles a solvent plays is as a liquid media surrounding the solid particles or molecules, which suspends them. In some cases, the solvent also provides charge, helps dissolve additives such as dispersants, surfactants,

or charging agents, and may participate in electrode reactions to help film forming. Generally, solvents for EPD can be divided into two main categories: water and organic solvents. Each category of solvent has advantages and disadvantages. Sometimes, mixtures of aqueous and organic solvents are used.

3.2.2.1 Aqueous solvents

Aqueous solvents are very popular for EPD because aqueous systems exhibit benefits such as being low cost, eco-friendly, and non-flammable and having low requirements for electric field strength compared with organic solvents. However, water-based solvents cause many problems in EPD. Firstly, electrolysis of water is almost inevitable during the EPD process. According to the following equations, electrolysis of water would produce bubbles, which is destructive for film forming:



Those bubbles tend to get trapped in the deposit, resulting in porous, low density, loosely packed films. This problem can be solved by using a porous mold or modulated electric field [2, 43, 44, 81]. A bubble-free deposit can be obtained on a porous mold placed between two electrodes, while bubbles evolve at the electrodes. Another problem related to the use of aqueous solvents is that high current density facilitates the oxidation of metallic electrodes, leading to electrode damage and adding impurities to the deposit. High

current density in an aqueous solvent also causes Joule heating to the suspension and the electrode [82]. Inserting dielectric layers with high electric impedance between the electrode and substrate effectively reduced problems such as electrochemical reactions, discharge, and Joule heating during EPD in an investigation by Miyajima et al. [83].

3.2.2.2 Organic solvents

Generally, organic liquid is superior to water as a solvent for EPD. Among organic solvents, alcohols are most widely utilized for EPD [84, 85]. Organic solvents exhibit higher chemical stability than water and are more inert with respect to particles. With organic solvents, gas formation from the electrolysis of water could be avoided, facilitating the formation of uniform and adhesive deposits. Moreover, a strong electric field can be applied to organic suspensions to raise the deposition efficiency [86]. Due to their low conductivity and dissociation power, they can avoid high current density, which significantly reduces Joule heating and electrochemical attacks against the electrode. Furthermore, because of the low relative permittivity of organic solvents, obstructions to the electric field intensity are minimized, and a more effective electric field strength can be retained to drive the movement of the charged particles.

The main disadvantage of organic solvents is that a high voltage is required for deposition. Moreover, most organic solvents cost more than water, and some are even toxic or flammable, which is not eco-friendly. Organic solvents with a lower boiling point will dry at a faster rate, which causes cracks in the films [87].

3.2.2.3 Mixed solvents

In several investigations, mixtures of two or more different liquids were used as solvents for EPD to promote deposition quality. Wang et al. [88] investigated EPD of yttria-stabilized zirconia (YSZ)/alumina composite coatings using various mixed solvents. They found deposit from mixed ethanol and acetylacetone suspension was more uniform and less porous than that from mixed ethanol and distilled water or from pure ethanol because the reaction between ethanol and acetylacetone promoted particle surface charging and diminished particle aggregation. Kang et al. [89] showed that the morphology of deposited iron oxide nanoparticles is highly related to the choice of solvents (hexane, toluene, and chloroform) and the ratio of their mixture because the solvent influences the surface charge and zeta potential of the nanoparticles.

3.2.3 Binders

Binders or binding agents were first used and regarded as critical aid materials in the field of ceramic processing to enhance the forming capabilities of discrete ceramic powders [90]. Binders were later introduced into the electrophoretic deposition industry to help increase the strength of the deposited films, provide adhesion to the substrate, and preventing cracking [1]. Although a binder is beneficial for forming an adhesive and crack-free film, it is not indispensable in EPD, and most EPD is performed without binders or only a minimal amount of binder when it is necessary [4]. Binders are mostly used for making films that are tens of microns thick using EPD [91-93].

The most common binder materials for EPD are polymer binders. Polymer binders in the suspension will adsorb on colloidal particles, not only offering charge to particles as ionizable polyelectrolytes, but also providing steric or electrosteric stabilization to the suspension. Metal oxides, alkoxides, or hydroxides such as $\text{Mg}(\text{OH})_2$ or MgO which have a high bonding strength have also been used as inorganic binders for EPD [94, 95] and deposited in the interstitial region between particles to provide adhesion [96].

Binders are multifunctional for the EPD process. For example, one commonly used binder for non-aqueous EPD, polyvinyl butyral (PVB), not only provided great strength, but also acted as a dispersant, which enhanced the stability of the suspension [97, 98]. In the EPD of silica particles [99] and polystyrene nanoparticles [100], poly (dimethyldiallylammonium chloride) (PDDA) not only served as a binder which adhered particles to the substrate, but also endowed the particles with charge to help with suspension stabilization. The suspension was more stable with higher PDDA content [100]. The water soluble, hydrophilic polymer polyvinyl alcohol (PVA) is famous for aqueous EPD. Chen et al. [101] found that when reinforcing with PVA an alginate-bioactive glass composite coating on stainless steel deposited by EPD, the amount of PVA significantly impacted the thickness, roughness, and adhesion strength of the composite coating.

3.3 Biosurfactants for EPD

Biosurfactants are a group of amphiphilic, surface-active compounds that help regulate surface and interfacial tension between two different phases [102]. Different from

traditional chemical surfactants, biosurfactants are produced from various microorganisms, such as bacteria, yeast, fungi etc., which are environmental friendly, low toxicity, and biodegradable [103]. These advanced properties make biosurfactants applicable in many areas, including the food industry, environmental protection, ceramic processing, pharmacology and medicine, and the oil and gas industry [103-106]. Biosurfactants are also widely applied in the EPD of colloidal particles [50]. The surfactants applied in an EPD process can also act as dispersants, charging agents, and film forming agents [107].

3.3.1 Bile acids and bile salts

Applying bile acids (BAs) as biosurfactants for EPD processing was motivated by their strong solubilization power and ability to solubilize cholesterol, vitamins, lipids, dietary fats, and other biomolecules in the human body [108]. This strong solubilization power was attributed to the rigid amphiphilic molecular structure of BAs with hydroxyl groups on their concave face, making it the hydrophilic side, and methyl groups on convex face, making it the hydrophobic side [109]. COOH or SO₃H groups on the end of bile acids are anionic groups, which facilitates their charging properties.

Major bile acids are cholic acid (ChA), deoxycholic acid (DCA), chenodeoxycholic acid (CDCA), lithocholic acid (LCA) and ursodeoxycholic acid (UDCA). Their carboxylic groups can conjugate with taurine or glycine residues to form other bile acids, as shown in Figure 3.7 [108, 109]. Most bile acids have poor water solubility when their ionisable functional groups have protonated; however, their corresponding bile salts (BSs) are highly

soluble [110, 111]. The solubility of bile acids is strongly related to the number, position, and orientation of their hydrophilic hydroxyl groups, which affiliate to water molecules through hydrogen bonding [111].

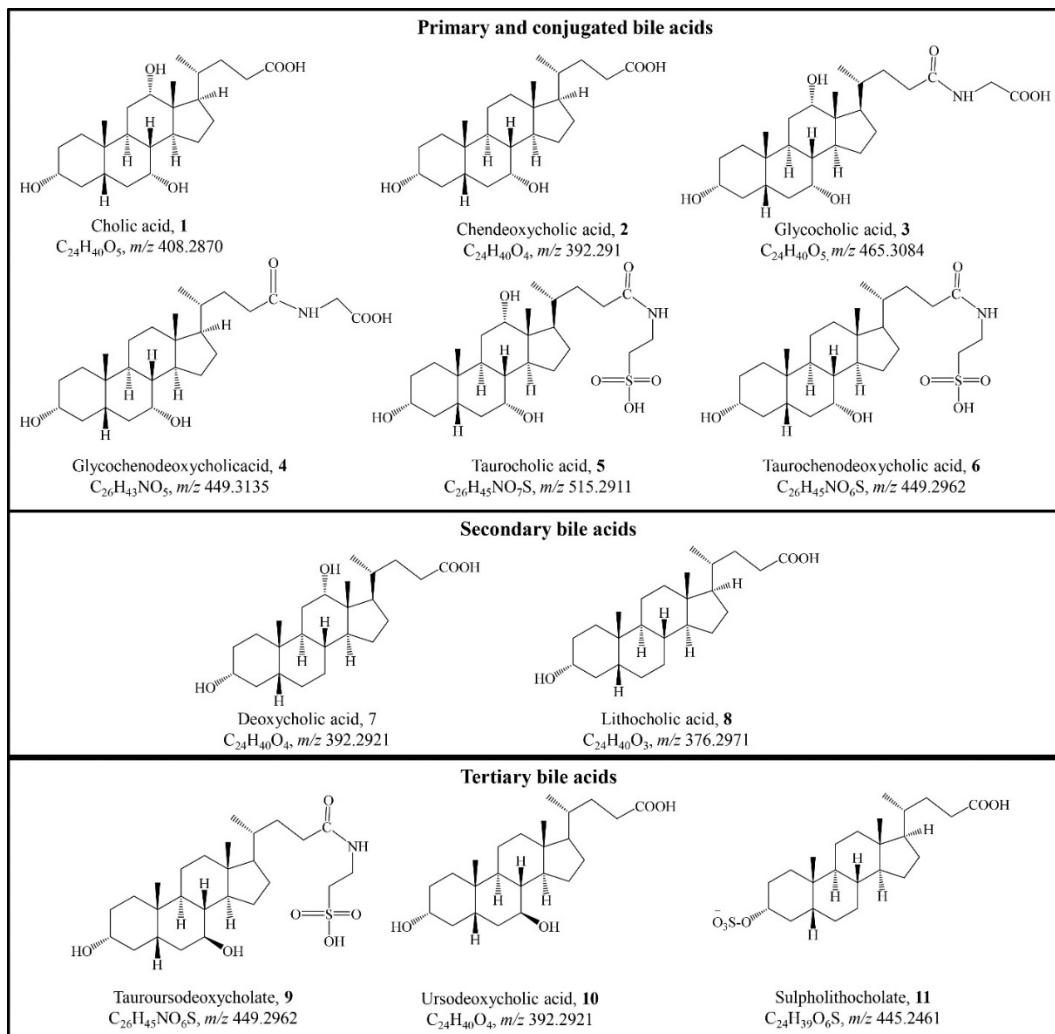


Figure 3.7 Chemical structures, molecular formula, and theoretical mass of bile acids. Reprinted with permission from [109]. Copyright {2019} American Chemical Society.

The mechanism through which bile acids or bile salts can solubilize many polar or nonpolar substances is their micellization behaviour. The micelle formation process has been well modeled by many researchers [112], involving two steps in primary and secondary micelle formation. Firstly, the primary micelles of BSs form from the hydrophobic interactions of the hydrophobic sides of the BSs molecules in an aqueous solution; secondly, by increasing the concentration of BSs, the primary micelles of BSs with OH groups that point outside tend to interact with each other through hydrogen bonding to form larger, secondary micelles, as illustrated in Figure 3.8 [108]. Critical micelle concentration (CMC) is an important factor reflecting the micellization properties of surfactants and their dispersion efficiency. CMC values are highly dependent on surfactant structure, temperature, pressure, ionic strength, pH, and the presence of other electrolytes. The CMC of different BSs has been investigated and measured using various techniques, and it was found that the CMC of BSs differed within a wide range [113-115]. Bile acids or bile salts are superior as biosurfactants to other conventional surfactants because of their unique amphiphilic structure, giving them a greater charge density, smaller micelle size, and lower CMC values [108, 112].

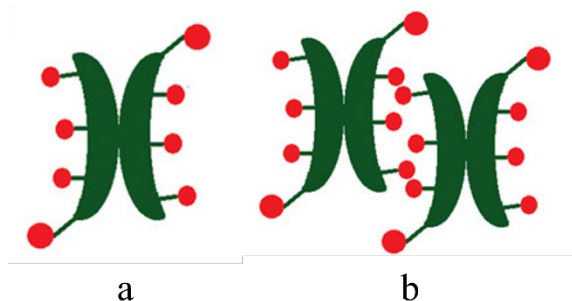


Figure 3.8 Formation of (a) primary and (b) secondary micelles of BAs/BSs molecules. Reprinted from [108] with permission from John Wiley and Sons.

Due to their high solubility in aqueous solutions, bile salts have been widely applied in aqueous EPD [116-120]. Very hydrophobic and poorly soluble carbon nanotubes (CNT), including single walled CNT (SWCNT) and multiwalled CNT (MWCNT), have been well dispersed with the sodium salts of cholic acid (ChA) and deoxycholic acid (DCA) to create products for energy storage, electronic devices, and sensor applications [25]. BSs showed strong adsorption on CNT, and it was found that steroidal BS molecules can wrap around CNT particles to form micelles. The hydrophobic side of BS molecules has a strong hydrophobic interaction with hydrophobic CNT particles, causing the hydrophilic side to point outward toward the water molecules, which unzips the large CNT particles into smaller ones as illustrated in [25].

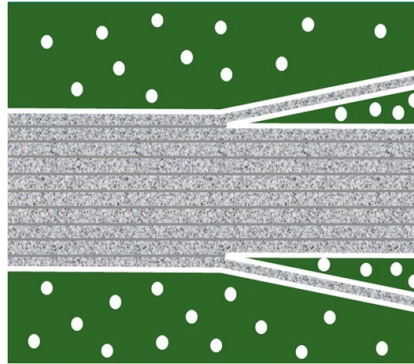
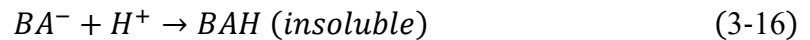


Figure 3.9 Schematic illustration of dispersion of CNT via the unzipping mechanism, in which white dots represent bile acid molecules. Reprinted from [25] with permission from Elsevier.

The EPD of ChA or DCA was due to their film-forming and gel-forming properties and the insolubility of their corresponding bile acids in water [118, 119]. During EPD, an electrochemical reaction of water at the anode electrode happened as follows, resulting in a local pH decrease,



The dissociation of ChA or DCA in water generated negative ChA^- or DCA^- ions, which moved toward the anode and protonated with hydrogen ions, forming water insoluble bile acid films at the anode's surface,



Unlike bile salts, most bile acids are water insoluble, but soluble in organic solvents like ethanol [121]. The EPD of chemically inert PTFE, PVDF, and composite films using bile

acids as surfactants in an ethanol solvent was investigated [56, 122-124]. It was found that using ethanol not only diminished gas generation induced film porosity during aqueous deposition, but also facilitated the dissociation of the bile acids used as dispersants and charging agents for the successful EPD of electrically neutral polymer particles.

3.3.2 Catecholates, gallates, and salicylates

Mussels can adsorb onto various material surfaces quickly and firmly to prevent damage from sea waves in the ocean. According to fundamental studies [125], this fast and strong adsorption results from the adhesive proteins confined to byssal plaques containing the amino acid, L-3,4-dihydroxyphenylalanine (DOPA). DOPA is an organic compound that has a catechol group with two adjacent OH groups attached on an unsaturated six-carbon ring, which is characteristic for catecholates. Catechol groups possess powerful complexing properties, in which two OH groups form bidentate bonding with atoms on different inorganic surfaces [50].

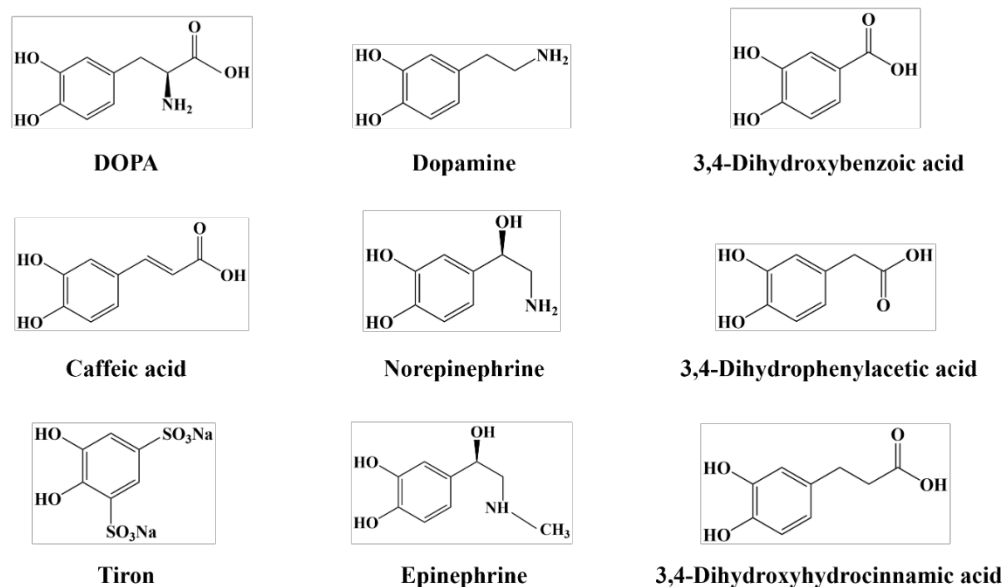


Figure 3.10 Chemical structures of various catecholic molecules.

Beside the catechol group on DOPA structures, there is a side chain containing an amino group and a carboxylic group (Figure 3.10), making DOPA a zwitterionic molecule that can offer charge to adsorbed particles through suspension acidity, facilitating dispersion and EPD. At a lower pH, the amino group protonates to NH_3^+ , offering positive charge. When the pH is increased, the amino, carboxylic, and phenolic groups deprotonate to contribute negative charge. Similar zwitterionic properties were also found for norepinephrine and epinephrine, whose chemical structures are shown in Figure 3.10.

The dopamine molecule belongs to the catecholamine family and exhibits cationic charging properties in acidic suspension and self-polymerization properties in basic suspension [50]. Dopamine has adsorbed onto oxide particles by chelation from a catechol group and onto CNT by π - π interaction. The EPD of various ceramic particles using dopamine as a

surfactant involved a charge neutralization deposition mechanism, and the deposited films showed improved functional properties for their particles [50].

Another characteristic molecule from the catechol family is caffeic acid (CA), which is famous for its antioxidation properties and as a corrosion inhibitor for stainless steels [123, 124]. The phenolic and carboxylic groups on CA have shown strong adsorption on various inorganic particles, involving either inner sphere or outer sphere bidentate chelating or bridging bonding, as schematically illustrated in Figure 3.11 [50]. The adsorption of CA on particles provided charging to particles by dissociating the carboxylic group. The catecholic molecules of 3,4-dihydroxybenzoic acid (DHB), 3,4-dihydroxyphenylacetic acid (DHP), and 3,4-dihydroxyhydrocinnamic acid (DHC) show similar chemical structures to CA and are also anionic surfactants due to their carboxylic groups. EPD investigations using DHB, DHP, and DHC molecules as charging and dispersing agents found that longer hydrocarbon chains show increased deposition yield due to improved dispersion efficiency [126]. The anionic properties of tiron are related to two SO_3^- groups and the adsorption of tiron is because it forms inner sphere complexes with metal atoms on the surfaces of particles [50].

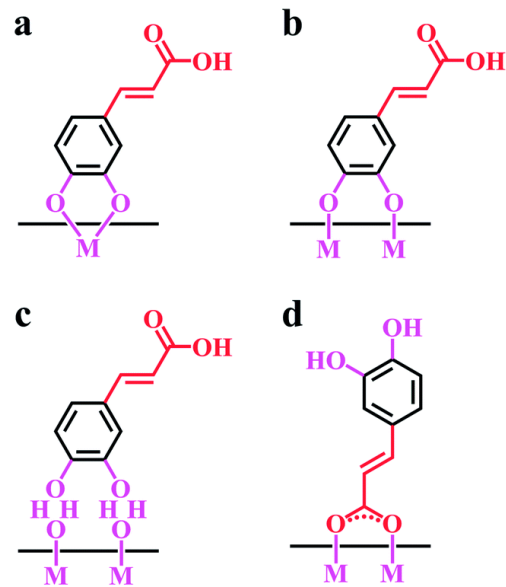
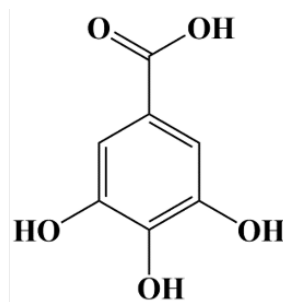


Figure 3.11 Schematic illustrations of the adsorption mechanisms of caffeic acid on inorganic particles: (a) bidentate chelating bonding, (b) inner sphere bidentate bridging bonding, (c) outer sphere bidentate bridging bonding, and (d) carboxylic group bonding [50].

Gallate-type molecules include gallic acids and gallic acid-based salts and esters. Gallic acid (GA) has three adjacent OH groups on the aromatic ring and a COOH group which is non-adjacent to either OH group (Figure 3.12). The adsorption mechanism of gallate-type molecules on oxides is similar to catecholate-type molecules, which is related to two of the three OH groups, forming complexations with the metal atoms in oxides. The third OH group showed a slight impact on the stability of the complexations [50]. However, EPD investigations revealed that GA with three OH groups exhibits improved dispersing and charging efficiencies compared to DHB with two OH groups [126]. Studies found that GA

can be used as a co-dispersant for the EPD of MnO₂-TiO₂ composites [127] and MnO₂-MWCNT composites [128].



Gallic acid

Figure 3.12 Chemical structures of gallic acid.

The characteristic structures of salicylate-type molecules contain at least one aromatic ring with an OH group and a carboxylic group bonded to two adjacent carbon atoms on the ring, as shown in Figure 3.13. Dissociation of the carboxylic groups provides anionic charge. The adsorption onto various ceramic particles is achieved by salicylate bonding involving the adjacent hydroxyl and carboxylic groups, as illustrated in Figure 3.14 [50].

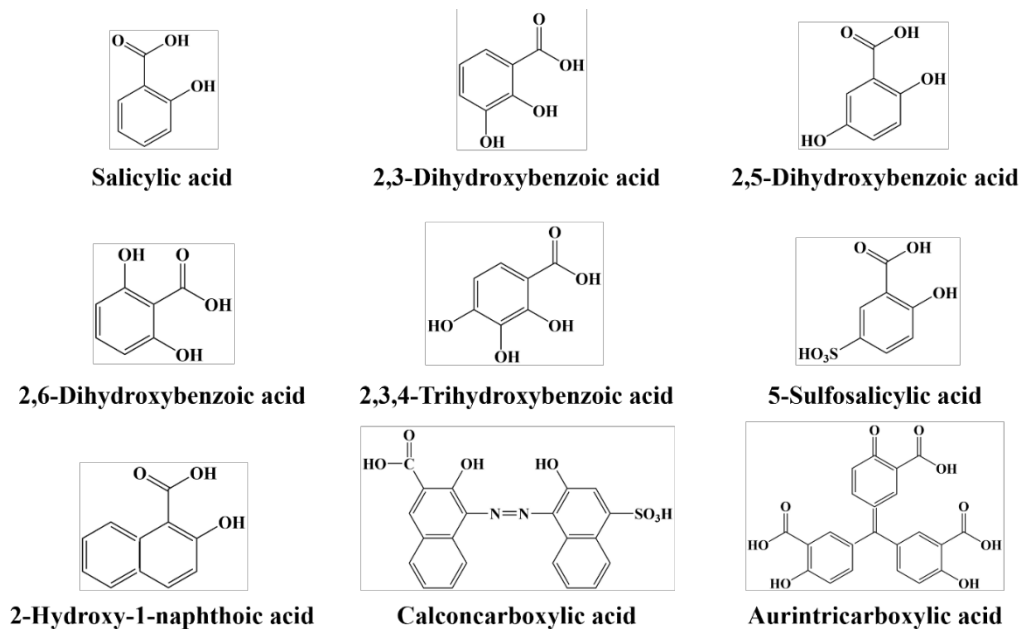


Figure 3.13 Chemical structures of salicylate-type molecules.

Investigations showed that 2,3-dihydroxybenzoic acid (DBA23) and 2,3,4-trihydroxybenzoic acid (TBA) can selectively form catecholate and salicylate bonding based on the nature of the adsorbed materials. However, other salicylate molecules in Figure 3.13, such as salicylic acid (SA), 2,5-dihydroxybenzoic acid (DBA25), 2,6-dihydroxybenzoic acid (DBA26), and 5-sulfosalicylic acid (SSA), can only form salicylate type bonding. EPD investigations of TiO_2 particles demonstrated that DBA23 exhibits a stronger adsorption ability on TiO_2 surfaces than DBA26 because DBA26 can only produce salicylate bonding [129]. The deposition kinetics studies in [129] found that SSA provides strong electrostatic repulsion at the electrode surface due to its two charged groups, SO_3^- and COO^- , which is detrimental to deposit growth. A comparison of the electrophoretic deposition yield of MnO_2 found that a TBA dispersed MnO_2 suspension had a significantly

higher yield than an SA dispersed one because of the enhanced dispersing capability of TBA [130]. The deposit mass versus concentration of 2-hydroxy-1-naphthoic acid in MnO_2 suspension revealed a charge reversal phenomenon due to competitive adsorption between the hydrogen ion and anionic 2-hydroxy-1-naphthoic acid.

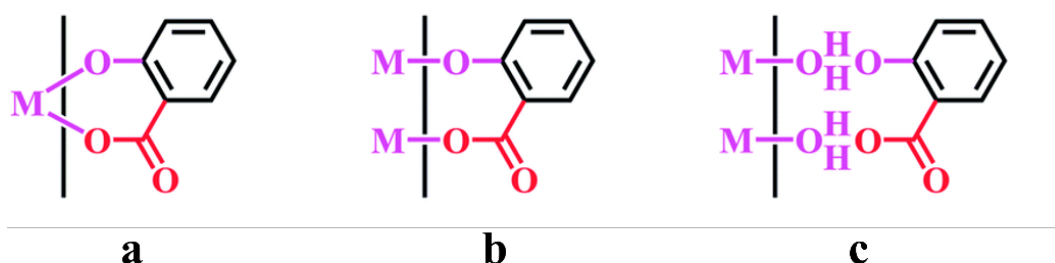


Figure 3.14 Salicylate bonding: (a) bidentate chelating bonding, (b) inner sphere bidentate bridging bonding, and (c) outer sphere bidentate bridging bonding [50].

3.3.3 Other natural surfactants

In addition to the abovementioned biosurfactants for EPD, there are many other natural surfactants already discovered or being discovered for applications in EPD. The natural surfactants from the carboxylic acid family, such as citric acid, oxalic acid, and malic acid, have been shown to be effective low molecule weight dispersants for the EPD of various oxide particles [131-134]. It was suggested that the adsorption mechanism of citric acid on oxide particles was due to a ligand exchange of surface-adsorbed hydroxyl groups with two carboxylate groups, in which two carboxylic groups of citric acid were coordinated, whereas only one group of oxalic acid was coordinated [131]. This adsorption was found

to be based on inner sphere complexes with TiO_2 nanoparticles, which is regarded as a stronger coordination because it is stable at all pH values [134]. Both citric and oxalic acid improved the suspension stability of ZrO_2 not only by enhancing the interparticle repulsion but also by providing a steric barrier to particle agglomeration, like commonly used, large molecule, polyelectrolyte dispersants [131]. This was concluded from an investigation of stable suspensions containing citric acid with a relative low zeta potential value. Higher concentrations of oxalic acid are needed to achieve similar dispersing effects to citric acid owing to its smaller effective size and smaller adsorption cross section [131].

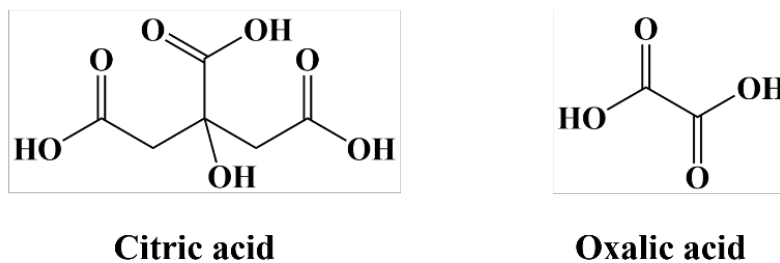


Figure 3.15 Chemical structures of citric acid and oxalic acid.

3.4 Challenges in EPD

3.4.1 Polymers

Interest in polymers is rapidly increasing, especially in biomedical applications [12], due to the advanced properties of polymer materials, such as their chemical stability, easy processability, corrosion resistance, biocompatibility, low cost, flexibility, high dielectric constant, etc. [56, 123, 124]. Compared to conventional film deposition methods, such as

thermal spraying or printing, EPD is superior because it avoids polymer degradation, is an easy operation, and has a low price point [123, 135]. EPD involves the electrophoresis of charged particles dispersed in a liquid towards the working electrode and deposited on it. However, most polymer materials are electrically neutral and cannot be deposited directly by EPD. Therefore, it is necessary to impart charge to polymer particles to make them usable for EPD. Polymer materials, such as PVDF or PTFE are chemically inert and hydrophobic, so surface modification through the adsorption of charged dispersants is challenging [56, 122]. Conventional charging agents show poor adsorption on the chemically inert surfaces of PVDF or PTFE [122]. Therefore, there is a need to develop advanced charged natural surfactants in order to create a stable polymer suspension suitable for EPD.

Another challenge for the EPD of polymer materials is to find appropriate, environmentally friendly solvents to prepare the deposition bath. Advanced engineered polymers such as PVDF and its copolymers are insoluble in water and have very limited solubility in common organic solvents. Typical solvents for dissolving PVDF are polar solvents such as dimethylformamide (DMF), dimethyl sulfoxide (DMSO), methyl ethyl ketone (MEK), and dimethylacetamide (DMAc) [136-138], which are harmful to the environment or human health. Previous investigations into the EPD of PVDF showed that to disperse PVDF well, not only were toxic solvents necessary but also a lifted stirring temperature of up to 120 °C and a stirring time up to 8 hours long [137, 138]. Therefore, it is imperative to seek environment friendly, non-toxic solvents that can effectively dissolve or suspend

chemically inert polymers like PVDF, and efficient biosurfactants for charging and dispersing them in order to widen their applications.

3.4.2 Carbon materials

Carbon materials, including CNT, graphene related materials (GRM), carbon fiber, carbon black, and diamond, have contributed to various applications due to their extraordinary electrical, thermal, and mechanical properties [25, 139]. The precondition for successful EPD of particulate materials is the preparation of a stable suspension of charged particles because the stability of the suspension affects the quality of the resulting deposits. The main challenge for successful EPD of carbon materials is their dispersal in suspension. For example, CNT is super hydrophobic and its particles often aggregate into bundles [25]. As-synthesised CNT is composed of different types with various diameters and chiral parameters. Those CNT aggregates contain different CNT types, causing heterogeneity, which has a strong negative impact on the performance of CNT products [140]. Therefore, advanced dispersants are required for CNT sorting and dispersion for the EPD of high-quality CNT films. A reported covalent modification of CNT caused damage to CNT and degradation of its properties [25]. Strategies of non-covalent modifications are based on the use of polymer-type or head-tail-type surfactants. Polymer surfactants tend to wrap around CNT bundles rather than individual CNT, which is not true dispersion of individual CNT [25]. Moreover, polymer wrapping causes insulating layers on CNT, which is detrimental to EPD. Investigations of using head-tail-type surfactants indicate that CNT has a low

dispersion efficiency, and, thus, a relatively high concentration of head-tail surfactants is necessary. However, a higher surfactant concentration induces micelle formation, which leads to depletion-induced aggregation of CNT [25].

The EPD of graphene related materials (GRM), including graphene, graphene oxide (GO), and reduced graphene oxide (rGO), is challenging because pristine graphene is hydrophobic and can not disperse easily [53]. To obtain a stable suspension in polar solvents, GO has commonly been used as a starting material in the EPD bath due to its oxygen-containing functional groups [53]. However, in-situ reduction of GO during EPD can compromise the stability of the suspension. In order to partially recover the properties of pristine graphene, GO films need to be further reduced to rGO, whether by in-situ reduction or post-EPD chemical reduction, which complicates the whole process. Various reducing agents that can be applied for the EPD of GO may introduce undesired contaminations to the final GRM films.

Because of the hydrophilic properties of GO, it can be dispersed relatively easily in aqueous media. Although water is an environmentally friendly and low-cost solvent, aqueous EPD tends to generate gases at the electrodes at high deposit voltages, creating a weak, heterogeneous, porous deposit. EPD of GRM is less common in organic solvents due to the difficulty with stabilizing a GRM suspension in many organic solvents [53]. Most of the organic solvents that can be used for the EPD of carbon materials are not environmentally friendly. Due to the lack of stability of GRM, various additives or chemical modifications

need to be applied to obtain a stable suspension. However, additives or chemical modifications can negatively affect the properties of GRM sheets [53].

Other issues with the EPD of GRM are side reactions, such aqueous electrolysis, the degradation of organic solvents, electrochemical reductions of additives, or the EPD-based reduction of GO at high deposit voltages [53].

3.4.3 Composite materials

Fabricating composite films has always been the most promising development direction in EPD technology, combining multi-component materials with various functionalities to satisfy different applications. However, the EPD of composite materials simultaneously from the same suspension is more complex than the EPD of a single material. There are several key challenges which need to be addressed to successfully create composite films through EPD.

The first requirement for composite coating via EPD is to ensure that each component has a similar charge sign and density, otherwise composite material deposition would not be possible because particles with different charging signs will deposit onto different electrodes. A low particle charge density results in porous and sponge-like deposits, and a high surface charge leads to a high particle packing density [141]. A comparable surface charge on multi-components is beneficial to obtain uniform composite coatings. Therefore,

it is important to add a suitable dispersant and it should act as an efficient co-dispersant for the co-deposition of multi-components in the suspension through EPD [120, 122].

Having a comparable deposition rate for each particle species is another requirement that must be satisfied to co-deposit homogeneous composite films. When the volume fractions of each species are relatively high, the particles deposit at a comparable rate; if the volume fractions are low, the deposition rate of each component relies on its individual electrophoretic mobility [4]. Therefore, it is critical to control the electrophoretic mobilities of each particle species.

3.5 Objectives

According to the preceding thorough review of fundamental literature, the overall objective designed for this project is to develop biomimetic strategies for the electrophoretic deposition of advanced polymers and composites containing multifunctional particles, which provide corrosion protection, enhanced mechanical strength, superparamagnetic, multiferroic, and biocompatible properties. To make the overall objective achievable, it was divided into the following short-term objectives:

1. Develop advanced biosurfactants for the dispersion, charging, and electrophoretic deposition of electrically neutral and chemically inert polymer coatings such as PTFE, PVDF, and PVDF-HFP;

2. Investigate the influence that the chemical structures of various bile acids have on the surface modification, dispersion efficiency, and deposition rate of the chemically inert polymer PVDF;
3. Develop composite organic and inorganic coatings with multifunctional properties for potential applications in corrosion protection, biomedical implants, and multiferroic materials;
4. Characterize the microstructure and multifunctional properties of films fabricated by EPD.

3.6 References

- [1] I. Zhitomirsky, "Cathodic electrodeposition of ceramic and organoceramic materials. Fundamental aspects," *Advances in colloid and interface science*, vol. 97, no. 1-3, pp. 279-317, 2002.
- [2] S. Hu, W. Li, H. Finklea, and X. Liu, "A review of electrophoretic deposition of metal oxides and its application in solid oxide fuel cells," *Advances in colloid and interface science*, vol. 276, p. 102102, 2020.
- [3] M. N. Rahaman, *Ceramic processing and sintering*. CRC press, 2017.
- [4] L. Besra and M. Liu, "A review on fundamentals and applications of electrophoretic deposition (EPD)," *Progress in Materials Science*, vol. 52, no. 1, pp. 1-61, 2007/01 2007.
- [5] B. Derjaguin and L. Landau, "Theory of the stability of strongly charged lyophobic sols and of the adhesion of strongly charged particles in solutions of electrolytes," vol. 43, no. 1-4, pp. 30-59, 1993.
- [6] E. J. W. Verwey, "Theory of the stability of lyophobic colloids," *The Journal of Physical Chemistry*, vol. 51, no. 3, pp. 631-636, 1947.

- [7] S.-J. Park and M.-K. Seo, "Intermolecular force," *Interface science and technology*, vol. 18, pp. 1-57, 2011.
- [8] P. Sennett and J. P. Olivier, "Colloidal dispersions, electrokinetic effects, and the concept of zeta potential," *Industrial & Engineering Chemistry*, vol. 57, no. 8, pp. 32-50, 1965.
- [9] K. Kiyofumi, "Structurally colored coating films with tunable iridescence fabricated via cathodic electrophoretic deposition of silica particles," (in English), *RSC advances*, vol. v. 8, no. no. 20, pp. pp. 10776-10784-2018 v.8 no.20, 0000 2018.
- [10] I. Zhitomirsky, "Electrophoretic Deposition of Organic–Inorganic Nanocomposites," *J Mater Sci*, vol. 41, pp. 8186-8195, 10/01 2006.
- [11] S. M. Doshi and E. T. Thostenson, "Thin and Flexible Carbon Nanotube-Based Pressure Sensors with Ultrawide Sensing Range," *ACS Sensors*, vol. 3, no. 7, pp. 1276-1282, 2018/07/27 2018.
- [12] R. Sikkema, K. Baker, and I. Zhitomirsky, "Electrophoretic deposition of polymers and proteins for biomedical applications," *Advances in Colloid and Interface Science*, vol. 284, p. 102272, 2020/10/01/ 2020.
- [13] E. Avcu, F. E. Baştan, H. Z. Abdullah, M. A. U. Rehman, Y. Y. Avcu, and A. R. Boccaccini, "Electrophoretic deposition of chitosan-based composite coatings for biomedical applications: A review," *Progress in Materials Science*, vol. 103, pp. 69-108, 2019.
- [14] K. Grandfield, F. Sun, M. FitzPatrick, M. Cheong, and I. Zhitomirsky, "Electrophoretic deposition of polymer-carbon nanotube–hydroxyapatite composites," *Surface and Coatings Technology*, vol. 203, no. 10, pp. 1481-1487, 2009/02/25/ 2009.
- [15] R. Sikkema, B. Keohan, and I. Zhitomirsky, "Alginate Acid Polymer-Hydroxyapatite Composites for Bone Tissue Engineering," *Polymers*, vol. 13, no. 18, 2021.
- [16] Y. Wang, I. Deen, and I. Zhitomirsky, "Electrophoretic deposition of polyacrylic acid and composite films containing nanotubes and oxide particles," *Journal of Colloid and Interface Science*, vol. 362, no. 2, pp. 367-374, 2011/10/15/ 2011.
- [17] D. Kuscer, T. Bakarič, B. Kozlevčar, and M. Kosec, "Interactions between Lead–Zirconate Titanate, Polyacrylic Acid, and Polyvinyl Butyral in Ethanol and Their

- Influence on Electrophoretic Deposition Behavior," *The Journal of Physical Chemistry B*, vol. 117, no. 6, pp. 1651-1659, 2013/02/14 2013.
- [18] T. Uchikoshi *et al.*, "Surface Modification of Complex Oxide Powder with Polyelectrolyte Layers Improving EPD Characteristics," vol. 654, pp. 255-260: Trans Tech Publ.
- [19] J. Cesarano Iii, I. A. Aksay, and A. Bleier, "Stability of aqueous α -Al₂O₃ suspensions with poly (methacrylic acid) polyelectrolyte," *Journal of the American Ceramic Society*, vol. 71, no. 4, pp. 250-255, 1988.
- [20] O. J. Rojas, P. M. Claesson, D. Muller, and R. D. Neuman, "The Effect of Salt Concentration on Adsorption of Low-Charge-Density Polyelectrolytes and Interactions between Polyelectrolyte-Coated Surfaces," *Journal of Colloid and Interface Science*, vol. 205, no. 1, pp. 77-88, 1998/09/01/ 1998.
- [21] S. Biggs and T. W. Healy, "Electrosteric stabilisation of colloidal zirconia with low-molecular-weight polyacrylic acid. An atomic force microscopy study," *Journal of the Chemical Society, Faraday Transactions*, vol. 90, no. 22, pp. 3415-3421, 1994.
- [22] P. Sarkar and P. S. Nicholson, "Electrophoretic deposition (EPD): mechanisms, kinetics, and application to ceramics," *Journal of the American Ceramic Society*, vol. 79, no. 8, pp. 1987-2002, 1996.
- [23] R. Damodaran and B. M. Moudgil, "Electrophoretic deposition of calcium phosphates from non-aqueous media," *Colloids and Surfaces A: Physicochemical and Engineering Aspects*, vol. 80, no. 2-3, pp. 191-195, 1993.
- [24] G. Wang, P. Sarkar, and P. S. Nicholson, "Influence of acidity on the electrostatic stability of alumina suspensions in ethanol," *Journal of the American Ceramic Society*, vol. 80, no. 4, pp. 965-972, 1997.
- [25] M. S. Ata, R. Poon, A. M. Syed, J. Milne, and I. Zhitomirsky, "New developments in non-covalent surface modification, dispersion and electrophoretic deposition of carbon nanotubes," *Carbon*, vol. 130, pp. 584-598, Apr 2018.
- [26] H. C. Hamaker, "Formation of a deposit by electrophoresis," *Transactions of the Faraday Society*, vol. 35, pp. 279-287, 1940.
- [27] H. C. Hamaker and E. J. W. Verwey, "Part II.—(C) Colloid stability. The role of the forces between the particles in electrodeposition and other phenomena," *Transactions of the Faraday Society*, vol. 35, pp. 180-185, 1940.

- [28] H. Koelmans and J. T. G. Overbeek, "Stability and electrophoretic deposition of suspensions in non-aqueous media," *Discussions of the Faraday Society*, vol. 18, pp. 52-63, 1954.
- [29] F. Grillon, D. Fayeulle, and M. Jeandin, "Quantitative image analysis of electrophoretic coatings," *Journal of materials science letters*, vol. 11, no. 5, pp. 272-275, 1992.
- [30] N. P. Bansal and A. R. Boccaccini, *Ceramics and composites processing methods*. John Wiley & Sons, 2012.
- [31] D. De and P. S. Nicholson, "Role of ionic depletion in deposition during electrophoretic deposition," *Journal of the American Ceramic Society*, vol. 82, no. 11, pp. 3031-3036, 1999.
- [32] L. Besra, T. Uchikoshi, T. S. Suzuki, and Y. Sakka, "Experimental verification of pH localization mechanism of particle consolidation at the electrode/solution interface and its application to pulsed DC electrophoretic deposition (EPD)," *Journal of the European Ceramic Society*, vol. 30, no. 5, pp. 1187-1193, 2010.
- [33] N. Koura, T. Tsukamoto, H. Shoji, and T. H. T. Hotta, "Preparation of various oxide films by an electrophoretic deposition method: a study of the mechanism," *Japanese journal of applied physics*, vol. 34, no. 3R, p. 1643, 1995.
- [34] B. E. Russ and J. B. Talbot, "An analysis of the binder formation in electrophoretic deposition," *Journal of the Electrochemical Society*, vol. 145, no. 4, p. 1253, 1998.
- [35] D. R. Brown and F. W. Salt, "The mechanism of electrophoretic deposition," *Journal of Applied Chemistry*, vol. 15, no. 1, pp. 40-48, 1965.
- [36] F. Bouyer and A. Foissy, "Electrophoretic deposition of silicon carbide," *Journal of the American Ceramic Society*, vol. 82, no. 8, pp. 2001-2010, 1999.
- [37] B. Ferrari and R. Moreno, "EPD kinetics: a review," *Journal of the European Ceramic Society*, vol. 30, no. 5, pp. 1069-1078, 2010.
- [38] B. Ferrari, R. Moreno, and J. A. Cuesta, "A resistivity model for electrophoretic deposition," vol. 314, pp. 175-180: Trans Tech Publ.
- [39] P. M. Biesheuvel and H. Verweij, "Theory of cast formation in electrophoretic deposition," *Journal of the American Ceramic Society*, vol. 82, no. 6, pp. 1451-1455, 1999.
- [40] R. J. Hunter, *Foundations of colloid science*. Oxford university press, 2001.

- [41] W. B. Russel, W. B. Russel, D. A. Saville, and W. R. Schowalter, *Colloidal dispersions*. Cambridge university press, 1991.
- [42] H. Ohshima, "Electrophoretic mobility of soft particles," *Colloids and Surfaces A: Physicochemical and Engineering Aspects*, vol. 103, no. 3, pp. 249-255, 1995.
- [43] M. Ammam, "Electrophoretic deposition under modulated electric fields: a review," *RSC advances*, vol. 2, no. 20, pp. 7633-7646, 2012.
- [44] B. Neirinck, O. Van der Biest, and J. Vleugels, "A current opinion on electrophoretic deposition in pulsed and alternating fields," *The Journal of Physical Chemistry B*, vol. 117, no. 6, pp. 1516-1526, 2013.
- [45] A. Chávez-Valdez and A. R. Boccaccini, "Innovations in electrophoretic deposition: Alternating current and pulsed direct current methods," *Electrochimica Acta*, vol. 65, pp. 70-89, 2012.
- [46] O. O. Van der Biest and L. J. Vandeperre, "Electrophoretic deposition of materials," *Annual Review of Materials Research*, vol. 29, p. 327, 1999.
- [47] S. Awasthi, S. K. Pandey, C. P. Pandey, and K. Balani, "Progress in electrochemical and electrophoretic deposition of nickel with carbonaceous allotropes: A review," *Advanced Materials Interfaces*, vol. 7, no. 1, p. 1901096, 2020.
- [48] A. R. Boccaccini and I. Zhitomirsky, "Application of electrophoretic and electrolytic deposition techniques in ceramics processing," *Current Opinion in Solid State and Materials Science*, vol. 6, no. 3, pp. 251-260, 2002.
- [49] P. Sarkar, D. De, and H. Rho, "Synthesis and microstructural manipulation of ceramics by electrophoretic deposition," *Journal of Materials Science*, vol. 39, no. 3, pp. 819-823, 2004.
- [50] M. S. Ata, Y. Liu, and I. Zhitomirsky, "A review of new methods of surface chemical modification, dispersion and electrophoretic deposition of metal oxide particles," *Rsc Advances*, vol. 4, no. 43, pp. 22716-22732, 2014.
- [51] A. R. Boccaccini, J. Cho, J. A. Roether, B. J. C. Thomas, E. J. Minay, and M. S. P. Shaffer, "Electrophoretic deposition of carbon nanotubes," *Carbon*, vol. 44, no. 15, pp. 3149-3160, 2006.
- [52] A. Chavez-Valdez, M. S. P. Shaffer, and A. R. Boccaccini, "Applications of graphene electrophoretic deposition. A review," *The Journal of Physical Chemistry B*, vol. 117, no. 6, pp. 1502-1515, 2013.

- [53] M. Diba, D. W. H. Fam, A. R. Boccaccini, and M. S. P. Shaffer, "Electrophoretic deposition of graphene-related materials: A review of the fundamentals," *Progress in Materials Science*, vol. 82, pp. 83-117, 2016.
- [54] M. Atiq Ur Rehman, Q. Chen, A. Braem, M. S. P. Shaffer, and A. R. Boccaccini, "Electrophoretic deposition of carbon nanotubes: recent progress and remaining challenges," *International Materials Reviews*, vol. 66, no. 8, pp. 533-562, 2021.
- [55] D. Zhitomirsky, J. A. Roether, A. R. Boccaccini, and I. Zhitomirsky, "Electrophoretic deposition of bioactive glass/polymer composite coatings with and without HA nanoparticle inclusions for biomedical applications," *Journal of Materials Processing Technology*, vol. 209, no. 4, pp. 1853-1860, 2009.
- [56] Q. Zhao, S. Veldhuis, R. Mathews, and I. Zhitomirsky, "Influence of chemical structure of bile acid dispersants on electrophoretic deposition of poly (vinylidene fluoride) and composites," *Colloids and Surfaces A: Physicochemical and Engineering Aspects*, vol. 627, p. 127181, 2021.
- [57] Y. Wang, X. Pang, and I. Zhitomirsky, "Electrophoretic deposition of chiral polymers and composites," *Colloids and Surfaces B: Biointerfaces*, vol. 87, no. 2, pp. 505-509, 2011.
- [58] A. R. Boccaccini, S. Keim, R. Ma, Y. Li, and I. Zhitomirsky, "Electrophoretic deposition of biomaterials," *Journal of the Royal Society Interface*, vol. 7, no. suppl_5, pp. S581-S613, 2010.
- [59] S. Bakhshandeh and S. A. Yavari, "Electrophoretic deposition: a versatile tool against biomaterial associated infections," *Journal of Materials Chemistry B*, vol. 6, no. 8, pp. 1128-1148, 2018.
- [60] B. Priyadarshini, M. Rama, Chetan, and U. Vijayalakshmi, "Bioactive coating as a surface modification technique for biocompatible metallic implants: a review," *Journal of Asian Ceramic Societies*, vol. 7, no. 4, pp. 397-406, 2019.
- [61] A. R. Boccaccini, C. Kaya, and K. K. Chawla, "Use of electrophoretic deposition in the processing of fibre reinforced ceramic and glass matrix composites: a review," *Composites Part A: Applied science and manufacturing*, vol. 32, no. 8, pp. 997-1006, 2001.
- [62] S. A. Batool, A. Wadood, S. W. Hussain, M. Yasir, and M. A. Ur Rehman, "A Brief Insight to the Electrophoretic Deposition of PEEK-, Chitosan-, Gelatin-, and Zein-Based Composite Coatings for Biomedical Applications: Recent Developments and Challenges," *Surfaces*, vol. 4, no. 3, pp. 205-239, 2021.

- [63] Y. Ma, J. Han, M. Wang, X. Chen, and S. Jia, "Electrophoretic deposition of graphene-based materials: A review of materials and their applications," *Journal of Materiomics*, vol. 4, no. 2, pp. 108-120, 2018.
- [64] G. Anné, K. Vanmeensel, J. Vleugels, and O. Van der Biest, "Electrophoretic deposition as a novel near net shaping technique for functionally graded biomaterials," vol. 492, pp. 213-218: Trans Tech Publ.
- [65] Y. Chen, X. Zhang, P. Yu, and Y. Ma, "Electrophoretic deposition of graphene nanosheets on nickel foams for electrochemical capacitors," *Journal of Power Sources*, vol. 195, no. 9, pp. 3031-3035, 2010/05/01/ 2010.
- [66] J. Ma, C. Wang, and K. W. Peng, "Electrophoretic deposition of porous hydroxyapatite scaffold," *Biomaterials*, vol. 24, no. 20, pp. 3505-3510, 2003.
- [67] Y. Li *et al.*, "Synthesis of hierarchical bio-inspired pine needle-shaped MnO₂/CNTs/carbon cloth composite as highly cycling stable symmetrical supercapacitor," *Int. J. Electrochem. Sci*, vol. 12, pp. 4733-4744, 2017.
- [68] I. Zhitomirsky, "Electrophoretic hydroxyapatite coatings and fibers," *Materials Letters*, vol. 42, no. 4, pp. 262-271, 2000.
- [69] J. H. Dickerson and A. R. Boccaccini, *Electrophoretic deposition of nanomaterials*. Springer, 2011.
- [70] P. Amrollahi, J. S. Krasinski, R. Vaidyanathan, L. Tayebi, and D. Vashaee, "Electrophoretic deposition (EPD): Fundamentals and applications from nano-to microscale structures," in *Handbook of nanoelectrochemistry*: Springer, 2016, pp. 561-591.
- [71] R. S. Hyam, K. M. Subhedar, and S. H. Pawar, "Effect of particle size distribution and zeta potential on the electrophoretic deposition of boron films," *Colloids and Surfaces A: Physicochemical and Engineering Aspects*, vol. 315, no. 1-3, pp. 61-65, 2008.
- [72] S. A. Guelcher, Y. Solomentsev, and J. L. Anderson, "Aggregation of pairs of particles on electrodes during electrophoretic deposition," *Powder technology*, vol. 110, no. 1-2, pp. 90-97, 2000.
- [73] N. Sato, M. Kawachi, K. Noto, N. Yoshimoto, and M. Yoshizawa, "Effect of particle size reduction on crack formation in electrophoretically deposited YBCO films," *Physica C: Superconductivity*, vol. 357, pp. 1019-1022, 2001.

- [74] C. Ji, I. P. Shapiro, and P. Xiao, "Fabrication of yttria-stabilized-zirconia coatings using electrophoretic deposition: Effects of agglomerate size distribution on particle packing," *Journal of the European Ceramic Society*, vol. 29, no. 15, pp. 3167-3175, 2009.
- [75] S. Seuss and A. R. Boccaccini, "Electrophoretic deposition of biological macromolecules, drugs, and cells," *Biomacromolecules*, vol. 14, no. 10, pp. 3355-3369, 2013.
- [76] K. Balagangadharan, S. Dhivya, and N. Selvamurugan, "Chitosan based nanofibers in bone tissue engineering," *International journal of biological macromolecules*, vol. 104, pp. 1372-1382, 2017.
- [77] M. Cheong and I. Zhitomirsky, "Electrodeposition of alginic acid and composite films," *Colloids and Surfaces A: Physicochemical and Engineering Aspects*, vol. 328, no. 1-3, pp. 73-78, 2008.
- [78] Y. Cheng, X. Luo, J. Betz, G. F. Payne, W. E. Bentley, and G. W. Rubloff, "Mechanism of anodic electrodeposition of calcium alginate," *Soft Matter*, vol. 7, no. 12, pp. 5677-5684, 2011.
- [79] F. Sun and I. Zhitomirsky, "Electrodeposition of hyaluronic acid and composite films," *Surface Engineering*, vol. 25, no. 8, pp. 621-627, 2009.
- [80] R. Ma, Y. Li, and I. Zhitomirsky, "Electrophoretic deposition of hyaluronic acid and composite films for biomedical applications," *JOM*, vol. 62, no. 6, pp. 72-75, 2010.
- [81] B. Neirinck, J. Fransaer, J. Vleugels, and O. Van der Biest, "Aqueous electrophoretic deposition at high electric fields," vol. 412, pp. 33-38: Trans Tech Publ.
- [82] M. Marín-Suárez *et al.*, "Electrophoretic deposition as a new approach to produce optical sensing films adaptable to microdevices," *Nanoscale*, vol. 6, no. 1, pp. 263-271, 2014.
- [83] S. Miyajima, S. Nagamatsu, S. S. Pandey, S. Hayase, K. Kaneto, and W. Takashima, "Electrophoretic deposition onto an insulator for thin film preparation toward electronic device fabrication," *Applied Physics Letters*, vol. 101, no. 19, p. 193305, 2012.
- [84] M. Farrokhi-Rad, "Electrophoretic deposition of hydroxyapatite nanoparticles in different alcohols: effect of Tris (tris (hydroxymethyl) aminomethane) as a dispersant," *Ceramics International*, vol. 42, no. 2, pp. 3361-3371, 2016.

- [85] M. Farrokhi-Rad and M. Ghorbani, "Electrophoretic deposition of titania nanoparticles in different alcohols: kinetics of deposition," *Journal of the American Ceramic Society*, vol. 94, no. 8, pp. 2354-2361, 2011.
- [86] M. Shan, X. Mao, J. Zhang, and S. Wang, "Electrophoretic shaping of sub-micron alumina in ethanol," *Ceramics International*, vol. 35, no. 5, pp. 1855-1861, 2009.
- [87] M. Farrokhi-Rad and T. Shahrabi, "Effect of suspension medium on the electrophoretic deposition of hydroxyapatite nanoparticles and properties of obtained coatings," *Ceramics International*, vol. 40, no. 2, pp. 3031-3039, 2014.
- [88] Z. Wang, J. Shemilt, and P. Xiao, "Fabrication of ceramic composite coatings using electrophoretic deposition, reaction bonding and low temperature sintering," *Journal of the European Ceramic Society*, vol. 22, no. 2, pp. 183-189, 2002.
- [89] H. Kang, Y. Park, Y.-K. Hong, S. Yoon, M.-H. Lee, and D.-H. Ha, "Solvent-induced charge formation and electrophoretic deposition of colloidal iron oxide nanoparticles," *Surfaces and Interfaces*, vol. 22, p. 100815, 2021.
- [90] J. A. Lewis, "Binder removal from ceramics," *Annual Review of Materials Science*, vol. 27, no. 1, pp. 147-173, 1997.
- [91] D. Kuscer, T. Bakaric, B. Kozlevčar, and M. Kosec, "Interactions between Lead–Zirconate Titanate, Polyacrylic Acid, and Polyvinyl Butyral in Ethanol and Their Influence on Electrophoretic Deposition Behavior," *The Journal of Physical Chemistry B*, vol. 117, no. 6, pp. 1651-1659, 2013.
- [92] H. Negishi, T. Yamaki, and A. Endo, "Preparation and characterization of mesoporous silica–polyvinyl butyral hybrid coatings by electrophoretic deposition," *Microporous and Mesoporous Materials*, vol. 292, p. 109710, 2020.
- [93] D. G. Gu, G. R. Li, Z. J. Xu, L. Y. Zheng, A. L. Ding, and Q. R. Yin, "Electrophoretic deposition of SrBi₄Ti₄O₁₅ thick films on Al₂O₃ substrate," *Journal of electroceramics*, vol. 21, no. 1, pp. 532-535, 2008.
- [94] C. Zhang *et al.*, "Antibacterial-functionalized Ag loaded-hydroxyapatite (HAp) coatings fabricated by electrophoretic deposition (EPD) process," *Materials Letters*, vol. 297, p. 129955, 2021.
- [95] C. Zhang, T. Uchikoshi, T. Kitabatake, Y. Sakka, and N. Hirosaki, "Surface modification of Ca- α -SiAlON: Eu²⁺ phosphor particles by SiO₂ coating and fabrication of its deposit by electrophoretic deposition (EPD) process," *Applied surface science*, vol. 280, pp. 229-234, 2013.

- [96] B. E. Russ and J. B. Talbot, "A study of the adhesion of electrophoretically deposited phosphors," *Journal of the Electrochemical Society*, vol. 145, no. 4, p. 1245, 1998.
- [97] G. F. Chen and J. L. Li, "Suspension development for electrophoretic deposition of mullite coating," vol. 546, pp. 1703-1706: Trans Tech Publ.
- [98] N. Wang, H. Lin, J. Li, X. Yang, and B. Chi, "Electrophoretic deposition and optical property of titania nanotubes films," *Thin Solid Films*, vol. 496, no. 2, pp. 649-652, 2006.
- [99] K. Katagiri, K. Uemura, R. Uesugi, K. Inumaru, T. Seki, and Y. Takeoka, "Structurally colored coating films with tunable iridescence fabricated via cathodic electrophoretic deposition of silica particles," *RSC advances*, vol. 8, no. 20, pp. 10776-10784, 2018.
- [100] Z. Yang, G. Chen, Y. Huang, Q. Liang, and H. Shen, "Development of bright and low angle dependent structural color coatings via electrophoretic deposition with variable voltage," *Surfaces and Interfaces*, vol. 24, p. 101045, 2021.
- [101] Q. Chen, S. Cabanas-Polo, O.-M. Goudouri, and A. R. Boccaccini, "Electrophoretic co-deposition of polyvinyl alcohol (PVA) reinforced alginate–Bioglass® composite coating on stainless steel: Mechanical properties and in-vitro bioactivity assessment," *Materials Science and Engineering: C*, vol. 40, pp. 55-64, 2014.
- [102] J. A. V. Costa, H. Treichel, L. O. Santos, and V. G. Martins, "Chapter 16 - Solid-State Fermentation for the Production of Biosurfactants and Their Applications," in *Current Developments in Biotechnology and Bioengineering*, A. Pandey, C. Larroche, and C. R. Soccol, Eds.: Elsevier, 2018, pp. 357-372.
- [103] W. Xi, Y. Ping, and M. A. Alikhani, "A Review on Biosurfactant Applications in the Petroleum Industry," *International Journal of Chemical Engineering*, vol. 2021, 2021.
- [104] M. A. Zahed, M. A. Matinvafa, A. Azari, and L. Mohajeri, "Biosurfactant, a green and effective solution for bioremediation of petroleum hydrocarbons in the aquatic environment," *Discover Water*, vol. 2, no. 1, pp. 1-20, 2022.
- [105] C. Nikolova and T. Gutierrez, "Biosurfactants and their applications in the oil and gas industry: current state of knowledge and future perspectives," *Frontiers in Bioengineering and Biotechnology*, vol. 9, p. 626639, 2021.
- [106] B. Shibulal, S. N. Al-Bahry, Y. M. Al-Wahaibi, A. E. Elshafie, A. S. Al-Bemani, and S. J. Joshi, "Microbial enhanced heavy oil recovery by the aid of inhabitant

- spore-forming bacteria: an insight review," *The Scientific World Journal*, vol. 2014, 2014.
- [107] X. Liu, S. Veldhuis, R. Mathews, and I. Zhitomirsky, "Carbenoxolone as a Multifunctional Vehicle for Electrodeposition of Materials," *Applied Sciences*, vol. 11, no. 19, 2021.
- [108] K. Baker, R. Sikkema, W. Liang, and I. Zhitomirsky, "Multifunctional Properties of Commercial Bile Salts for Advanced Materials Engineering," *Advanced Engineering Materials*, vol. 23, no. 5, p. 2001261, 2021.
- [109] J. Singh, R. Metrani, S. R. Shivanagoudra, G. K. Jayaprakasha, and B. S. Patil, "Review on bile acids: Effects of the gut microbiome, interactions with dietary fiber, and alterations in the bioaccessibility of bioactive compounds," *Journal of agricultural and food chemistry*, vol. 67, no. 33, pp. 9124-9138, 2019.
- [110] A. Fini, A. Roda, R. Fugazza, and B. Grigolo, "Chemical properties of bile acids: III. Bile acid structure and solubility in water," *Journal of solution chemistry*, vol. 14, no. 8, pp. 595-603, 1985.
- [111] A. Roda and A. Fini, "Effect of nuclear hydroxy substituents on aqueous solubility and acidic strength of bile acids," *Hepatology*, vol. 4, no. S2, pp. 72S-76S, 1984.
- [112] N. A. Malik, "Solubilization and interaction studies of bile salts with surfactants and drugs: a review," *Applied biochemistry and biotechnology*, vol. 179, no. 2, pp. 179-201, 2016.
- [113] B. R. Simonović and M. Momirović, "Determination of critical micelle concentration of bile acid salts by micro-calorimetric titration," *Microchimica Acta*, vol. 127, no. 1, pp. 101-104, 1997.
- [114] M. C. Carey, J. C. Montet, M. C. Phillips, M. J. Armstrong, and N. A. Mazer, "Thermodynamic and molecular basis for dissimilar cholesterol-solubilizing capacities by micellar solutions of bile salts: cases of sodium chenodeoxycholate and sodium ursodeoxycholate and their glycine and taurine conjugates," *Biochemistry*, vol. 20, no. 12, pp. 3637-3648, 1981.
- [115] K. Matsuoka and A. Yamamoto, "Study on micelle formation of bile salt using nuclear magnetic resonance spectroscopy," *Journal of Oleo Science*, vol. 66, no. 10, pp. 1129-1137, 2017.
- [116] A. Clifford and I. Zhitomirsky, "Aqueous electrophoretic deposition of drugs using bile acids as solubilizing, charging and film-forming agents," *Materials Letters*, vol. 227, pp. 1-4, 2018/09/15/ 2018.

- [117] X. Liu, Q. Zhao, S. Veldhuis, and I. Zhitomirsky, "Cholic acid is a versatile coating-forming dispersant for electrophoretic deposition of diamond, graphene, carbon dots and polytetrafluoroethylene," *Surface and Coatings Technology*, vol. 384, p. 125304, 2020/02/25/ 2020.
- [118] M. S. Ata and I. Zhitomirsky, "Electrochemical deposition of composites using deoxycholic acid dispersant," *Materials and Manufacturing Processes*, vol. 31, no. 1, pp. 67-73, 2016.
- [119] M. S. Ata and I. Zhitomirsky, "Colloidal methods for the fabrication of carbon nanotube–manganese dioxide and carbon nanotube–polypyrrole composites using bile acids," *Journal of Colloid and Interface Science*, vol. 454, pp. 27-34, 2015/09/15/ 2015.
- [120] Q. Zhao, X. Liu, S. Veldhuis, and I. Zhitomirsky, "Sodium deoxycholate as a versatile dispersing and coating-forming agent: A new facet of electrophoretic deposition technology," *Colloids and Surfaces A: Physicochemical and Engineering Aspects*, vol. 588, p. 124382, 2020.
- [121] M. C. Carey, "Bile acids and bile salts: ionization and solubility properties," *Hepatology*, vol. 4, no. S2, pp. 66S-71S, 1984.
- [122] Q. Zhao, X. Liu, and I. Zhitomirsky, "Electrophoretic deposition of materials using lithocholic acid as a dispersant," *Materials Letters*, vol. 275, p. 128129, 2020.
- [123] Q. Zhao, X. Liu, S. Veldhuis, and I. Zhitomirsky, "Versatile Strategy for Electrophoretic Deposition of Polyvinylidene Fluoride-Metal Oxide Nanocomposites," *Materials*, vol. 14, no. 24, p. 7902, 2021.
- [124] Q. Zhao and I. Zhitomirsky, "Biomimetic strategy for electrophoretic deposition of composite ferroelectric poly (vinylidene, fluoride-co-hexafluoropropylene)-ferrimagnetic NiFe₂O₄ films," *Colloids and Surfaces A: Physicochemical and Engineering Aspects*, p. 129743, 2022.
- [125] B. P. Lee, P. B. Messersmith, J. N. Israelachvili, and J. H. Waite, "Mussel-inspired adhesives and coatings," *Annual review of materials research*, vol. 41, p. 99, 2011.
- [126] M. S. Ata and I. Zhitomirsky, "Electrophoretic nanotechnology of ceramic films," *Advances in Applied Ceramics*, vol. 111, no. 5-6, pp. 345-350, 2012.
- [127] K. Wu, Y. Wang, and I. Zhitomirsky, "Electrophoretic deposition of TiO₂ and composite TiO₂–MnO₂ films using benzoic acid and phenolic molecules as charging additives," *Journal of colloid and interface science*, vol. 352, no. 2, pp. 371-378, 2010.

- [128] Y. Wang and I. Zhitomirsky, "Effect of phenolic molecules on electrophoretic deposition of manganese dioxide–carbon nanotube nanocomposites," *Colloids and Surfaces A: Physicochemical and Engineering Aspects*, vol. 369, no. 1-3, pp. 211-217, 2010.
- [129] Y. Sun, Y. Wang, and I. Zhitomirsky, "Dispersing agents for electrophoretic deposition of TiO₂ and TiO₂–carbon nanotube composites," *Colloids and Surfaces A: Physicochemical and Engineering Aspects*, vol. 418, pp. 131-138, 2013.
- [130] M. S. Ata and I. Zhitomirsky, "Preparation of MnO₂ and composites for ultracapacitors," *Materials and manufacturing processes*, vol. 28, no. 9, pp. 1014-1018, 2013.
- [131] D. Hanaor, M. Michelazzi, C. Leonelli, and C. C. Sorrell, "The effects of carboxylic acids on the aqueous dispersion and electrophoretic deposition of ZrO₂," *Journal of the European Ceramic Society*, vol. 32, no. 1, pp. 235-244, 2012.
- [132] P. C. Hidber, T. J. Graule, and L. J. Gauckler, "Influence of the dispersant structure on properties of electrostatically stabilized aqueous alumina suspensions," *Journal of the European Ceramic Society*, vol. 17, no. 2-3, pp. 239-249, 1997.
- [133] M. F. De Riccardis, D. Carbone, and A. Rizzo, "A novel method for preparing and characterizing alcoholic EPD suspensions," *Journal of Colloid and Interface Science*, vol. 307, no. 1, pp. 109-115, 2007.
- [134] I. A. Mudunkotuwa and V. H. Grassian, "Citric acid adsorption on TiO₂ nanoparticles in aqueous suspensions at acidic and circumneutral pH: surface coverage, surface speciation, and its impact on nanoparticle–nanoparticle interactions," *Journal of the American Chemical Society*, vol. 132, no. 42, pp. 14986-14994, 2010.
- [135] M. F. De Riccardis, V. Martina, and D. Carbone, "Study of polymer particles suspensions for electrophoretic deposition," *The Journal of Physical Chemistry B*, vol. 117, no. 6, pp. 1592-1599, 2013.
- [136] M. Li *et al.*, "Controlling the microstructure of poly (vinylidene-fluoride)(PVDF) thin films for microelectronics," *Journal of Materials Chemistry C*, vol. 1, no. 46, pp. 7695-7702, 2013.
- [137] K. T. Lau, M. S. M. Suan, M. Zaimi, J. Abd Razak, M. A. Azam, and N. Mohamad, "Microstructure and Phase of Poly (Vinyliden Fluoride) Films by Electrophoretic Deposition: Effect of Polymer Dispersion's Stirring Conditions," *Journal of Advanced Manufacturing Technology (JAMT)*, vol. 10, no. 2, pp. 57-66, 2016.

- [138] K. T. Lau *et al.*, "Electrophoretic deposition and heat treatment of steel-supported PVDF-graphite composite film," vol. 761, pp. 412-416: Trans Tech Publ.
- [139] A. R. Boccaccini, J. Cho, T. Subhani, C. Kaya, and F. Kaya, "Electrophoretic deposition of carbon nanotube–ceramic nanocomposites," *Journal of the European Ceramic Society*, vol. 30, no. 5, pp. 1115-1129, 2010.
- [140] D. Janas, "Towards monochiral carbon nanotubes: A review of progress in the sorting of single-walled carbon nanotubes," *Materials Chemistry Frontiers*, vol. 2, no. 1, pp. 36-63, 2018.
- [141] H. G. Krüger, A. Knote, U. Schindler, H. Kern, and A. R. Boccaccini, "Composite ceramic-metal coatings by means of combined electrophoretic deposition and galvanic methods," *Journal of materials science*, vol. 39, no. 3, pp. 839-844, 2004.

Chapter 4 DChNa for EPD of Composite Coatings

This chapter is reproduced from **Q. Zhao, X. Liu, S. Veldhuis, I. Zhitomirsky**, *Sodium deoxycholate as a versatile dispersing and coating-forming agent: A new facet of electrophoretic deposition technology*, *Colloids and Surfaces A: Physicochemical and Engineering Aspects*, Volume 588, 2020, 124382 (<https://doi.org/10.1016/j.colsurfa.2019.124382>), with permission from Copyright © 2019 Elsevier B.V. The author of this thesis is the first author and the main contributor of this publication, including conceiving the initial ideas, development of approach and methodology, carrying out experiments, analysis of data and preparation of the manuscript.

4.1 Abstract

The unique dispersion power of bile acid salts offers a tremendous potential for the development of new biomimetic strategies for colloidal processing of materials. This paper reports the feasibility of electrophoretic deposition (EPD) of polytetrafluoroethylene (PTFE), diamond and carbon dots (CDs) using commercial sodium deoxycholate (DChNa) as a charged dispersant and coating-forming agent. The amphiphilic DChNa structure is beneficial for adsorption of this molecule on chemically inert hydrophobic surfaces and particle dispersion. The electrochemical film formation mechanism is based on the electrogenerated acid formation, protonation and charge neutralization of anionic DCh⁻ species. SEM and FTIR are used for the analysis of film morphology and composition.

Potentiodynamic and impedance spectroscopy studies show that PTFE films deposited by EPD provide protection of steel from corrosion. The use of DChNa allows the fabrication of composites by combined electrochemical strategies. Diamond-polypyrrole (PPy) films are prepared by an EPD-electropolymerization method. DChNa is a versatile co-dispersant for co-deposition of different materials by EPD or combined electrochemical methods.

4.2 Introduction

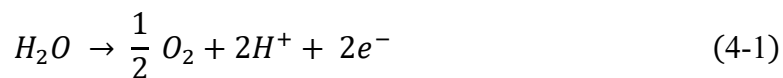
Electrophoretic deposition of materials (EPD) is increasingly being used for the manufacturing of advanced films for electronic, energy generation and storage, photovoltaic, biomedical, corrosion protection and sensor applications [1-5]. Especially important are EPD applications in the nanotechnology of composite materials. EPD involves electromigration of charged molecules or particles toward the electrode surface and film deposition [6-9]. One of the challenges in the development of EPD technology is the particle dispersion and charging [10-12]. The key to achieving efficient particle dispersion is the strong adsorption of a dispersant on the particle [13, 14]. The EPD of multicomponent composite materials requires the use of co-dispersants for individual particles [6]. Another challenge of EPD is to overcome particle dispersive forces at the electrode surface and obtain continuous adherent films.

Materials innovations in dispersants and coating-forming agents are expected to enable significant advances in the EPD technology. Recently, interest has been generated in application of commercial bile acid salts (BSs) for dispersion and EPD of materials. It is

known that BSs allow for efficient dispersion of various biomolecules [15] due to their unique steroid-like structure [15-17], which facilitates adsorption on materials. BSs molecules were used for the dispersion of carbon nanotubes (CNT) [18-23]. It was demonstrated that such molecules allowed enhanced CNT dispersion, as compared to other surfactants [24]. BSs have generated interest for drug delivery technologies [25]. It was found [26-30] that BSs facilitated solubilization of various promising drug molecules in water and allowed the development of new drug delivery techniques [15, 31-33].

Deoxycholic acid (DChH) is one of the primary bile acids. Sodium deoxycholate (DChNa) was found to be an efficient dispersant for CNT [34] and a structure-directing agent for the formation of ordered structures. The use of DChNa as a dispersant allowed CNT sorting by length for application in thin film transistors [35]. The non-covalent graphene functionalization with adsorbed DChNa facilitated the formation of polymer-graphene composites, containing well-dispersed graphene particles in the polymer matrix [36]. DChNa exhibits promising gel-forming properties for various biomedical applications [37, 38].

Recently DChH [39] films were formed by EPD from DChNa solutions. The EPD strategy was based on the anaphoresis of DCh^- and the local pH decrease at anode, which resulted from the following reaction:



The DCh^- protonation of discharge resulted in the deposition of water insoluble $DChH$ films:



The use of $DChNa$ as a dispersant and coating-forming agent facilitated the EPD of CNT [21, 39]. Moreover, $DChNa$ was used for the solubilization of drug molecules and their EPD [40]. Previous investigations indicated that $DChNa$ can potentially be used to solve different problems related to EPD of various functional materials.

The objective of this work was the EPD of polytetrafluoroethylene (PTFE), diamond and carbon dots (CDs) using $DChNa$. We presented experimental evidence that PTFE films can be formed by anodic EPD and such films provided protection of steel from corrosion. We demonstrated that $DChNa$ is a versatile charged dispersant and coating-forming agent for EPD and co-EPD of carbon materials, such as diamond and CDs. The experimental results described below indicated that $DChNa$ can be used for the electrodeposition of composite coatings by a combined EPD-electropolymerization method. This investigation opens a new and unexplored route for the electrodeposition of composites by EPD or combined electrochemical methods.

4.3 Experimental Procedures

$DChNa$, submicrometric polytetrafluoroethylene (PTFE) and diamond particles, pyrrole (Py) and Tiron (Aldrich) were used. Carbon dots (CDs) were synthesized according to the

procedure, described in the literature [41]. EPD of PTFE films was carried out from PTFE particle suspensions in an ethanol-water medium (40 % ethanol), containing dissolved DChNa. The use of ethanol facilitated PTFE dispersion. Diamonds and CDs were dispersed in aqueous DChNa solutions for film formation by EPD. Anodic electropolymerization of polypyrrole (PPy) was performed from 0.1 M Py solutions, containing 0.01 M Tiron. Diamond particles were dispersed using DChNa and added to the electropolymerization bath for the manufacturing of composites.

The EPD cell contained a substrate (type 304 stainless steel, dimensions $25 \times 30 \times 0.1 \text{ mm}^3$) and a Pt counter electrode ($25 \times 30 \times 0.1 \text{ mm}^3$). The electrode separation was 15 mm. Electrodeposition was performed at cell voltages of 7-50 V. PTFE coatings were thermally treated at $350 \text{ }^\circ\text{C}$ for 1 h.

Electrochemical testing of the PTFE coatings was performed using a PARSTAT 2273 potentiostat in 3% NaCl solutions. A 3-electrode cell contained a steel substrate working electrode, Pt counter electrode and a saturated calomel electrode (SCE) as a reference electrode. Potentiodynamic investigations were carried out at a rate of $1 \text{ mV} \cdot \text{s}^{-1}$. Electrochemical impedance spectroscopy (EIS) studies were performed at frequencies 10 mHz-10 kHz and AC voltage of 5 mV. Film porosity was estimated from the electrochemical testing data by the method described in the literature [42, 43] and a ZSimpWin software (Ametek). Zeta potential studies were performed by the electrophoretic transport method [44], which allows zeta potential measurements at the same conditions as conditions of the EPD experiments. Scanning electron microscopy

(SEM) investigations were performed using JEOL JSM-7000F microscope. FTIR data was obtained using a Bruker Vertex 70 spectrometer. The coating adhesion strength was measured according to the ASTM D3359-17 standard. The electrical conductivity of PPy films was measured by a conventional four-probe method.

4.4 Results and Discussion

Figure 4.1 shows the chemical structure of DChNa, which contains different functional groups. The steroid amphiphilic DChNa structure contains convex hydrophobic and concave hydrophilic sides [21]. The negative charge of the dissociated DChNa molecules in solutions is attributed to their COO^- groups. The hydrophobic side of DChNa facilitates its adsorption on hydrophobic surfaces, whereas the hydrophilic side, containing OH and COO^- groups, governs the dissolution and electrokinetic behavior of DChNa in water.

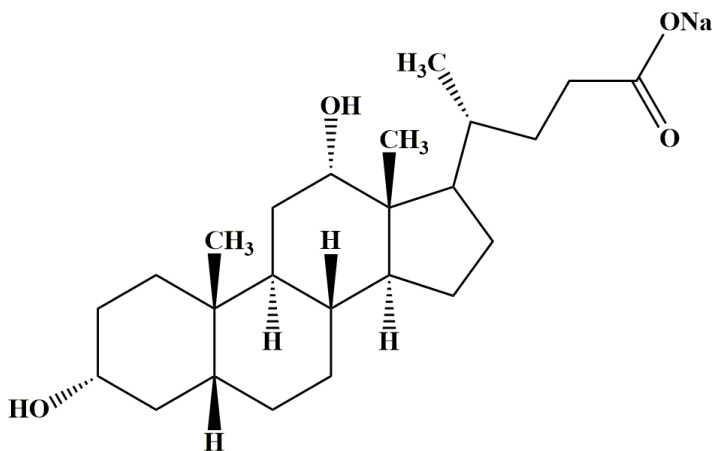


Figure 4.1 Chemical structure of DChNa.

In this investigation we found that DChNa can be used for dispersion of PTFE, diamond and quantum dots (QDs). Table S4.1 and Table S4.2 in the Supplementary information present data on zeta potentials of particles and conductivities of suspensions used for EPD. Zeta potential measurements showed that the particles were negatively charged due to DChNa adsorption. The suspensions prepared without DChNa showed sedimentation during the 3-5 min. The addition of DChNa resulted in improved suspension stability. The bath compositions for EPD were optimized and testing results were presented for optimized conditions, specified in figure captions and supplementary information. The suspensions of diamond, PTFE and QDs, prepared using DChNa were stable for 2, 5 and 7 days, respectively.

Figure 4.2 shows the PTFE film microstructure at different magnifications. EPD allowed the fabrication of relatively dense crack-free films, containing submicrometric PTFE particles at a deposition rate of $12 \mu\text{g}\cdot\text{cm}^{-2}\cdot\text{s}^{-1}$. However, the films showed small pores with a typical size of 100-350 nm. Such pores resulted from PTFE packing or O_2 evolution at the electrode surface. The deposition of PTFE was confirmed by the analysis of the FTIR spectra. The FTIR spectrum (Figure 4.3) of as-received PTFE revealed strong absorptions at 1150 and 1204 cm^{-1} . The absorption at 1204 cm^{-1} resulted from symmetric C-F₂ vibration [45, 46]. The asymmetric C-F₂ and C-C vibrations [45, 46] resulted in the absorption at 1150 cm^{-2} . Such absorptions were also observed in the FTIR data of the deposited material and indicated that PTFE was deposited by EPD. The annealing of the PTFE films above the melting temperature facilitated the formation of denser films (Figure

4.4A). However, the SEM images of the film surface at a higher magnification (Figure 4.4B) revealed nanopores. The adhesion strength of the sintered PTFE film, measured according to ASTM D3359-17 standard, corresponded to 5B classification. The SEM studies of film cross section indicated that film thickness above 10 μm was achieved at the deposition duration of 5 min (Supplementary information, Figure S4.1).

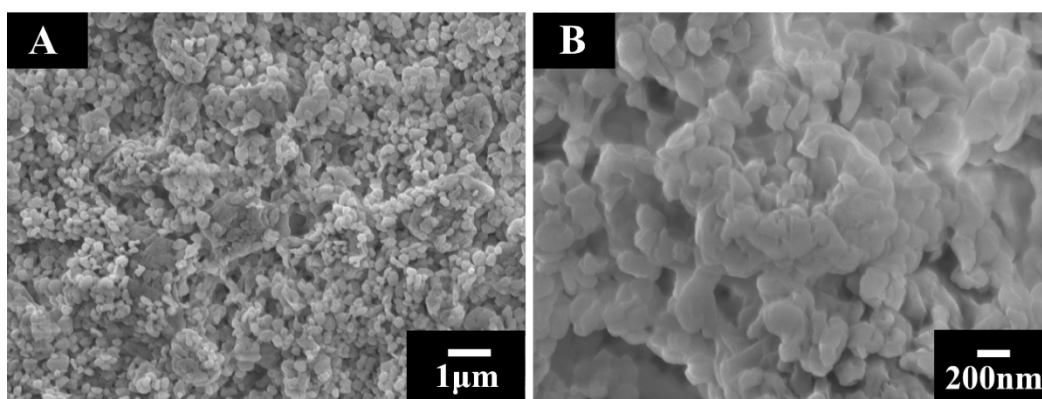


Figure 4.2 SEM images of films, prepared from 1 $\text{g}\cdot\text{L}^{-1}$ DChNa solutions, containing 5 $\text{g}\cdot\text{L}^{-1}$ PTFE at a deposition voltage of 50 V.

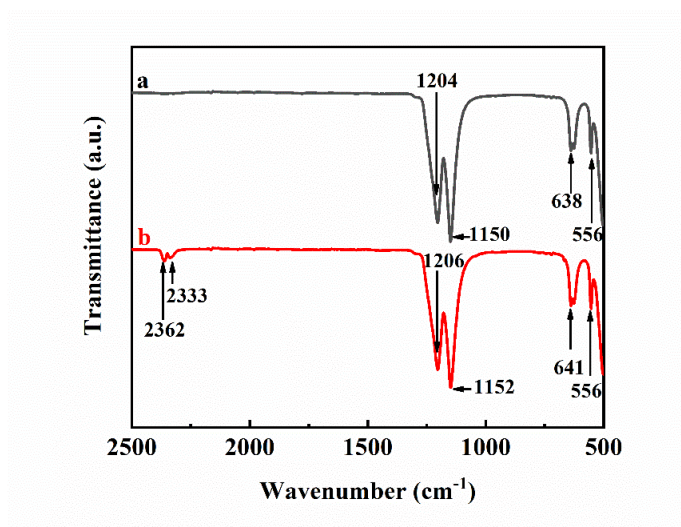


Figure 4.3 FTIR spectra of (a) as-received PTFE and (b) deposit, prepared from $1 \text{ g}\cdot\text{L}^{-1}$ DChNa solutions, containing $5 \text{ g}\cdot\text{L}^{-1}$ PTFE at a deposition voltage of 50 V.

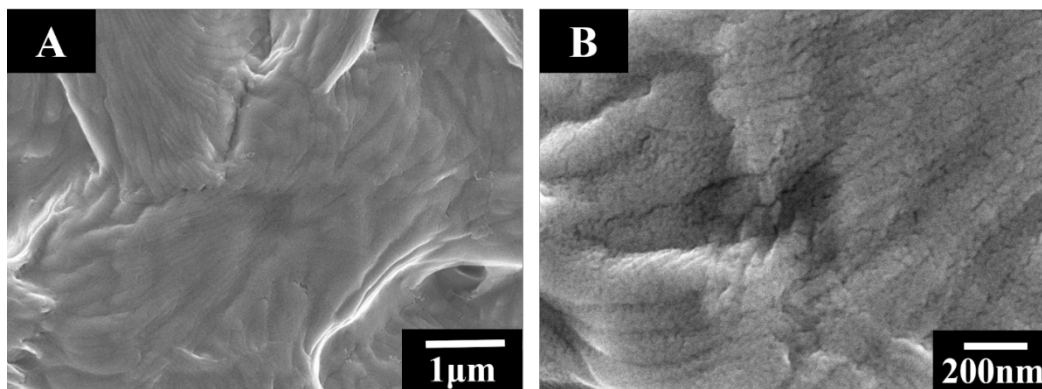


Figure 4.4 SEM images at different magnifications of films, prepared from $1 \text{ g}\cdot\text{L}^{-1}$ DChNa solutions, containing $5 \text{ g}\cdot\text{L}^{-1}$ PTFE at a deposition voltage of 50 V and annealed at $350 \text{ }^\circ\text{C}$ for 1 hour.

It is important to note that PTFE is a chemically inert and hydrophobic material. Therefore, the surface modification and charging of PTFE particles presents difficulties. However, from the experimental data described above it becomes obvious that anion DCh^- species adsorbed on PTFE and negatively charged the PTFE particles. The adsorbed DCh^- molecules allowed for electrostatic dispersion of PTFE and anaphoretic transport of PTFE to the anodic substrate. The pH dependent solubility and charge, as well as binding and coating-forming properties of DCh^- allowed for charge neutralization and coagulation of the PTFE particles at the anode surface, which facilitated film formation. It is expected that this approach can potentially be utilized for EPD of other electrically neutral functional polymers.

The feasibility of PTFE film formation by EPD paves the way for various applications, such as electrical insulation, biomedical implants, fuel cells, and formation of lubricating and nonstick hydrophobic surfaces [47, 48]. Of particular interest are applications of PTFE films for corrosion protection [49]. Therefore, we investigated protective properties of the PTFE films prepared by EPD. The comparison of the Tafel plots (Figure 4.5) for uncoated and coated steel indicated that the coated sample exhibited significantly lower anodic current and higher corrosion potential. The corrosion current density decreased from $2.59 \mu\text{A}\cdot\text{cm}^{-2}$ for the uncoated stainless steel to $0.34 \mu\text{A}\cdot\text{cm}^{-2}$ for the coated stainless steel.

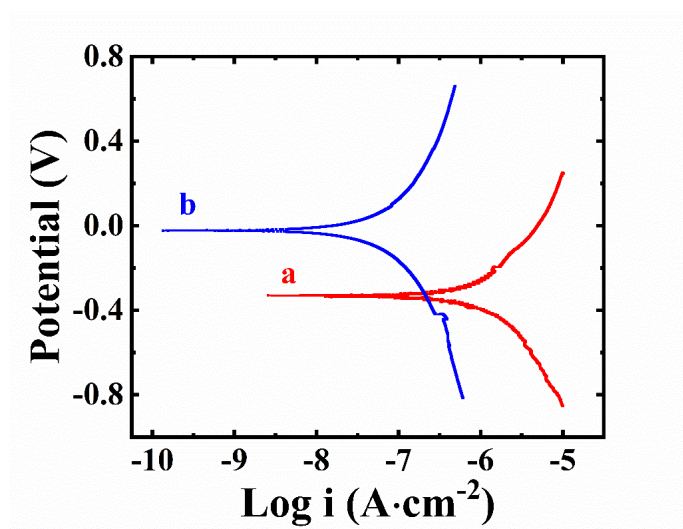


Figure 4.5 Tafel plots for stainless steel: (a) uncoated and (b) coated from $1 \text{ g}\cdot\text{L}^{-1}$ DChNa solutions, containing $5 \text{ g}\cdot\text{L}^{-1}$ PTFE at a deposition voltage of 50 V during 5 min and annealed at $350 \text{ }^\circ\text{C}$ for 1 hour.

EIS studies (Figure 4.6) showed increased impedance of the coated samples, which confirmed that the PTFE coating acted as a barrier, which limited the electrolyte access to

the electrode surface. The absolute value of impedance (Figure 4.6A) of the coated sample was practically independent on frequency below 1 kHz due to insulating properties of the coating. In contrast, the uncoated sample showed reduction of impedance with increasing frequency. The insulating properties of the coated sample resulted in low phase shift (Figure 4.6B) at low frequencies. The analysis of EIS data was performed using an equivalent circuit (Supplementary information, Figure S4.2), similar to that proposed in Ref. [42]. According to [42], the performance of a coating, containing small porosity can be described by an equivalent circuit, containing electrolyte resistance R_s , resistance in pores R_{pore} and charge transfer resistance R_{CT} . The constant phase elements described capacitive behavior of the coating and double layer capacitance in pores. In this model [42], the use of constant phase elements instead of capacitances was necessary due to some inhomogeneity of pore size distribution and coating microstructure. Modeling results showed good fitting of experimental and modeling data (Supplementary information, Figure S4.3). The film porosity (F) was analyzed by the method, described in the literature [43, 50] using the following equation:

$$F = \frac{R_{ss}}{R_c} \times 10^{-\left|\frac{\Delta E}{\beta}\right|} \quad (4-3)$$

where R_{ss} – is the polarization resistance of the substrate, R_c – is polarization resistance of the coated substrate, ΔE – is the corrosion potential difference of the coated and uncoated substrate, β – is the anodic Tafel slope of the substrate. The film porosity was found to be 2.5%. It is expected that further development of the EPD method and optimization of the

annealing procedure will result in reduced porosity and enhanced protective properties of the PTFE films.

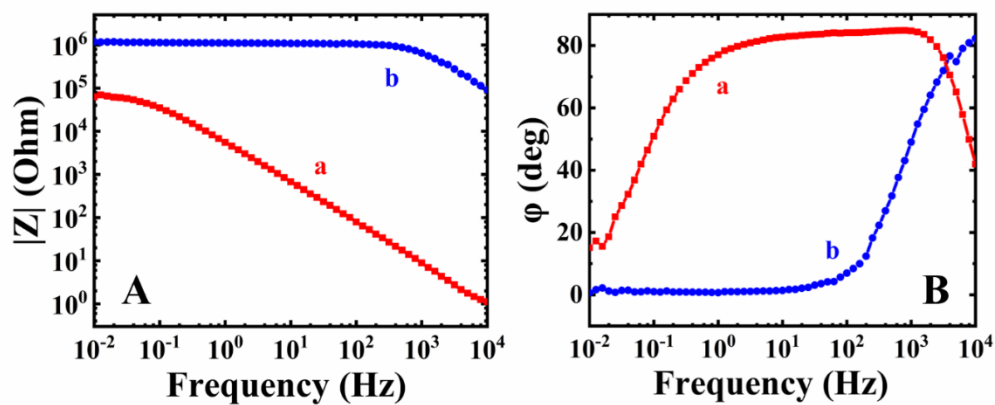


Figure 4.6 Bode plots of impedance data for stainless steel (a) uncoated and (b) coated from $1 \text{ g}\cdot\text{L}^{-1}$ DChNa solutions, containing $5 \text{ g}\cdot\text{L}^{-1}$ PTFE at a deposition voltage of 50 V during 5 min and annealed at $350 \text{ }^\circ\text{C}$ for 1 hour.

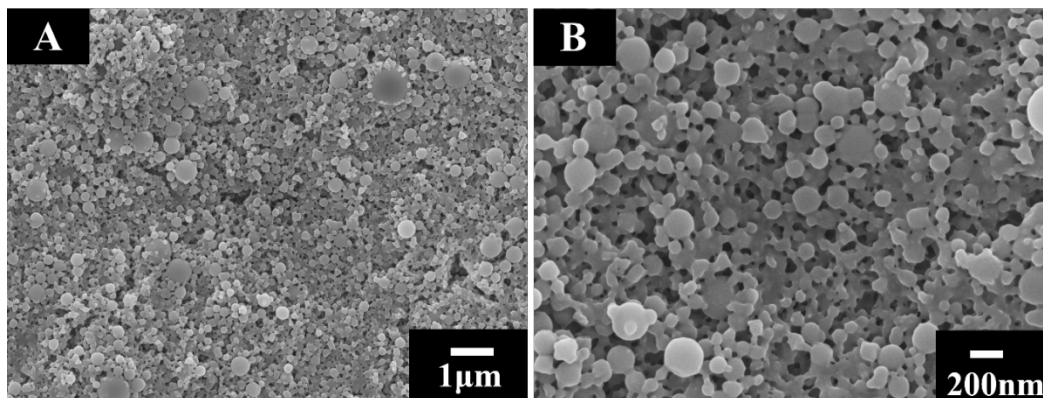


Figure 4.7 SEM images of films, deposited from solutions, containing $0.5 \text{ g}\cdot\text{L}^{-1}$ CDs and $0.5 \text{ g}\cdot\text{L}^{-1}$ DChNa at a cell voltage of 15 V.

DChNa has also been investigated as a dispersant, charging and film-forming agent for EPD of CDs and diamonds. Figure 4.7 presents SEM images of a coating, deposited by EPD from a CDs suspension, containing DChNa. SEM studies (Figure 4.7A) showed the formation of continuous films. The SEM image at higher magnification (Figure 4.7B) showed film porosity with a pore size on a scale below 100 nm. The film contained many spherical particles with diameters of 30-200 nm. The deposition rate was found to be $8.6 \mu\text{g}\cdot\text{cm}^{-2}\cdot\text{s}^{-1}$. The incorporation of CDs into the DChH films was confirmed by the FTIR analysis. Figure 4.8 presents FTIR spectra of as-received DChNa, deposited DChH, as-prepared CDs and co-deposited CDs and DChH. The bands at 2929 and 2865 cm^{-1} of as-received DChNa were related to C-H stretching. Such absorption was also found in the spectra of deposited DChH, as-prepared CDs and co-deposited DChH and CDs. Figure 4.8 (a) shows absorption peak at 1561 and 1406 cm^{-1} due to stretching COO^- asymmetric and symmetric vibrations, respectively [50]. Observed band at 1042 cm^{-1} resulted from C-O stretching [22]. The FTIR spectrum of deposited DChH showed peaks at 1711 and 1379 cm^{-1} , assigned to stretching of COOH groups [22] and C-OH bending [51], respectively (Figure 4.8 (b)). Such absorptions were also observed for a composite DChH-CDs film (Figure 4.8 (d)). The FTIR analysis of CDs (Figure 4.8 (c)) revealed peaks at 2364 and 2335 cm^{-1} assigned to C-H vibrations [52]. The bands at 1668 and 1454 cm^{-1} were due to C-C/C=C stretching [51]. Such peaks were observed for a composite DChH-CDs film (Figure 4.8 (d)). The broad absorption peak at 1240 cm^{-1} (Figure 4.8 (d)) resulted from C-H stretching in DChH and CDs.

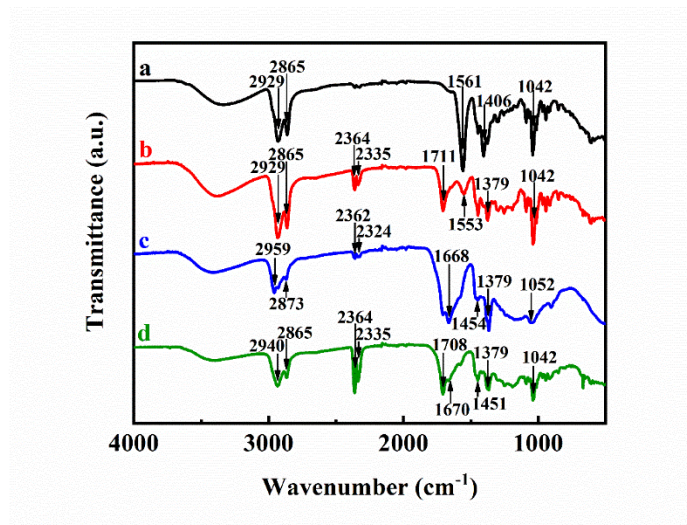


Figure 4.8 FTIR spectra of (a) as received DChNa, (b) deposit, prepared from $0.5 \text{ g}\cdot\text{L}^{-1}$ DChNa solution, (c) as-prepared CDs, (d) deposit, prepared from a solution, containing $0.5 \text{ g}\cdot\text{L}^{-1}$ CDs and $0.5 \text{ g}\cdot\text{L}^{-1}$ DChNa.

Figure 4.9 presents microstructures of the diamond films prepared using DChNa. The films contained diamond particles with typical size $0.5\text{-}0.8 \mu\text{m}$ and DChH particles of irregular shape. EPD deposition rate was found to be $3.5 \mu\text{g}\cdot\text{cm}^{-2}\cdot\text{s}^{-1}$. The feasibility of diamond deposition by EPD indicated that negatively charged DCh^- adsorbed on the diamond particles and charged the particles. The adsorption of anionic DCh^- species on diamonds allowed for electromigration of the particles to the substrate. The charge neutralization in the reaction (4-2) facilitated film formation. Moreover, the electrophoresis of non-adsorbed DCh^- resulted in the independent deposition of DChH, as described in the previous investigation [39].

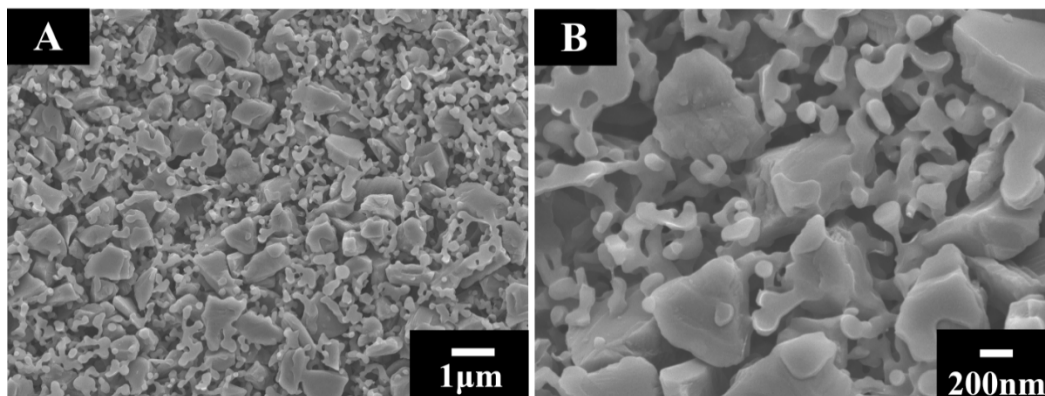


Figure 4.9 SEM images of films, prepared from 2 g·L⁻¹ DChNa solutions, containing 4 g·L⁻¹ diamond at a deposition voltage of 7 V.

The use of DChNa as a charging, dispersing and film-forming agent opens an efficient and unexplored route in the EPD of diamond and composite films. Diamond particles are known to have poor colloidal stability in various solvents, such as water and alcohols [53]. Moreover, surface modification of chemically inert diamond particles by charged dispersants presents difficulties. Previous investigations were based on the use of weak natural charge [54] of diamonds in different solvents for seeding [55, 56] of separate particles by EPD, following by the formation of continuous films by CVD. The drawback of using weak natural charge of diamond is related to poor control of particle charge and film formation mechanism. Acid-treated diamonds showed a negative charge, which allowed for film formation by anaphoresis [57]. A cataphoretic strategy [58] involved the generation H⁺ in acetone-iodine reactions and H⁺ adsorption on diamond particles. Later, this method has been utilized for the EPD of nanodiamond [59] and co-deposition of diamonds with oxide or glass materials [60, 61]. Metal ion adsorption [58, 62] has also

been used for diamond charging and cathodic EPD. The use of iodine-acetone mixture or metal ions for particle charging generates various problems, such as corrosion of electrodes, deposit contamination, poor control of particle charge and low suspension stability.

In contrast to previous studies, we found that diamond dispersion and EPD can be achieved using a dispersant, such as DChNa. The advantages of using DChNa involve good suspension stability, control of particle charge and film formation in reactions (4-1, 4-2). Moreover, DChNa can potentially be used as a co-dispersant for the EPD of composite coatings. Therefore, the results of this investigations, coupled with the previous studies [39, 40] showed that DChNa can be used for deposition of carbon nanotubes, PTFE, CDs, drugs and diamonds. DChNa is a promising co-dispersant for co-EPD of different materials and composite design. Composite materials can also be prepared by combining different electrochemical techniques [63]. The use of DChNa for EPD of diamonds is beneficial for the deposition of composites by combined electrodeposition techniques. In this investigation composite PPy-diamond films have been deposited by a combined electropolymerization-EPD method.

The comparison of SEM images of pure PPy films, prepared by anodic electropolymerization (Figure 4.10) and images of PPy-diamond films, prepared by a combined electropolymerization-EPD method (Figure 4.11), revealed difference in film morphology and confirmed the fabrication of PPy-diamond composite films. PPy is a conductive polymer. The conductivity of pure PPy film prepared in this investigation was $86 \text{ S}\cdot\text{cm}^{-1}$. The pure PPy film (Figure 4.10) was relatively smooth. In contrast, the

composite film (Figure 4.11) showed increased surface roughness. The film contained PPy coated and uncoated diamond particles. It is expected that EPD of diamonds can also be combined with electrosynthesis of oxides and anodic electrodeposition of anionic polymers.

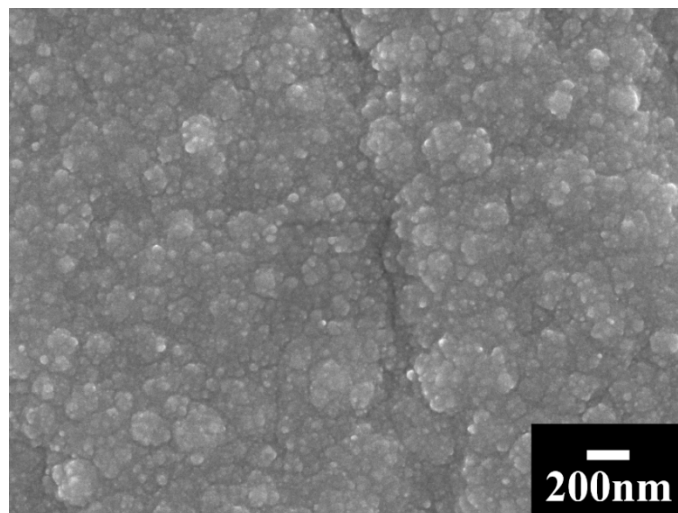


Figure 4.10 SEM image of a PPy film, prepared from 0.1 M Py solution containing 0.01 M Tiron at a deposition voltage of 7 V.

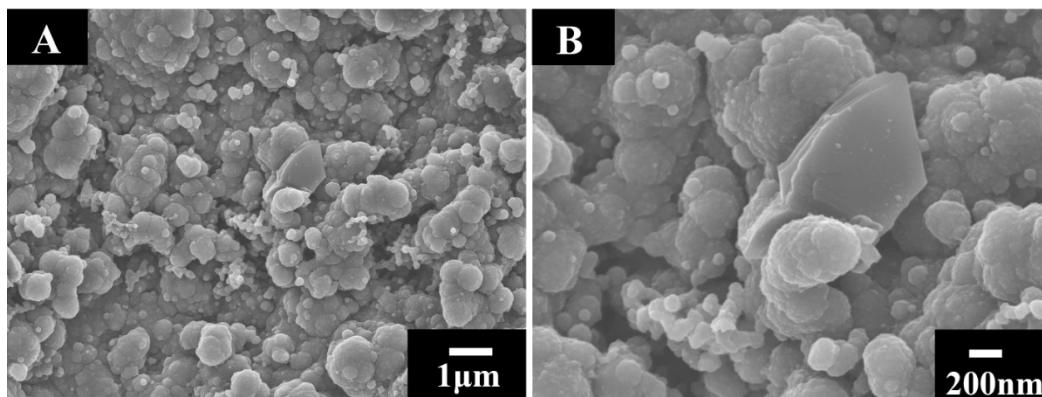


Figure 4.11 SEM images for PPy-diamond films, prepared from 0.1 M Py solution, containing 0.01 M Tiron, $1 \text{ g}\cdot\text{L}^{-1}$ diamond and $0.5 \text{ g}\cdot\text{L}^{-1}$ DChNa at a cell voltage of 7 V.

4.5 Conclusions

DChNa is a versatile charged dispersant and coating-forming molecule, which allows for EPD of PTFE, diamond and CDs. The EPD mechanism involved anaphoresis of the particles, containing adsorbed DCh^- toward the anodic substrate, electrochemical acid generation at anode, protonation and charge neutralization of DCh^- , particle coagulation at the substrate surface and assembly of films, containing particles bonded by water insoluble DChH. DChNa can be utilized as a co-dispersant for co-deposition of multicomponent composite films by EPD. Potentiodynamic and EIS testing showed that PTFE films provide protection of steel from corrosion. Building on the benefits offered by DChNa, we fabricated composite PPy-diamond deposits by a new electrodeposition method, which was based on PPy electropolymerization combined with anodic EPD of diamond. The colloidal-electrochemical methods designed in this study can potentially be utilized for deposition of different materials, such as various electrically neutral polymers and carbon materials. Moreover, new composite materials can be prepared by co-EPD or combined electrochemical methods, based on EPD and other electrochemical deposition techniques such as electropolymerization, electrosynthesis, polymer-mediated electrosynthesis and other techniques.

Especially promising is the use of DChNa-mediated EPD for electrodeposition of composites, containing various functional materials in a polymer matrix. It is expected that other bile salts and steroid molecules can also be used for EPD of functional materials. Rich chemistry of such molecules can provide a basis for a breakthrough in EPD technology.

4.6 Acknowledgements

The authors gratefully acknowledge the Natural Sciences and Engineering Research Council of Canada for the financial support.

4.7 Supplementary Data

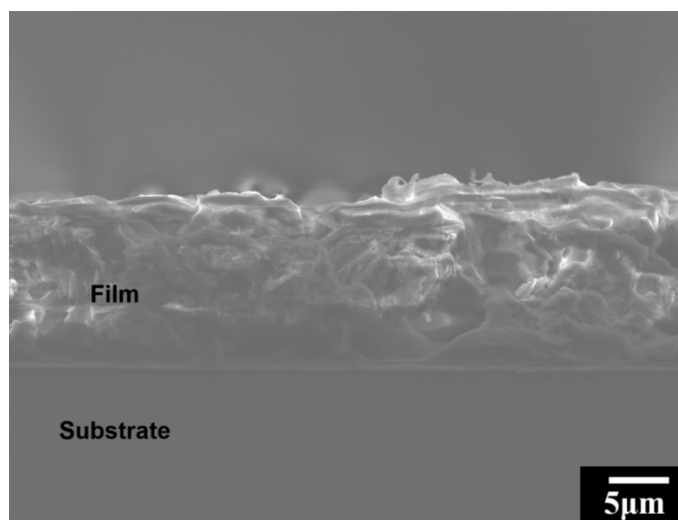


Figure S4.1 Cross section of annealed PTFE film, prepared from $1 \text{ g}\cdot\text{L}^{-1}$ DChNa solution, containing $5 \text{ g}\cdot\text{L}^{-1}$ PTFE at a cell voltage of 50 V and deposition time of 5 min.

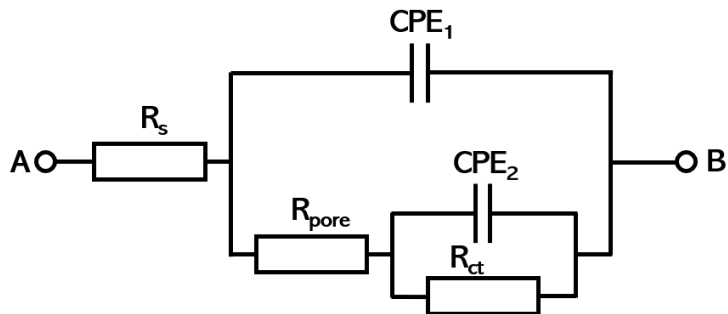


Figure S4.2 Equivalent circuit of PTFE coating: R_S -solution resistance, R_{pore} -resistance of electrolyte in pores, R_{CT} -charge transfer resistance, CPE1 and CPE2 constant phase elements, describing coating capacitance and double layer capacitance at the electrode interface formed by penetrating electrolyte.

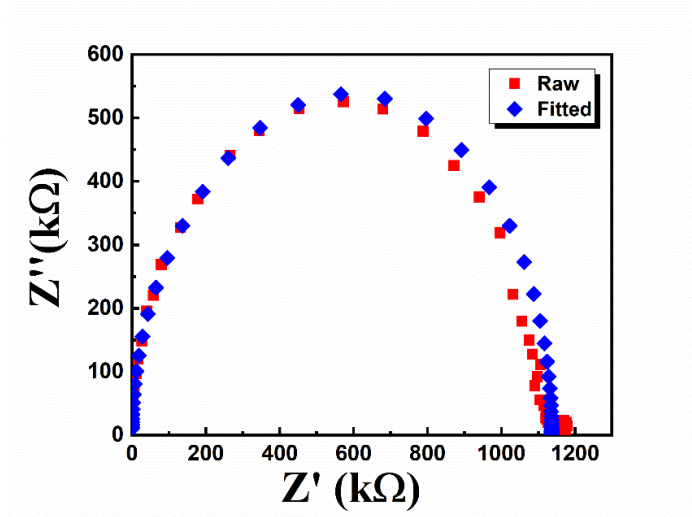


Figure S4.3 Nyquist plot of AC impedance for PTFE coating.

Table S4.1 Zeta potentials of materials

Material	Zeta potential (mV)
Diamond	-61
PTFE	-32
CDs	-98

Table S4.2 Conductivities of suspensions

Suspension	Conductivity ($\text{mS}\cdot\text{cm}^{-1}$)
$4 \text{ g}\cdot\text{L}^{-1}$ diamond + $1 \text{ g}\cdot\text{L}^{-1}$ DChNa	0.17
$5 \text{ g}\cdot\text{L}^{-1}$ PTFE + $1 \text{ g}\cdot\text{L}^{-1}$ DChNa	0.13
$0.5 \text{ g}\cdot\text{L}^{-1}$ CDs + $0.5 \text{ g}\cdot\text{L}^{-1}$ DChNa	0.09

4.8 References

- [1] R. Alheli Herrada, A. Medel, F. Manriquez, I. Sires, and E. Bustos, "Preparation of IrO₂-Ta₂O₅ vertical bar Ti electrodes by immersion, painting and electrophoretic deposition for the electrochemical removal of hydrocarbons from water," *Journal of Hazardous Materials*, vol. 319, pp. 102-110, Dec 5 2016.
- [2] L. Besra and M. Liu, "A review on fundamentals and applications of electrophoretic deposition (EPD)," *Progress in Materials Science*, vol. 52, no. 1, pp. 1-61, Jan 2007.
- [3] G. Falk, A. Nold, and B. Wiegand, "Experimental and numerical analysis of electrophoretic deposition on charge selective surfaces in external electric fields," *Advances in Applied Ceramics*, vol. 113, no. 1, pp. 55-64, Jan 2014.
- [4] X. Pang, I. Zhitomirsky, and M. Niewczas, "Cathodic electrolytic deposition of zirconia films," *Surface & Coatings Technology*, vol. 195, no. 2-3, pp. 138-146, May 31 2005.
- [5] E. Zanchi, B. Talic, A. G. Sabato, S. Molin, A. R. Boccaccini, and F. Smeacetto, "Electrophoretic co-deposition of Fe₂O₃ and Mn_{1.5}Co_{1.5}O₄: Processing and oxidation performance of Fe-doped Mn-Co coatings for solid oxide cell interconnects," *Journal of the European Ceramic Society*, vol. 39, no. 13, pp. 3768-3777, Oct 2019.
- [6] A. R. Boccaccini and I. Zhitomirsky, "Application of electrophoretic and electrolytic deposition techniques in ceramics processing," *Current Opinion in Solid State & Materials Science*, vol. 6, no. 3, pp. 251-260, Jun 2002, Art. no. Pii s1359-0286(02)00080-3.
- [7] A. Singh, N. J. English, and K. M. Ryan, "Highly Ordered Nanorod Assemblies Extending over Device Scale Areas and in Controlled Multilayers by Electrophoretic Deposition," *Journal of Physical Chemistry B*, vol. 117, no. 6, pp. 1608-1615, Feb 14 2013.
- [8] S. Molin *et al.*, "Microstructural and electrical characterization of Mn-Co spinel protective coatings for solid oxide cell interconnects," *Journal of the European Ceramic Society*, vol. 37, no. 15, pp. 4781-4791, Dec 2017.
- [9] K. Grandfield and I. Zhitomirsky, "Electrophoretic deposition of composite hydroxyapatite-silica-chitosan coatings," *Materials Characterization*, vol. 59, no. 1, pp. 61-67, Jan 2008.

- [10] M. Cheong and I. Zhitomirsky, "Electrophoretic deposition of manganese oxide films," *Surface Engineering*, vol. 25, no. 5, pp. 346-352, Jul 2009.
- [11] Y. Li, K. Wu, and I. Zhitomirsky, "Electrodeposition of composite zinc oxide-chitosan films," *Colloids and Surfaces a-Physicochemical and Engineering Aspects*, vol. 356, no. 1-3, pp. 63-70, Mar 5 2010.
- [12] I. Zhitomirsky and L. Gal-Or, "Formation of hollow fibers by electrophoretic deposition," *Materials Letters*, vol. 38, no. 1, pp. 10-17, Jan 1999.
- [13] R. M. E. Silva, R. Poon, J. Milne, A. Syed, and I. Zhitomirsky, "New developments in liquid-liquid extraction, surface modification and agglomerate-free processing of inorganic particles," *Advances in Colloid and Interface Science*, vol. 261, pp. 15-27, Nov 2018.
- [14] K. Grandfield, F. Sun, M. FitzPatrick, M. Cheong, and I. Zhitomirsky, "Electrophoretic deposition of polymer-carbon nanotube-hydroxyapatite composites," *Surface & Coatings Technology*, vol. 203, no. 10-11, pp. 1481-1487, Feb 25 2009.
- [15] L. Galantini *et al.*, "Bile salts and derivatives: Rigid unconventional amphiphiles as dispersants, carriers and superstructure building blocks," *Current Opinion in Colloid & Interface Science*, vol. 20, no. 3, pp. 170-182, Jun 2015.
- [16] W. C. Herndon, "Structure of choleic acids," *Journal of Chemical Education*, vol. 44, no. 12, pp. 724-&, 1967 1967.
- [17] S. Mukhopadhyay and U. Maitra, "Chemistry and biology of bile acids," *Current Science*, vol. 87, no. 12, pp. 1666-1683, Dec 25 2004.
- [18] P. Kumar and H. B. Bohidar, "Aqueous dispersion stability of multi-carbon nanoparticles in anionic, cationic, neutral, bile salt and pulmonary surfactant solutions," *Colloids and Surfaces a-Physicochemical and Engineering Aspects*, vol. 361, no. 1-3, pp. 13-24, May 20 2010.
- [19] Z. Sun, V. Nicolosi, D. Rickard, S. D. Bergin, D. Aherne, and J. N. Coleman, "Quantitative evaluation of surfactant-stabilized single-walled carbon nanotubes: Dispersion quality and its correlation with zeta potential," *Journal of Physical Chemistry C*, vol. 112, no. 29, pp. 10692-10699, Jul 24 2008.
- [20] M. Gubitosi *et al.*, "Characterization of Carbon Nanotube Dispersions in Solutions of Bile Salts and Derivatives Containing Aromatic Substituents," *Journal of Physical Chemistry B*, vol. 118, no. 4, pp. 1012-1021, Jan 30 2014.

- [21] M. S. Ata, R. Poon, A. M. Syed, J. Milne, and I. Zhitomirsky, "New developments in non-covalent surface modification, dispersion and electrophoretic deposition of carbon nanotubes," *Carbon*, vol. 130, pp. 584-598, 2018.
- [22] M. S. Ata and I. Zhitomirsky, "Colloidal methods for the fabrication of carbon nanotube-manganese dioxide and carbon nanotube-polypyrrole composites using bile acids," *Journal of Colloid and Interface Science*, vol. 454, pp. 27-34, Sep 15 2015.
- [23] K. Shi, X. Yang, E. D. Cranston, and I. Zhitomirsky, "Efficient Lightweight Supercapacitor with Compression Stability," *Advanced Functional Materials*, vol. 26, no. 35, pp. 6437-6445, Sep 2016.
- [24] W. Wenseleers, Vlasov, II, E. Goovaerts, E. D. Obraztsova, A. S. Lobach, and A. Bouwen, "Efficient isolation and solubilization of pristine single-walled nanotubes in bile salt micelles," *Advanced Functional Materials*, vol. 14, no. 11, pp. 1105-1112, Nov 2004.
- [25] S. Kalepu and V. Nekkanti, "Insoluble drug delivery strategies: review of recent advances and business prospects," *Acta Pharmaceutica Sinica B*, vol. 5, no. 5, pp. 442-453, Sep 2015.
- [26] M. Posa, J. Csanadi, K. E. Koeber, V. Guzsanyi, and G. Batta, "Molecular interactions between selected sodium salts of bile acids and morphine hydrochloride," *Colloids and Surfaces B-Biointerfaces*, vol. 94, pp. 317-323, Jun 1 2012.
- [27] S. Glanzer *et al.*, "Structural and Functional Implications of the Interaction between Macrolide Antibiotics and Bile Acids," *Chemistry-a European Journal*, vol. 21, no. 11, pp. 4350-4358, Mar 9 2015.
- [28] M. A. Rub *et al.*, "Aggregation behaviour of amphiphilic drug and bile salt mixtures at different compositions and temperatures," *Journal of Chemical Thermodynamics*, vol. 64, pp. 28-39, Sep 2013.
- [29] S. Sen, B. K. Paul, and N. Guchhait, "Differential interaction behaviors of an alkaloid drug berberine with various bile salts," *Journal of Colloid and Interface Science*, vol. 505, pp. 266-277, Nov 1 2017.
- [30] T. Yadav, D. Tikariha, S. Sinha, and K. K. Ghosh, "Biophysical studies on the interactions between antidepressant drugs and bile salts," *Journal of Molecular Liquids*, vol. 233, pp. 23-28, May 2017.

- [31] J. Park, J. U. Choi, K. Kim, and Y. Byun, "Bile acid transporter mediated endocytosis of oral bile acid conjugated nanocomplex," *Biomaterials*, vol. 147, pp. 145-154, Dec 2017.
- [32] H. Chen *et al.*, "Electrochemical conversion of Ni-2(OH)(2)CO₃ into Ni(OH)(2) hierarchical nanostructures loaded on a carbon nanotube paper with high electrochemical energy storage performance," *Journal of Materials Chemistry A*, vol. 3, no. 5, pp. 1875-1878, 2015 2015.
- [33] Q. Gao *et al.*, "Fabrication and characterization of metal stent coating with drug-loaded nanofiber film for gallstone dissolution," *Journal of Biomaterials Applications*, vol. 31, no. 5, pp. 784-796, Nov 2016.
- [34] E. K. Hobbie, J. A. Fagan, M. L. Becker, S. D. Hudson, N. Fakhri, and M. Pasquali, "Self-Assembly of Ordered Nanowires in Biological Suspensions of Single-Wall Carbon Nanotubes," *Acs Nano*, vol. 3, no. 1, pp. 189-196, Jan 2009.
- [35] R. Si, H. Wang, L. Wei, Y. Chen, Z. Wang, and J. Wei, "Length-dependent performances of sodium deoxycholate-dispersed single-walled carbon nanotube thin-film transistors," *Journal of Materials Research*, vol. 28, no. 7, pp. 1004-1011, Apr 2013.
- [36] L. Wang, R. Liao, Z. Tang, Y. Lei, and B. Guo, "Sodium deoxycholate functionalized graphene and its composites with polyvinyl alcohol," *Journal of Physics D-Applied Physics*, vol. 44, no. 44, Nov 9 2011, Art. no. 445302.
- [37] A. Jover, F. Meijide, E. R. Nunez, and J. V. Tato, "Dynamic rheology of sodium deoxycholate gels," *Langmuir*, vol. 18, no. 4, pp. 987-991, Feb 19 2002.
- [38] X. Sun, X. Xin, N. Tang, L. Guo, L. Wang, and G. Xu, "Manipulation of the Gel Behavior of Biological Surfactant Sodium Deoxycholate by Amino Acids," *Journal of Physical Chemistry B*, vol. 118, no. 3, pp. 824-832, Jan 23 2014.
- [39] M. S. Ata and I. Zhitomirsky, "Electrochemical Deposition of Composites Using Deoxycholic Acid Dispersant," *Materials and Manufacturing Processes*, vol. 31, no. 1, pp. 67-73, Jan 2 2016.
- [40] A. Clifford and I. Zhitomirsky, "Aqueous electrophoretic deposition of drugs using bile acids as solubilizing, charging and film-forming agents," *Materials Letters*, vol. 227, pp. 1-4, Sep 15 2018.
- [41] H. Hou, C. E. Banks, M. Jing, Y. Zhang, and X. Ji, "Carbon Quantum Dots and Their Derivative 3D Porous Carbon Frameworks for Sodium-Ion Batteries with

- Ultralong Cycle Life," *Advanced Materials*, vol. 27, no. 47, pp. 7861-7866, Dec 16 2015.
- [42] S. H. Ahn, J. H. Lee, H. G. Kim, and J. G. Kim, "A study on the quantitative determination of through-coating porosity in PVD-grown coatings," *Applied Surface Science*, vol. 233, no. 1-4, pp. 105-114, Jun 30 2004.
- [43] W. Tato and D. Landolt, "Electrochemical determination of the porosity of single and duplex PVD coatings of titanium and titanium nitride on brass," *Journal of the Electrochemical Society*, vol. 145, no. 12, pp. 4173-4181, Dec 1998.
- [44] M. Hashiba, H. Okamoto, Y. Nurishi, and K. Hiramatsu, "The zeta-potential measurement for concentrated aqueous suspension by improved electrophoretic mass-transport apparatus - application to Al₂O₃, ZrO₃ and SiC suspensions," *Journal of Materials Science*, vol. 23, no. 8, pp. 2893-2896, Aug 1988.
- [45] H. W. Starkweather Jr, R. C. Ferguson, D. B. Chase, and J. M. Minor, "Infrared spectra of amorphous and crystalline poly (tetrafluoroethylene)," *Macromolecules*, vol. 18, no. 9, pp. 1684-1686, 1985.
- [46] R. Wang, G. Xu, and Y. He, "Structure and properties of polytetrafluoroethylene (PTFE) fibers," *E-Polymers*, vol. 17, no. 3, pp. 215-220, May 2017.
- [47] G. J. Puts, P. Crouse, and B. M. Ameduri, "Polytetrafluoroethylene: synthesis and characterization of the original extreme polymer," *Chemical reviews*, vol. 119, no. 3, pp. 1763-1805, 2019.
- [48] P. Gao *et al.*, "Carbon composite coatings on Ti for corrosion protection as bipolar plates of proton exchange membrane fuel cells," *Micro & Nano Letters*, vol. 13, no. 7, pp. 931-935, Jul 2018.
- [49] K. Grytsenko, Y. V. Kolomzarov, O. Belyaev, and S. Schrader, "Protective applications of vacuum-deposited perfluoropolymer films," *Semiconductor Physics Quantum Electronics & Optoelectronics*, 2016.
- [50] D. C. Culita, L. Patron, V. S. Teodorescu, and L. Balint, "Synthesis and characterization of spinelic ferrites obtained from coordination compounds as precursors," *Journal of Alloys and Compounds*, vol. 432, no. 1-2, pp. 211-216, Apr 25 2007.
- [51] I. A. Jankovic, Z. V. Saponjic, M. I. Comor, and J. M. Nedeljkovic, "Surface modification of colloidal TiO₂ nanoparticles with bidentate benzene derivatives," *The Journal of Physical Chemistry C*, vol. 113, no. 29, pp. 12645-12652, 2009.

- [52] D. Philip, A. John, C. Y. Panicker, and H. T. Varghese, "FT-Raman, FT-IR and surface enhanced Raman scattering spectra of sodium salicylate," *Spectrochimica Acta Part A: Molecular and Biomolecular Spectroscopy*, vol. 57, no. 8, pp. 1561-1566, 2001.
- [53] L. La-Torre-Riveros, K. Soto, M. A. Scibioh, and C. R. Cabrera, "Electrophoretically fabricated diamond nanoparticle-based electrodes," *Journal of The Electrochemical Society*, vol. 157, no. 6, pp. B831-B836, 2010.
- [54] Y. Wang *et al.*, "Preparing porous diamond composites via electrophoretic deposition of diamond particles on foam nickel substrate," *Materials Letters*, vol. 138, pp. 52-55, Jan 1 2015.
- [55] J. Valdes, J. Mitchel, J. Mucha, L. Seibles, and H. Huggins, "Selected-Area Nucleation and Patterning of Diamond Thin Films by Electrophoretic Seeding," *Journal of the Electrochemical Society*, vol. 138, no. 2, pp. 635-636, 1991.
- [56] D.-G. Lee and R. K. Singh, "Synthesis of (111) oriented diamond thin films by electrophoretic deposition process," *Applied physics letters*, vol. 70, no. 12, pp. 1542-1544, 1997.
- [57] B. Dzepina, I. Sigalas, M. Herrmann, and R. Nilen, "The aqueous electrophoretic deposition (EPD) of diamond–diamond laminates," *International Journal of Refractory Metals and Hard Materials*, vol. 36, pp. 126-129, 2013/01/01/ 2013.
- [58] I. Zhitomirsky, "Cathodic electrophoretic deposition of diamond particles," *Materials Letters*, vol. 37, no. 1-2, pp. 72-78, Sep 1998.
- [59] A. Affoune, B. Prasad, H. Sato, and T. Enoki, "Electrophoretic deposition of nanosized diamond particles," *Langmuir*, vol. 17, no. 2, pp. 547-551, 2001.
- [60] K. Kamada, K. Maehara, M. Mukai, S. Ida, and Y. Matsumoto, "Fabrication of metal oxide–diamond composite films by electrophoretic deposition and anodic dissolution," *Journal of materials research*, vol. 18, no. 12, pp. 2826-2831, 2003.
- [61] Y. Wang, Q. Chen, J. Cho, and A. Boccaccini, "Electrophoretic co-deposition of diamond/borosilicate glass composite coatings," *Surface and Coatings Technology*, vol. 201, no. 18, pp. 7645-7651, 2007.
- [62] S. Yu *et al.*, "Fabrication of SiC/diamond composite coatings by electrophoretic deposition and chemical vapor deposition," *International Journal of Applied Ceramic Technology*, vol. 14, no. 4, pp. 644-651, Jul-Aug 2017.

- [63] I. Zhitomirsky and A. Petric, "Electrochemical deposition of yttrium oxide," *Journal of Materials Chemistry*, vol. 10, no. 5, pp. 1215-1218, May 2000.

Chapter 5 LCA for PTFE Composites

This chapter is reproduced from **Q. Zhao, X. Liu, I. Zhitomirsky**, *Electrophoretic deposition of materials using lithocholic acid as a dispersant*, *Materials Letters*, Volume 275, 2020, 128129, (<https://doi.org/10.1016/j.matlet.2020.128129>), with permission from Copyright © 2020 Elsevier B.V. The author of this thesis is the first author and the main contributor of this publication, including conceiving the initial ideas, development of approach and methodology, carrying out experiments, analysis of data and preparation of the manuscript.

5.1 Abstract

Lithocholic acid (LCA) was used as an anionic biosurfactant for the dispersion and electrophoretic deposition (EPD) of electrically neutral materials, such as poly(tetrafluoroethylene) (PTFE) and diamond from suspensions in ethanol. The steroid structure of LCA facilitated its adsorption on PTFE and diamond, which allowed for particle charging and deposition by anodic EPD. LCA was used as a co-dispersant for the fabrication of composite PTFE-diamond coatings. PTFE coatings provided corrosion protection of stainless steel in 3% NaCl solutions. Potentiodynamic studies revealed increased corrosion potential and decreased corrosion current of coated steel in comparison with uncoated steel. Impedance spectroscopy studies and analysis of the equivalent circuit showed that PTFE coating acted a barrier for electrolyte diffusion. LCA is a promising surfactant for EPD of other hydrophobic electrically neutral materials.

5.2 Introduction

Electrophoretic deposition (EPD) offers unique opportunities in deposition of films and coatings of different materials [1-3]. EPD involves electrophoretic motion of charged molecules or particles in a slurry under the influence of an electric field and their deposition on a substrate [4-6]. Organic solvents are preferable of the fabrication of slurries for EPD, because electric fields of sufficient strength must be applied for electrophoresis and film formation. It is important to note that relatively low fields can be applied to aqueous slurries, because electrolysis of water and related gas evolution result in porous films, which show poor adhesion. EPD is a promising method for deposition of diamond and hydrophobic polymers, such as poly(tetrafluoroethylene) (PTFE). PTFE is an advanced coating material for biomedical implants, pharmaceutical, automotive, electrical and corrosion protection applications [7, 8]. Diamond films and composites are used for various biomedical applications, such as prostheses, heart valves, microelectromechanical devices and biosensors as well as electrochemical, optical, catalytic and electronic applications [9]. Diamond particles are also used for polymer strengthening [9]. However, conventional charging additives show poor adsorption on chemically inert surfaces of PTFE and diamond in organic solvents. The goal of this investigation was EPD of PTFE and diamond and their co-EPD in an organic solvent. We discovered that lithocholic acid (LCA) can be used for efficient particle charging and dispersion in ethanol. Following the goal of this investigation we deposited PTFE, diamond and composite PTFE-diamond films. The PTFE films acted as a barrier for corrosion protection of steel.

5.3 Experimental Procedures

PTFE powder (average size 1 μm), lithocholic acid (LCA) and diamond (average size 1 μm) (Aldrich) were used. EPD was performed from PTFE and diamond suspensions in ethanol. The concentrations of PTFE, diamond and LCA in the suspensions were 5, 5 and 1 $\text{g}\cdot\text{L}^{-1}$, respectively. LCA was dissolved in ethanol and then PTFE and diamond particles were added. The obtained suspensions were ultrasonicated before EPD. Stainless steel (304 type) anodes and Pt cathodes were used for anodic EPD. The deposition voltage was 50 V, the distance between electrodes was 1.5 cm. A scanning electron microscope (SEM, JSM-7000F, JEOL) was used for microstructure investigations. A spectrometer Vertex 70 (Bruker) was used for the Fourier Transform Infrared Spectroscopy (FTIR) investigations. The coating adhesion strength was analyzed using ASTM D3359-17 standard. Electrochemical characterization was performed in 3 $\text{g}\cdot\text{L}^{-1}$ NaCl aqueous solutions using a PARSTAT (Ametek, model 2273) potentiostat. Potentiodynamic studies at a sweep rate of 1 $\text{mV}\cdot\text{s}^{-1}$ and electrochemical impedance spectroscopy (EIS) analysis in the frequency range 10 mHz-10 kHz were used for the characterization of protective properties of the coatings.

5.4 Results and Discussion

Figure 5.1A shows a chemical structure of LCA, which contains a steroid core and an anionic carboxylic group. It was hypothesized that the steroid skeleton will facilitate the LCA adsorption on hydrophobic surfaces, whereas the carboxylic group will provide a

charge required for EPD. It was found that PTFE and diamond particles can be dispersed and charged in ethanol using LCA as a surfactant and a charging agent. EPD experiments showed the formation of PTFE and diamond films. FTIR analysis confirmed deposition of PTFE.

Figure 5.1B compares FTIR spectra of as-received PTFE and deposited PTFE. The spectrum of as-received PTFE shows peaks at 1150 and 1204 cm^{-1} due to CF_2 asymmetric and symmetric vibrations, respectively [10, 11]. The C–C vibrations can also contribute to the absorption at 1150 cm^{-1} . Similar peaks were observed in the spectrum of the deposit, prepared from the PTFE suspension.

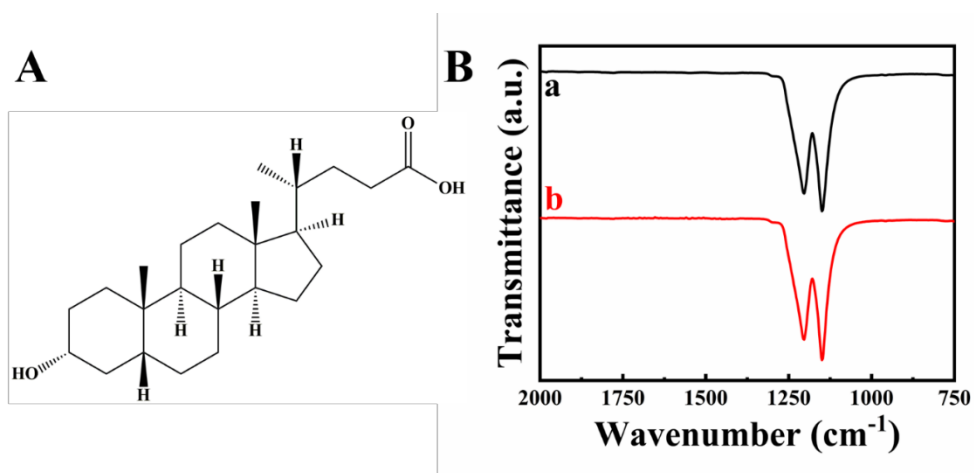


Figure 5.1 (A) Chemical structure of LCA and (B) FTIR data of (a) as-received PTFE and (b) PTFE deposit, prepared from 5 $\text{g}\cdot\text{L}^{-1}$ PTFE suspension, containing 1 $\text{g}\cdot\text{L}^{-1}$ LCA.

SEM studies of the deposited PTFE showed (Figure 5.2A) submicrometric PTFE particles, the voids between the particles resulted from their packing. Coating annealing resulted in reduced porosity (Figure 5.2B). The SEM image of the annealed sample showed nanocracks in the surface layer. SEM studies showed that diamond particles can be deposited using LCA as a dispersant (Figure 5.2C). Moreover, LCA was used as a co-dispersant for diamond and PTFE. SEM image of the deposit prepared from mixed suspensions showed particles of diamond and PTFE (Figure 5.2D).

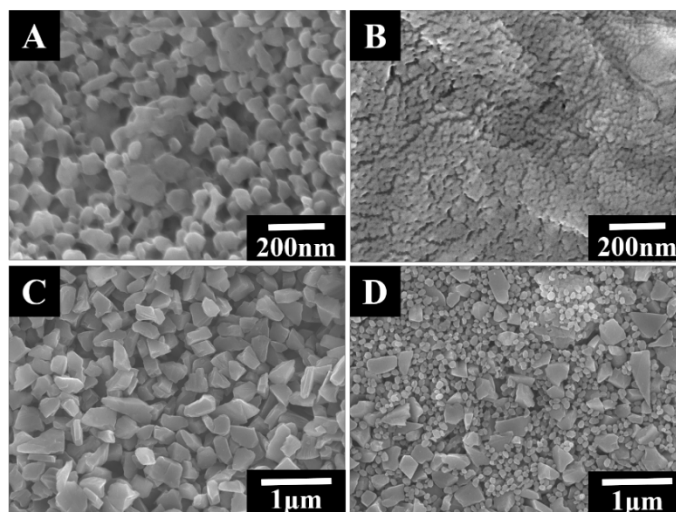


Figure 5.2 SEM images of films: (A) PTFE, as-deposited; (B) PTFE, annealed at 350 °C, prepared from 5 g·L⁻¹ PTFE suspension, containing 1 g·L⁻¹ LCA; (C) as-deposited diamond from 5 g·L⁻¹ diamond suspension, containing 1 g·L⁻¹ LCA; (D) as-deposited PTFE-diamond composite, prepared from a suspension, containing 5 g·L⁻¹ PTFE, 5 g·L⁻¹ diamond and 1 g·L⁻¹ LCA.

The PTFE coatings prepared by anodic EPD provided corrosion protection of stainless-steel substrates. Figure 5.3 shows Tafel plots for coated and uncoated samples. Coated

samples showed increased corrosion potential and decreased anodic current, which indicate corrosion protection [12]. The corrosion current decreased from $2.63 \mu\text{A}\cdot\text{cm}^{-2}$ for uncoated stainless steel to $0.93 \mu\text{A}\cdot\text{cm}^{-2}$ for coated stainless steel. Coated stainless steel showed significantly higher impedance $|Z|$ (Figure 5.4), compared to uncoated stainless steel due to insulating properties and low capacitance of the coating. The impedance of uncoated stainless steel is influenced by the capacitive properties of the electrical double layer [13, 14] at the solution/electrode interface. As a result, the impedance $|Z|$ of the uncoated steel decreased with increasing frequency (Figure 5.4). A defect-free polymer coating acts as a barrier to electrolyte diffusion and prevents corrosion [13]. However, small defects in coatings [15] create low resistance channels for electrolyte diffusion.

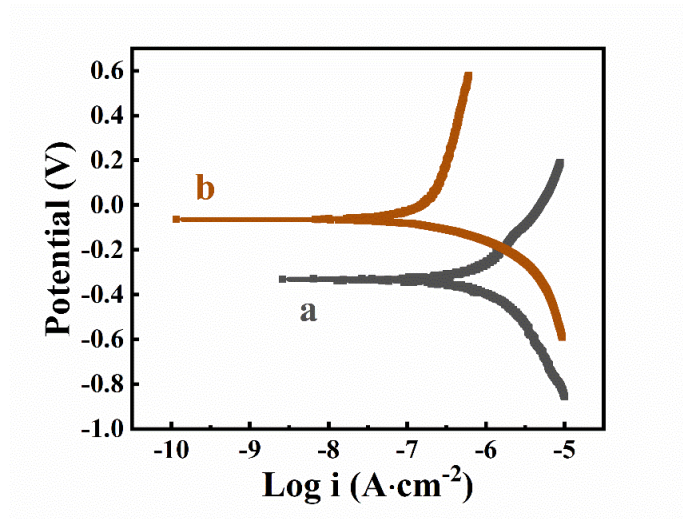


Figure 5.3 Tafel dependences for steel: (a) uncoated and (b) coated from $5 \text{ g}\cdot\text{L}^{-1}$ PTFE suspension, containing $1 \text{ g}\cdot\text{L}^{-1}$ LCA and annealed at $350 \text{ }^\circ\text{C}$ for 1 h.

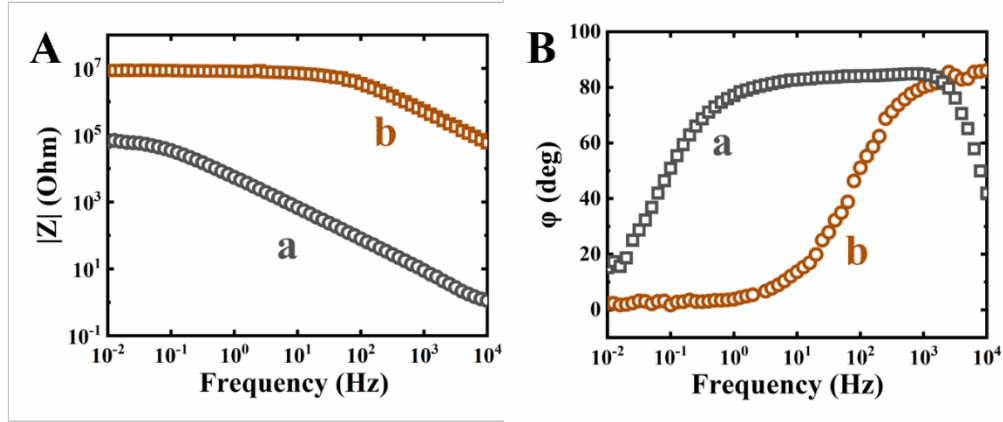


Figure 5.4 EIS Bode plots for steel (A) absolute value of impedance $|Z|$ versus frequency, (B) phase angle versus frequency for (a) uncoated and (b) coated from $5 \text{ g}\cdot\text{L}^{-1}$ PTFE suspension, containing $1 \text{ g}\cdot\text{L}^{-1}$ LCA and annealed at $350 \text{ }^\circ\text{C}$ for 1 h.

The electrochemical impedance of coated stainless steel is usually described by a transmission line circuit [13, 16], which includes different parameters, such as coating capacitance C , coating resistance perpendicular to the surface R_p , solution resistance R_s , impedance at the metal/coating interface Z_i , coating resistance tangential to surface R_t , and interfacial resistance R_i . At low frequencies (ω) the impedance of the coated electrode can be described by the equation [13, 16]:

$$Z = R_s + R_p + \frac{R_t}{2} + \sqrt{\frac{R_t^2}{4} + \frac{R_t R_i}{1 - \omega j C R_i}} \quad (5-1)$$

At low frequencies the impedance is nearly independent on the frequency [13, 16]. Indeed, the impedance $|Z|$ of the uncoated sample (Figure 5.4) showed very small variations in the range of 10 mHz-100 Hz. The decrease of $|Z|$ and increase of phase angle at higher frequencies are attributed to reduced impedance of the capacitive component (Figure 5.4).

The approach developed in this study can potentially be used for the deposition of other electrically neutral materials from organic solvents.

5.5 Conclusions

We received evidence that LCA is a promising charged surfactant for EPD of electrically neutral chemically inert materials such as PTFE and diamond. The use of ethanol as a solvent eliminates problems related to gas evolution in aqueous suspensions and allows for applications of relatively high fields, which allow for reduced porosity and high deposition yield. LCA can be used as a co-surfactant for the deposition of composite films. The analysis of Tafel plots and EIS data showed that PTFE coatings provided corrosion protection of stainless steel.

5.6 Acknowledgements

The authors thank the Natural Sciences and Engineering Research Council of Canada for the financial support and Canadian Centre for Electron microscopy for SEM studies.

5.7 References

- [1] A. R. Boccaccini and I. Zhitomirsky, "Application of electrophoretic and electrolytic deposition techniques in ceramics processing," *Current Opinion in Solid State & Materials Science*, vol. 6, no. 3, pp. 251-260, Jun 2002, Art. no. Pii s1359-0286(02)00080-3.
- [2] R. Alheli Herrada, A. Medel, F. Manriquez, I. Sires, and E. Bustos, "Preparation of IrO₂-Ta₂O₅ vertical bar Ti electrodes by immersion, painting and electrophoretic

- deposition for the electrochemical removal of hydrocarbons from water," *Journal of Hazardous Materials*, vol. 319, pp. 102-110, Dec 5 2016.
- [3] A. Braun, M. Wolff, C. Oetzel, J. Tabellion, G. Falk, and R. Clasen, "Alumina ceramics by means of electrophoretic deposition of submicron powders," in *28th International Conference on Advanced Ceramics and Composites B: Ceramic Engineering and Science Proceedings*, 2004, vol. 25, pp. 591-596: Wiley Online Library.
- [4] K. Shi and I. Zhitomirsky, "Electrophoretic nanotechnology of graphene-carbon nanotube and graphene-polypyrrole nanofiber composites for electrochemical supercapacitors," *Journal of Colloid and Interface Science*, vol. 407, pp. 474-481, Oct 1 2013.
- [5] Y. Wang, I. Deen, and I. Zhitomirsky, "Electrophoretic deposition of polyacrylic acid and composite films containing nanotubes and oxide particles," *Journal of Colloid and Interface Science*, vol. 362, no. 2, pp. 367-374, Oct 15 2011.
- [6] A. Jankovic, S. Erakovic, M. Vukasinovic-Sekulic, V. Miskovic-Stankovic, S. J. Park, and K. Y. Rhee, "Graphene-based antibacterial composite coatings electrodeposited on titanium for biomedical applications," *Progress in Organic Coatings*, vol. 83, pp. 1-10, Jun 2015.
- [7] M.-K. Lee, C. Park, T.-S. Jang, H.-E. Kim, and S.-H. Jeong, "Enhanced mechanical stability of PTFE coating on nano-roughened NiTi for biomedical applications," *Materials Letters*, vol. 216, pp. 12-15, Apr 1 2018.
- [8] E. Dhanumalayan and G. M. Joshi, "Performance properties and applications of polytetrafluoroethylene (PTFE)-a review," *Advanced Composites and Hybrid Materials*, vol. 1, no. 2, pp. 247-268, Jun 2018.
- [9] S. Kumar, M. Nehra, D. Kedia, N. Dilbaghi, K. Tankeshwar, and K.-H. Kim, "Nanodiamonds: Emerging face of future nanotechnology," *Carbon*, vol. 143, pp. 678-699, Mar 2019.
- [10] H. W. Starkweather, R. C. Ferguson, D. B. Chase, and J. M. Minor, "Infrared-Spectra Of Amorphous And Crystalline Poly(Tetrafluoroethylene)," *Macromolecules*, vol. 18, no. 9, pp. 1684-1686, 1985 1985.
- [11] R. Wang, G. Xu, and Y. He, "Structure and properties of polytetrafluoroethylene (PTFE) fibers," *E-Polymers*, vol. 17, no. 3, pp. 215-220, May 2017.
- [12] K. Grandfield, F. Sun, M. FitzPatrick, M. Cheong, and I. Zhitomirsky, "Electrophoretic deposition of polymer-carbon nanotube-hydroxyapatite

- composites," *Surface & Coatings Technology*, vol. 203, no. 10-11, pp. 1481-1487, Feb 25 2009.
- [13] J. R. Scully, "Electrochemical impedance of organic-coated steel - correlation of impedance parameters with long-term coating deterioration," *Journal of the Electrochemical Society*, vol. 136, no. 4, pp. 979-990, Apr 1989.
- [14] F. Mansfeld, "Use of electrochemical impedance spectroscopy for the study of corrosion protection by polymer-coatings," *Journal of Applied Electrochemistry*, vol. 25, no. 3, pp. 187-202, Mar 1995.
- [15] A. Amirudin and D. Thierry, "Application of electrochemical impedance spectroscopy to study the degradation of polymer-coated metals," *Progress in Organic Coatings*, vol. 26, no. 1, pp. 1-28, Aug 1995.
- [16] M. Kendig, F. Mansfeld, and S. Tsai, "Determination of the long-term corrosion behavior of coated steel with ac impedance measurements," *Corrosion Science*, vol. 23, no. 4, pp. 317-329, 1983 1983.

Chapter 6 Influence of Bile Acids on EPD of PVDF

Composites

This chapter is reproduced from **Q. Zhao**, *S. Veldhuis*, *R. Mathews*, *I. Zhitomirsky*, *Influence of chemical structure of bile acid dispersants on electrophoretic deposition of poly(vinylidene fluoride) and composites*, *Colloids and Surfaces A: Physicochemical and Engineering Aspects*, Volume 627, 2021, 127181, (<https://doi.org/10.1016/j.colsurfa.2021.127181>) with permission from Copyright © 2021 Elsevier B.V. The author of this thesis is the first author and the main contributor of this publication, including conceiving the initial ideas, development of approach and methodology, carrying out experiments, analysis of data, writing the initial draft and preparation of the manuscript.

6.1 Abstract

A biomimetic strategy has been developed for the dispersion of poly(vinylidene fluoride) (PVDF) particles using commercial analogs of bile acids (BAs), such as lithocholic acid (LCA), chenodeoxycholic acid (CDCA), deoxycholic acid (DCA), ursodeoxycholic acid (UDCA), and cholic acid (ChA). BAs were used as anionic surfactants for electrophoretic deposition of PVDF films. The EPD method allowed controlled deposition of PVDF films at high deposition rates. The PVDF deposition yield, obtained using different BAs, increased in the order LCA<CDCA<DCA<UDCA<ChA. It depends on the number of OH

groups and their positions and orientation in the BAs structures. Annealed PVDF films provided corrosion protection of stainless steel in 3% NaCl solutions. ChA was used as a co-surfactant for diamond, silica and PVDF particles and allowed for the deposition of PVDF-diamond and PVDF-silica films of varied compositions. The biomimetic approach developed in this investigation opens a new strategy for the chemical modification and charging of electrically neutral hydrophobic materials and deposition of functional polymers and composites by EPD from colloidal suspensions.

6.2 Introduction

PVDF is an advanced functional polymer, which exhibits valuable properties, such as high mechanical strength, excellent chemical resistance, piezoelectric and ferroelectric properties, high dielectric constant, good processability and low flammability [1-4]. PVDF coatings and films are gaining attention for many applications [5-7]. Good resistance to organic and inorganic acids as well as to various chemicals and solvents, low melting temperature and low permeability are important factors for PVDF applications for corrosion protection of metals and alloys [8-10]. PVDF films were developed for electrical insulation, piezoelectric transducers, pyroelectric sensors, actuators and capacitors [1, 11, 12]. Moreover, PVDF films were used as separators for batteries and fuel cells, membranes for water treatment, pollutants removal, gas separation and other applications [13-16].

The interest in applications of PVDF films and coatings has generated the need in the development of advanced deposition techniques. Electrophoretic deposition (EPD) has

generated significant interest for the deposition of organic and inorganic materials [17-19]. Fundamental aspects of the EPD technique have been described in review papers [20-24]. Main challenges in the EPD of advanced materials include the development of efficient techniques for surface modification of particles, their charging and fabrication of stable colloidal suspensions [24, 25].

PVDF is an electrically neutral polymer. Therefore, there is a need in the development of charged surfactants, which must be adsorbed on the PVDF particles for their dispersion and charging. Several investigations [26-29] reported co-EPD of inorganic or carbon materials with a small amount of PVDF as a binder. In those approaches, PVDF was dissolved in a solvent and co-deposited together with particles of other materials. Pure PVDF films were deposited from PVDF solutions in various organic solvents or suspensions in a mixed 2-butanone-water solvent without the use of charging agents [30, 31]. PVDF films were also deposited from suspensions formed in a mixed N-methyl-2-pyrrolidinone-ethanol solvent [32]. However, the mechanisms of PVDF co-deposition with charged particles [26-29] and deposition of pure PVDF without charging additives [30, 32] have not been described. EPD method has also been applied [33, 34] for the deposition of poly(vinylidene fluoride-co-hexafluoropropylene) co-polymer (PVDF-HFP) from its solution in acetone. The proposed charging mechanism involved adsorption of water from the moist air, dissociation of water molecules, bonding of OH^- ions to acetone and interaction of PVDF-HFP with anionic acetone- OH^- species [34]. Despite the progress achieved in the deposition of PVDF and PVDF-HFP from their solutions in different solvents, there is a need in the development of

advanced dispersing and charging agents for controlled deposition of PVDF films and composites at high deposition rates using suspensions of PVDF particles.

This investigation was motivated by unique properties of advanced natural surfactants, such as synthetic bile acids (BAs) and bile salts (BSs), which were used for colloidal processing of materials [35-37]. BSs are natural anionic surfactants, which facilitate solubilization and dispersion of various biomolecules and drugs. BAs and BSs exhibit interesting adsorption properties resulting from their amphiphilic facial structures, containing hydrophobic and hydrophilic sides.

The goal of this investigation was EPD of PVDF and composites from suspensions in an ethanol solvent using BAs as dispersing and charging agents. The experimental results showed that various BAs can be used for dispersion and charging of PVDF particles and EPD of PVDF films. Our investigation revealed strong influence of the chemical structure of BAs on surface modification of PVDF and the deposition yield. Testing results indicated that the deposition yield depended on the number of OH groups, their location and orientation in the BA structure. The method allowed the fabrication of PVDF films, which provided corrosion protection of stainless steel. The protective properties of the films prepared using different BAs were linked to the deposition kinetics and morphologies of the obtained films. BAs allowed surface modification of other materials, such as silica and diamonds, which were co-deposited with PVDF using BAs as co-dispersants. We demonstrated the fabrication of composite PVDF-diamond and PVDF-silica films. The approach developed in this investigation opens a new strategy for the chemical

modification and charging of chemically inert materials and deposition of functional polymers and composites by EPD from colloidal suspensions.

6.3 Experimental Procedures

Poly(vinylidene fluoride) powder (PVDF, Alfa Aesar Company), lithocholic acid (LCA), chenodeoxycholic acid (CDCA), deoxycholic acid (DCA), ursodeoxycholic acid (UDCA), cholic acid (ChA), NaCl, synthetic monocrystalline diamond powder (average size $\leq 1 \mu\text{m}$, Millipore-Sigma Company), silica powder (average size 0.5 micron, PCR Inc.) were used. BAs were dissolved in ethanol for film formation by EPD. The BAs concentration in the solutions was $1 \text{ g}\cdot\text{L}^{-1}$. PVDF films were deposited from $10 \text{ g}\cdot\text{L}^{-1}$ PVDF suspensions in the BAs solutions. EPD of composite films was performed from $10 \text{ g}\cdot\text{L}^{-1}$ PVDF suspensions, containing $1\text{-}5 \text{ g}\cdot\text{L}^{-1}$ diamond or $1\text{-}5 \text{ g}\cdot\text{L}^{-1}$ silica in the BAs solutions. The suspensions were ultrasonicated prior to EPD.

The EPD cell contained a type 304 stainless steel (dimensions $25\times 30\times 0.1 \text{ mm}^3$) served as the working electrode and a platinum sheet (dimensions $25\times 30\times 0.1 \text{ mm}^3$) served as the counter electrode with a separation distance of 15 mm between them. EPD was carried out with EPS 2A200 external power supply from Amersham Biosciences. The constant deposition voltage applied between two electrodes varied between 10~150 V for 1~20 min. After deposition, films were dried at room temperature and thermally treated at $200 \text{ }^\circ\text{C}$ for 1 h in the furnace for further characterization.

Electrochemical characterizations of coated and uncoated substrates were performed using a PARSTAT 2273 potentiostat from Ametek in 3.0 wt% aqueous NaCl solution with a 3-electrode cell including a uncoated or coated stainless steel substrate as a working electrode, a saturated calomel reference electrode (SCE) and a Pt mesh counter electrode. A PowerSuite software was used to control the testing procedure and data analysis. Prior to each test, the aqueous NaCl solution was deoxygenated for at least 30 min using inert nitrogen gas to minimize effect of oxygen. Potentiodynamic polarization tests were conducted at a sweeping rate of $1.0 \text{ mV}\cdot\text{s}^{-1}$ from negative to positive direction. Electrochemical impedance spectroscopy (EIS) studies were performed under a sinusoidal excitation potential of 10 mV in the frequency range of 10 mHz-10 kHz. A JEOL JSM-7000F scanning electron microscope (SEM) was used for microstructure investigation.

6.4 Results and Discussion

In this investigation EPD of PVDF was performed from PVDF particle suspensions in ethanol, containing dissolved BAs. It is well known that organic solvents, such as ethanol, are preferable for EPD of various materials. It is in this regard that the use of water as a solvent for EPD generates a problem of significant H_2 and O_2 evolution related to electrochemical decomposition of water in cathodic and anodic reactions, respectively. Another difficulty is related to high electrical conductivity of aqueous solutions. Therefore, aqueous EPD can be performed at very low voltages. However, higher voltages are necessary for creation of sufficiently high electric fields in the suspensions for

electrophoresis of colloidal particles. BAs are practically insoluble in water, however they are well-soluble in ethanol. Therefore, in this investigation various BAs were used as surfactants for EPD of PVDF in ethanol. It will be shown below that the choice of BA molecules was crucial to achieving high deposition yield.

Figure 6.1 shows chemical structures of BAs used in this investigation. BAs are steroid amphiphilic molecules, which have a hydrophobic hydrocarbon convex face and a concave hydrophilic face with a carboxylic and OH groups. The chemical structure of LCA includes one OH group. CDCA, DCA and UDCA have two OH groups. The OH groups have different positions in the structures of CDCA and DCA. UDCA is the 7 β -OH epimer of CDCA [38] and C7-OH groups have different space orientations in the structures of CDCA and UDCA. The chemical structure of ChA contains three OH groups.

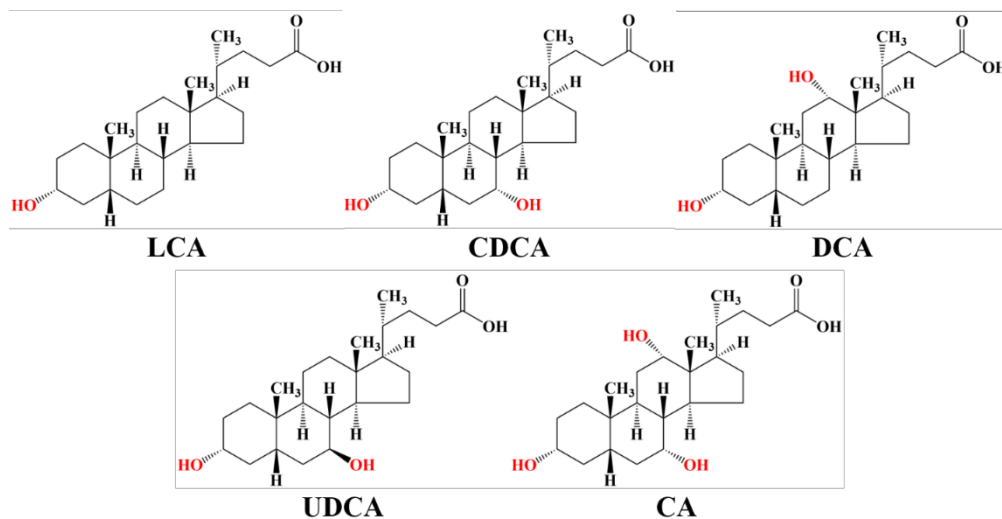


Figure 6.1 Chemical structures of BAs.

The use of BAs as surfactants allowed for anodic EPD of PVDF from stable suspensions. The ability to form PVDF films by EPD indicated that dissociated BAs adsorbed on the PVDF particles and imparted a negative charge to the particles. Figure 6.2 shows deposit mass achieved in the presence of surfactants at a deposition voltage of 50 V and deposition time of 5 min.

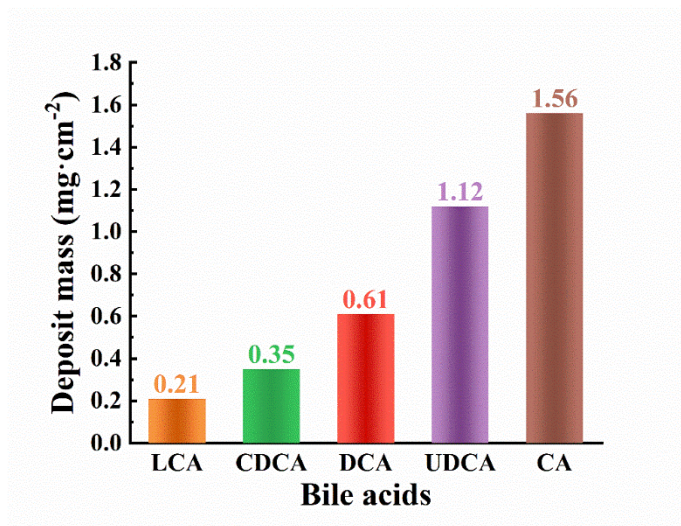


Figure 6.2 Deposit mass of PVDF films deposited using various BAs as surfactants from 10 g·L⁻¹ PVDF suspensions in ethanol solutions, containing 1 g·L⁻¹ BAs at a deposition voltage of 50 V and deposition time of 5 min.

The deposition yield increased in the order LCA<CDCA<DCA<UDCA<ChA. The use of LCA as a surfactant, containing one OH group, resulted in a relatively small deposition yield. Higher deposition yields were achieved using BAs surfactants with two OH groups, such as CDCA, DCA, and UDCA. The highest deposition yield was obtained using ChA with three OH groups. The increase in deposition yield with increasing number of OH groups in the BAs structure can result from enhanced BAs adsorption on the PVDF

particles. The comparison of the deposition yields achieved using CDCA and DCA indicated that positions of the two OH groups in their structure also exert influence on the surfactant efficiency. The deposition yield achieved using UDCA was significantly higher than that for CDCA. This result indicated that orientation of OH groups in the surfactant structure is another important factor, controlling surfactant efficiency. It is suggested that adsorption of BAs on the PVDF surface was based on a hydrophobic interaction mechanism [39], which involved interaction of the hydrophobic side of the BAs molecules and hydrophobic PVDF particles. This suggestion can be supported by literature data on hydrophobic interactions between hydrophobic face of ChA and PVDF membranes in ethanol [40]. However, the influence of the BAs structures on the deposition yield is not well understood. It is known that the surfactant efficiency is influenced by different factors governing their behavior in solvents, such as critical micelle concentration (CMC), solubility, hydrophilicity, and other factors.

The behavior of various BSs in aqueous solution has been widely investigated. However, relatively limited information is available on behavior of BAs in ethanol and other organic solvents. It is known that properties of BSs are influenced not only by the number of OH groups, but also by their position and orientation [41]. Hydrophilicity of BSs increases with increasing number of OH groups. The analysis of BSs showed that salts of CDCA and DCA exhibit comparable hydrophilicities, whereas hydrophilic properties of UDCA are similar to ChA [41]. Hydrophilicity of surfactants belongs to the important factors controlling micelle formation. It is also known that the formation of BSs micelles is influenced by the

number, position and orientation of OH groups of BSs molecules [35, 42]. The analysis of micelle formation of BSs revealed a two step mechanism, which results in a relatively wide CMC ranges instead of specific CMC values [35]. Moreover, the CMC data reported in the BSs literature varied to a great extent between various methods and within the same technique [35]. It was found that micelle formation resulted in the reduced ChA adsorption on PVDF [40]. Therefore, it can be suggested that the difference in the chemical structure of the BAs dispersants exerts influence on their aggregation in the ethanol solutions and their efficiency as dispersants for PVDF.

The film mass can be varied by the variation of the deposition voltage at a fixed deposition time or by variation of deposition time at a constant voltage (Figure 6.3). Therefore, the amount of the deposited material can be easily varied and controlled. The deposition yield data deviated from linear Hamaker law [21] dependences (Figure 6.3). Such deviations can be attributed to different factors, discussed in the literature, such as reduction of electric field in the bulk suspension due to the increasing voltage drop in the growing films [24, 43], and reduction of the particle concentration in the bulk suspension with increasing deposition time [22, 24]. Moreover, the deposition yield depends not only on mass transport rate, described by the Hamaker law, but it is also influenced by the mechanism of film formation [24, 44].

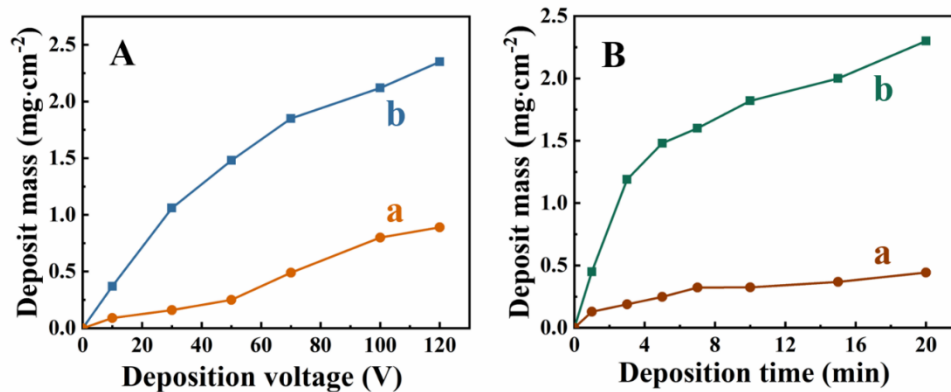


Figure 6.3 Deposit mass versus (A) deposition voltage at a deposition time of 5 min and (B) deposition time at a deposition voltage of 50 V for 10 g·L⁻¹ PVDF suspensions in ethanol, containing dissolved (a) 1 g·L⁻¹ LCA and (b) 1 g·L⁻¹ ChA.

Figure 6.4 compares the SEM images of as-deposited and annealed PVDF films prepared using different BAs at a deposition voltage of 50V and deposition time of 5 min.

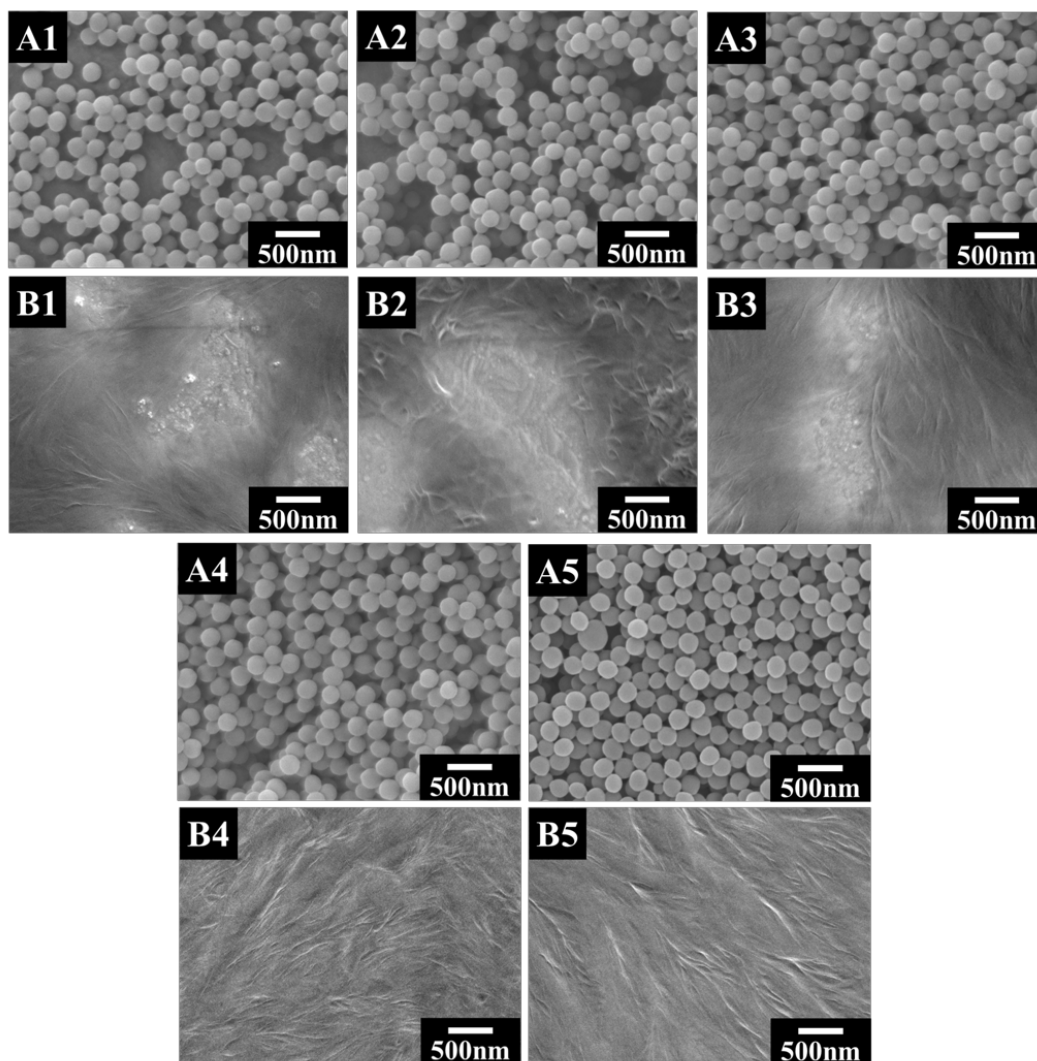


Figure 6.4 SEM images of (A1-A5) as deposited and (B1-B5) annealed films, prepared from $10 \text{ g}\cdot\text{L}^{-1}$ PVDF suspensions in ethanol, containing dissolved (A1, B1) $1 \text{ g}\cdot\text{L}^{-1}$ LCA, (A2, B2) $1 \text{ g}\cdot\text{L}^{-1}$ CDCA and (A3, B3) $1 \text{ g}\cdot\text{L}^{-1}$ DCA, (A4, B4) $1 \text{ g}\cdot\text{L}^{-1}$ UDCA and (A5, B5) $1 \text{ g}\cdot\text{L}^{-1}$ ChA.

The low deposition yield achieved using LCA resulted in poor coverage of the substrate at a deposition time of 5 min. The SEM image (Figure 6.4 A1) shows that some areas of the substrate remained uncovered by the particles. The higher deposition yield achieved using

CDCA and DCA resulted in improved substrate coverage (Figure 6.4 (A2, A3)). Annealing of the films at the temperature that slightly higher than its melting temperature resulted in deposited PVDF powder melting. The melting PVDF material flowed around the substrates and recrystallized to film form, covering the substrate completely. However, the films were very thin, non-uniform and non-smooth due to inhomogeneous and limited deposition of PVDF particles (Figure 6.4 (B1-B3)). The high deposition rate achieved using UDCA and ChA allowed for the good coverage of the substrates (Figure 6.4 (A4, A5)). The SEM images shows spherical PVDF particles with a typical size of 0.2 μm which formed relatively dense packed films (Figure 6.4 (A4, A5)). Annealing resulted in the formation of crack-free, smooth, dense, and uniform films (Figure 6.4 (B4, B5)).

It was found that annealed films provided corrosion protection of stainless steel substrates in 3% NaCl solutions. Figure 6.5 shows Tafel plots of the coated and uncoated samples. The coated samples showed significant increase in the corrosion potential and reduction of anodic current, compared to the uncoated samples. As pointed out in the Introduction, advanced chemical and physical properties of PVDF make it an important material for corrosion protection of metals and alloys. Therefore, EPD is a promising method for the fabrication of PVDF coatings for corrosion protection. The results of EIS studies are presented as Bode plots in Figure 6.6. The comparison of the impedance data for the coated and uncoated samples indicated that coated samples showed enhanced impedance, which resulted from the insulating properties of the PVDF films. The high resistance of the films

prepared using UDCA and ChA at frequencies 10 Hz -10 kHz indicated that such films provided enhanced barrier to the electrolyte diffusion to the substrate surface.

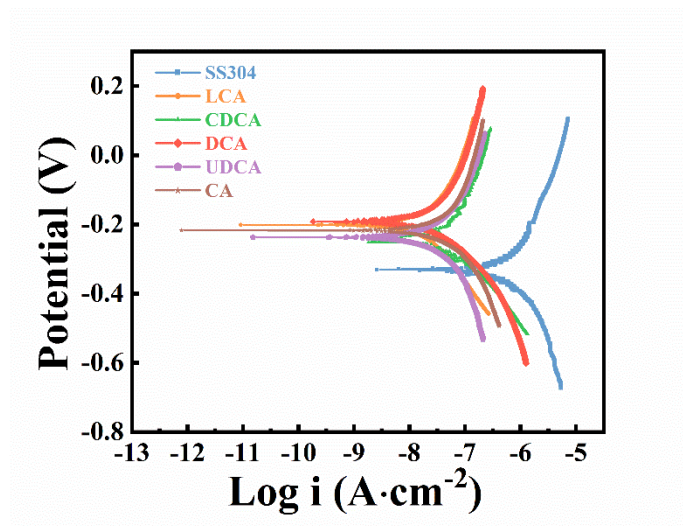


Figure 6.5 Tafel plots for uncoated 304 type stainless steel and coated from 10 g·L⁻¹ PVDF suspensions containing different BAs at deposition voltage of 50 V and deposition time of 5 min and annealed at 200 °C for 1 hour.

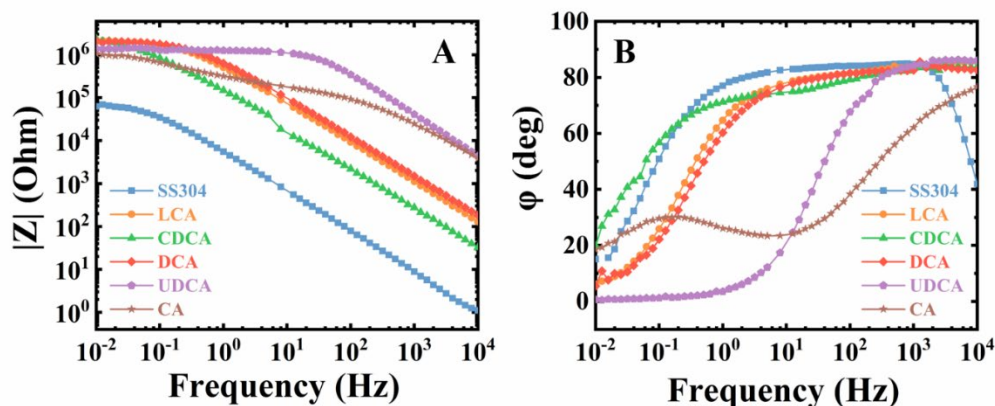


Figure 6.6 EIS Bode plots for uncoated 304 type stainless steel and coated from 10 g·L⁻¹ PVDF suspensions containing different BAs at deposition voltage of 50 V and deposition time of 5 min and annealed at 200 °C for 1 hour.

The feasibility of PVDF deposition using BAs as dispersants, opens a strategy for the deposition of composites. Of particular interest is the deposition of PVDF-diamond films and PVDF-silica films. The co-deposition of diamond and PVDF is a promising strategy for the fabrication of films with enhanced piezoelectric, pyroelectric, thermal conductivity, and mechanical properties [45, 46]. PVDF-silica composites are of significant interest for biomedical applications [47] and fabrication of films with enhanced piezoelectric, thermal and mechanical properties [48]. Therefore, in this investigation ChA was used as a co-dispersant for deposition of PVDF-diamond and PVDF-silica films.

Figure 6.7 (A1, A2) shows SEM images of as-deposited films from $10 \text{ g}\cdot\text{L}^{-1}$ PVDF suspensions containing $1 \text{ g}\cdot\text{L}^{-1}$ diamond. The SEM images show small spherical PVDF particles and larger diamond particles of irregular shapes. The increase of diamond concentration in the suspensions resulted in the increasing amount of diamond in the films (Figure 6.7 (A3, A4)). The SEM images indicate that ChA can be used as a co-dispersant for the co-deposition of PVDF and diamond. Small PVDF particles filled the voids between the larger diamond particles and allowed the formation of relatively dense deposits. Annealing resulted in melting of PVDF particles and formation of crack-free continuous PVDF layers, embedded with diamond particles (Figure 6.7 (B1-B4)). The comparison of images of the sintered films confirmed that the increase in diamond concentration in the suspension resulted in larger amount of the diamond particles in the films. The SEM images of films prepared from the $10 \text{ g}\cdot\text{L}^{-1}$ PVDF suspensions containing $1 \text{ g}\cdot\text{L}^{-1}$ silica showed small spherical PVDF particles and larger silica particles of a spherical shape (Figure 6.8

(A1, A2)). The increase in the silica concentration in the suspension to $5 \text{ g}\cdot\text{L}^{-1}$ resulted in larger amount of silica in the deposited films (Figure 6.8 (A3, A4)). Therefore, ChA acted as a co-dispersant and allowed co-deposition of silica and PVDF. Annealing resulted in melting of PVDF particles and formation a continuous layer, containing spherical silica particles. The comparison of the SEM images of the annealed films confirmed that the increase in the silica concentration in the suspension resulted in the increasing amount of silica in the deposited films (Figure 6.8 (B3, B4)). Therefore, the results of SEM studies showed that the composition of the coatings can be varied by the variation of diamond and silica concentration in the suspensions.

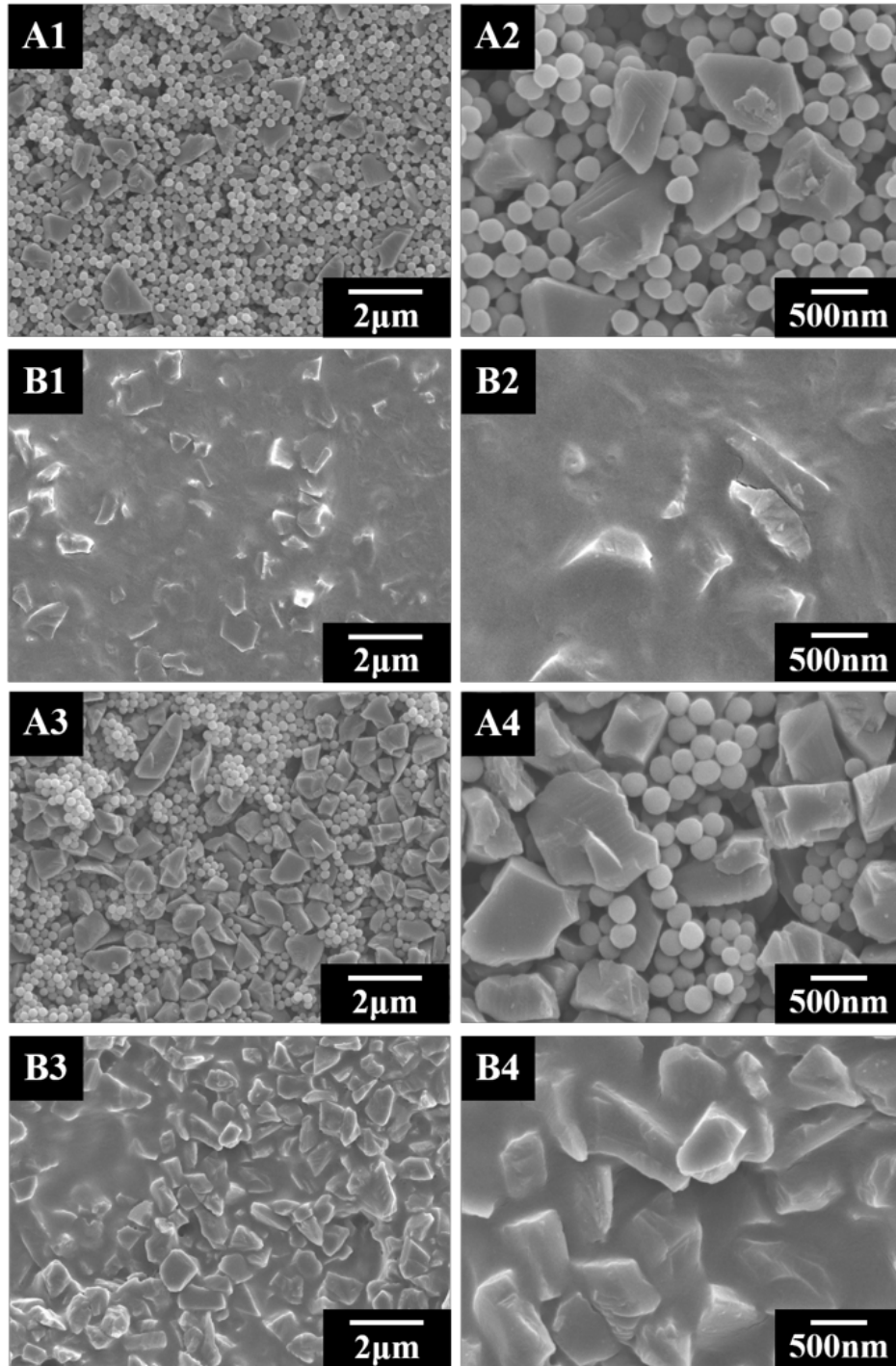


Figure 6.7 SEM images of (A1-A4) as-deposited and (B1-B4) annealed films at (A1, B1, A3, B3) low magnification and (A2, B2, A4, B4) high magnifications for deposition from

10 g·L⁻¹ PVDF suspensions, containing (A1, A2, B1, B2) 1 g·L⁻¹ diamond and (A3, A4, B3, B4) 5 g·L⁻¹ diamond and 1 g·L⁻¹ ChA for deposition voltage of 50 V.

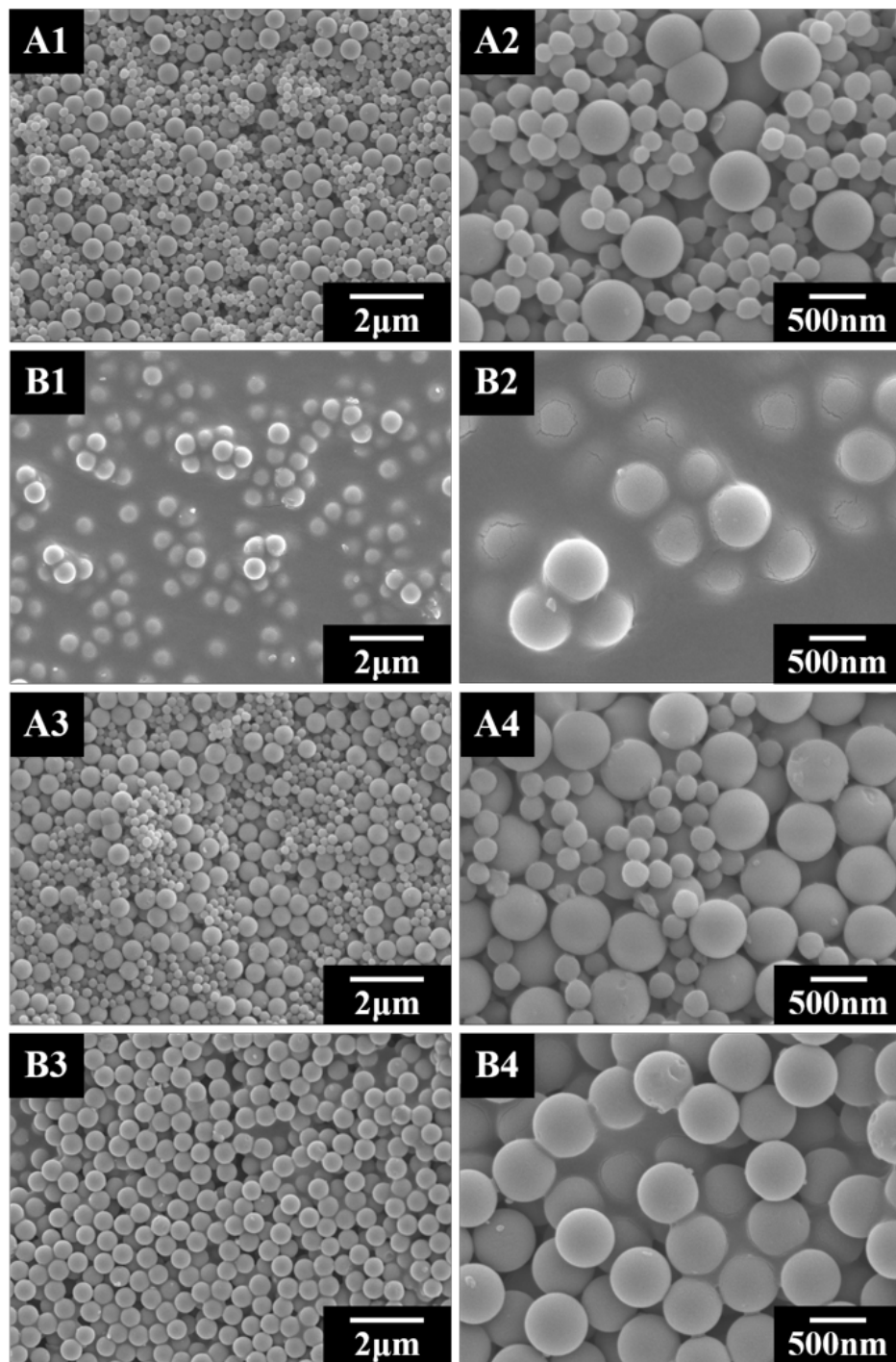


Figure 6.8 SEM images of (A1-A4) as-deposited and (B1-B4) annealed films at (A1, B1, A3, B3) low magnification and (A2, B2, A4, B4) high magnifications for deposition from $10 \text{ g}\cdot\text{L}^{-1}$ PVDF suspensions, containing (A1, A2, B1, B2) $1 \text{ g}\cdot\text{L}^{-1}$ silica and (A3, A4, B3, B4) $5 \text{ g}\cdot\text{L}^{-1}$ silica and $1 \text{ g}\cdot\text{L}^{-1}$ ChA for deposition voltage of 50 V.

6.5 Conclusions

BAs can be used as anionic surfactants for EPD of PVDF films in ethanol solvent. The PVDF deposition yield, obtained using different BAs, increased in the order $\text{LCA} < \text{CDCA} < \text{DCA} < \text{UDCA} < \text{ChA}$. It depends on the number of OH groups and their positions and orientation in the structures of the anionic BAs surfactants. The use of BAs allowed controlled deposition of PVDF films at high deposition rates. Annealed PVDF films provided corrosion protection of stainless steel in 3% NaCl solutions. ChA was used as a co-surfactant for diamond, silica and PVDF particles and allowed for the deposition of PVDF-diamond and PVDF silica films of controlled composition. The biomimetic approach developed in this investigation opens a new strategy for the chemical modification and charging of electrically neutral hydrophobic materials and deposition of functional polymers and composites by EPD from colloidal suspensions.

6.6 Acknowledgments

This research was funded by the Natural Sciences and Engineering Research Council of Canada, grant number RGPIN-2018-04014. SEM investigations were performed at the Canadian Centre for Electron Microscopy.

6.7 References

- [1] C. Ribeiro *et al.*, "Electroactive poly (vinylidene fluoride)-based structures for advanced applications," vol. 13, no. 4, pp. 681-704, 2018.
- [2] B. Ji-Hun and C. Seung-Hwan, "PVDF-based ferroelectric polymers and dielectric elastomers for sensor and actuator applications: a review," *Functional Composites and Structures*, vol. 1, no. 1, p. 012003 (19 pp.), 03/ 2019.
- [3] J. Inderherbergh, "Polyvinylidene fluoride (PVDF) appearance, general properties and processing," *Ferroelectrics*, vol. 115, no. 4, pp. 295-302, 1991.
- [4] J. Zhong *et al.*, "Modulation of the interfacial architecture enhancing the efficiency and energy density of ferroelectric nanocomposites via the irradiation method," *Journal of Colloid and Interface Science*, vol. 586, pp. 30-38, 2021/03/15/ 2021.
- [5] S. K. Gupta, C. Hernandez, J. P. Zuniga, K. Lozano, and Y. Mao, "Luminescent PVDF nanocomposite films and fibers encapsulated with La 2 Hf 2 O 7: Eu 3+ nanoparticles," *SN Applied Sciences*, vol. 2, no. 4, pp. 1-11, 2020.
- [6] Y. Wang *et al.*, "A renewable low-frequency acoustic energy harvesting noise barrier for high-speed railways using a Helmholtz resonator and a PVDF film," *Applied Energy*, vol. 230, pp. 52-61, 2018.
- [7] P. Hu, L. Yan, C. Zhao, Y. Zhang, and J. Niu, "Double-layer structured PVDF nanocomposite film designed for flexible nanogenerator exhibiting enhanced piezoelectric output and mechanical property," *Composites Science and Technology*, vol. 168, pp. 327-335, 2018/11/10/ 2018.
- [8] N. Ghazali, W. J. Basirun, A. Mohammed Nor, and M. R. Johan, "Super-amphiphobic coating system incorporating functionalized nano-Al₂O₃ in polyvinylidene fluoride (PVDF) with enhanced corrosion resistance," *Coatings*, vol. 10, no. 4, p. 387, 2020.
- [9] A. M. Pornea, J. M. C. Puguán, V. G. Deonikar, and H. Kim, "Fabrication of multifunctional wax infused porous PVDF film with switchable temperature response surface and anti corrosion property," *Journal of Industrial and Engineering Chemistry*, vol. 82, pp. 211-219, 2020.
- [10] Y. H. Kim, Y. S. Kwon, M. Y. Shon, and M. J. Moon, "Corrosion protection performance of PVDF/PMMA-blended coatings by electrochemical impedance method," *Journal of Electrochemical Science and Technology*, vol. 9, no. 1, pp. 1-8, 2018.

- [11] J. H. Park, N. Kurra, M. AlMadhoun, I. N. Odeh, and H. N. Alshareef, "A two-step annealing process for enhancing the ferroelectric properties of poly (vinylidene fluoride)(PVDF) devices," *Journal of Materials Chemistry C*, vol. 3, no. 10, pp. 2366-2370, 2015.
- [12] F. S. Foster, K. A. Harasiewicz, and M. D. Sherar, "A history of medical and biological imaging with polyvinylidene fluoride (PVDF) transducers," *IEEE transactions on ultrasonics, ferroelectrics, and frequency control*, vol. 47, no. 6, pp. 1363-1371, 2000.
- [13] G.-d. Kang and Y.-m. Cao, "Application and modification of poly (vinylidene fluoride)(PVDF) membranes—A review," *Journal of membrane science*, vol. 463, pp. 145-165, 2014.
- [14] J. C. Barbosa *et al.*, "Enhanced ionic conductivity in poly(vinylidene fluoride) electrospun separator membranes blended with different ionic liquids for lithium ion batteries," *Journal of Colloid and Interface Science*, vol. 582, pp. 376-386, 2021/01/15/ 2021.
- [15] Y. Cui *et al.*, "Synergistic interaction of Z-scheme 2D/3D g-C₃N₄/BiOI heterojunction and porous PVDF membrane for greatly improving the photodegradation efficiency of tetracycline," *Journal of Colloid and Interface Science*, vol. 586, pp. 335-348, 2021/03/15/ 2021.
- [16] N. Wei *et al.*, "Scalable and low-cost fabrication of hydrophobic PVDF/WS₂ porous membrane for highly efficient solar steam generation," *Journal of Colloid and Interface Science*, vol. 588, pp. 369-377, 2021/04/15/ 2021.
- [17] K. Shi and I. Zhitomirsky, "Electrophoretic nanotechnology of graphene–carbon nanotube and graphene–polypyrrole nanofiber composites for electrochemical supercapacitors," *Journal of Colloid and Interface Science*, vol. 407, pp. 474-481, 2013/10/01/ 2013.
- [18] M. Cheong and I. Zhitomirsky, "Electrophoretic deposition of manganese oxide films," *Surface Engineering*, vol. 25, no. 5, pp. 346-352, Jul 2009.
- [19] M. Fayette, A. Nelson, and R. D. Robinson, "Electrophoretic deposition improves catalytic performance of Co₃O₄ nanoparticles for oxygen reduction/oxygen evolution reactions," *Journal of Materials Chemistry A*, vol. 3, no. 8, pp. 4274-83, 02/28 2015.
- [20] L. Besra and M. Liu, "A review on fundamentals and applications of electrophoretic deposition (EPD)," *Progress in Materials Science*, vol. 52, no. 1, pp. 1-61, Jan 2007.

- [21] O. O. Van der Biest and L. J. Vandeperre, "Electrophoretic deposition of materials," *Annual Review of Materials Science*, vol. 29, no. 1, pp. 327-352, 1999.
- [22] P. Sarkar and P. S. Nicholson, "Electrophoretic deposition (EPD): mechanisms, kinetics, and application to ceramics," *Journal of the American Ceramic Society*, vol. 79, no. 8, pp. 1987-2002, 1996.
- [23] I. Zhitomirsky, "Cathodic electrodeposition of ceramic and organoceramic materials. Fundamental aspects," *Advances in Colloid and Interface Science*, vol. 97, no. 1, pp. 279-317, 2002/03/29/ 2002.
- [24] B. Ferrari and R. Moreno, "EPD kinetics: a review," *Journal of the European Ceramic Society*, vol. 30, no. 5, pp. 1069-1078, 2010.
- [25] I. Deen, X. Pang, and I. Zhitomirsky, "Electrophoretic deposition of composite chitosan-halloysite nanotube-hydroxyapatite films," *Colloids and Surfaces A: Physicochemical and Engineering Aspects*, vol. 410, pp. 38-44, 2012/09/20/ 2012.
- [26] N. A. Kyeremateng, D. Gukte, M. Ferch, J. Buk, T. Hrebicek, and R. Hahn, "Preparation of a Self-Supported SiO₂ Membrane as a Separator for Lithium-Ion Batteries," *Batteries & Supercaps*, vol. 3, no. 5, pp. 456-462, 2020.
- [27] K. Prasanna, T. Subburaj, Y. N. Jo, and C. W. Lee, "Optimization of electrophoretic suspension to fabricate Li [Ni_{1/3}Co_{1/3}Mn_{1/3}] O₂ based positive electrode for Li-ion batteries," *Electrochimica Acta*, vol. 95, pp. 295-300, 2013.
- [28] J. Hagberg *et al.*, "Lithium iron phosphate coated carbon fiber electrodes for structural lithium ion batteries," *Composites Science and Technology*, vol. 162, pp. 235-243, 2018.
- [29] K. Ui, K. OKURA, N. Koura, S. Tsumeda, and K. Tamamitsu, "Fabrication of the electrode for capacitor cell prepared by the electrophoretic deposition method," *Electrochemistry*, vol. 75, no. 8, pp. 604-606, 2007.
- [30] K. T. Lau, M. S. M. Suan, M. Zaimi, J. Abd Razak, M. Azam, and N. Mohamad, "Microstructure And Phase Of Poly (Vinyliden Fluoride) Films By Electrophoretic Deposition: Effect Of Polymer Dispersion's Stirring Conditions," *Journal of Advanced Manufacturing Technology (JAMT)*, vol. 10, no. 2, pp. 57-66, 2016.
- [31] K. T. Lau *et al.*, "Electrophoretic deposition and heat treatment of steel-supported PVDF-graphite composite film," in *Applied Mechanics and Materials*, 2015, vol. 761, pp. 412-416: Trans Tech Publ.

- [32] J. Yin *et al.*, "Fabrication of protective KB/PVdF composite films on stainless steel substrates for PEFCs through electrophoretic deposition," *Journal of the Ceramic Society of Japan*, vol. 116, no. 1350, pp. 201-204, 2008.
- [33] T. He *et al.*, "A solid-electrolyte-reinforced separator through single-step electrophoretic assembly for safe high-capacity lithium ion batteries," *Journal of Power Sources*, vol. 448, p. 227469, 2020.
- [34] Y. Han *et al.*, "Direct electrophoretic deposition of an ultra-strong separator on an anode in a surfactant-free colloidal system for lithium ion batteries," *Journal of Materials Chemistry A*, vol. 7, no. 4, pp. 1410-1417, 2019.
- [35] K. Baker, R. Sikkema, W. Liang, and I. Zhitomirsky, "Multifunctional Properties of Commercial Bile Salts for Advanced Materials Engineering," *Advanced Engineering Materials*, vol. 23, p. 2001261, 2021.
- [36] M. S. Ata, R. Poon, A. M. Syed, J. Milne, and I. Zhitomirsky, "New developments in non-covalent surface modification, dispersion and electrophoretic deposition of carbon nanotubes," *Carbon*, vol. 130, pp. 584-598, 2018.
- [37] K. Baker, R. Sikkema, and I. Zhitomirsky, "Application of bile acids for biomedical devices and sensors," *Medical Devices & Sensors*, vol. 3, no. 6, p. e10119, 2020.
- [38] P. Lepercq *et al.*, "Epimerization of chenodeoxycholic acid to ursodeoxycholic acid by *Clostridium baratii* isolated from human feces," *FEMS microbiology letters*, vol. 235, no. 1, pp. 65-72, 2004.
- [39] S. Paria and K. C. Khilar, "A review on experimental studies of surfactant adsorption at the hydrophilic solid-water interface," *Advances in colloid and interface science*, vol. 110, no. 3, pp. 75-95, 2004.
- [40] M.-X. Hu, J.-N. Li, S.-L. Zhang, L. Li, and Z.-K. Xu, "Hydrophilic modification of PVDF microfiltration membranes by adsorption of facial amphiphile cholic acid," *Colloids and Surfaces B: Biointerfaces*, vol. 123, pp. 809-813, 2014.
- [41] J. M. Roe and B. W. Barry, "Bile salt association (cholate, deoxycholate, chenodeoxycholate, and ursodeoxycholate) and interactions with aromatic alcohols (benzyl, 2-phenylethanol, and 3-phenylpropanol)," *Journal of colloid and interface science*, vol. 107, no. 2, pp. 398-404, 1985.
- [42] Q. Dou and Z. Jiang, "A facile route to ursodeoxycholic acid based on stereocontrolled conversion and aggregation behavior research," *Synthesis*, vol. 48, no. 04, pp. 588-594, 2016.

- [43] I. Zhitomirsky and L. Gal-Or, "Formation of hollow fibers by electrophoretic deposition," *Materials Letters*, vol. 38, no. 1, pp. 10-17, Jan 1999.
- [44] I. Zhitomirsky and A. Petric, "Electrochemical deposition of yttrium oxide," *Journal of Materials Chemistry*, 10.1039/B000311P vol. 10, no. 5, pp. 1215-1218, 2000.
- [45] S. Sodagar, B. Jaleh, P. Fakhri, M. Kashfi, B. F. Mohazzab, and A. Momeni, "Flexible piezoelectric PVDF/NDs nanocomposite films: Improved electroactive properties at low concentration of nanofiller and numerical simulation using finite element method," *Journal of Polymer Research*, vol. 27, no. 8, pp. 1-10, 2020.
- [46] W. Li *et al.*, "High pyroelectric effect in poly (vinylidene fluoride) composites cooperated with diamond nanoparticles," *Materials Letters*, vol. 267, p. 127514, 2020.
- [47] S. A. Haddadi, S. Ghaderi, M. Amini, and S. A. Ramazani, "Mechanical and piezoelectric characterizations of electrospun PVDF-nanosilica fibrous scaffolds for biomedical applications," *Materials Today: Proceedings*, vol. 5, no. 7, pp. 15710-15716, 2018.
- [48] S. A. Haddadi, A. Ramazani SA, S. Talebi, S. Fattahpour, and M. Hasany, "Investigation of the effect of nanosilica on rheological, thermal, mechanical, structural, and piezoelectric properties of poly (vinylidene fluoride) nanofibers fabricated using an electrospinning technique," *Industrial & Engineering Chemistry Research*, vol. 56, no. 44, pp. 12596-12607, 2017.

Chapter 7 Versatile Strategies for EPD of PVDF

Nanocomposites

This chapter is reproduced from **Q. Zhao, X. Liu, S. Veldhuis, I. Zhitomirsky**, *Versatile Strategy for Electrophoretic Deposition of Polyvinylidene Fluoride-Metal Oxide Nanocomposites*, *Materials* 2021, 14, 7902, (<https://doi.org/10.3390/ma14247902>) with permission from Copyright © 1996-2022 MDPI. The author of this thesis is the first author and the main contributor of this publication, including conceiving the initial ideas, development of approach and methodology, carrying out experiments, analysis of data, writing the initial draft and preparation of the manuscript.

7.1 Abstract

Polyvinylidene fluoride (PVDF) is an advanced functional polymer which exhibits excellent chemical and thermal stability, and good mechanical, piezoelectric and ferroelectric properties. This work opens a new strategy for the fabrication of nanocomposites, combining the functional properties of PVDF and advanced inorganic nanomaterials. Electrophoretic deposition (EPD) has been developed for the fabrication of films containing PVDF and nanoparticles of TiO₂, MnO₂ and NiFe₂O₄. An important finding was the feasibility of EPD of electrically neutral PVDF and inorganic nanoparticles using caffeic acid (CA) and catechol violet (CV) as co-dispersants. The experiments revealed strong adsorption of CA and CV on PVDF and inorganic nanoparticles, which

involved different mechanisms and facilitated particle dispersion, charging and deposition. The analysis of the deposition yield data, chemical structure of the dispersants and the microstructure and composition of the films provided an insight into the adsorption and dispersion mechanisms and the influence of deposition conditions on the deposition rate, film microstructure and composition. PVDF films provided the corrosion protection of stainless steel. Overcoming the limitations of other techniques, this investigation demonstrates a conceptually new approach for the fabrication of PVDF-NiFe₂O₄ films, which showed superparamagnetic properties. The approach developed in this investigation offers versatile strategies for the EPD of advanced organic-inorganic nanocomposites.

7.2 Introduction

Poly (vinylidene fluoride) (PVDF) is an advanced functional polymer, which has outstanding chemical resistance, thermal stability, mechanical strength, piezoelectric and ferroelectric properties [1-6]. Significant interest has been generated in the fabrication of advanced nanocomposites, combining functional properties of PVDF and inorganic nanomaterials [7]. Flexible PVDF-MnO₂ nanocomposites showed enhanced piezoelectric and mechanical properties [8]. Moreover, such nanocomposites are of particular interest for energy storage applications [9] due to the outstanding pseudocapacitive properties of MnO₂. PVDF-TiO₂ nanocomposites have been developed [10] for application in separation membranes, which showed enhanced fouling resistance. Ferrimagnetic NiFe₂O₄ nanoparticles were added to PVDF [11] in order to obtain composites, combining the

ferroelectric and piezoelectric properties of PVDF and the magnetic properties of NiFe₂O₄. The addition of NiFe₂O₄ nanoparticles resulted in enhanced formation of ferroelectric β phase of PVDF [12]. Nanocomposites of PVDF and NiFe₂O₄ showed magnetoelectric properties, which were analyzed by investigating the influence of the magnetic field on ferroelectric properties [13]. Many applications of PVDF-metal oxide nanocomposites involved the use of films and significant attention has been focused on the development of film deposition techniques. The combination of organic and inorganic materials in composites offers a possibility of fabricating multifunctional materials with advanced properties [14-16].

Colloidal film deposition techniques are of particular interest for nanotechnology of composites due to the possibility of composite design on the nanometric scale. Currently, there are several methods which are commonly used for the fabrication of PVDF films: solvent casting, spin coating, and electrospinning [17]. Such techniques are based on the use of PVDF solutions. PVDF dissolves in a few non-ecofriendly organic solvents such as dimethylformamide, dimethyl sulfoxide, N-methyl pyrrolidone or dimethylacetamide, and there is a significant interest in replacing such solvents with more environmentally friendly solvents.

Electrochemical deposition methods are very promising for the deposition of PVDF and composite films. Various electrochemical strategies have been utilized for the fabrication of polymer-metal oxide nanocomposites [18, 19]. Electrophoretic deposition (EPD) is a colloidal technique, which offers advantages for the deposition of nanocomposites due to

high deposition rate, simple control of film thickness, and uniformity [20-26]. This technique is especially important for the deposition of nanoparticles as uniform monolayers or multilayers on substrates of complex shape [27]. Several previous investigations reported the EPD of pure PVDF films in different organic solvents without the use of surfactants [28-30]. It should be noted that PVDF is an electrically neutral polymer, and the use of charged surfactants facilitates the control of particle charge and EPD yield. Co-surfactants are highly desired for the co-deposition of PVDF with inorganic nanoparticles. Inorganic nanoparticles are prone to forming agglomerates due to their high surface energy. It is challenging to disperse magnetic nanoparticles due to their magnetic interactions, which promote agglomeration. In a previous investigation [31], bile salts were used as charged surfactants for PVDF. However, bile salts show poor adsorption on metal oxide surfaces and their applications for EPD of PVDF-metal oxide films present difficulties. The EPD of metal oxide nanoparticles requires the use of efficient surfactants with a very small size and strong adsorption on the particle surface. It is challenging to develop co-dispersants with strong adsorption on metal oxide nanoparticles and hydrophobic PVDF particles. In our investigation we addressed this problem using a biomimetic strategy, which is based on the use of catecholate-type molecules as dispersants.

The goal of this investigation was the fabrication of PVDF-metal oxide films by EPD using chelating catecholate molecules as co-dispersants for PVDF and metal oxide nanoparticles. Due to significant interest in the fabrication of PVDF composites containing MnO_2 , TiO_2 and NiFe_2O_4 nanoparticles, we selected such nanomaterials as model metal oxides of

different types for the feasibility studies, which showed the versatility of our approach. The biomimetic approach of our investigation was based on the analysis of the mechanism of mussel protein adhesion to different surfaces, which involves the super-strong catecholate type bonding to inorganic surfaces. The investigations of deposition efficiency provided an insight into the influence of the chemical structure of the dispersant molecules and charged groups on their adsorption on PVDF and metal oxide nanoparticles and related adsorption mechanisms. We demonstrate the feasibility of deposition of nanocomposite films using ethanol as a non-toxic solvent and report valuable properties of the deposited films, such as corrosion protection and superparamagnetic properties. Following the work objective we investigated the microstructure, composition, and properties of the films deposited at different conditions.

7.3 Experimental Procedures

7.3.1 Materials

Poly (vinylidene fluoride) (PVDF) and catechol violet (CV) were purchased from Alfa Aesar (Haverhill, MA, US). Caffeic acid (CA), titanium oxide (TiO₂, 21 nm) nanopowder, iron nickel oxide (NiFe₂O₄, < 50 nm) nanopowder, and KMnO₄ were purchased from Aldrich (St. Louis, MO, US). Nanoparticles of MnO₂ with an average size of 50 nm were prepared by a chemical reduction of KMnO₄ aqueous solutions with ethanol, as was described in the previous investigation [32]. The nanoparticles prepared by this method were amorphous [32].

7.3.2 Film deposition

PVDF particles were dispersed in pure ethanol using CA or CV dispersants. The concentration of PVDF was 5-10 g·L⁻¹. The concentration of CA or CV was 0.2-1 g·L⁻¹. TiO₂, MnO₂, and NiFe₂O₄ were added for the fabrication of composite films, and their concentrations were 1-3 g·L⁻¹. EPD was performed using these suspensions after ultrasonication and stirring. A stainless-steel substrate (304 type, 20×30×0.1 mm³) and a platinum sheet (20×30×0.1 mm³) served as a working electrode and counter electrode, respectively, with 15 mm separation in electrochemical deposition cell for EPD. A deposition voltage of 20-100 V was applied for 5 min. EPD resulted in the accumulation of particles at the substrate surface. The films were dried at room temperature and then annealed at 200 °C for 1 h. The annealing process was essential for the formation of dense films.

7.3.3 Characterization

Zeta-potential measurements were performed using the mass transport method [33]. Electrochemical studies were performed in 3% aqueous NaCl solution using a potentiostat (PARSTAT 2273, Princeton Applied Research, Oak Ridge, TN, US) and a 3-electrode cell with coated or uncoated stainless steel as a working electrode, a platinum counter electrode, and a saturated calomel electrode (SCE) as a reference electrode. Potentiodynamic studies were conducted at a sweeping rate of 1 mV·s⁻¹ from the negative to positive direction and obtained data was presented in Tafel plots. Electrochemical impedance spectroscopy (EIS)

studies were performed under a sinusoidal excitation voltage of 10 mV in the frequency range of 10 mHz-10 kHz. A JEOL JSM-7000 F microscope (Tokyo, Japan) was used for scanning electron microscopy (SEM) investigations. Talos 200 X microscope (Waltham, MA, USA) was used for transmission electron microscopy (TEM) studies. FTIR studies were performed using a Bruker Vertex 70 spectrometer (Billerica, MA, US). X-ray diffraction (XRD) was carried out using a Nicolet I2 powder diffractometer with monochromatized Co K α radiation. Magnetic measurements were conducted using a Quantum Design PPMS-9 system (San Diego, CA, US).

7.4 Results and Discussion

TEM investigations showed that as-received PVDF particles were of spherical shape with a diameter of about 200 nm (Figure S7.1). A significant challenge in the EPD of PVDF is obtaining stable suspensions of charged PVDF particles. This can be achieved using efficient dispersants, which must be adsorbed on the particle surface to impart colloidal stability and electric charge. Difficulties are related to poor adsorption of traditional dispersants on the surface of chemically inert electrically neutral hydrophobic PVDF particles. Another challenge is to find co-dispersants suitable for the co-dispersion of PVDF with metal oxide nanoparticles. Previous investigations showed that mutual repulsion of charged particles or polymer macromolecules at the electrode surface can prevent their deposition [19]. Particle coagulation and deposit formation at the electrode surface are

influenced by the properties of the dispersant and local pH changes at the electrode [19]. Such challenges were addressed using CV and CA as dispersants (Figure 7.1).

The chemical structures of CV and CA contain a catechol group with two phenolic OH groups bonded to adjacent carbon atoms of the aromatic ring. The catechol molecules were chosen due to the ability of catechol bonding to metal atoms on material surfaces [34]. The interest in dispersant with catechol anchoring groups resulted from the investigation of mechanism of mussel protein adsorption on rock surfaces in sea water [34]. The catechol adsorption involves two phenolic OH groups. Various bonding mechanisms are based on bidentate bridging or chelating bonding in the inner sphere or outer sphere modes [34].

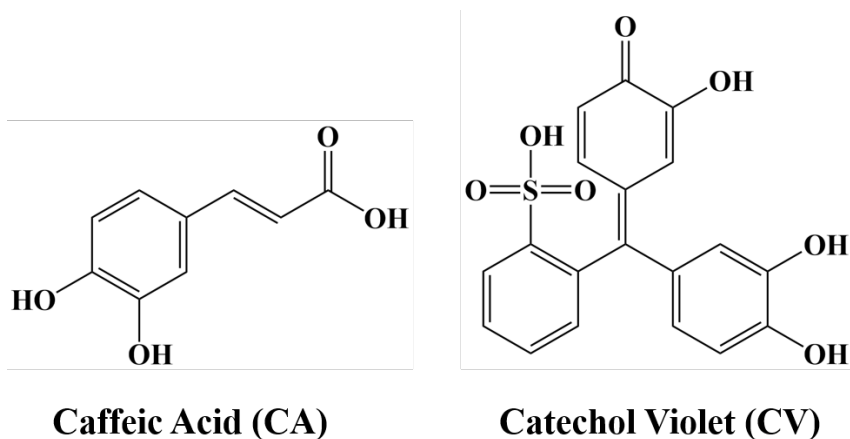


Figure 7.1 Chemical structures of dispersants.

The catechol adsorption on different surfaces is influenced by solvents, the nature of the surface atoms, and the chemical structure of the material. CA is a monoaromatic molecule,

whereas the chemical structure of CV contains three aromatic groups. The anionic properties of CA and CV are related to their COOH and SO₃H groups, respectively.

In this investigation, CA and CV were used as dispersing and charging agents for EPD of PVDF powder from its suspension in ethanol. PVDF suspensions in ethanol were unstable and quick sedimentation was unavoidable even with ultrasonic treatment or stirring. No deposition was achieved from pure PVDF suspension because PVDF powder is electrically neutral. The addition of CA and CV molecules resulted in improved stability of PVDF suspensions by electrostatic stabilization, and anodic films were deposited by EPD. It was hypothesized that CA or CV molecules dissociated in ethanol, adsorbed on PVDF particles, and their deprotonated anionic groups imparted a negative charge to the PVDF particles. As a result, the negatively charged PVDF particles were deposited anodically from the suspensions containing catecholate molecules as additives. The deposition yield measurements indicated that the film mass increased significantly with increasing concentration of PVDF powder (Figure 7.2A). The PVDF particles in 10 g·L⁻¹ PVDF suspensions, containing 0.5 g·L⁻¹ CA and 0.5 g·L⁻¹ CV showed zeta potentials of -11 mV and -26 mV, respectively.

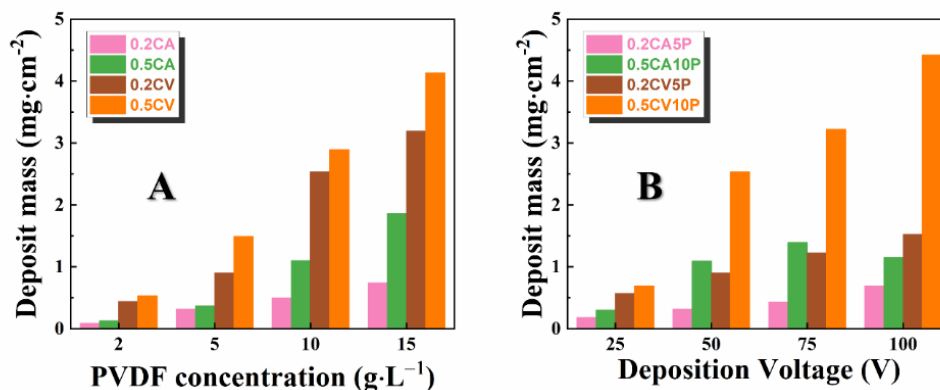


Figure 7.2 (A) Deposit mass versus PVDF concentration for suspensions, containing 0.2 g·L⁻¹ CA (0.2CA), 0.5 g·L⁻¹ CA (0.5CA), 0.2 g·L⁻¹ CV (0.2CV), 0.5 g·L⁻¹ CV (0.5 CV) at a deposition voltage of 50 V and a deposition time of 5 min and (B) deposit mass versus deposition voltage for suspensions containing 0.2 g·L⁻¹ CA and 5 g·L⁻¹ PVDF (0.2CA5P); 0.5 g·L⁻¹ CA and 10 g·L⁻¹ PVDF (0.5CA10P); 0.2 g·L⁻¹ CV and 5 g·L⁻¹ PVDF (0.2CV5P); and 0.5 g·L⁻¹ CV and 10 g·L⁻¹ PVDF (0.5CV10P) for deposition time of 5 min.

CA and CV catechol molecules showed sufficient charging and dispersing effects in a wide range of PVDF concentrations. The PVDF films produced with CV had higher deposit mass than that with CA, which indicated that CV allowed higher deposition efficiency than CA. It was suggested that adsorption of CA and CV molecules on PVDF particles involved hydrophobic interactions of the aromatic rings of the molecules with hydrophobic PVDF surfaces. The larger number of aromatic rings in the CV structure resulted in stronger interactions, which allowed for better adsorption CV and enhanced PVDF dispersion and charging. Figure 7.2B shows deposit mass versus deposition voltage dependencies. The deposit mass presented increasing trends with increasing deposition voltage, indicating higher efficiency of particles motion and packing on the substrates. Therefore, the mass of

the deposited PVDF films can be varied and controlled by EPD bath composition and deposition voltage.

Morphologies of the as-deposited and heat-treated PVDF films fabricated using CA and CV were analyzed by SEM. Figure 7.3 (A, B) shows that the as-deposited spherical PVDF powder was relatively densely packed on the stainless steel 304 substrates, offering good coverage of the substrates. However, there were still some nanosized voids between the PVDF spheres. After heat treatment at the temperature right above the melting point of PVDF for 1 h, PVDF spherical particles were completely melted and re-solidified into uniform and crack-free films (Figure 7.3 (C, D)).

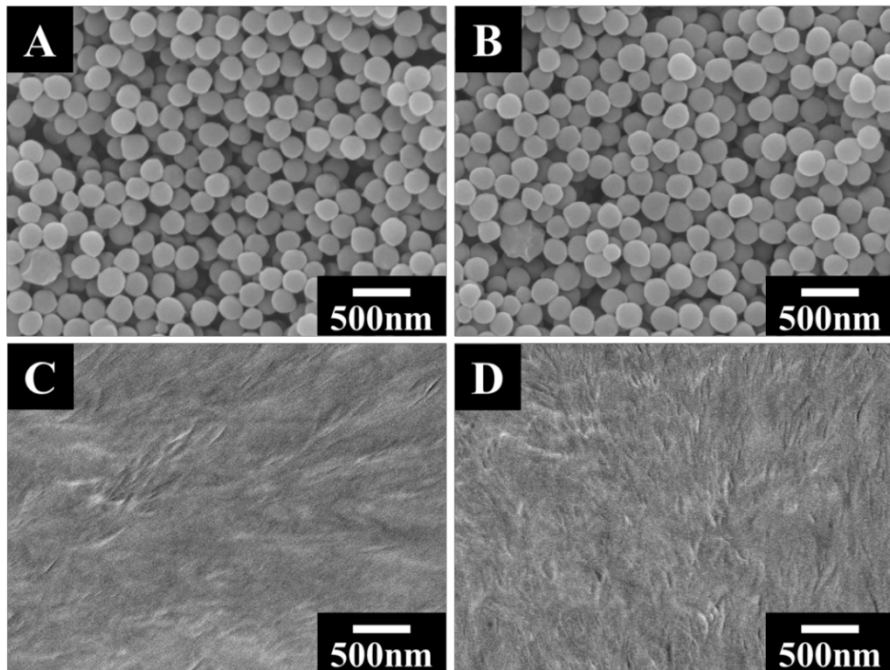


Figure 7.3 SEM images of films at different magnifications prepared from suspensions containing $10 \text{ g}\cdot\text{L}^{-1}$ PVDF with **(A, C)** $0.5 \text{ g}\cdot\text{L}^{-1}$ CA or **(B, D)** $0.5 \text{ g}\cdot\text{L}^{-1}$ CV at a deposition voltage of 50 V for 5 min; **(A, B)** as-deposited and **(C, D)** annealed at $200 \text{ }^\circ\text{C}$.

The as-deposited PVDF films prepared using CA and CV were also analyzed by FTIR (Figure 7.4). Several previous investigations showed that aromatic dispersants can be deposited by EPD to form particles of different shapes at the substrate surface [25, 35, 36]. Therefore, FTIR studies were used to confirm the deposition of PTFE. The FTIR data of as-received PVDF showed strong absorptions at 1399 , 1179 , and 873 cm^{-1} . The absorption at 1399 cm^{-1} resulted from wagging of CH_2 and antisymmetric stretching of C-C bonds [37]. The bands at 1179 and 873 cm^{-1} were associated with the stretching and rocking of the CF_2 bonds [37, 38]. Those absorptions were also achieved for deposited PVDF films using CA or CV, which confirmed successful deposition of PVDF.

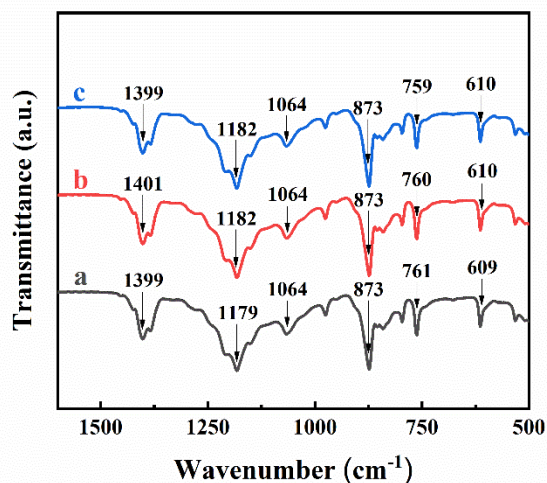


Figure 7.4 FTIR spectra of (a) as-received PVDF and (b, c) as-deposited PVDF, prepared from $0.5 \text{ g}\cdot\text{L}^{-1}$ (b) CA or (c) CV solution containing $10 \text{ g}\cdot\text{L}^{-1}$ PVDF at a deposition voltage of 50 V during 5 min.

The heat-treated PVDF films were studied for corrosion protection of stainless steel in 3% NaCl solutions by potentiodynamic analysis and electrochemical impedance spectroscopy. It was found that the annealed films offered corrosion protection of stainless steel (304-type) substrates. Testing results were presented in Tafel plots (Figure 7.5). Compared to the bare substrates, the coated samples showed significantly higher corrosion potential and lower anodic current (Figure 7.5). The calculated corrosion currents of coated samples were $0.17 \mu\text{A}\cdot\text{cm}^{-2}$ and $0.083 \mu\text{A}\cdot\text{cm}^{-2}$, for films prepared using CA and CV, respectively at a deposition voltage of 50 V and deposition duration of 5 min. The lower corrosion currents for the films, prepared using CV can result from higher film mass (Figure 7.2). The corrosion currents decreased significantly compared to that of uncoated samples ($2.6 \mu\text{A}\cdot\text{cm}^{-2}$). The PVDF-coated sample prepared using CV showed an even lower corrosion current than that prepared using CA. Bode plots in Figure 7.6 showed enhanced absolute impedance in a wide frequency range for coated samples. This indicated that annealed PVDF films acted as barriers for the corrosive electrolyte diffusion to the substrate, insulating the substrates from corrosion damage.

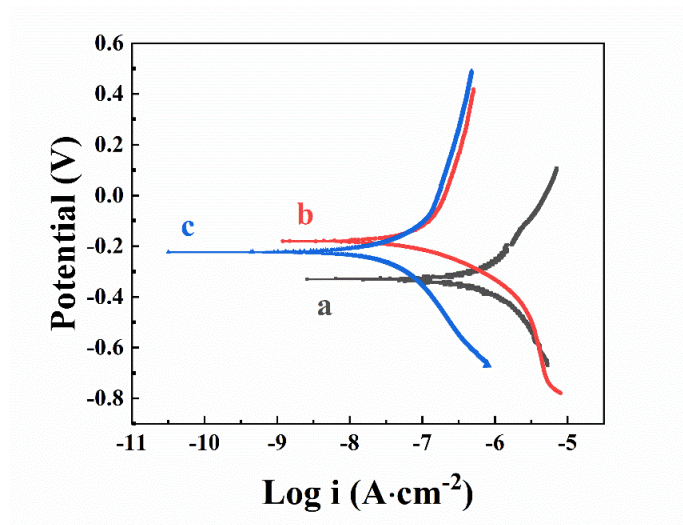


Figure 7.5 Tafel plots for stainless steel (a) uncoated and (b, c) coated from $0.5 \text{ g}\cdot\text{L}^{-1}$ (b) CA or (c) CV solutions, containing $10 \text{ g}\cdot\text{L}^{-1}$ PVDF at a deposition voltage of 50 V during 5 min and annealed at $200 \text{ }^\circ\text{C}$ for 1 hour.

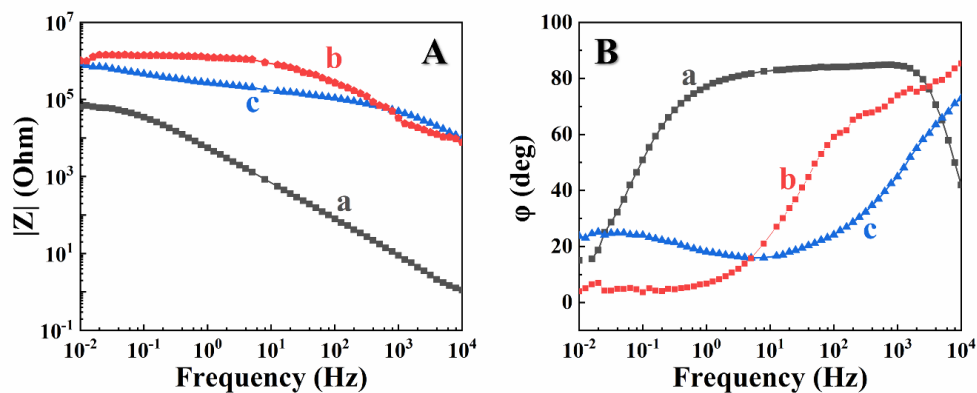


Figure 7.6 (A) Absolute impedance and (B) Phase versus frequency impedance data for stainless steel (a) uncoated and (b, c) coated from $0.5 \text{ g}\cdot\text{L}^{-1}$ (b) CA or (c) CV solutions, containing $10 \text{ g}\cdot\text{L}^{-1}$ PVDF at a deposition voltage of 50 V during 5 min and annealed at $200 \text{ }^\circ\text{C}$ for 1 hour.

The feasibility of EPD of PVDF using CA and CV as surfactants paved the way for the fabrication of nanocomposites, containing functional metal oxide nanoparticles. Following the objective of this investigation, we used MnO_2 , TiO_2 , and NiFe_2O_4 nanoparticles as model metal oxide materials with advanced functionality for the fabrication of composite films. The use of CA and CV for EPD was based on different structural features of the dispersants, which facilitated their adsorption on PVDF or metal oxides. As pointed out above, the aromatic rings of the dispersant molecules facilitated their adsorption on PVDF. However, catecholate type bonding [34] involving phenolic OH groups is beneficial for adsorption on metal oxide nanoparticles. Co-deposition experiments were focused on the use of CA or CV as co-dispersants. The SEM images of the as-deposited films showed co-deposited PVDF and metal oxide nanoparticles (Figure 7.7 (A-C)). Annealing of as-deposited films caused the melting of PVDF particles and the formation of crack-free continuous PVDF matrix layers with imbedded nanoparticles (Figure 7.7 (D-F)).

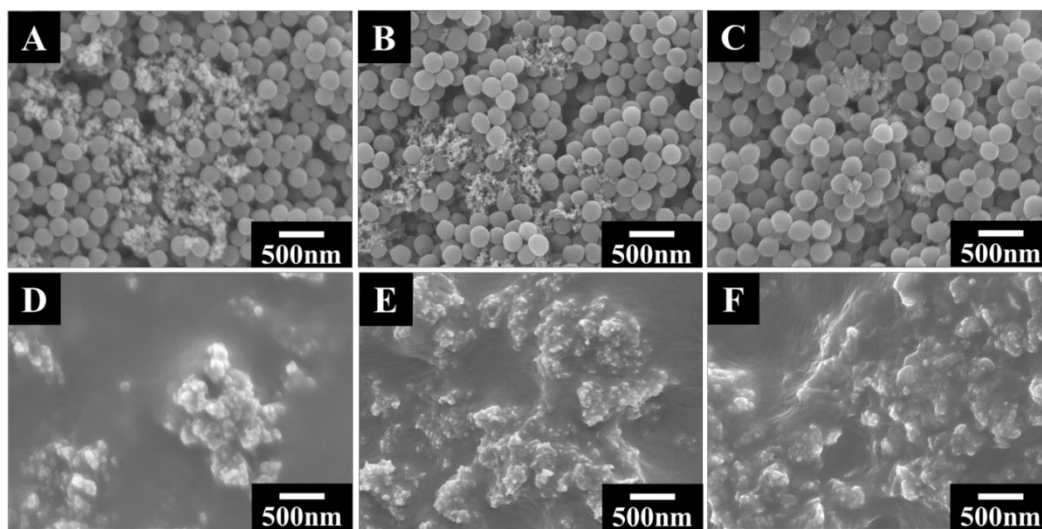


Figure 7.7 SEM images of films, prepared from $5 \text{ g}\cdot\text{L}^{-1}$ PVDF solutions, containing **(A, D)** $1 \text{ g}\cdot\text{L}^{-1}$ CA and $1 \text{ g}\cdot\text{L}^{-1}$ MnO_2 , **(B, E)** $1 \text{ g}\cdot\text{L}^{-1}$ CV and $1 \text{ g}\cdot\text{L}^{-1}$ TiO_2 , **(C, F)** $1 \text{ g}\cdot\text{L}^{-1}$ CV and $1 \text{ g}\cdot\text{L}^{-1}$ NiFe_2O_4 at a deposition voltage of 50 V and **(D, E, F)** annealed at $200 \text{ }^\circ\text{C}$ for 1 hour.

The SEM images of the annealed films showed agglomeration of the oxide particles (Figure 7.7 (D-F) and Supplementary materials, Figure S7.2 (A-C)). The typical size of the agglomerates was in the range of 200-600 nm. Such agglomeration can result from different factors, such as discharge of the particles at the electrode surface and their reduced electrostatic repulsion, hydrophobic interactions between polymer macromolecules, hydrophilic interactions of the inorganic particles, and magnetic interactions of ferrimagnetic NiFe_2O_4 particles. The composite films, containing PVDF and metal oxide nanoparticles were studied by X-ray diffraction method (Figure 7.8).

The X-ray diffraction peaks of PVDF (corresponding to JCPDS file 00-061-1403) were observed in X-ray diffraction patterns of pure PVDF (Figure 7.8a) and composite films (Figure 7.8 (b-d)). The composite films prepared from suspensions containing TiO_2 showed XRD peaks of the anatase phase of TiO_2 (JCPDS file 00-064-0863) and very small peaks of the rutile TiO_2 phase (04-003-0648). The synthesis method [32] used in this investigation allowed for the formation of amorphous MnO_2 . As a result, the X-ray diffraction pattern of the composite PVDF- MnO_2 films showed peaks of PVDF and a broad halo related to the amorphous MnO_2 phase. X-ray diffraction studies of PVDF- NiFe_2O_4 films showed peaks of NiFe_2O_4 corresponding to JCPDS file 00-054-0964 in addition to peaks of PVDF.

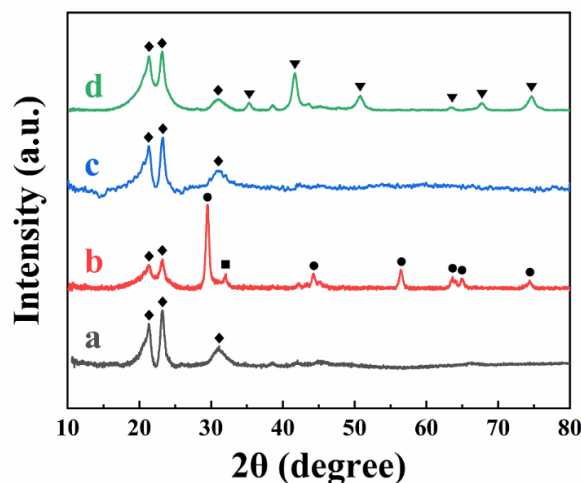


Figure 7.8 X-ray diffraction pattern of films (a) pure PVDF, (b) PVDF and TiO₂, (c) PVDF and MnO₂, and (d) PVDF and NiFe₂O₄ (peaks corresponding to ♦ JCPDS file 00-061-1403, ● JCPDS file 00-064-0863, ■ JCPDS file 04-003-0648, ▼ JCPDS file 00-054-0964). EPD conditions are similar to Figure 7.7.

The results of this investigation showed the feasibility of co-deposition of PVDF with nanoparticles of TiO₂, MnO₂, and NiFe₂O₄. As pointed out in Introduction, the investigation of nanocomposites containing such metal oxide nanoparticles is important for various applications. As a step in this direction, we investigated the magnetic properties of PVDF-NiFe₂O₄ nanocomposites. Figure 7.9a shows that as-received NiFe₂O₄ particles exhibit a superparamagnetic behavior, as indicated by the S-shaped dependence of magnetization on magnetic field. The composite materials showed a similar dependence with reduced mass normalized magnetization (Figure 7.9b). Therefore, the EPD method allows fabrication of nanocomposites, combining the magnetic properties of NiFe₂O₄ with the inherent

functional properties of PVDF, such as piezoelectric, ferroelectric, corrosion protection, and other properties.

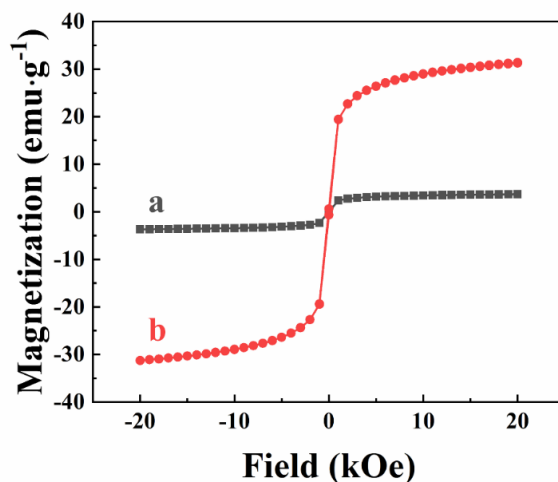


Figure 7.9 Magnetization versus magnetic field for (a) as received NiFe_2O_4 nanoparticles and (b) PVDF- NiFe_2O_4 composites prepared from $5 \text{ g}\cdot\text{L}^{-1}$ PVDF solutions containing $1 \text{ g}\cdot\text{L}^{-1}$ CV and $1 \text{ g}\cdot\text{L}^{-1}$ NiFe_2O_4 at a deposition voltage of 50 V.

7.5 Conclusions

An EPD method has been developed for the deposition of PVDF and composite films containing nanoparticles of TiO_2 , MnO_2 , NiFe_2O_4 , which were used as model materials with advanced functionality for the deposition of the organic-inorganic nanocomposites by the EPD method. It was found that CA and CV adsorbed on chemically inert, electrically neutral PVDF, providing dispersion and charging of the PVDF particles. The dispersant adsorption was a key factor for the successful EPD of the PVDF films. The deposition yield measurements showed that the amount of the deposited material can be controlled by the

PVDF concentration in the suspensions, the deposition voltage, and the concentration of selected dispersant. The results of the potentiodynamic and impedance spectroscopy studies showed that PVDF films provided corrosion protection of stainless-steel substrates. The adsorption of CA and CV on the PVDF particles involved hydrophobic interactions, whereas the catecholate-type bonding facilitated their adsorption on the metal oxide nanoparticles. The unique ability of CA and CV to adsorb on different materials was a key factor for their use as co-dispersants for the EPD of nanocomposites. The co-deposition of PVDF with metal oxides was confirmed by the results of SEM, FTIR, and XRD studies. The ability to combine the functional properties of PVDF with the functional properties of metal oxides was demonstrated by the investigation of PVDF-NiFe₂O₄ films, which showed superparamagnetic properties. The approach developed in this investigation paves the way for the EPD of other chemically inert, electrically neutral polymers and their co-deposition with inorganic materials for the fabrication of novel nanocomposites with advanced functionality.

7.6 Acknowledgments

SEM investigations were performed at the Canadian Centre for Electron Microscopy. This research was funded by the Natural Sciences and Engineering Research Council of Canada grant number RGPIN-2018-04014.

7.7 Supplementary Data

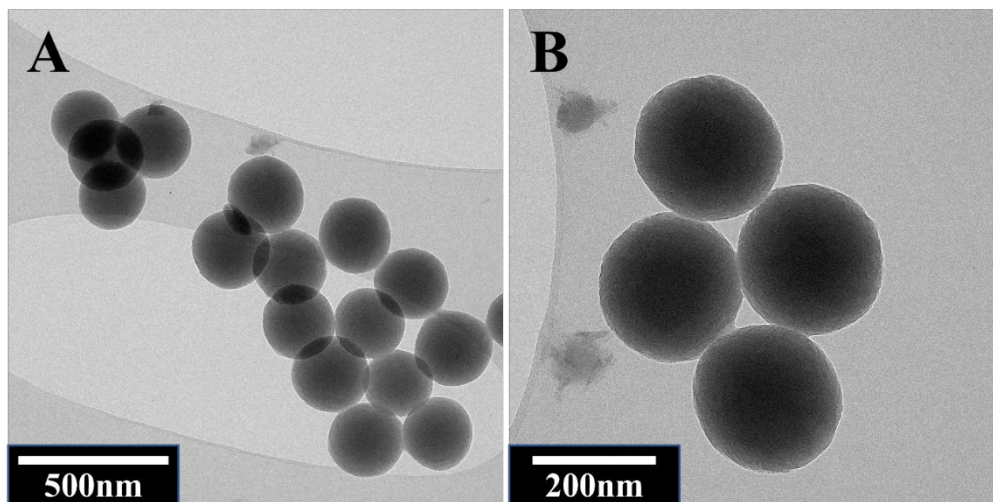


Figure S7.1 TEM images of as received PVDF particles.

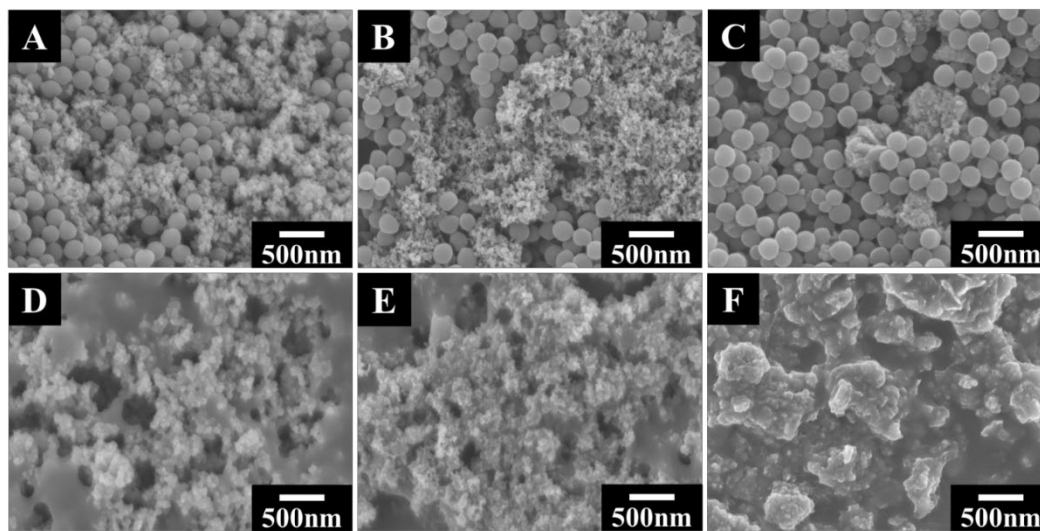


Figure S7.2 SEM images of annealed composite films.

7.8 References

- [1] C. Ribeiro *et al.*, "Electroactive poly (vinylidene fluoride)-based structures for advanced applications," *Nature protocols*, vol. 13, no. 4, pp. 681-704, 2018.
- [2] J.-H. Bae and S.-H. Chang, "PVDF-based ferroelectric polymers and dielectric elastomers for sensor and actuator applications: a review," *Functional Composites and Structures*, vol. 1, no. 1, p. 012003, 2019.
- [3] J. Inderherbergh, "Polyvinylidene fluoride (PVDF) appearance, general properties and processing," *Ferroelectrics*, vol. 115, no. 4, pp. 295-302, 1991.
- [4] J. Zhong *et al.*, "Modulation of the interfacial architecture enhancing the efficiency and energy density of ferroelectric nanocomposites via the irradiation method," *Journal of Colloid and Interface Science*, vol. 586, pp. 30-38, 2021.
- [5] L. Lu, W. Ding, J. Liu, and B. Yang, "Flexible PVDF based piezoelectric nanogenerators," *Nano Energy*, p. 105251, 2020.
- [6] N. Chamankar, R. Khajavi, A. A. Yousefi, A. Rashidi, and F. Golestanifard, "A flexible piezoelectric pressure sensor based on PVDF nanocomposite fibers doped with PZT particles for energy harvesting applications," *Ceramics International*, vol. 46, no. 12, pp. 19669-19681, 2020.
- [7] N. Ghazali, W. J. Basirun, A. Mohammed Nor, and M. R. Johan, "Super-amphiphobic coating system incorporating functionalized nano-Al₂O₃ in polyvinylidene fluoride (PVDF) with enhanced corrosion resistance," *Coatings*, vol. 10, no. 4, p. 387, 2020.
- [8] Q. Zhao *et al.*, "Flexible textured MnO₂ nanorods/PVDF hybrid films with superior piezoelectric performance for energy harvesting application," *Composites Science and Technology*, vol. 199, p. 108330, 2020.
- [9] Q. Zhao *et al.*, "Ultra-high discharged energy density in PVDF based composites through inducing MnO₂ particles with optimized geometric structure," *Nano Energy*, vol. 65, p. 104007, 2019.
- [10] S. J. Oh, N. Kim, and Y. T. Lee, "Preparation and characterization of PVDF/TiO₂ organic-inorganic composite membranes for fouling resistance improvement," *Journal of Membrane Science*, vol. 345, no. 1-2, pp. 13-20, 2009.

- [11] T. Prabhakaran and J. Hemalatha, "Magnetoelectric investigations on poly (vinylidene fluoride)/NiFe₂O₄ flexible films fabricated through a solution casting method," *RSC advances*, vol. 6, no. 90, pp. 86880-86888, 2016.
- [12] E. Botero, J. Nobrega, and D. Trombini, "Influence of NiFe₂O₄ on β phase formation in PVDF composites," *Material Sci & Eng*, vol. 4, no. 3, pp. 83-86, 2020.
- [13] P. D. Prasad and J. Hemalatha, "Energy harvesting performance of magnetoelectric poly (vinylidene fluoride)/NiFe₂O₄ nanofiber films," *Journal of Magnetism and Magnetic Materials*, vol. 532, p. 167986, 2021.
- [14] M. Rehan, A. A. Nada, T. A. Khattab, N. A. Abdelwahed, and A. A. Abou El-Kheir, "Development of multifunctional polyacrylonitrile/silver nanocomposite films: Antimicrobial activity, catalytic activity, electrical conductivity, UV protection and SERS-active sensor," *Journal of Materials Research and Technology*, vol. 9, no. 4, pp. 9380-9394, 2020.
- [15] D. Huang *et al.*, "Graphitic carbon nitride-based heterojunction photoactive nanocomposites: applications and mechanism insight," *ACS applied materials & interfaces*, vol. 10, no. 25, pp. 21035-21055, 2018.
- [16] S. Choi, S. I. Han, D. Kim, T. Hyeon, and D.-H. Kim, "High-performance stretchable conductive nanocomposites: materials, processes, and device applications," *Chemical Society Reviews*, vol. 48, no. 6, pp. 1566-1595, 2019.
- [17] S. Guo, X. Duan, M. Xie, K. C. Aw, and Q. Xue, "Composites, fabrication and application of polyvinylidene fluoride for flexible electromechanical devices: A review," *Micromachines*, vol. 11, no. 12, p. 1076, 2020.
- [18] I. Zhitomirsky and A. Petric, "Electrochemical deposition of yttrium oxide," *Journal of Materials Chemistry*, 10.1039/B000311P vol. 10, no. 5, pp. 1215-1218, 2000.
- [19] I. Zhitomirsky, "Cathodic electrodeposition of ceramic and organoceramic materials. Fundamental aspects," *Advances in colloid and interface science*, vol. 97, no. 1-3, pp. 279-317, 2002.
- [20] A. Singh, N. J. English, and K. M. Ryan, "Highly ordered nanorod assemblies extending over device scale areas and in controlled multilayers by electrophoretic deposition," *The Journal of Physical Chemistry B*, vol. 117, no. 6, pp. 1608-1615, 2013.

- [21] F. Smeacetto *et al.*, "Electrophoretic deposition of Mn_{1.5}Co_{1.5}O₄ on metallic interconnect and interaction with glass-ceramic sealant for solid oxide fuel cells application," *Journal of Power Sources*, vol. 280, pp. 379-386, 2015.
- [22] M. Djošić *et al.*, "Electrochemical synthesis of nanosized monetite powder and its electrophoretic deposition on titanium," *Colloids and Surfaces A: Physicochemical and Engineering Aspects*, vol. 341, no. 1-3, pp. 110-117, 2009.
- [23] R. Mayén-Mondragón, G. Falk, and R. Clasen, "Electrophoretic Impregnation/Deposition Complemented with Polymeric Templating for the Fabrication of Functionalized-Porosity Layered-Ceramics: A Solid-Oxide-Fuel-Cells Approach," *Journal of the American Ceramic Society*, vol. 95, no. 2, pp. 593-599, 2012.
- [24] O. O. Otelaja, D.-H. Ha, T. Ly, H. Zhang, and R. D. Robinson, "Highly conductive Cu_{2-x}S nanoparticle films through room-temperature processing and an order of magnitude enhancement of conductivity via electrophoretic deposition," *ACS Applied Materials & Interfaces*, vol. 6, no. 21, pp. 18911-18920, 2014.
- [25] Y. Su and I. Zhitomirsky, "Electrophoretic deposition of graphene, carbon nanotubes and composite films using methyl violet dye as a dispersing agent," *Colloids and Surfaces A: Physicochemical and Engineering Aspects*, vol. 436, pp. 97-103, 2013/09/05/ 2013.
- [26] R. Sikkema, K. Baker, and I. Zhitomirsky, "Electrophoretic deposition of polymers and proteins for biomedical applications," *Advances in Colloid and Interface Science*, vol. 284, p. 102272, 2020/10/01/ 2020.
- [27] I. Zhitomirsky and L. Gal-Or, "Formation of hollow fibers by electrophoretic deposition," *Materials Letters*, vol. 38, no. 1, pp. 10-17, Jan 1999.
- [28] K. T. Lau *et al.*, "Electrophoretic deposition and heat treatment of steel-supported PVDF-graphite composite film," in *Applied Mechanics and Materials*, 2015, vol. 761, pp. 412-416: Trans Tech Publ.
- [29] K. T. Lau, M. S. M. Suan, M. Zaimi, J. Abd Razak, M. Azam, and N. Mohamad, "Microstructure And Phase Of Poly (Vinyliden Fluoride) Films By Electrophoretic Deposition: Effect Of Polymer Dispersion's Stirring Conditions," *Journal of Advanced Manufacturing Technology (JAMT)*, vol. 10, no. 2, pp. 57-66, 2016.
- [30] J. Yin *et al.*, "Fabrication of protective KB/PVdF composite films on stainless steel substrates for PEFCs through electrophoretic deposition," *Journal of the Ceramic Society of Japan*, vol. 116, no. 1350, pp. 201-204, 2008.

- [31] Q. Zhao, S. Veldhuis, R. Mathews, and I. Zhitomirsky, "Influence of chemical structure of bile acid dispersants on electrophoretic deposition of poly (vinylidene fluoride) and composites," *Colloids and Surfaces A: Physicochemical and Engineering Aspects*, vol. 627, p. 127181, 2021.
- [32] M. Cheong and I. Zhitomirsky, "Electrophoretic deposition of manganese oxide films," *Surface Engineering*, vol. 25, no. 5, pp. 346-352, Jul 2009.
- [33] M. Hashiba, H. Okamoto, Y. Nurishi, and K. Hiramatsu, "The zeta-potential measurement for concentrated aqueous suspension by improved electrophoretic mass transport apparatus—application to Al₂O₃, ZrO₃ and SiC suspensions," *Journal of materials science*, vol. 23, no. 8, pp. 2893-2896, 1988.
- [34] M. Ata, Y. Liu, and I. Zhitomirsky, "A review of new methods of surface chemical modification, dispersion and electrophoretic deposition of metal oxide particles," *Rsc Advances*, vol. 4, no. 43, pp. 22716-22732, 2014.
- [35] Y. Su and I. Zhitomirsky, "Electrophoretic assembly of organic molecules and composites for electrochemical supercapacitors," *Journal of Colloid and Interface Science*, vol. 392, pp. 247-255, 2013/02/15/ 2013.
- [36] Y. Su and I. Zhitomirsky, "Cataphoretic assembly of cationic dyes and deposition of carbon nanotube and graphene films," *Journal of Colloid and Interface Science*, vol. 399, pp. 46-53, 2013/06/01/ 2013.
- [37] M. Kobayashi, K. Tashiro, and H. Tadokoro, "Molecular vibrations of three crystal forms of poly (vinylidene fluoride)," *Macromolecules*, vol. 8, no. 2, pp. 158-171, 1975.
- [38] Z. Zeng *et al.*, "Graphene oxide quantum dots covalently functionalized PVDF membrane with significantly-enhanced bactericidal and antibiofouling performances," *Scientific reports*, vol. 6, no. 1, pp. 1-11, 2016.

Chapter 8 EPD of PVDF-HFP-NiFe₂O₄ Composites

This chapter is reproduced from **Q. Zhao, I. Zhitomirsky**, *Biomimetic strategy for electrophoretic deposition of composite ferroelectric poly(vinylidene, fluoride-co-hexafluoropropylene) – ferrimagnetic NiFe₂O₄ films*, *Colloids and Surfaces A: Physicochemical and Engineering Aspects*, Volume 651, 2022, 129743, (<https://doi.org/10.1016/j.colsurfa.2022.129743>) with permission from Copyright © 2022 Elsevier B.V. The author of this thesis is the first author and the main contributor of this publication, including conceiving the initial ideas, development of approach and methodology carrying out experiments, analysis of data, writing the initial draft and preparation of the manuscript.

8.1 Abstract

This investigation is motivated by interest in fabrication of composite films combining ferrimagnetic properties of spinel ferrites with multifunctional properties of ferroelectric polymers. It addresses the need in the development of surface modification techniques for inorganic materials and polymers and their electrophoretic deposition (EPD) for the fabrication of composite films. This article describes for the first time the fabrication of composite ferroelectric poly(vinylidene fluoride-co-hexafluoropropylene) (PVDF-HFP) - ferrimagnetic NiFe₂O₄ films by EPD. The approach is based on feasibility of fabrication, surface modification and EPD of PVDF HFP particles using natural biosurfactants, such as

catechol-type caffeic acid (CA) and bile acid-type cholic acid (ChA). The analysis of chemical structure of CA and ChA provides an insight into the surface modification mechanisms and EPD efficiency. Film morphologies and corrosion protection properties are analyzed. An important finding is the ability of CA to act as a charging dispersant for materials of different types, such as PVDF-HFP polymer particles and inorganic nanoparticles of NiFe_2O_4 spinel and fabrication of composite films by EPD. The film deposition yield, morphology and composition of PVDF-HFP- NiFe_2O_4 films are analyzed. NiFe_2O_4 content and magnetic properties of the composites are varied by variation of EPD bath composition. This investigation provides a platform for EPD of composite films combining ferrimagnetic properties of spinel ferrites with multifunctional properties of ferroelectric polymers.

8.2 Introduction

Poly(vinylidene fluoride-co-hexafluoropropylene) (PVDF-HFP) co-polymer exhibits ferroelectric, piezoelectric properties, high chemical stability, flexibility, biocompatibility and optical transparency [1-4]. The advanced functionality of PVDF-HFP provides a platform for various practical applications [5-7].

PVDF-HFP showed promising properties for applications in lithium battery separators and electrolytes [8, 9]. Researchers have employed PVDF-HFP for biosensors [10] and fuel cells [11]. Composites were developed for magnetically controllable oil-water separation

[12], distillation membranes [13], batteries [14], magnetoelectric devices [15], triboelectric nanogenerators [16], and energy storage devices [17].

PVDF-HFP ferroelectric copolymer is a promising material for the development of multiferroics. Materials, combining ferroelectric and magnetic ordering [18], also known as multiferroics [19], have generated significant interest for various applications based on magnetoelectric effects. It has been widely reported that individual compounds and solid solutions of different types, such as hexagonal manganite, perovskites, boracites, BaMeF_4 (Me = Mn, Fe, Co, Ni) and hexagonal BaTiO_3 type oxides exhibit multiferroic properties [18, 20]. A significant challenge in the development of multiferroics for practical applications is obtaining ferri- or ferromagnetic ordering and ferroelectric ordering at room temperature in a single material. Many multiferroic materials exhibit antiferromagnetic properties, other materials have ferromagnetic Curie points or ferrimagnetic Neel points at very low temperatures. Such materials usually show high conductivity, which is detrimental for the observation of ferroelectric properties. Therefore, the combination of ferroelectric polymers such as PVDF-HFP and magnetic particles in composite materials is a promising approach for the fabrication of multiferroic materials.

PVDF-HFP and composite films addressed the need for various applications [9] and significant attention was focused on the development of film deposition techniques. Thin films were obtained by spin-coating [10], electrospinning [21], spray coating [10], and dip coating [12]. Electrophoretic deposition (EPD) offers many advantages for deposition of polymer films and composites [22-27]. EPD method combines benefits of high yields and

deposition rates with the advantages of deposition selectivity, film uniformity, and purity [28-30]. This method is technically simple with a significant potential for upscaling [31-34]. Another key benefit is the possibility of composite manufacturing [35-40]. The choice of dispersants [26, 41-43] plays a crucial role in materials deposition by EPD.

Several investigations focused on EPD of PVDF-HFP. This co-polymer was used as a binder for EPD of TiO₂ nanoparticles [44]. PVDF-HFP content in the EPD deposits was 8.5 wt%. Charging of TiO₂ particles was achieved using iodine-acetone mixture [44]. The transport of TiO₂ particles through 30% PVDF-HFP solution facilitated deposition of a thin PVDF-HFP layer on the TiO₂ film [44]. EPD of PVDF-HFP was also performed from a surfactant-free colloidal suspension in acetone [45]. This approach was based on moisture adsorption from air by an acetone bath. It was suggested [45] that chemical interaction of acetone and adsorbed water resulted in dissociation of water and charging of PVDF-HFP particles. A similar approach was used for co-EPD of PVDF-HFP with Al-doped Li_{6.75}La₃Zr_{1.75}Ta_{0.25}O₁₂ [46] and Li-montmorillonite [47] for applications in lithium ion batteries.

This investigation was motivated by increasing interest in composite films based on ferroelectric PVDF-HFP polymer and magnetic particles. It addressed the need in the development of advanced EPD strategies, based on the use of surfactants. The goal of this investigation was EPD of PVDF-HFP-NiFe₂O₄ films. The biomimetic approach was based on the use of natural biosurfactants of different types, such as caffeic acid (CA) and cholic

acid (ChA). Figure 8.1 shows chemical structures of CA and ChA molecules used in this study.

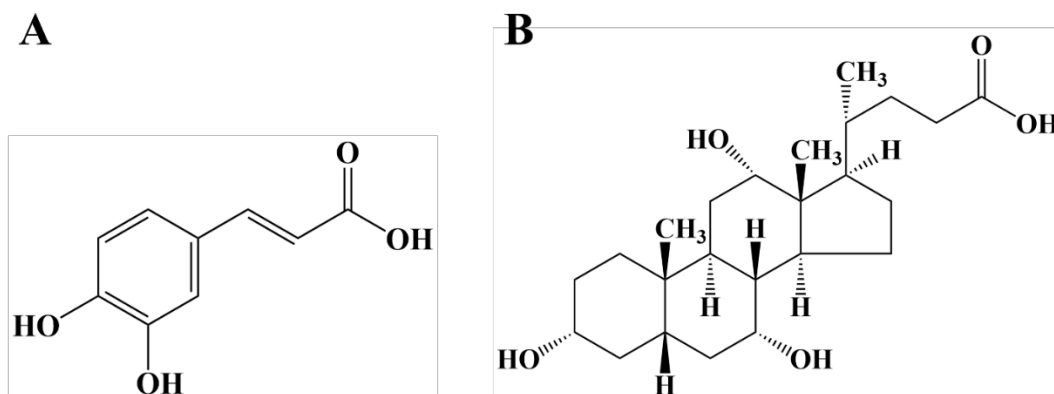


Figure 8.1 Chemical structures of (A) CA and (B) ChA.

CA belongs to the catechol family of organic molecules. The interest in catecholate molecules for EPD of inorganic materials has been motivated by the analysis of strong bonding of catecholate monomers of mussel proteins to inorganic surfaces [48-50]. Previous investigations of small charged catecholate molecules resulted in discovery of advanced dispersants, which strongly adsorbed on inorganic particles in ethanol and facilitated their electrostatic dispersion and EPD [51]. The anionic properties of CA molecule are related to its COOH group. CA was used for EPD of TiO₂, MnO₂, and ZrO₂ from their suspensions in ethanol [51, 52]. Adsorption of CA on positively charged MnO₂ particles in ethanol resulted in charge reversal and MnO₂ films were prepared by anodic EPD [53]. In this investigation CA was used for EPD of PVDF-HFP polymer and inorganic NiFe₂O₄ nanoparticles.

ChA is another promising anionic dispersant for EPD of PVDF-HFP particles. ChA is a natural bile acid molecule, containing anionic COOH group. The facial amphiphilicity of bile acids is an important factor governing their interaction with different organic materials, which resulted in exceptional dispersion power. Previous investigations showed that bile acids can be used for charging and EPD of PVDF particles in ethanol [54]. The comparison of deposition yields of PVDF achieved using different bile acids showed that ChA is the most efficient dispersant for EPD of PVDF films [54]. Therefore, it was hypothesized that ChA can also be used for EPD of PVDF-HFP particles. The experimental results presented below demonstrate EPD of PVDF-HFP-NiFe₂O₄ films and describe film properties, composition and microstructure.

8.3 Experimental Procedures

Poly(vinylidene fluoride-co-hexafluoropropylene) (PVDF-HFP, average M_w of 400000, beads, diameter 5 mm, density 1.77 g/mL at 25 °C, quality level 100, ISO 9001), N-methyl-2-pyrrolidone (NMP, $\geq 99.5\%$), caffeic acid (CA, $\geq 98.0\%$), cholic acid (ChA, $\geq 98\%$), absolute ethanol ($\geq 99.995\%$) and iron nickel oxide (NiFe₂O₄, size <50 nm, $\geq 98\%$) nanopowder (MilliporeSigma, Canada) were used.

20 g·L⁻¹ solution of PVDF-HFP in 20 mL NMP was prepared and slowly (~600 drops) added to ethanol, containing dissolved CA or ChA dispersants at a stirring speed of 200 rpm. The final concentrations of PVDF-HFP and dispersants in the mixed solvent were 5 g·L⁻¹ and 1 g·L⁻¹, respectively. This procedure allowed the fabrication of stable colloidal

suspensions of fine charged particles, which were used for EPD of PVDF-HFP films. NiFe₂O₄ was added to the suspensions of PVDF-HFP, containing CA for fabricating composite films. The mass ratio of PVDF-HFP:NiFe₂O₄ was 1:1 or 1:9. These suspensions were stirred and ultrasonicated before EPD. The EPD cell contained a 304-type stainless steel foil substrate and a platinum foil counter electrode with 15 mm separation. The films were deposited under the voltages of 10-100 V for 1-11 min.

The film microstructure was investigated using JEOL JSM-7000F microscope. Zeta potential measurements were performed by a mass transfer method [55]. Electrochemical studies were performed in 3% aqueous NaCl solution using a potentiostat (PARSTAT 2273, Princeton Applied Research) and a 3-electrode cell with coated or uncoated stainless steel as a working electrode, platinum counter electrode and a saturated calomel electrode (SCE) reference. Potentiodynamic studies were conducted at a sweeping rate of 1 mV·s⁻¹. Electrochemical impedance spectroscopy (EIS) studies were performed under a sinusoidal excitation voltage of 10 mV in the frequency range of 10 mHz-10 kHz. A Bruker Vertex 70 spectrometer was used for FTIR studies by attenuated total reflectance (ATR) method. X-ray diffraction (XRD) was carried out using a Nicolet I2 powder diffractometer with monochromatized Cu K α radiation. As deposited films were scraped off from stainless steel electrodes and collected for magnetic measurements, FTIR, XRD, thermogravimetric analysis (TGA) and differential thermal analysis (DTA). TGA and DTA studies were performed using Netzsch STH-409 thermoanalyzer between room temperature and 1000 °C

at a heating rate of $5\text{ }^{\circ}\text{C}\cdot\text{min}^{-1}$. Magnetic measurements were conducted using a Quantum Design PPMS-9 system using powder samples.

8.4 Results and Discussion

The fabrication of PVDF-HFP suspensions presented difficulties due to the large size of as-received PVDF-HFP beads ($\sim 5\text{ mm}$). Moreover, PVDF-HFP is an electrically neutral polymer. Therefore, as-received PVDF-HFP cannot be used for EPD. The experimental procedure described above facilitated the fabrication of stable colloidal suspensions of charged PVDF-HFP particles for film formation by EPD. The size of polymer particles precipitated from solutions is influenced by different factors, such as polymer solubility in a solvent, polymer concentration, nature of antisolvent, mixing rate, stirring rate, temperature, nature of dispersants and other factors discussed in the literatures [56-58]. It is known that PVDF-HFP shows good solubility in NMP [59, 60], however this polymer is insoluble in ethanol. Therefore, NMP and ethanol were used as a solvent and an antisolvent, respectively.

Figure 8.2 (A, B) shows TEM images of PVDF-HFP particles. The particles were formed by adding PVDF-HFP solution in NMP to ethanol, which is an antisolvent for PVDF-HFP, in the presence of CA or ChA. It is seen that a typical size of the PVDF-HFP particles was about $1\text{-}2\text{ }\mu\text{m}$. Drying resulted in necks formation between the particles (Figure 8.2B).

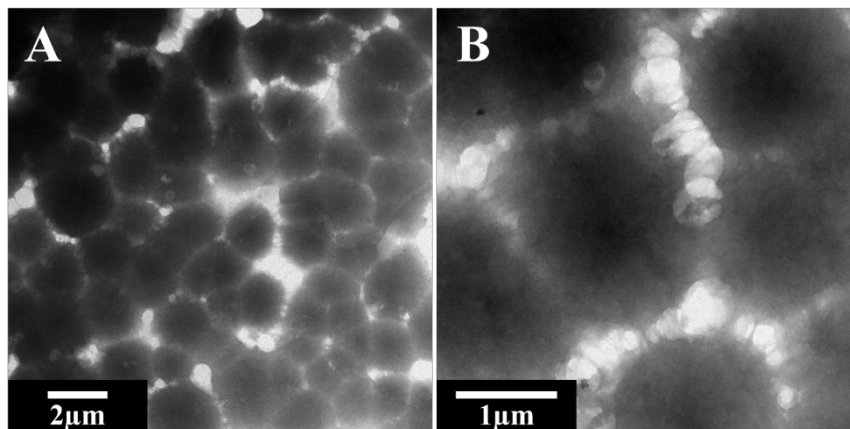


Figure 8.2 TEM images at different magnifications of PVDF-HFP particles.

Natural organic molecules such as CA and ChA were used for the fabrication of colloidal suspensions of PVDF-HFP particles and film formation by EPD. CA and ChA facilitated the fabrication of stable suspensions of PVDF-HFP particles and imparted them a negative charge, which allowed for PVDF-HFP film deposition by EPD. PVDF-HFP films were obtained at a deposition voltage of 20-50 V using CA. However, higher deposition voltages of about 100 V were necessary for EPD of PVDF-HFP films using ChA. Therefore, PVDF-HFP films were deposited at a deposition voltage of 100 V using ChA in order to achieve a comparable deposit mass at the same deposition time with that obtained using CA at a deposition voltage of 50 V. PVDF-HFP particles, dispersed using CA and ChA showed zeta potentials of -28 and -11 mV, respectively. It should be noted that dispersants provide charging and dispersion of the particles in the bulk of the suspensions. However, the same particles must coagulate at the electrode surface. According to the literature [61] a certain value of an electric field is necessary to overcome particle mutual repulsion at the electrode surface for deposit formation. The required electric field can be different for suspensions

stabilized using different surfactants. It depends on zeta potential of the particles, size and properties of adsorbed dispersants. It is suggested that larger size of adsorbed ChA, compared to that of CA, was detrimental for particle coagulation at the electrode surface and the deposition process required a higher voltage.

Figure 8.3 shows morphologies of the films prepared using CA and ChA. EPD resulted in deposition of relatively dense, continuous and crack-free films. However, small pores were observed in high magnification SEM images. Such pores can result from packing of polymer particles [62, 63]. The morphology of EPD coatings is dependent [61] on the applied voltage and dispersant. Fast packing of particles at high voltages can result in enhanced porosity [61]. More adherent films with reduced number of defects can be obtained at moderate voltages [61]. The SEM images of cross sections indicate that film thickness is about 1.5-2 μm . Since PVDF-HFP is hydrophobic, and the as-deposited films were relatively dense, the corrosion resistance of the films was expected. Therefore, corrosion studies were performed in aqueous 3% NaCl solutions by potentiodynamic method and testing results were presented in the Tafel plots (Figure 8.4). In comparison to uncoated 304 stainless steel (Figure 8.4 (a)), the PVDF-HFP coated substrates (Figure 8.4 (b, c)) presented substantially increased corrosion potential and lowered anodic current. The calculated corrosion current decreased from 2.6 $\mu\text{A}\cdot\text{cm}^{-2}$ for uncoated substrate to 0.13 $\mu\text{A}\cdot\text{cm}^{-2}$ and 0.25 $\mu\text{A}\cdot\text{cm}^{-2}$ for substrates coated with PVDF-HFP using CA and ChA, respectively.

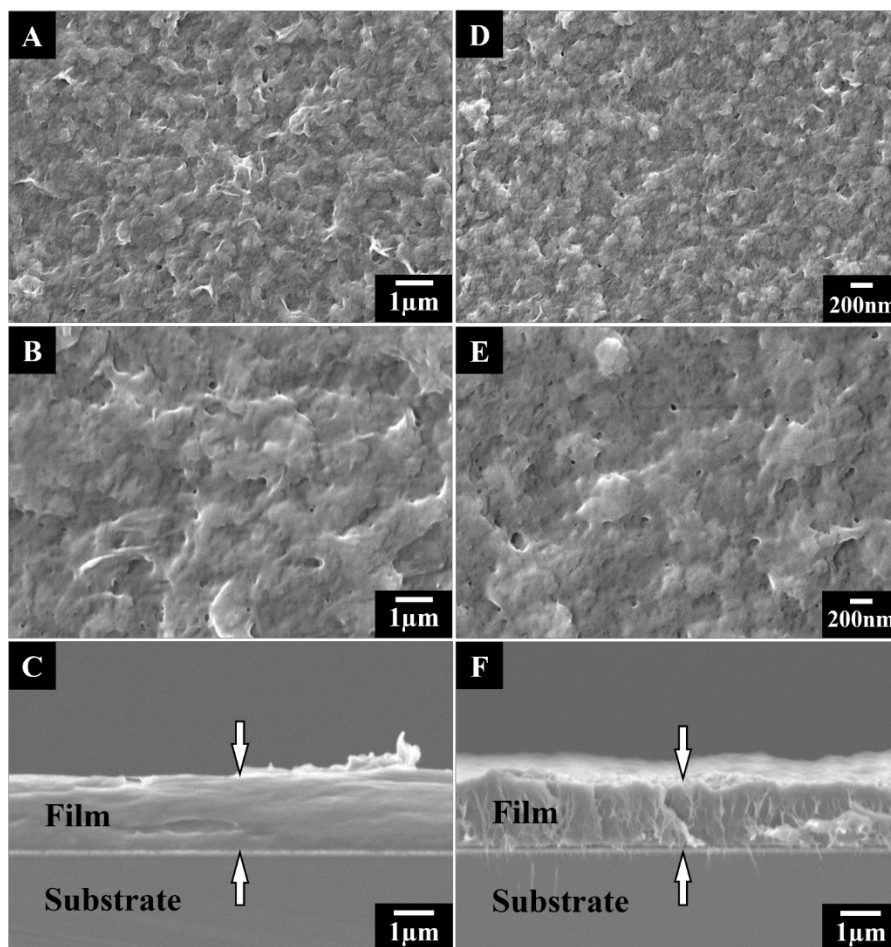


Figure 8.3 SEM images for PVDF-HFP films prepared using (A-C) CA at 50 V and (D-F) ChA at 100 V: (A, B, D, E) film surfaces at different magnifications, (C, F) cross sections, arrows show film thickness.

EIS data showed that the PVDF-HFP film was a barrier preventing the electrolyte from reaching the substrate surface. Bode plots (Figure 8.5A) revealed a significantly higher absolute impedance of both coated samples than the bare substrate across a broad frequency range from 10 Hz to 10 kHz. This corrosion resistance property of the coated sample led to low phase shift (Figure 8.5B) at low frequencies. The protective properties of the coatings

were optimized at deposition time of 5 min. At lower deposition times (Supplementary Information, Figure S8.1 and Figure S8.2) the corrosion protection is less efficient. The increase in the deposition time above 5 min did not show improvement in corrosion protection.

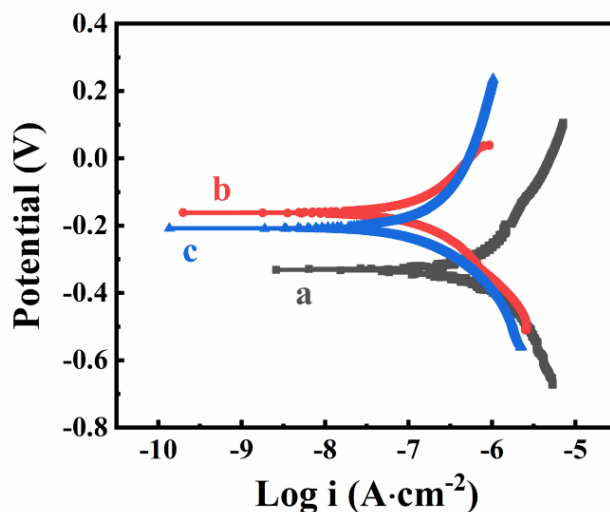


Figure 8.4 Tafel plots of (a) uncoated and (b, c) coated stainless steel. The coatings were prepared from PVDF-HFP suspensions at optimized deposition conditions: (b) CA at 50 V (c) ChA at 100 V and deposition time of 5 min.

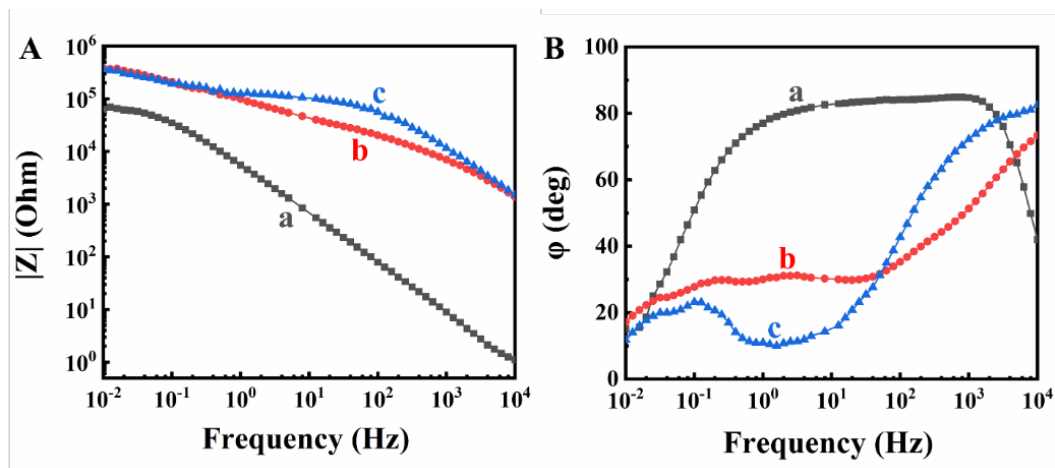


Figure 8.5 EIS data of (a) uncoated and (b, c) coated stainless steel. The coatings were prepared from PVDF-HFP suspensions at optimized deposition conditions using (b) CA at 50 V (c) ChA at 100 V and deposition time of 5 min.

Following the goal of this investigation, EPD experiments were performed on co-deposition of PVDF-HFP and NiFe_2O_4 . Sedimentation tests showed poor dispersion of NiFe_2O_4 in the presence of ChA. However, CA allowed enhanced stability of NiFe_2O_4 suspensions. NiFe_2O_4 particles, dispersed using CA showed zeta potential of -32 mV. Therefore, CA was used for co-deposition of PVDF-HFP and NiFe_2O_4 . Figure 8.6 shows X-ray diffraction patterns of pure NiFe_2O_4 and composite films.

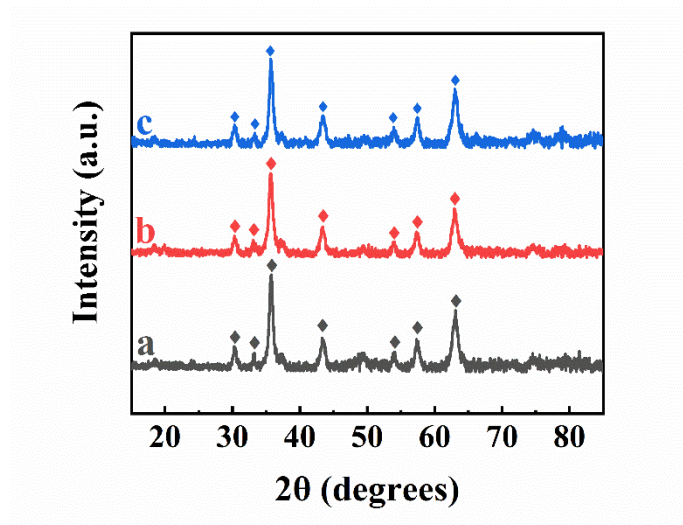


Figure 8.6 XRD patterns of (a) as-received NiFe_2O_4 , and deposits obtained from $5 \text{ g}\cdot\text{L}^{-1}$ PVDF-HFP suspensions, containing $1 \text{ g}\cdot\text{L}^{-1}$ CA with (b) $5 \text{ g}\cdot\text{L}^{-1}$ NiFe_2O_4 (c) $45 \text{ g}\cdot\text{L}^{-1}$ NiFe_2O_4 at 20 V and deposition time of 5 min (\blacklozenge peaks corresponding to JCPDS file 54-0964)

As-received NiFe_2O_4 powder showed XRD peaks corresponding to the JCPDS file 54-0964. Similar peaks were observed in the diffraction patterns of deposited materials and indicated NiFe_2O_4 deposition. The formation of composite materials was confirmed by FTIR studies. The broad peak centered at 549 cm^{-1} for as-received NiFe_2O_4 in Figure 8.7 (a) was attributed to Fe-O and Ni-O stretching [64]. The FTIR spectrum of PVDF-HFP (Figure 8.7 (b)) showed peak at 1398 cm^{-1} assigned to -C-F stretching and the bands at 1178 and 1064 cm^{-1} were ascribed to the symmetrical stretching mode of CF_2 [65]. The amorphous phase of the polymer contributed to the bands at 876 and 841 cm^{-1} [66]. The vibrational bands observed at 757 and 611 cm^{-1} are characteristic absorptions of the crystalline phase VDF

unit [67]. The composite films showed the characteristic peaks of both NiFe_2O_4 and PVDF-HFP, which demonstrated the successful co-deposition of NiFe_2O_4 and PVDF-HFP.

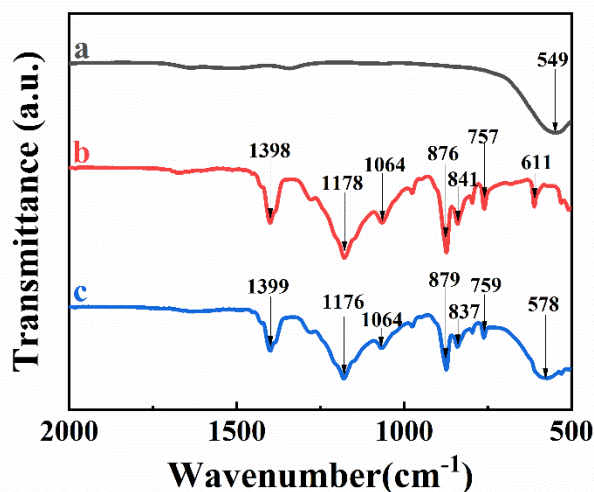


Figure 8.7 FTIR spectra of (a) as-received NiFe_2O_4 , (b) PVDF-HFP deposit, prepared from $5 \text{ g}\cdot\text{L}^{-1}$ PVDF-HFP suspension, containing $1 \text{ g}\cdot\text{L}^{-1}$ CA at 50 V and deposition time of 5 min and (c) PVDF-HFP- NiFe_2O_4 deposit, prepared from $5 \text{ g}\cdot\text{L}^{-1}$ PVDF-HFP and $5 \text{ g}\cdot\text{L}^{-1}$ NiFe_2O_4 suspension, containing $1 \text{ g}\cdot\text{L}^{-1}$ CA at 20 V and deposition time of 5 min.

TGA and DTA studies (Figure 8.8) were used for the analysis of film composition. TGA data showed stepwise sample mass reduction below $600 \text{ }^\circ\text{C}$ and the sample mass remained nearly constant at higher temperatures. The total mass loss at $900 \text{ }^\circ\text{C}$ was found to be 56.0 and 29.2 mass% for deposits prepared from $5 \text{ g}\cdot\text{L}^{-1}$ PVDF-HFP suspension, containing $1 \text{ g}\cdot\text{L}^{-1}$ CA with 5 and $45 \text{ g}\cdot\text{L}^{-1}$ NiFe_2O_4 , respectively. The decrease of samples mass with temperature was mainly attributed to the pyrolysis of the copolymer. The TGA data indicated that the increase in NiFe_2O_4 concentration in suspension resulted in increasing NiFe_2O_4 concentration in the deposited film. The DTA curves in Figure 8.8 were in

agreement with TGA investigations. The exothermic peaks between 460 °C and 620 °C were related to the burning out of PVDF-HFP polymer. The sample with larger NiFe₂O₄ and lower PVDF-HFP content showed reduced exothermic peak. The difference in TGA mass loss (Figure 8.8A (a, b)) and DTA peak positions (Figure 8.8B (a, b)) can be explained by the dynamic nature of the TGA/DTA test, which was performed at a heating rate of 5 °C·min⁻¹ and difference in the polymer content in the samples. In the experimental conditions of such a dynamic TGA/DTA test for the samples with different compositions, the burning out of the polymer occurs in a range of temperatures. During TGA/DTA experiments, oxygen diffuses through composite and CO₂ gas diffuses away. The process is governed by the rate of oxygen supply to the polymer component and the rate of CO₂ release. The lower content of the inorganic phase in the composite facilitates gas diffusion and burning out of the polymer, resulting in a sharp reduction of sample mass (Figure 8.8A (a)) at temperatures above 460 °C. The sharp reduction of sample mass also resulted from larger polymer content. In the sample with larger content of the inorganic phase and lower polymer content, the inorganic phase limits the diffusion processes. As a result, the sample mass (Figure 8.8A (b)) decreases gradually and reduced exothermic peak for this sample is observed at higher temperatures (Figure 8.8B (b)).

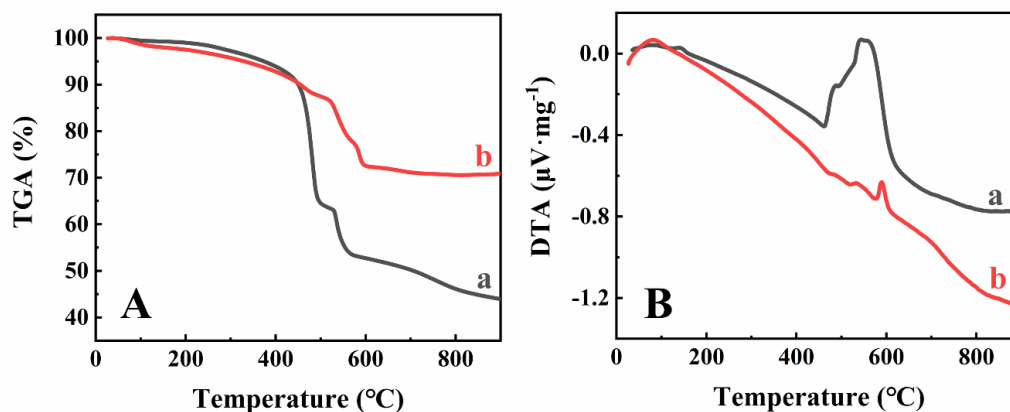


Figure 8.8 (A) TGA and (B) DTA data for deposits prepared from $5 \text{ g}\cdot\text{L}^{-1}$ PVDF-HFP suspensions, containing $1 \text{ g}\cdot\text{L}^{-1}$ CA with (a) 5 and (b) $45 \text{ g}\cdot\text{L}^{-1}$ NiFe_2O_4 at 20 V and deposition time of 5 min.

Figure 8.9 shows SEM images of composite films at different magnifications. The films prepared from $5 \text{ g}\cdot\text{L}^{-1}$ PVDF-HFP suspensions, containing $1 \text{ g}\cdot\text{L}^{-1}$ CA with $5 \text{ g}\cdot\text{L}^{-1}$ NiFe_2O_4 were relatively dense, crack-free and smooth. The films prepared from $5 \text{ g}\cdot\text{L}^{-1}$ PVDF-HFP suspensions, containing $1 \text{ g}\cdot\text{L}^{-1}$ CA with $45 \text{ g}\cdot\text{L}^{-1}$ NiFe_2O_4 showed higher porosity. It should be noted that PVDF-HFP acted as a binder for NiFe_2O_4 particles. The sample with larger NiFe_2O_4 content and lower PVDF-HFP content showed enlarged porosity due to packing of NiFe_2O_4 particles. Energy-dispersive X-ray spectroscopy (EDX) mapping of film surfaces showed relatively uniform distribution of NiFe_2O_4 particles (Figure S8.3). Only a low number of small agglomerates were observed in the images and EDX maps of composites with lower NiFe_2O_4 content. The analysis of cross section (Figure S8.4) of such films also showed that some agglomeration which resulted in deviation from uniform distribution of NiFe_2O_4 phase in some areas of the films. In contrast, the EDX

studies of cross sections of the films with larger NiFe₂O₄ content showed uniform distribution of NiFe₂O₄ in the film (Figure S8.4).

The results of thermogravimetry showed that film composition and morphology can be varied by the variation of NiFe₂O₄ particle concentration in the suspensions. Moreover, deposition yield studies showed that the amount of the deposited materials can be varied by variation of deposition time at a constant voltage or voltage at constant deposition time (Figure 8.10). The decrease in the deposition rate with time (Figure 8.10), especially at deposition times above 6 min, can result from the decreasing voltage drop in the suspension due to the increasing voltage drop in the deposited layer [68, 69]. At low deposition times, such as 1 min, the deposit mass was low and substrate coverage was incomplete; at high deposition times, such as 15 min, the deposit spalling was observed due to the large mass of the deposited material. The deposition voltages used for deposition of composite materials were lower than the deposition voltages for pure polymer. The deposition voltages were limited to 40 V and the optimized deposition voltage for the composite film was 20V. This was attributed to electric field induced agglomeration of NiFe₂O₄ particles. The effect of electric field induced agglomeration of inorganic nanoparticles was discovered by W. M. Winslow [70]. This effect was observed in other investigations and attributed to dipole-dipole interactions [71].

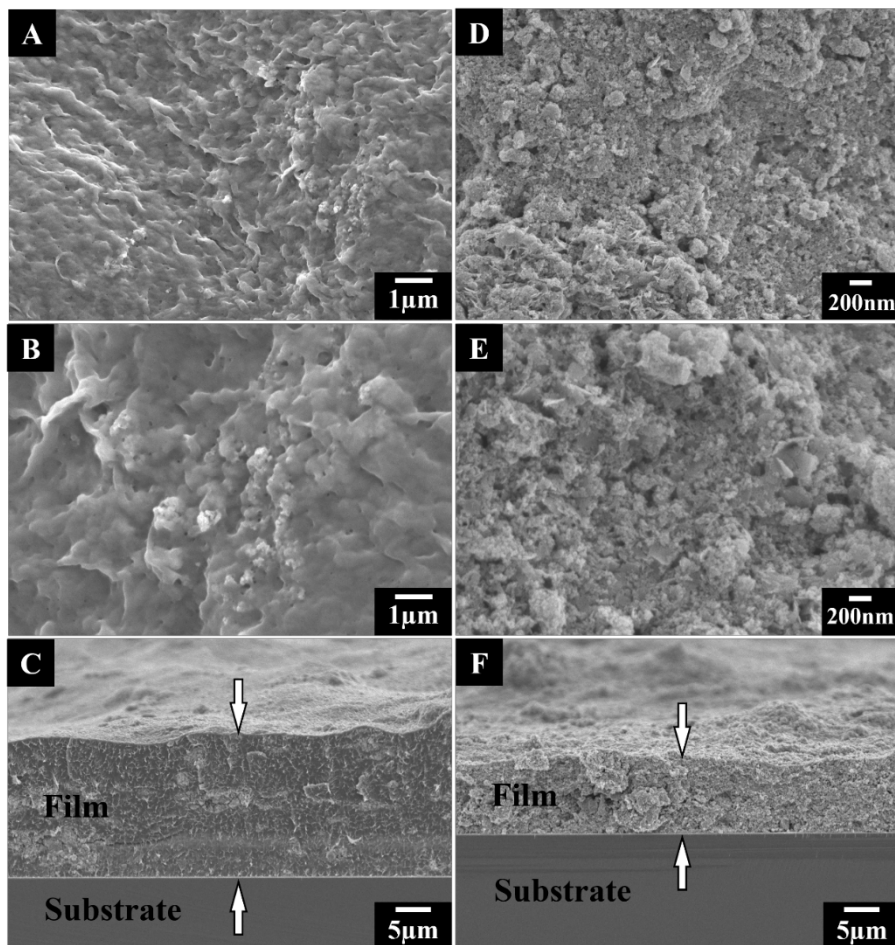


Figure 8.9 SEM images for films prepared at a deposition voltage of 20 V and deposition time of 5 min from 5 g·L⁻¹ PVDF-HFP suspensions, containing 1 g·L⁻¹ CA with (A-C) 5 and (D-F) 45 g·L⁻¹ NiFe₂O₄: (A, B, D, E) surfaces at different magnifications, (C, F) cross sections, arrows show film thickness.

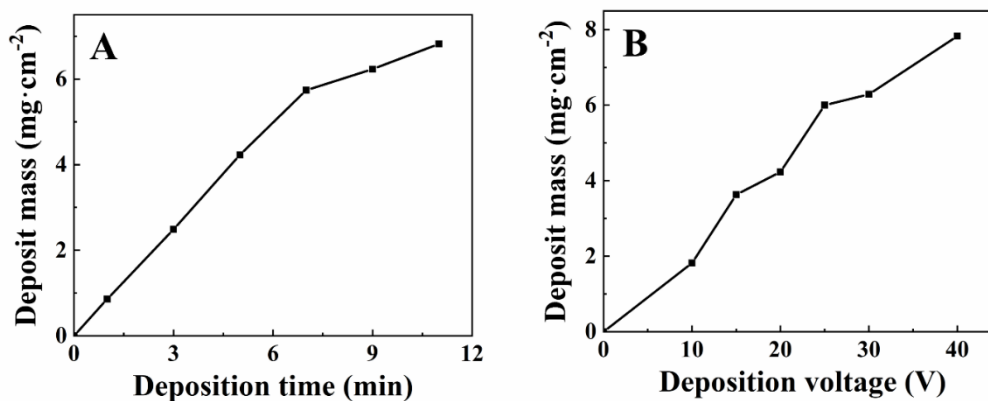


Figure 8.10 Deposit mass versus (A) deposition time at a deposition voltage of 20 V and (B) voltage at a deposition time of 5 min for films prepared from 5 g·L⁻¹ PVDF-HFP suspensions, containing 1 g·L⁻¹ CA with 5 g·L⁻¹ NiFe₂O₄.

Investigations also showed that magnetic properties of the composites can be varied. Figure 8.11 compares magnetization data for as-received NiFe₂O₄ and composite deposits.

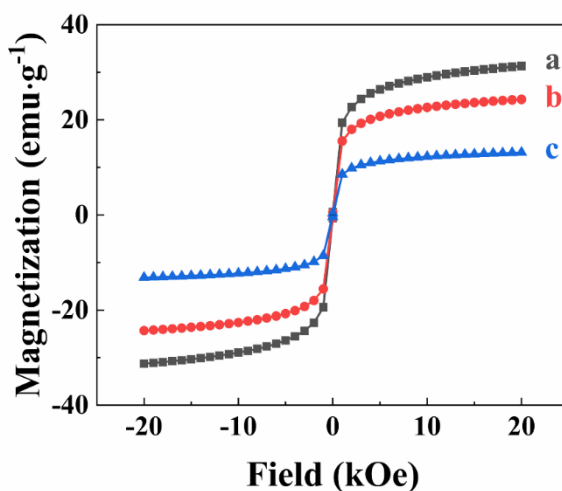


Figure 8.11 Magnetization versus magnetic field for (a) as-received NiFe₂O₄ and composite deposits prepared from 5 g·L⁻¹ PVDF-HFP suspensions, containing 1 g·L⁻¹ CA and (b) 45 and (c) 5 g·L⁻¹ NiFe₂O₄ at 20 V and deposition time of 5 min.

The magnetization data for as-received NiFe_2O_4 show ferrimagnetic behavior of this material at room temperature. As expected, composite materials also showed magnetic properties, but with lower magnetization. Magnetization data confirmed incorporation of NiFe_2O_4 into the composites. PVDF-HFP polymer is a diamagnetic material, which gives a negative contribution to the total magnetization. Therefore, magnetic properties of the composites are governed by their composition. Figure 8.11 indicated that magnetization decreased with decreasing NiFe_2O_4 content in the composites. It should be noted that FTIR data indicated only co-deposition of PVDF-HFP with NiFe_2O_4 , whereas TGA/DTA data coupled with magnetic measurements testing results also showed that film composition and magnetic properties can be varied by the variation of bath composition. Therefore, obtained composites combined magnetic properties of NiFe_2O_4 with functional properties of PVDF-HFP. EPD of PVDF-HFP- NiFe_2O_4 composites offers inherent processing advantages of EPD technique, such as simple and low cost equipment, fast deposition rate, good control of the deposition rate, electric field controlled film uniformity and possibility of deposition on substrates of complex shape and large area [30, 72]. Moreover, EPD offers benefits for the fabrication of advanced composites with different phase connectivities of ferroelectric and ferro-/ferrimagnetic phases [73]. This investigation provides a platform for EPD of composite films combining ferrimagnetic properties of spinel ferrites with multifunctional properties of ferroelectric polymers. It should be noted that a combination of ferrimagnetic and ferroelectric materials doesn't necessarily lead [74] to the multiferroic properties of the composite. Magnetoelectric coupling in the multiferroic materials requires various

interactions [74] between the individual components, which are based on magnetostrictive, piezoelectric and other properties of the individual materials.

8.5 Conclusions

This study showed the feasibility of fabrication, surface modification and EPD of PVDF-HFP particles using natural biosurfactants, such as CA and ChA. The EPD method allowed fabrication of dense films, which exhibited corrosion protection properties. CA allowed PVDF-HFP deposition at reduced deposition voltages. An important finding was the possibility of co-EPD of different type materials, such as PVDF-HFP polymer and magnetic NiFe₂O₄ spinel nanoparticles using CA. The use of biosurfactants offered benefits of controlled EPD of materials. For the first time EPD method was applied for the fabrication of composite ferroelectric poly(vinylidene fluoride-co-hexafluoropropylene) (PVDF-HFP) - ferrimagnetic NiFe₂O₄ films. The composition, microstructure, deposition rate and magnetic properties of the composite films can be varied. The method developed in this investigation provide a simple and versatile strategy for the fabrication of composite films, combining ferrimagnetic properties of spinel oxides with multifunctional properties of ferroelectric polymers.

8.6 Acknowledgements

This research was funded by Natural Sciences and Engineering Research Council of Canada, grant RGPIN-2018-04014. SEM studies were conducted at the Canadian Centre for Electron Microscopy.

8.7 Supplementary Data

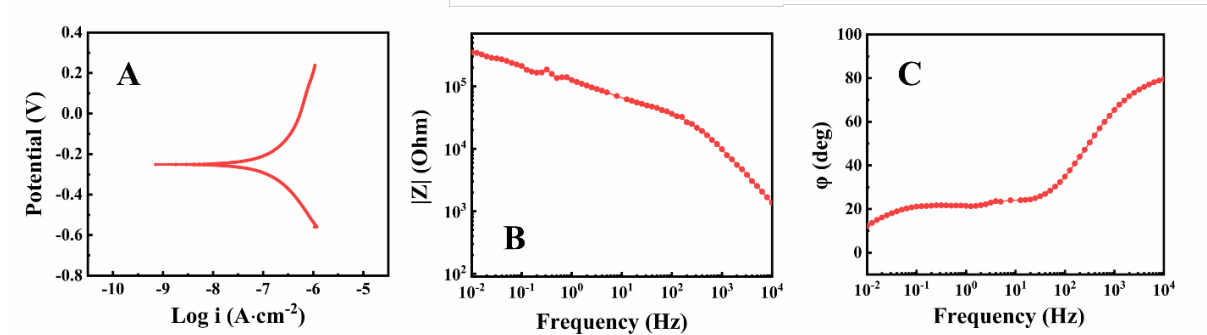


Figure S8.1 (A) Tafel plot and (B, C) Bode plot of complex impedance for coated stainless steel. The coating was prepared from PVDF-HFP suspensions using CA at 50 V and deposition time of 2 min.

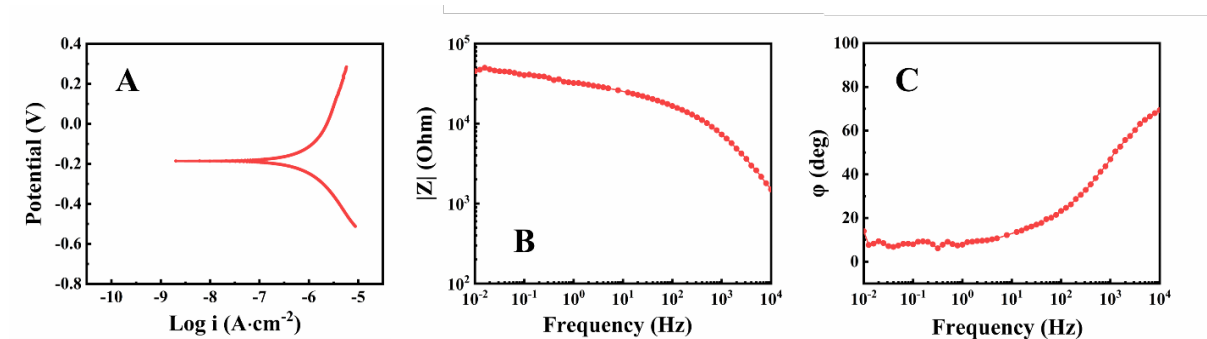


Figure S8.2 (A) Tafel plot and (B, C) Bode plot of complex impedance for coated stainless

steel. The coating was prepared from PVDF-HFP suspensions using ChA at 100 V and deposition time of 2 min.

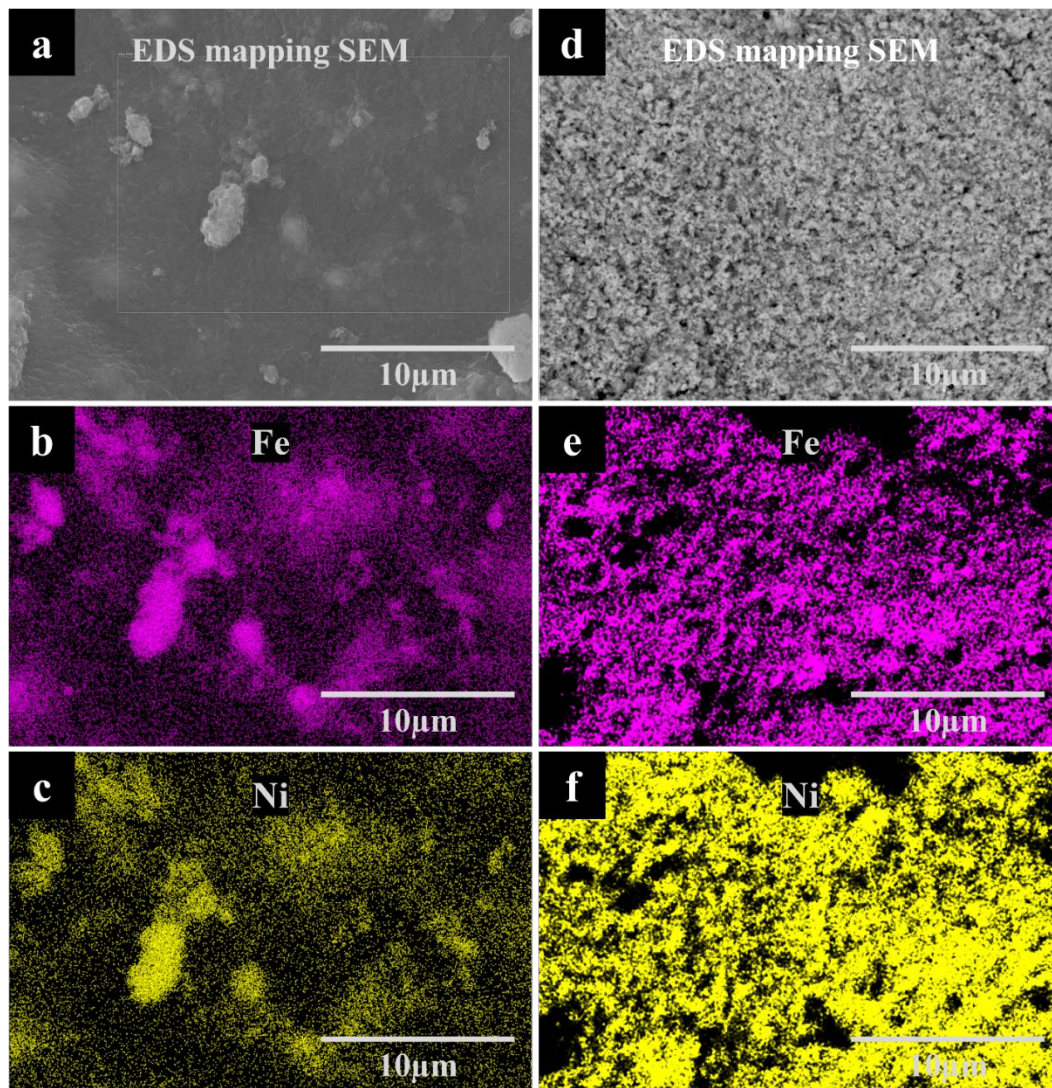


Figure S8.3 Electron microscopy data for deposits prepared from 5 g·L⁻¹ PVDF-HFP suspensions, containing 1 g·L⁻¹ CA with (a-c) 5 and (d-f) 45 g·L⁻¹ NiFe₂O₄ at 20 V and deposition time of 5 min: (a, d) SEM and (b, c, e, f) corresponding EDX.

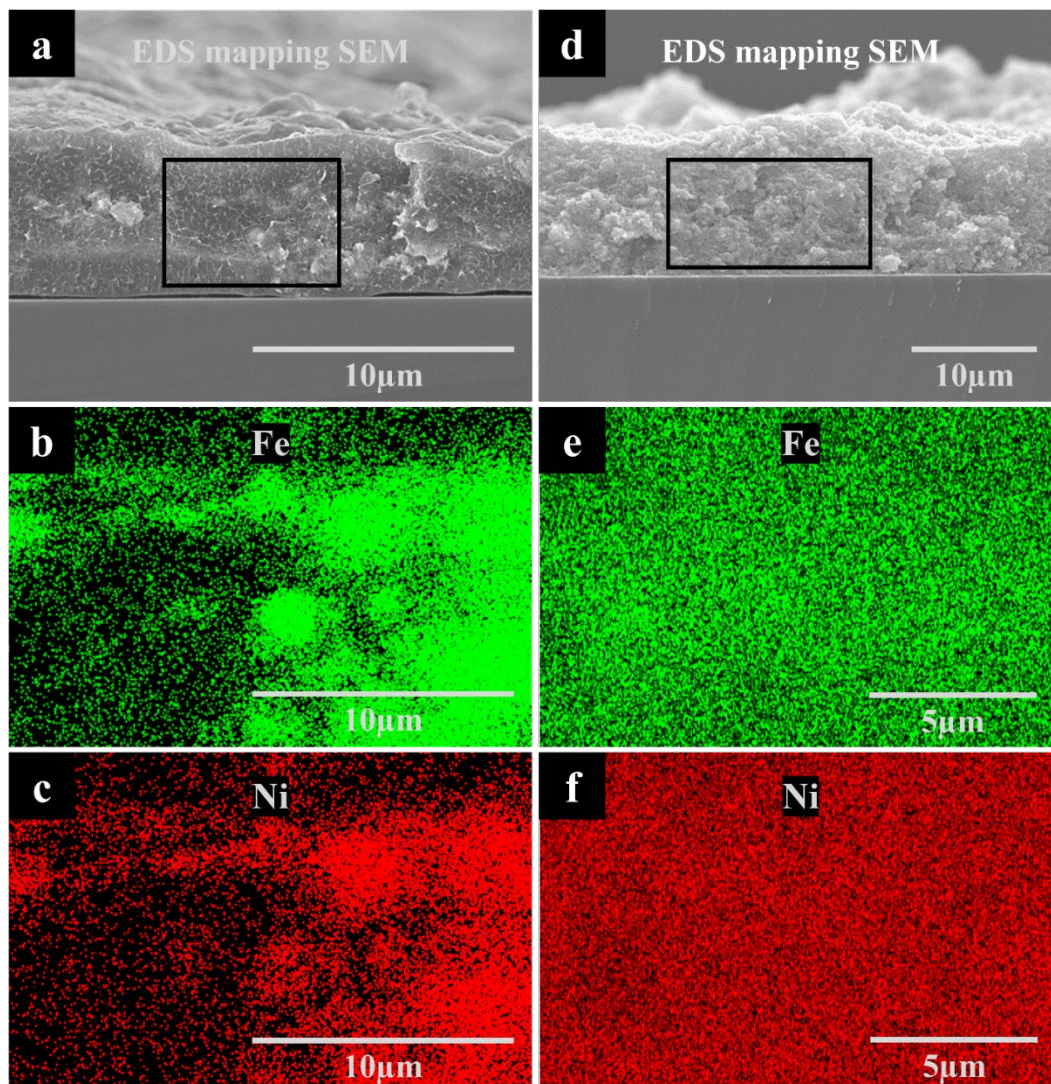


Figure S8.4 Electron microscopy data for deposits prepared from $5 \text{ g}\cdot\text{L}^{-1}$ PVDF-HFP suspensions, containing $1 \text{ g}\cdot\text{L}^{-1}$ CA with (a-c) 5 and (d-f) $45 \text{ g}\cdot\text{L}^{-1}$ NiFe_2O_4 at 20 V and deposition time of 5 min: (a, d) Cross-sectional SEM and (b, c, e, f) corresponding EDX.

8.8 References

- [1] S. Chaipo and C. Putson, "Preparation and ferroelectric properties of poly (vinylidene fluoride-hexafluoropropylene)(PVDF-HFP) filled with graphene-

- nanoplatelets film composites," in *IOP Conference Series: Materials Science and Engineering*, 2020, vol. 773, no. 1, p. 012021: IOP Publishing.
- [2] P. Huang *et al.*, "Carbon quantum dots inducing formation of β phase in PVDF-HFP to improve the piezoelectric performance," *Sensors and Actuators A: Physical*, vol. 330, p. 112880, 2021.
- [3] S. Zhang, W. Tong, J. Wang, W. Wang, Z. Wang, and Y. Zhang, "Modified sepiolite/PVDF-HFP composite film with enhanced piezoelectric and dielectric properties," *Journal of Applied Polymer Science*, vol. 137, no. 9, p. 48412, 2020.
- [4] X. He, K. Yao, and B. K. Gan, "Phase transition and properties of a ferroelectric poly (vinylidene fluoride-hexafluoropropylene) copolymer," *Journal of applied physics*, vol. 97, no. 8, p. 084101, 2005.
- [5] A. Yadav, R. V. Patel, B. G. Vyas, P. K. Labhsetwar, and V. K. Shahi, "Recovery of CaSO₄ and NaCl from sub-soil brine using CNT@MOF5 incorporated poly(vinylidene fluoride-hexafluoropropylene) membranes via vacuum-assisted distillation," *Colloids and Surfaces A: Physicochemical and Engineering Aspects*, vol. 645, p. 128918, 2022/07/20/ 2022.
- [6] A. Rajput, J. Sharma, S. K. Raj, and V. Kulshrestha, "Dehydrofluorinated poly(vinylidene fluoride-co-hexafluoropropylene) based crosslinked cation exchange membrane for brackish water desalination via electrodialysis," *Colloids and Surfaces A: Physicochemical and Engineering Aspects*, vol. 630, p. 127576, 2021/12/05/ 2021.
- [7] A. Yadav, J. R. Mandal, A. B. Panda, and V. K. Shahi, "Structural tailoring of ceria nanoparticles for fabricating fouling resistant nanocomposite membranes with high flux distillation," *Colloids and Surfaces A: Physicochemical and Engineering Aspects*, vol. 633, p. 127858, 2022/01/20/ 2022.
- [8] A. M. Stephan, "Review on gel polymer electrolytes for lithium batteries," *European polymer journal*, vol. 42, no. 1, pp. 21-42, 2006.
- [9] J. C. Barbosa, J. P. Dias, S. Lanceros-Méndez, and C. M. Costa, "Recent advances in poly (vinylidene fluoride) and its copolymers for lithium-ion battery separators," *Membranes*, vol. 8, no. 3, p. 45, 2018.
- [10] A. Daneshkhah, S. Shrestha, M. Agarwal, and K. Varahramyan, "Poly (vinylidene fluoride-hexafluoropropylene) composite sensors for volatile organic compounds detection in breath," *Sensors and Actuators B: Chemical*, vol. 221, pp. 635-643, 2015.

- [11] T. Y. Inan, H. Doğan, and A. Güngör, "PVdF-HFP membranes for fuel cell applications: effects of doping agents and coating on the membrane's properties," *Ionics*, vol. 19, no. 4, pp. 629-641, 2013.
- [12] J. Li, M. Tenjimbayashi, N. S. Zacharia, and S. Shiratori, "One-step dipping fabrication of Fe₃O₄/PVDF-HFP composite 3D porous sponge for magnetically controllable oil–water separation," *ACS Sustainable Chemistry & Engineering*, vol. 6, no. 8, pp. 10706-10713, 2018.
- [13] H. Nassrullah, O. Mekanjuola, I. Janajreh, F. A. AlMarzooqi, and R. Hashaikeh, "Incorporation of nanosized LTL zeolites in dual-layered PVDF-HFP/cellulose membrane for enhanced membrane distillation performance," *Journal of Membrane Science*, vol. 611, p. 118298, 2020.
- [14] T. Liang, J.-H. Cao, W.-H. Liang, Q. Li, L. He, and D.-Y. Wu, "Asymmetrically coated LAGP/PP/PVDF–HFP composite separator film and its effect on the improvement of NCM battery performance," *RSC Advances*, vol. 9, no. 70, pp. 41151-41160, 2019.
- [15] S. K. Chacko, M. Rahul, B. Raneesh, and N. Kalarikkal, "Enhanced magnetoelectric coupling and dielectric constant in flexible ternary composite electrospun fibers of PVDF-HFP loaded with nanoclay and NiFe₂O₄ nanoparticles," *New Journal of Chemistry*, vol. 44, no. 26, pp. 11356-11364, 2020.
- [16] A. Maitra *et al.*, "Trielectric nanogenerator driven self-charging and self-healing flexible asymmetric supercapacitor power cell for direct power generation," *ACS applied materials & interfaces*, vol. 11, no. 5, pp. 5022-5036, 2019.
- [17] D. Ponnamma, O. Aljarod, H. Parangusan, and M. A. A. Al-Maadeed, "Electrospun nanofibers of PVDF-HFP composites containing magnetic nickel ferrite for energy harvesting application," *Materials Chemistry and Physics*, vol. 239, p. 122257, 2020.
- [18] Y. N. Venevtsev, V. V. Gagulin, and I. D. Zhitomirsky, "Material science aspects of seignette-magnetism problem," *Ferroelectrics*, vol. 73, no. 1, pp. 221-248, 1987/06/01 1987.
- [19] H. Schmid, "Multi-ferroic magnetoelectrics," *Ferroelectrics*, vol. 162, no. 1, pp. 317-338, 1994.
- [20] J. Ahmad *et al.*, "A facile strategy for the preparation of bismuth ferrite nanoparticles: Influence of calcination temperature on structural, dielectric, and morphological characteristics," *Colloids and Surfaces A: Physicochemical and Engineering Aspects*, vol. 628, p. 127328, 2021/11/05/ 2021.

- [21] E.-J. Lee, A. K. An, P. Hadi, S. Lee, Y. C. Woo, and H. K. Shon, "Advanced multi-nozzle electrospun functionalized titanium dioxide/polyvinylidene fluoride-co-hexafluoropropylene (TiO₂/PVDF-HFP) composite membranes for direct contact membrane distillation," *Journal of Membrane Science*, vol. 524, pp. 712-720, 2017.
- [22] V. B. Mišković-Stanković, "Electrophoretic deposition of ceramic coatings on metal surfaces," in *Electrodeposition and surface finishing*: Springer, 2014, pp. 133-216.
- [23] G. Amor, A. Vázquez, S. Obregón, and B. Kharisov, "Calcium carbonate hierarchical structures formed by a combined electrophoretic/electrochemical deposition," *Materials Letters*, vol. 295, p. 129856, 2021/07/15/ 2021.
- [24] G. Bree, H. Geaney, and K. M. Ryan, "Electrophoretic Deposition of Tin Sulfide Nanocubes as High-Performance Lithium-Ion Battery Anodes," *ChemElectroChem*, vol. 6, no. 12, pp. 3049-3056, 2019.
- [25] S. D. Perera *et al.*, "Enhanced Supercapacitor Performance for Equal Co-Mn Stoichiometry in Colloidal Co₃-xMnxO₄ Nanoparticles, in Additive-Free Electrodes," *Chemistry of Materials*, vol. 27, no. 23, pp. 7861-7873, 2015/12/08 2015.
- [26] B. Ferrari and R. Moreno, "EPD kinetics: a review," *Journal of the European Ceramic Society*, vol. 30, no. 5, pp. 1069-1078, 2010.
- [27] W. Huang *et al.*, "Electrophoretic deposited boron nitride nanosheets-containing chitosan-based coating on Mg alloy for better corrosion resistance, biocompatibility and antibacterial properties," *Colloids and Surfaces A: Physicochemical and Engineering Aspects*, vol. 638, p. 128303, 2022/04/05/ 2022.
- [28] J. Li and I. Zhitomirsky, "Cathodic electrophoretic deposition of manganese dioxide films," *Colloids and Surfaces A: Physicochemical and Engineering Aspects*, vol. 348, no. 1, pp. 248-253, 2009/09/20/ 2009.
- [29] G. Falk, A. Nold, and B. Wiegand, "Experimental and numerical analysis of electrophoretic deposition on charge selective surfaces in external electric fields," *Advances in Applied Ceramics*, vol. 113, no. 1, pp. 55-64, 01/ 2014.
- [30] O. O. Van der Biest and L. J. Vandeperre, "Electrophoretic deposition of materials," *Annual Review of Materials Science*, vol. 29, no. 1, pp. 327-352, 1999.
- [31] A. Singh, N. J. English, and K. M. Ryan, "Highly ordered nanorod assemblies extending over device scale areas and in controlled multilayers by electrophoretic

- deposition," *The Journal of Physical Chemistry B*, vol. 117, no. 6, pp. 1608-1615, 2013.
- [32] R. Mayén-Mondragón, G. Falk, and R. Clasen, "Electrophoretic Impregnation/Deposition Complemented with Polymeric Templating for the Fabrication of Functionalized-Porosity Layered-Ceramics: A Solid-Oxide-Fuel-Cells Approach," *Journal of the American Ceramic Society*, vol. 95, no. 2, pp. 593-599, 2012.
- [33] J. A. Argüello, J. M. Rojo, and R. Moreno, "Electrophoretic deposition of manganese oxide and graphene nanoplatelets on graphite paper for the manufacture of supercapacitor electrodes," *Electrochimica Acta*, vol. 294, pp. 102-109, 2019.
- [34] K. Shi and I. Zhitomirsky, "Electrophoretic nanotechnology of graphene-carbon nanotube and graphene-polypyrrole nanofiber composites for electrochemical supercapacitors," *Journal of Colloid and Interface Science*, vol. 407, pp. 474-481, 2013/10/01/ 2013.
- [35] R. Sikkema, K. Baker, and I. Zhitomirsky, "Electrophoretic deposition of polymers and proteins for biomedical applications," *Advances in Colloid and Interface Science*, vol. 284, p. 102272, 2020/10/01/ 2020.
- [36] I. Zhitomirsky, "New Developments in Electrolytic Deposition of Ceramic Films," *American Ceramic Society Bulletin*, vol. 79, no. 9, pp. 57-62, 2000.
- [37] X. Pang, I. Zhitomirsky, and M. Niewczas, "Cathodic electrolytic deposition of zirconia films," *Surface and Coatings Technology*, vol. 195, no. 2, pp. 138-146, 2005/05/31/ 2005.
- [38] I. Zhitomirsky and A. Petric, "Electrochemical deposition of yttrium oxide," *Journal of Materials Chemistry*, 10.1039/B000311P vol. 10, no. 5, pp. 1215-1218, 2000.
- [39] O. O. Otelaja, D.-H. Ha, T. Ly, H. Zhang, and R. D. Robinson, "Highly conductive Cu_{2-x}S nanoparticle films through room-temperature processing and an order of magnitude enhancement of conductivity via electrophoretic deposition," *ACS Applied Materials & Interfaces*, vol. 6, no. 21, pp. 18911-18920, 2014.
- [40] J. A. Argüello, A. Cerpa, and R. Moreno, "Reinforcing effect of graphene nanoplatelets in the electrochemical behaviour of manganese oxide-based supercapacitors produced by EPD," *Ceramics International*, vol. 45, no. 11, pp. 14316-14321, 2019.

- [41] B. I. Kharisov, O. V. Kharissova, and A. V. Dimas, "The dispersion, solubilization and stabilization in "solution" of single-walled carbon nanotubes," *RSC advances*, vol. 6, no. 73, pp. 68760-68787, 2016.
- [42] Y. Su and I. Zhitomirsky, "Electrophoretic deposition of graphene, carbon nanotubes and composite films using methyl violet dye as a dispersing agent," *Colloids and Surfaces A: Physicochemical and Engineering Aspects*, vol. 436, pp. 97-103, 2013/09/05/ 2013.
- [43] C. Mendoza, Z. González, Y. Castro, E. Gordo, and B. Ferrari, "Improvement of TiN nanoparticles EPD inducing steric stabilization in non-aqueous suspensions," *Journal of the European Ceramic Society*, vol. 36, no. 2, pp. 307-317, 2016.
- [44] B. S. Lalia, C. Garlisi, G. Palmisano, and R. Hashaikeh, "Photocatalytic activity of an electrophoretically deposited composite titanium dioxide membrane using carbon cloth as a conducting substrate," *RSC advances*, vol. 6, no. 69, pp. 64219-64227, 2016.
- [45] Y. Han *et al.*, "Direct electrophoretic deposition of an ultra-strong separator on an anode in a surfactant-free colloidal system for lithium ion batteries," *Journal of Materials Chemistry A*, vol. 7, no. 4, pp. 1410-1417, 2019.
- [46] T. He *et al.*, "A solid-electrolyte-reinforced separator through single-step electrophoretic assembly for safe high-capacity lithium ion batteries," *Journal of Power Sources*, vol. 448, p. 227469, 2020.
- [47] J. Zhao *et al.*, "Atomic interlamellar ion path in polymeric separator enables long-life and dendrite-free anode in lithium ion batteries," *Journal of Power Sources*, vol. 451, p. 227773, 2020.
- [48] B. P. Lee, P. B. Messersmith, J. N. Israelachvili, and J. H. Waite, "Mussel-inspired adhesives and coatings," *Annual review of materials research*, vol. 41, pp. 99-132, 2011.
- [49] H. Lee, B. P. Lee, and P. B. Messersmith, "A reversible wet/dry adhesive inspired by mussels and geckos," *Nature*, vol. 448, no. 7151, pp. 338-341, 2007.
- [50] N. Xu *et al.*, "A mussel-inspired strategy for CNT/carbon fiber reinforced epoxy composite by hierarchical surface modification," *Colloids and Surfaces A: Physicochemical and Engineering Aspects*, vol. 635, p. 128085, 2022/02/20/ 2022.
- [51] M. Ata, Y. Liu, and I. Zhitomirsky, "A review of new methods of surface chemical modification, dispersion and electrophoretic deposition of metal oxide particles," *Rsc Advances*, vol. 4, no. 43, pp. 22716-22732, 2014.

- [52] K. Wu, Y. Wang, and I. Zhitomirsky, "Electrophoretic deposition of TiO₂ and composite TiO₂-MnO₂ films using benzoic acid and phenolic molecules as charging additives," *Journal of colloid and interface science*, vol. 352, no. 2, pp. 371-378, 2010.
- [53] Y. Wang and I. Zhitomirsky, "Bio-inspired catechol chemistry for electrophoretic nanotechnology of oxide films," *Journal of colloid and interface science*, vol. 380, no. 1, pp. 8-15, 2012.
- [54] Q. Zhao, S. Veldhuis, R. Mathews, and I. Zhitomirsky, "Influence of chemical structure of bile acid dispersants on electrophoretic deposition of poly (vinylidene fluoride) and composites," *Colloids and Surfaces A: Physicochemical and Engineering Aspects*, vol. 627, p. 127181, 2021.
- [55] M. Hashiba, H. Okamoto, Y. Nurishi, and K. Hiramatsu, "The zeta-potential measurement for concentrated aqueous suspension by improved electrophoretic mass transport apparatus—application to Al₂O₃, ZrO₃ and SiC suspensions," *Journal of materials science*, vol. 23, no. 8, pp. 2893-2896, 1988.
- [56] C. Zhao *et al.*, "Particle formation mechanisms in the nanoprecipitation of polystyrene," *Langmuir*, vol. 36, no. 44, pp. 13210-13217, 2020.
- [57] J. S. Hong, D. Srivastava, and I. Lee, "Fabrication of poly (lactic acid) nano-and microparticles using a nanomixer via nanoprecipitation or emulsion diffusion," *Journal of Applied Polymer Science*, vol. 135, no. 18, p. 46199, 2018.
- [58] C. Mora-Huertas, H. Fessi, and A. Elaissari, "Influence of process and formulation parameters on the formation of submicron particles by solvent displacement and emulsification–diffusion methods: Critical comparison," *Advances in colloid and interface science*, vol. 163, no. 2, pp. 90-122, 2011.
- [59] M. J. Toh, P. C. Oh, T. L. Chew, and A. L. Ahmad, "Antiwettability enhancement of PVDF-HFP membrane via superhydrophobic modification by SiO₂ nanoparticles," *Comptes Rendus Chimie*, vol. 22, no. 5, pp. 369-372, 2019.
- [60] S. Wongchitphimon, R. Wang, R. Jiratananon, L. Shi, and C. H. Loh, "Effect of polyethylene glycol (PEG) as an additive on the fabrication of polyvinylidene fluoride-co-hexafluoropropylene (PVDF-HFP) asymmetric microporous hollow fiber membranes," *Journal of Membrane Science*, vol. 369, no. 1, pp. 329-338, 2011/03/01/ 2011.
- [61] I. Zhitomirsky and L. Gal-Or, "Electrophoretic deposition of hydroxyapatite," *Journal of Materials Science: Materials in Medicine*, vol. 8, no. 4, pp. 213-219, 1997.

- [62] Q. Zhao, X. Liu, S. Veldhuis, and I. Zhitomirsky, "Sodium deoxycholate as a versatile dispersing and coating-forming agent: A new facet of electrophoretic deposition technology," *Colloids and Surfaces A: Physicochemical and Engineering Aspects*, vol. 588, p. 124382, 2020.
- [63] Q. Zhao, X. Liu, and I. Zhitomirsky, "Electrophoretic deposition of materials using lithocholic acid as a dispersant," *Materials Letters*, p. 128129, 2020.
- [64] A. Naseri, M. Goodarzi, and D. Ghanbari, "Green synthesis and characterization of magnetic and effective photocatalyst NiFe₂O₄-NiO nanocomposites," *Journal of Materials Science: Materials in Electronics*, vol. 28, no. 23, pp. 17635-17646, 2017.
- [65] S. Mahendrakar, M. Anna, and J. Reddy, "Structural, morphological and FTIR of PVDF-HFP and lithium tetrafluoroborate salt as polymer electrolyte membrane in lithium ion batteries," *Int. J. Chem. Technol. Res.*, vol. 8, pp. 319-328, 2015.
- [66] P. Tuhania *et al.*, "PVDF-HFP and 1-ethyl-3-methylimidazolium thiocyanate-doped polymer electrolyte for efficient supercapacitors," *High Performance Polymers*, vol. 30, no. 8, pp. 911-917, 2018.
- [67] L. Yesappa *et al.*, "Optical properties and ionic conductivity studies of an 8 MeV electron beam irradiated poly (vinylidene fluoride-co-hexafluoropropylene)/LiClO₄ electrolyte film for opto-electronic applications," *RSC Advances*, vol. 8, no. 28, pp. 15297-15309, 2018.
- [68] N. Tarutani, R. Uesugi, K. Uemura, K. Katagiri, K. Inumaru, and Y. Takeoka, "Understanding the Electrophoretic Deposition Accompanied by Electrochemical Reactions Toward Structurally Colored Bilayer Films," *ACS Applied Materials & Interfaces*, 2022.
- [69] I. Zhitomirsky, "Electrophoretic hydroxyapatite coatings and fibers," *Materials Letters*, vol. 42, no. 4, pp. 262-271, 2000.
- [70] W. M. Winslow, "Induced fibrillation of suspensions," *Journal of applied physics*, vol. 20, no. 12, pp. 1137-1140, 1949.
- [71] I. Zhitomirsky, "Cathodic electrodeposition of ceramic and organoceramic materials. Fundamental aspects," *Advances in colloid and interface science*, vol. 97, no. 1-3, pp. 279-317, 2002.
- [72] K. Grandfield and I. Zhitomirsky, "Electrophoretic deposition of composite hydroxyapatite-silica-chitosan coatings," *Materials Characterization*, vol. 59, no. 1, pp. 61-67, 2008/01/01/ 2008.

- [73] A. Mahajan and E. V Ramana, "Patents on magnetoelectric multiferroics and their processing by electrophoretic deposition," *Recent Patents on Materials Science*, vol. 7, no. 2, pp. 109-130, 2014.
- [74] Y. Wang, J. Hu, Y. Lin, and C.-W. Nan, "Multiferroic magnetoelectric composite nanostructures," *NPG asia materials*, vol. 2, no. 2, pp. 61-68, 2010.

Chapter 9 EPD of PVDF-HFP-CuFe₂O₄ Composites

This chapter is reproduced from **Q. Zhao and I. Zhitomirsky**, *Colloidal processing of ferroelectric poly(vinylidene fluoride-co-hexafluoropropylene) – ferrimagnetic pseudocapacitive CuFe₂O₄ composite films*, *Colloid Polymer Science* 300, 1197–1204 (2022), (<https://doi.org/10.1007/s00396-022-05022-9>) with permission from Copyright © 2022 Elsevier B.V. The author of this thesis is the first author and the main contributor of this publication, including conceiving the initial ideas, carrying out experiments, development of approach and methodology, analysis of data, writing the initial draft and preparation of the manuscript.

9.1 Abstract

Composite polymer-ceramic films are prepared from colloidal suspensions by electrophoretic deposition (EPD). Co-deposition of ferrimagnetic CuFe₂O₄ with ferroelectric poly(vinylidene fluoride-co-hexafluoropropylene) (PVDF-HFP) polymer is achieved using a co-dispersant, which is also used for the preparation of PVDF-HFP particles. The mechanism of co-dispersant adsorption on CuFe₂O₄ and PVDF-HFP in colloidal suspensions is analyzed. Electrochemical studies of CuFe₂O₄ reveal good pseudocapacitive properties of this material in a negative potential range, which make it a material of choice for magnetocapacitive devices. A capacitance of 1.72 F·cm⁻² (43.1 F·g⁻¹) is observed at 2 mV·s⁻¹ for pure material in a neutral Na₂SO₄ electrolyte. The

microstructure and composition of PVDF-HFP-CuFe₂O₄ films are analyzed. Composite films show ferrimagnetic properties, which are analyzed in a wide temperature range. EPD method represents a versatile strategy for the fabrication of composite films based on functional properties of CuFe₂O₄ and PVDF-HFP.

9.2 Introduction

Poly(vinylidene fluoride-co-hexafluoropropylene) (PVDF-HFP) is an important functional polymer for various applications [1-3] due to its high chemical stability, biocompatibility, flexibility, optical transparency, ferroelectric and piezoelectric properties [4-7]. PVDF-HFP has generated significant interest for fuel cells [8], biosensors [9], and lithium batteries [10, 11]. Many applications are based on the use of PVDF-HFP composites for triboelectric nanogenerators [12], magnetoelectric devices [13], batteries [14], distillation membranes [15], energy storage devices [16] and magnetically controllable oil-water separation [17].

Ferroelectric PVDF-HFP is a very promising polymer for the fabrication of multiferroic composite materials, combining ferroelectric and magnetic properties. Multiferroic composites offer advantages compared to individual multiferroic compounds. The analysis of review literature [18, 19] on multiferroic compounds indicates that such compounds exhibit antiferroelectric properties or weak ferro-/ferrimagnetic properties at low temperatures. The combination of ferroelectric PVDF-HFP with advanced ferrites in composite materials can potentially result in the fabrication of multiferroic composites with high magnetization. Moreover, recent studies revealed pseudocapacitive properties of

spinel ferrites [20-22]. The theoretical capacitance of such materials is by many orders of magnitude higher than the capacitance of the best ferroelectric materials. Therefore, the incorporation of spinel ferrites into PVDF-HFP matrix can impart advanced capacitive properties to the composites.

CuFe_2O_4 is a promising ferrimagnetic spinel material for the fabrication of PVDF-HFP composites. This material exhibits advanced magnetic and photocatalytic properties [23]. Magnetic properties of CuFe_2O_4 spinel depend on distribution of Cu^{2+} and Fe^{3+} ions in crystallographic tetrahedral and octahedral positions [24, 25]. It is known that Fe^{3+} cations in oxide materials can be reduced electrochemically [26-28] to Fe^{2+} , whereas Cu^{2+} cations can be reduced [29-31] to Cu^+ . Therefore, interesting pseudocapacitive properties of CuFe_2O_4 can be expected in a negative potential range. However, pseudocapacitive properties of CuFe_2O_4 were observed in a positive potential range [32-36]. The investigation of pseudocapacitive properties of CuFe_2O_4 in the negative potential range is of particular interest for the analysis of potential magnetocapacitive effects. Such effects can result from changes in magnetization due to changes in magnetic moments of ions during the reduction process.

Many applications of multiferroic and magnetocapacitive materials involve the use of thin films and significant attention was focused on the development of film deposition techniques [37-40]. PVDF-HFP is a promising polymer for the fabrication of composite films due to its high chemical stability and flexibility. PVDF-HFP films were deposited by dip coating [17], spray coating [9], electrospinning [41], and spin-coating [9]. Colloidal

techniques, such as electrophoretic deposition (EPD) [42-45], offer advantages for the fabrication of composite films. EPD facilitates uniform deposition on substrates of complex shape at a high deposition rate [46, 47]. This method allows excellent control of deposit stoichiometry, which is critically important for the deposition of complex oxides with advanced functionality [48]. The success in the fabrication of composites by colloidal method is inevitably related to the development of advanced techniques for surface functionalization and dispersion of particles [49-51]. EPD of composites requires the use of co-dispersants, suitable for deposition of individual components [52-54]. Recent studies showed that EPD of CuFe_2O_4 can be achieved using $\text{Mg}(\text{NO}_3)_2$ as a charging and dispersing agent. However, the use of $\text{Mg}(\text{NO}_3)_2$ can result in film contamination due to the cathodic electrosynthesis [55] of $\text{Mg}(\text{OH})_2$. Moreover, this strategy cannot be used for co-deposition of CuFe_2O_4 with PVDF-HFP.

The goal of this investigation was the fabrication of PVDF-HFP- CuFe_2O_4 films by EPD. The results presented below demonstrate good pseudocapacitive properties of CuFe_2O_4 in a negative potential range. Co-deposition of PVDF-HFP and CuFe_2O_4 films was achieved using caffeic acid as a co-dispersant. Composite films showed ferrimagnetic properties. The EPD method represents a versatile strategy for the fabrication of composite films with advanced functional properties. The incorporation of CuFe_2O_4 into PVDF-HFP offers benefits for the fabrication of films with advanced functionality, due to magnetic, pseudocapacitive and photocatalytic properties of CuFe_2O_4 .

9.3 Experimental Procedures

CuFe₂O₄ nanopowder (size<100 nm), poly(vinylidene fluoride-co-hexafluoropropylene) (PVDF-HFP, M_w~400 kDa), absolute ethanol, N-methyl-2-pyrrolidone (NMP) and caffeic acid (CA) were obtained from (MilliporeSigma, Canada). As-received PVDF-HFP contained beads with a typical size of 0.5 cm. The PVDF-HFP beads were dissolved in NMP solvent and added dropwise to ethanol, containing dissolved CA. Obtained 5 g·L⁻¹ suspensions of PVDF-HFP particles, dispersed using CA in a mixed solvent of 75% ethanol-25% NMP were used for electrophoretic deposition of pure PVDF-HFP. Composite PVDF-HFP-CuFe₂O₄ films were obtained from suspensions, containing 5 g·L⁻¹ PVDF-HFP and 5 g·L⁻¹ CuFe₂O₄, which were dispersed in 75% ethanol-25% NMP solvent using CA as a co-dispersant. The concentration of dissolved CA in suspensions used for EPD was 1 g·L⁻¹.

304 stainless steel and Pt foils were used as anodic substrates and cathodes, respectively, for anodic EPD. The deposition voltages were 50 V for PVDF-HFP films and 30 V for composite PVDF-HFP-CuFe₂O₄ films. The distance between electrodes was 1.5 cm. The suspensions were ultrasonicated for 30 min before EPD. The deposition time was 5 min.

Microstructure characterization was performed by a scanning electron microscope (SEM, JSM-7000F, JEOL) and a transmission electron microscope (TEM, Talos 200X). Pseudocapacitive properties of CuFe₂O₄ were studied using electrodes with high active mass loadings of 40 mg·cm⁻² for comparison with other pseudocapacitive materials [56].

The electrode fabrication procedure was similar to that used for other pseudocapacitive materials [56-58]. Slurries of CuFe_2O_4 in NMP, containing dissolved PVDF-HFP were used for impregnation of Ni foam (Vale, Canada) current collectors. PVDF-HFP acted as a binder for CuFe_2O_4 particles. The binder content in the electrode material was 5%. The initial thickness of the porous current collectors (95% porosity) was 1.6 mm. After impregnation and drying, the obtained electrodes were pressed to 30% on the initial thickness in order to reduce porosity and improve electric contact of active material with current collector. Electrochemical testing was performed using PARSTAT 2273 (Ametek) potentiostat and a 3-electrode cell, containing a working electrode with area of 1 cm^2 , saturated calomel electrode (SCE) and Pt mesh counter electrode in $0.5 \text{ M Na}_2\text{SO}_4$ electrolyte. Cyclic voltammetry studies were performed in a negative potential range of -0.8 - 0.0 V versus SCE. Complex impedance (Z^*) measurements were performed at a voltage amplitude of 5 mV in a frequency (f) range of 10 mHz - 10 kHz . Electrode area normalized capacitance (C_s) and mass normalized capacitances (C_m) were calculated from the CV and impedance data.

The following equation was used for capacitance calculations from CV data:

$$C = \frac{\Delta Q}{\Delta U} = \frac{\left| \int_0^{t(U_{max})} I dt \right| + \left| \int_{t(U_{max})}^0 I dt \right|}{2U_{max}} \quad (9-1)$$

where ΔQ is charge, ΔU is the potential range, I is current and t is time.

The impedance $Z^*(\omega) = Z'(\omega) + iZ''(\omega)$ data at different frequencies $\omega = 2\pi f$ was used for the calculation of complex capacitance $C^*(\omega) = C'(\omega) - iC''(\omega)$:

$$C'(\omega) = \frac{-Z''(\omega)}{\omega|Z(\omega)|^2} \quad (9-2)$$

$$C''(\omega) = \frac{Z'(\omega)}{\omega|Z(\omega)|^2} \quad (9-3)$$

Deposited films were scraped off from the substrates and powder samples obtained were used for X-ray diffraction (XRD) studies, magnetic measurements, Fourier transform infrared spectroscopy (FTIR) studies, thermogravimetric analysis (TGA) and differential thermal analysis (DTA). XRD studies (diffractometer Bruker D8, Cu-K α radiation, UK) were performed at the rate of 0.01 degrees per second.

Magnetic properties were studied using a Quantum Design PPMS-9 system. Magnetization hysteresis loops were obtained by applying external magnetic field at the sweep rate of 10 Oe \cdot min $^{-1}$. The temperature dependence of the magnetization was studied by both zero-field-cooled (ZFC) and field-cooled (FC) procedures. The sample was cooled down to 1.9 K in the zero external field (ZFC) and then magnetization was measured during heating to 300 K under the applied field of 100 Oe. The sample was subsequently cooled back to 1.9 K under an applied field of 100 Oe (FC) and the measurements of magnetization were carried out during heating to 300 K.

FTIR studies were performed using a Bruker Vertex 70 spectrometer (USA) in the range of 400-4000 cm^{-1} . The TGA and DTA studies were performed using a thermoanalyzer (Netzsch STH-409), which was operated in air between room temperature and 1000 $^{\circ}\text{C}$ at a heating rate of 5 $^{\circ}\text{C}\cdot\text{min}^{-1}$.

9.4 Results and Discussion

Figure 9.1 shows results of magnetic measurements of pure CuFe_2O_4 material. Magnetic measurements indicated that as-received CuFe_2O_4 particles showed ferrimagnetic behavior at room temperature.

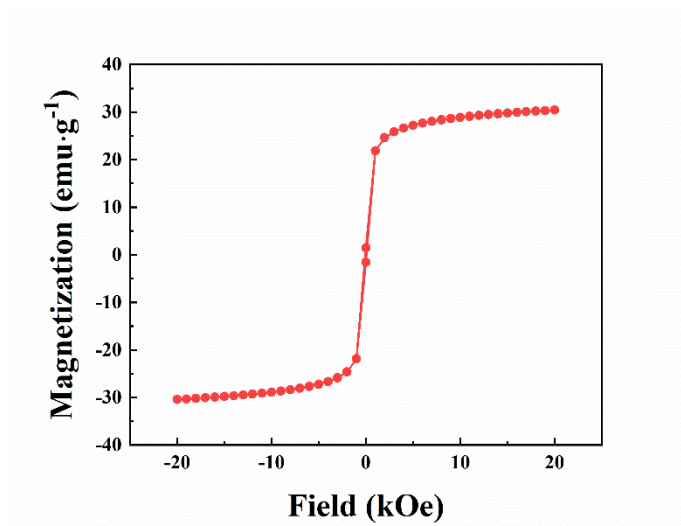


Figure 9.1 Magnetization versus magnetic field for as-received CuFe_2O_4 .

Electrochemical studies showed pseudocapacitive properties of CuFe_2O_4 in the negative potential range. Figure 9.2A shows CVs for CuFe_2O_4 electrodes in the potential range of -0.8-0.0 V versus SCE.

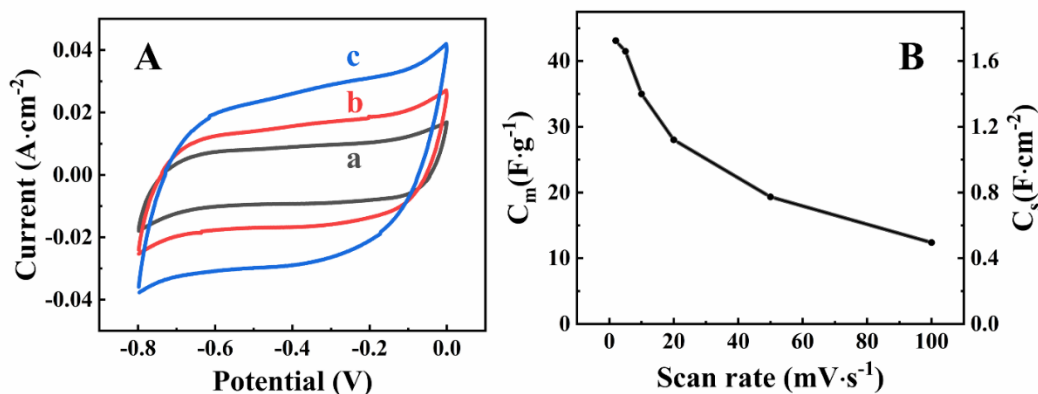


Figure 9.2 (A) CVs at sweep rates of (a) 5, (b) 10 and (c) 20 $\text{mV}\cdot\text{s}^{-1}$ and (B) capacitance, calculated from CV data versus scan rate for CuFe_2O_4 electrodes.

For an ideal capacitor $Q=CU$, therefore a constant current $I=dQ/dt=CdU/dt$ is observed at a constant scan rate (dU/dt). The analysis of CV data at low scan rates revealed nearly constant charge/discharge currents without redox peaks, which indicated pseudocapacitive behavior. However, CVs were slightly tilted at higher scan rates. This can result from ion diffusion limitations in pores of the material at high scan rates. The capacitance of $1.72 \text{ F}\cdot\text{cm}^{-2}$ ($43.1 \text{ F}\cdot\text{g}^{-1}$) was observed at $2 \text{ mV}\cdot\text{s}^{-1}$. The capacitance decreased with increasing scan rate to the level of $0.5 \text{ F}\cdot\text{cm}^{-2}$ ($12.4 \text{ F}\cdot\text{g}^{-1}$) at $100 \text{ mV}\cdot\text{s}^{-1}$. A relatively high capacitance of CuFe_2O_4 makes it a promising energy storage material. As pointed out above the high capacitance in the negative potential range can result in magnetocapacitive effects in this material, because reduction of metal ions in this range results in changing of their magnetic moments, which influence superexchange interactions of the ions and ferrimagnetic behavior of the material. Figure 9.3 shows impedance spectroscopy data for the CuFe_2O_4

electrodes. The Nyquist plot of complex impedance showed a relatively low resistance of the electrode.

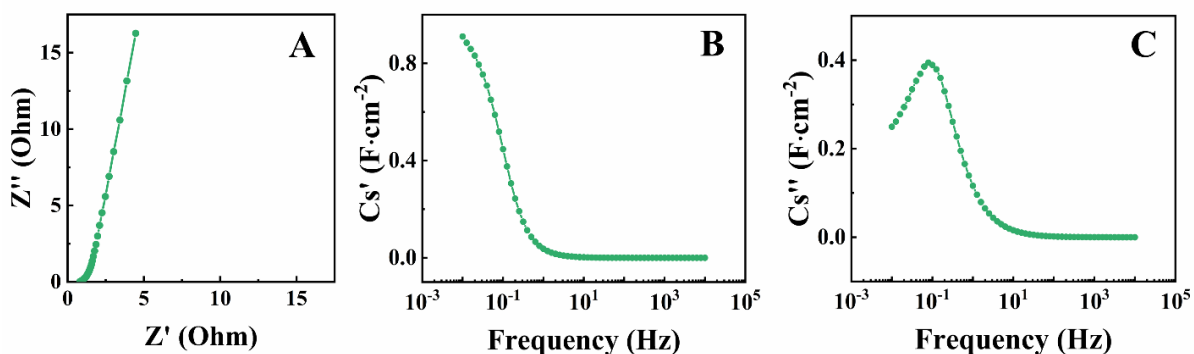


Figure 9.3 (A) Nyquist plot, (B,C) frequency dependences of (B) C_s' and (C) C_s'' for CuFe_2O_4 .

It should be noted that capacitance C_s' obtained from impedance data depends on frequency, whereas C_s derived from the CV data depends on scan rate. Therefore, the capacitances must be compared at similar charge-discharge time scales. It was found that such comparison gives comparable capacitances measured by both methods. The frequency, corresponding to the maximum in the C_s'' is a relaxation frequency, which was relatively high and indicated good material performance.

Following the goal of this investigation, EPD method was used for the fabrication of PVDF-HFP- CuFe_2O_4 films. Figure 9.4 shows a TEM image of PVDF-HFP particles prepared in this investigation. It should be noted that original large PVDF-HFP beads cannot be used for EPD due to their large size. The particle preparation procedure resulted in the fabrication of relatively small particles with a typical size of 1.5-2 μm . Drying resulted in

neck formation between the particles and facilitated the formation of relatively dense films by EPD (Figure 9.5). It is suggested that adsorbed anionic CA imparted a negative charge to the particles for their anodic EPD. Moreover, CA acted as a co-dispersant for PVDF-HFP and CuFe_2O_4 and facilitated their co-EPD from colloidal suspensions. SEM images in Figure 9.5 show that small CuFe_2O_4 nanoparticles were co-deposited with PVDF-HFP and incorporated into the PVDF-HFP matrix. It should be noted that CuFe_2O_4 nanoparticles are prone to agglomeration in colloidal suspensions due to van der Waals and magnetic attraction forces. The use of CA allowed for their efficient dispersion, charging and deposition.

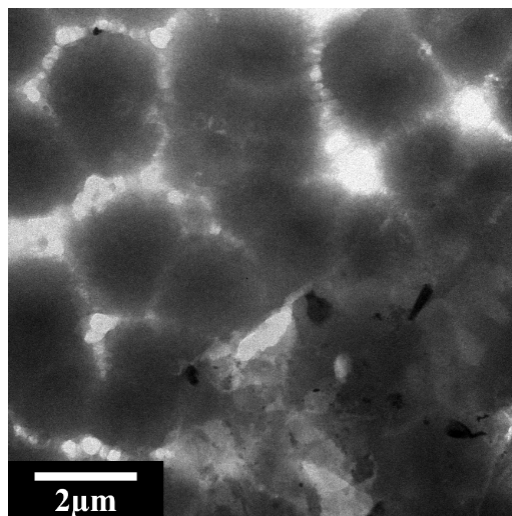


Figure 9.4 TEM image of PVDF-HFP particles.

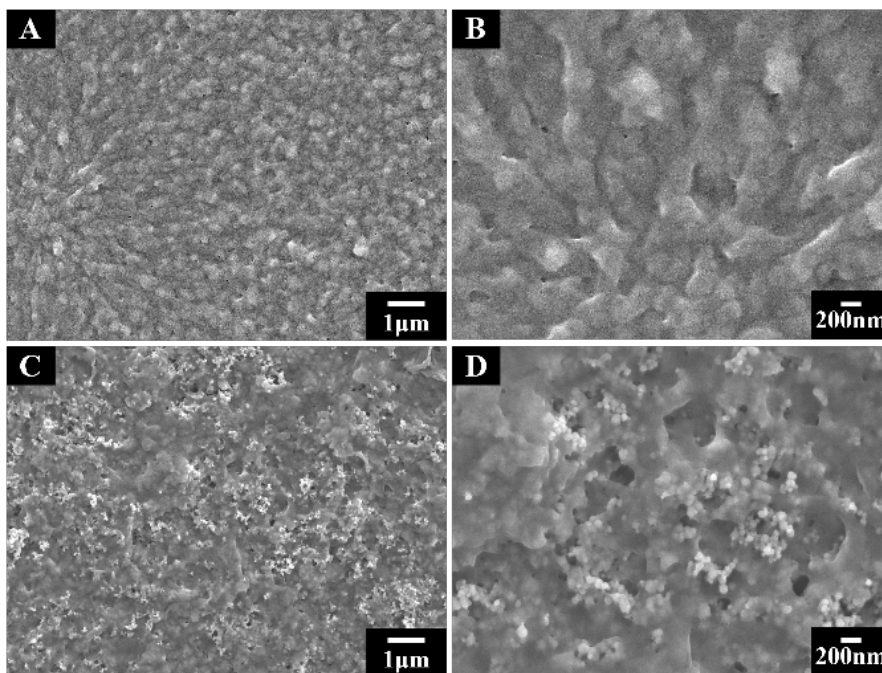


Figure 9.5 SEM images at different magnifications for (A, B) PVDF-HFP and (C, D) PVDF-HFP-CuFe₂O₄ films prepared by EPD.

Figure 9.6A shows the chemical structure of CA. This molecule belongs to the catecholate group of materials [59], which show strong adsorption on inorganic surfaces by creation of bidentate chelating or bridging bonding (Figure 9.6 (B, C)). The electric charge of adsorbed CA allows EPD of materials [59].

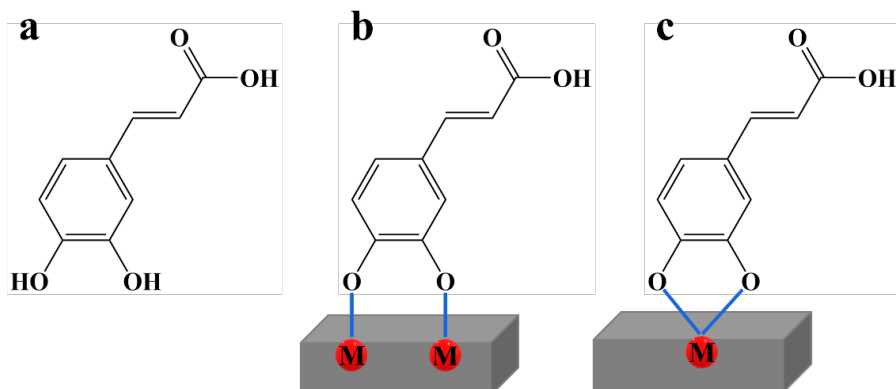


Figure 9.6 (A) Chemical structure of CA, (B, C) CA adsorption on particle surface by bidentate (A) bridging or (C) chelating bonding, involving metal atoms $M = \text{Cu}$ or Fe on the surface.

The interest in catecholite dispersants [53, 59] for EPD of inorganic materials has been fueled by analysis of strong mussel adsorption on surfaces, which involves catecholite-type amino acid monomers of mussel proteins [60, 61]. It is suggested that the adsorption of CA on PVDF-HFP involved hydrophobic interactions. Many commercial dispersants fail to provide co-EPD of materials of different materials classes. In contrast, CA co-dispersant allowed co-EPD of PVDF-HFP polymer and inorganic CuFe_2O_4 particles.

The co-deposition of CuFe_2O_4 and of PVDF-HFP was confirmed by XRD, FTIR, TGA/DTA and magnetic measurements. Figure 9.7 shows X-ray diffraction patterns of as-received CuFe_2O_4 and PVDF-HFP- CuFe_2O_4 composite.

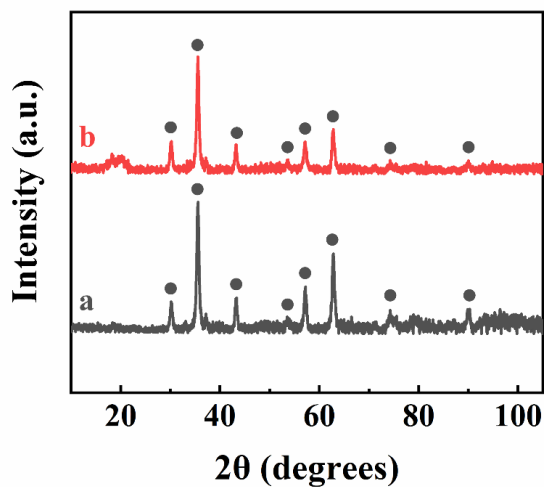


Figure 9.7 X-ray diffraction patterns of (a) as-received CuFe_2O_4 and (b) PVDF-HFP- CuFe_2O_4 deposit prepared by EPD (● peaks, corresponding to JCPDS file 04-006-6233 of CuFe_2O_4).

As-received CuFe_2O_4 showed peaks, corresponding to JCPDS file 04-006-6233. The deposited PVDF-HFP- CuFe_2O_4 films showed similar peaks and confirmed deposition of CuFe_2O_4 .

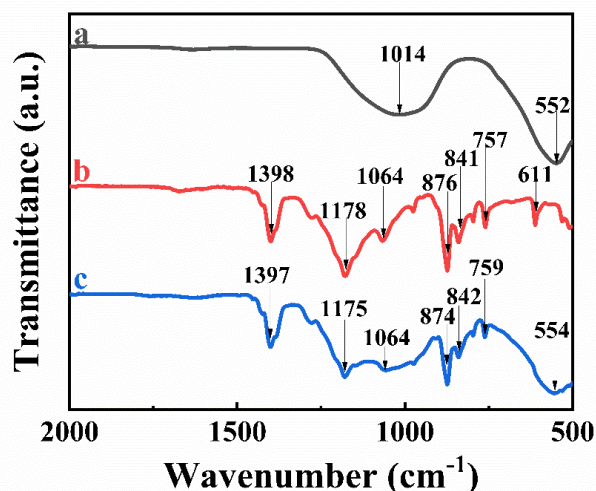


Figure 9.8 FTIR spectra of (a) as-received CuFe_2O_4 , (b) deposited PVDF-HFP film and (c) deposited PVDF-HFP- CuFe_2O_4 composite film.

Figure 9.8 shows FTIR spectra of as-received CuFe_2O_4 nanoparticles, deposited PVDF-HFP and PVDF-HFP- CuFe_2O_4 composites. The spectrum of CuFe_2O_4 showed broad peaks around 552 and 1014 cm^{-1} , which can be attributed to M-O vibrations ($\text{M}=\text{Cu, Fe}$) and surface vibrations of M-OH groups, respectively [62, 63].

The absorptions at 611 and 757 cm^{-1} in the spectrum of PVDF-HFP are attributed to characteristic vibrations of the crystalline VDF group [64]. The amorphous phase contributed to peaks at 841 and 876 cm^{-1} [65]. The absorptions at 1064 and 1178 cm^{-1} resulted from the stretching symmetrical vibrations of CF_2 [66]. The absorption at 1398 cm^{-1} resulted from -C-F stretching [66]. The spectrum of deposited PVDF-HFP- CuFe_2O_4 composite film showed peaks related to PVDF-HFP as well as CuFe_2O_4 and confirmed their co-deposition.

TGA studies showed mass loss, related to burning out of PVDF-HFP. The remaining mass of the composite material at high temperatures represents the mass of CuFe_2O_4 . The DTA data showed an exothermic peak due to burning out of PVDF-HFP, corresponding to the step in the TGA data (Figure 9.9). Therefore, TGA/DTA data also confirms co-deposition of PVDF-HFP with CuFe_2O_4 .

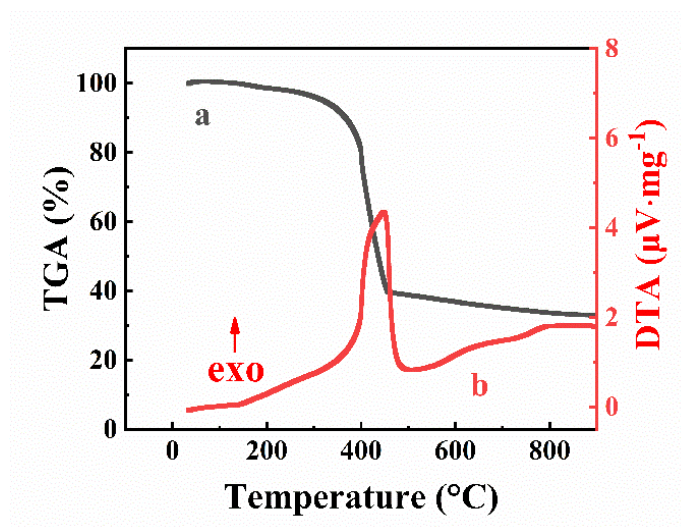


Figure 9.9 (a) TGA and (b) DTA data for PVDF-HFP- CuFe_2O_4 composite deposit.

Figure 9.10 shows magnetic measurement data for the composite film. The magnetization versus magnetic field dependence shows ferrimagnetic behavior of the composite film. The composite showed a relatively high magnetization. As expected, the mass normalized magnetization is lower than that for pure CuFe_2O_4 material. ZFC and FC curves confirmed ferrimagnetic behavior of the composite material. ZFC curve in the range of 1.9-298 K did not show a maximum related to blocking temperature of transition from the ferrimagnetic to a superparamagnetic state.

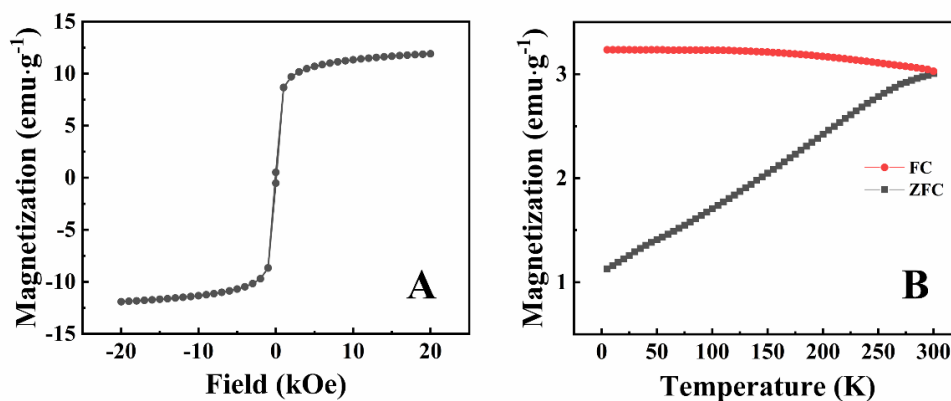


Figure 9.10 (A) Magnetization versus magnetic field at 300 K and (B) ZFC and FC magnetization data for PVDF-HFP-CuFe₂O₄ composite.

Testing results indicate that PVDF-HFP-CuFe₂O₄ composite material, combining functional properties of PVDF-HFP and CuFe₂O₄ can be prepared by EPD. Further investigations will be focused on the variation of film composition, which can be achieved by variation of mass ratio of PVDF-HFP and CuFe₂O₄ in the EPD bath. It should be noted that PVDF-HFP exhibits low conductivity, which is detrimental for observation of pseudocapacitive properties of CuFe₂O₄. Therefore, advanced pseudocapacitive, magnetic and photocatalytic properties [23] can be observed at a high CuFe₂O₄ content in the composite. A relatively high conductivity of CuFe₂O₄ is beneficial for the pseudocapacitive charging mechanism [67]. Such films can potentially exhibit magnetocapacitive effects due to redox-active properties of CuFe₂O₄ in the negative potential range. In contrast, ferroelectric properties of PVDF-HFP can be combined with magnetic properties of CuFe₂O₄ at high PVDF-HFP content. The relatively high dielectric constant of CuFe₂O₄ [67] can result in enhanced dielectric constant of such composites.

9.5 Conclusions

EPD method has been developed for the fabrication of composite films of ferrimagnetic CuFe_2O_4 and ferroelectric PVDF-HFP. Electrochemical studies revealed advanced pseudocapacitive properties of CuFe_2O_4 in a negative potential range. A capacitance of $1.72 \text{ F}\cdot\text{cm}^{-2}$ ($43.1 \text{ F}\cdot\text{g}^{-1}$) was observed at $2 \text{ mV}\cdot\text{s}^{-1}$ for pure material in a neutral Na_2SO_4 electrolyte. The high pseudocapacitance of CuFe_2O_4 in a negative potential range makes it a material of choice for energy storage devices. CA facilitated the fabrication of PVDF-HFP particles. The challenges related to dispersion of ferrimagnetic CuFe_2O_4 nanoparticles in colloidal suspensions were addressed using CA, which acted as a co-dispersant and charging agent for co-deposition of CuFe_2O_4 and PVDF-HFP. Composite films showed ferrimagnetic properties. EPD method represents a versatile strategy for the fabrication of composite films and opens an avenue for the fabrication of composites with different functional properties. High pseudocapacitance and magnetization can be expected at high concentrations of CuFe_2O_4 nanoparticles in the composite films. Moreover, such composites can potentially exhibit magnetocapacitive properties due to redox-active properties of CuFe_2O_4 in the negative potential range and other functional properties of CuFe_2O_4 , such as photocatalytic properties. At high PVDF-HFP content, the enhanced ferroelectric properties can be expected. The incorporation of CuFe_2O_4 into the PVDF-HFP can impart enlarged dielectric constant and ferrimagnetic properties to such composites.

9.6 Acknowledgments

This research was funded by the Natural Sciences and Engineering Research Council of Canada, grant number RGPIN-2018-04014 and CRC program. SEM investigations were performed at the Canadian Centre for Electron Microscopy.

9.7 References

- [1] A. Yadav, R. V. Patel, B. G. Vyas, P. K. Labhasetwar, and V. K. Shahi, "Recovery of CaSO₄ and NaCl from sub-soil brine using CNT@MOF5 incorporated poly(vinylidene fluoride-hexafluoropropylene) membranes via vacuum-assisted distillation," *Colloids and Surfaces A: Physicochemical and Engineering Aspects*, vol. 645, p. 128918, 2022/07/20/ 2022.
- [2] A. Rajput, J. Sharma, S. K. Raj, and V. Kulshrestha, "Dehydrofluorinated poly(vinylidene fluoride-co-hexafluoropropylene) based crosslinked cation exchange membrane for brackish water desalination via electrodialysis," *Colloids and Surfaces A: Physicochemical and Engineering Aspects*, vol. 630, p. 127576, 2021/12/05/ 2021.
- [3] A. Yadav, J. R. Mandal, A. B. Panda, and V. K. Shahi, "Structural tailoring of ceria nanoparticles for fabricating fouling resistant nanocomposite membranes with high flux distillation," *Colloids and Surfaces A: Physicochemical and Engineering Aspects*, vol. 633, p. 127858, 2022/01/20/ 2022.
- [4] S. Chaipo and C. Putson, "Preparation and ferroelectric properties of poly(vinylidene fluoride-hexafluoropropylene)(PVDF-HFP) filled with graphene-nanoplatelets film composites," in *IOP Conference Series: Materials Science and Engineering*, 2020, vol. 773, no. 1, p. 012021: IOP Publishing.
- [5] P. Huang *et al.*, "Carbon quantum dots inducing formation of β phase in PVDF-HFP to improve the piezoelectric performance," *Sensors and Actuators A: Physical*, vol. 330, p. 112880, 2021.
- [6] S. Zhang, W. Tong, J. Wang, W. Wang, Z. Wang, and Y. Zhang, "Modified sepiolite/PVDF-HFP composite film with enhanced piezoelectric and dielectric properties," *Journal of Applied Polymer Science*, vol. 137, no. 9, p. 48412, 2020.

- [7] X. He, K. Yao, and B. K. Gan, "Phase transition and properties of a ferroelectric poly (vinylidene fluoride-hexafluoropropylene) copolymer," *Journal of applied physics*, vol. 97, no. 8, p. 084101, 2005.
- [8] T. Y. Inan, H. Doğan, and A. Güngör, "PVdF-HFP membranes for fuel cell applications: effects of doping agents and coating on the membrane's properties," *Ionics*, vol. 19, no. 4, pp. 629-641, 2013.
- [9] A. Daneshkhah, S. Shrestha, M. Agarwal, and K. Varahramyan, "Poly (vinylidene fluoride-hexafluoropropylene) composite sensors for volatile organic compounds detection in breath," *Sensors and Actuators B: Chemical*, vol. 221, pp. 635-643, 2015.
- [10] A. M. Stephan, "Review on gel polymer electrolytes for lithium batteries," *European polymer journal*, vol. 42, no. 1, pp. 21-42, 2006.
- [11] J. C. Barbosa, J. P. Dias, S. Lanceros-Méndez, and C. M. Costa, "Recent advances in poly (vinylidene fluoride) and its copolymers for lithium-ion battery separators," *Membranes*, vol. 8, no. 3, p. 45, 2018.
- [12] A. Maitra *et al.*, "Trielectric nanogenerator driven self-charging and self-healing flexible asymmetric supercapacitor power cell for direct power generation," *ACS applied materials & interfaces*, vol. 11, no. 5, pp. 5022-5036, 2019.
- [13] S. K. Chacko, M. Rahul, B. Raneesh, and N. Kalarikkal, "Enhanced magnetoelectric coupling and dielectric constant in flexible ternary composite electrospun fibers of PVDF-HFP loaded with nanoclay and NiFe₂O₄ nanoparticles," *New Journal of Chemistry*, vol. 44, no. 26, pp. 11356-11364, 2020.
- [14] T. Liang, J.-H. Cao, W.-H. Liang, Q. Li, L. He, and D.-Y. Wu, "Asymmetrically coated LAGP/PP/PVDF-HFP composite separator film and its effect on the improvement of NCM battery performance," *RSC Advances*, vol. 9, no. 70, pp. 41151-41160, 2019.
- [15] H. Nassrullah, O. Mäkanjuola, I. Janajreh, F. A. AlMarzooqi, and R. Hashaikeh, "Incorporation of nanosized LTL zeolites in dual-layered PVDF-HFP/cellulose membrane for enhanced membrane distillation performance," *Journal of Membrane Science*, vol. 611, p. 118298, 2020.
- [16] D. Ponnamma, O. Aljarod, H. Parangusan, and M. A. A. Al-Maadeed, "Electrospun nanofibers of PVDF-HFP composites containing magnetic nickel ferrite for energy harvesting application," *Materials Chemistry and Physics*, vol. 239, p. 122257, 2020.

- [17] J. Li, M. Tenjimbayashi, N. S. Zacharia, and S. Shiratori, "One-step dipping fabrication of Fe₃O₄/PVDF-HFP composite 3D porous sponge for magnetically controllable oil–water separation," *ACS Sustainable Chemistry & Engineering*, vol. 6, no. 8, pp. 10706-10713, 2018.
- [18] Y. N. Venevtsev, V. V. Gagulin, and I. D. Zhitomirsky, "Material science aspects of seignette-magnetism problem," *Ferroelectrics*, vol. 73, no. 1, pp. 221-248, 1987/06/01 1987.
- [19] H. Schmid, "Multi-ferroic magnetoelectrics," *Ferroelectrics*, vol. 162, no. 1, pp. 317-338, 1994.
- [20] J. Acharya, B. G. S. Raj, T. H. Ko, M.-S. Khil, H.-Y. Kim, and B.-S. Kim, "Facile one pot sonochemical synthesis of CoFe₂O₄/MWCNTs hybrids with well-dispersed MWCNTs for asymmetric hybrid supercapacitor applications," *international journal of hydrogen energy*, vol. 45, no. 4, pp. 3073-3085, 2020.
- [21] X. Gao *et al.*, "Morphology-controllable preparation of NiFe₂O₄ as high performance electrode material for supercapacitor," *Electrochimica Acta*, vol. 296, pp. 181-189, 2019.
- [22] M. Nawwar, R. Poon, R. Chen, R. P. Sahu, I. K. Puri, and I. Zhitomirsky, "High areal capacitance of Fe₃O₄-decorated carbon nanotubes for supercapacitor electrodes," *Carbon Energy*, vol. 1, no. 1, pp. 124-133, 2019.
- [23] K. Atacan, B. Topaloğlu, and M. Özacar, "New CuFe₂O₄/amorphous manganese oxide nanocomposites used as photocatalysts in photoelectrochemical water splitting," *Applied Catalysis A: General*, vol. 564, pp. 33-42, 2018.
- [24] T. F. Marinca, I. Chicinaş, and O. Isnard, "Structural and magnetic properties of the copper ferrite obtained by reactive milling and heat treatment," *Ceramics International*, vol. 39, no. 4, pp. 4179-4186, 2013.
- [25] D. Birajdar, U. Devatwal, and K. Jadhav, "X-ray, IR and bulk magnetic properties of Cu_{1+x}Mn_xFe_{2-2x}O₄ ferrite system," *Journal of materials science*, vol. 37, no. 7, pp. 1443-1448, 2002.
- [26] V. D. Nithya and N. S. Arul, "Review on α -Fe₂O₃ based negative electrode for high performance supercapacitors," *Journal of Power Sources*, vol. 327, pp. 297-318, 2016/09/30/ 2016.
- [27] K. Xie *et al.*, "Highly ordered iron oxide nanotube arrays as electrodes for electrochemical energy storage," *Electrochemistry communications*, vol. 13, no. 6, pp. 657-660, 2011.

- [28] T. Liu *et al.*, "Investigation of hematite nanorod–nanoflake morphological transformation and the application of ultrathin nanoflakes for electrochemical devices," *Nano Energy*, vol. 12, pp. 169-177, 2015.
- [29] J. Shaikh, R. Pawar, A. Moholkar, J. Kim, and P. Patil, "CuO–PAA hybrid films: chemical synthesis and supercapacitor behavior," *Applied Surface Science*, vol. 257, no. 9, pp. 4389-4397, 2011.
- [30] M. Ates, M. A. Serin, I. Ekmen, and Y. N. Ertas, "Supercapacitor behaviors of polyaniline/CuO, polypyrrole/CuO and PEDOT/CuO nanocomposites," *Polymer Bulletin*, vol. 72, no. 10, pp. 2573-2589, 2015.
- [31] G. P. Awasthi, M. B. Poudel, M. Shin, K. P. Sharma, H. J. Kim, and C. Yu, "Facile synthesis of a copper oxide/molybdenum disulfide heterostructure for asymmetric supercapacitors of high specific energy," *Journal of Energy Storage*, vol. 42, p. 103140, 2021.
- [32] S. B. Bandgar, M. M. Vadiyar, U. P. Suryawanshi, C. L. Jambhale, J.-H. Kim, and S. S. Kolekar, "Rotational reflux chemistry approach derived flat holey CuFe₂O₄ nanosheets for supercapacitors application," *Materials Letters*, vol. 279, p. 128514, 2020.
- [33] M. Zhu, D. Meng, C. Wang, and G. Diao, "Facile fabrication of hierarchically porous CuFe₂O₄ nanospheres with enhanced capacitance property," *ACS applied materials & interfaces*, vol. 5, no. 13, pp. 6030-6037, 2013.
- [34] B. Saravanakumar, S. Ramachandran, G. Ravi, V. Ganesh, R. K. Guduru, and R. Yuvakkumar, "Electrochemical performances of monodispersed spherical CuFe₂O₄ nanoparticles for pseudocapacitive applications," *Vacuum*, vol. 168, p. 108798, 2019.
- [35] Y. Guo, Y. Chen, X. Hu, Y. Yao, and Z. Li, "Tween modified CuFe₂O₄ nanoparticles with enhanced supercapacitor performance," *Colloids and Surfaces A: Physicochemical and Engineering Aspects*, vol. 631, p. 127676, 2021.
- [36] W. Zhang *et al.*, "One-step facile solvothermal synthesis of copper ferrite–graphene composite as a high-performance supercapacitor material," *ACS applied materials & interfaces*, vol. 7, no. 4, pp. 2404-2414, 2015.
- [37] C. Lu, W. Hu, Y. Tian, and T. Wu, "Multiferroic oxide thin films and heterostructures," *Applied physics reviews*, vol. 2, no. 2, p. 021304, 2015.
- [38] S. Roy and S. Majumder, "Recent advances in multiferroic thin films and composites," *Journal of Alloys and Compounds*, vol. 538, pp. 153-159, 2012.

- [39] A. Kumar and K. Yadav, "Enhanced magnetocapacitance sensitivity in BiFeO₃-poly (vinylidene-fluoride) hot pressed composite films," *Journal of alloys and compounds*, vol. 528, pp. 16-19, 2012.
- [40] Y. Chen *et al.*, "Magnetocapacitance effects of Pb_{0.7}Sr_{0.3}TiO₃/La_{0.7}Sr_{0.3}MnO₃ thin film on Si substrate," *Applied Physics Letters*, vol. 98, no. 5, p. 052910, 2011.
- [41] E.-J. Lee, A. K. An, P. Hadi, S. Lee, Y. C. Woo, and H. K. Shon, "Advanced multi-nozzle electrospun functionalized titanium dioxide/polyvinylidene fluoride-co-hexafluoropropylene (TiO₂/PVDF-HFP) composite membranes for direct contact membrane distillation," *Journal of Membrane Science*, vol. 524, pp. 712-720, 2017.
- [42] Y. Han *et al.*, "Direct electrophoretic deposition of an ultra-strong separator on an anode in a surfactant-free colloidal system for lithium ion batteries," *Journal of Materials Chemistry A*, vol. 7, no. 4, pp. 1410-1417, 2019.
- [43] R. Sikkema, K. Baker, and I. Zhitomirsky, "Electrophoretic deposition of polymers and proteins for biomedical applications," *Advances in Colloid and Interface Science*, vol. 284, p. 102272, 2020/10/01/ 2020.
- [44] X. Pang, I. Zhitomirsky, and M. Niewczas, "Cathodic electrolytic deposition of zirconia films," *Surface and Coatings Technology*, vol. 195, no. 2, pp. 138-146, 2005/05/31/ 2005.
- [45] I. Zhitomirsky and A. Petric, "Electrochemical deposition of yttrium oxide," *Journal of Materials Chemistry*, 10.1039/B000311P vol. 10, no. 5, pp. 1215-1218, 2000.
- [46] J. Yus, Y. Bravo, A. J. Sanchez-Herencia, B. Ferrari, and Z. Gonzalez, "Electrophoretic deposition of RGO-NiO core-shell nanostructures driven by heterocoagulation method with high electrochemical performance," *Electrochimica Acta*, vol. 308, pp. 363-372, 2019.
- [47] J. Li and I. Zhitomirsky, "Cathodic electrophoretic deposition of manganese dioxide films," *Colloids and Surfaces A: Physicochemical and Engineering Aspects*, vol. 348, no. 1, pp. 248-253, 2009/09/20/ 2009.
- [48] O. O. Van der Biest and L. J. Vandeperre, "Electrophoretic deposition of materials," *Annual Review of Materials Science*, vol. 29, no. 1, pp. 327-352, 1999.
- [49] Z. Zhang *et al.*, "Graphene oxide-Fe₃O₄ nanocomposite used as aniline adsorbent with a wide pH range," *Colloid and Polymer Science*, vol. 300, no. 1, pp. 83-93, 2022/01/01 2022.

- [50] Z. Pu, X. Fan, J. Su, M. Zhu, and Z. Jiang, "Aqueous dispersing mechanism study of nonionic polymeric dispersant for organic pigments," *Colloid and Polymer Science*, vol. 300, no. 3, pp. 167-176, 2022/03/01 2022.
- [51] Y. Gong, G. Liu, Q. Wang, A. Zhu, P. Liu, and Q. Wu, "Synthesis of a novel mesoporous Fe₃O₄@SiO₂/CTAB-SiO₂ composite material and its application in the efficient removal of bisphenol A from water," *Colloid and Polymer Science*, vol. 299, no. 5, pp. 807-822, 2021/05/01 2021.
- [52] Y. Su and I. Zhitomirsky, "Electrophoretic deposition of graphene, carbon nanotubes and composite films using methyl violet dye as a dispersing agent," *Colloids and Surfaces A: Physicochemical and Engineering Aspects*, vol. 436, pp. 97-103, 2013/09/05/ 2013.
- [53] K. Wu, Y. Wang, and I. Zhitomirsky, "Electrophoretic deposition of TiO₂ and composite TiO₂-MnO₂ films using benzoic acid and phenolic molecules as charging additives," *Journal of colloid and interface science*, vol. 352, no. 2, pp. 371-378, 2010.
- [54] K. Shi and I. Zhitomirsky, "Electrophoretic nanotechnology of graphene-carbon nanotube and graphene-polypyrrole nanofiber composites for electrochemical supercapacitors," *Journal of Colloid and Interface Science*, vol. 407, pp. 474-481, 2013/10/01/ 2013.
- [55] I. Zhitomirsky, "New Developments in Electrolytic Deposition of Ceramic Films," *American Ceramic Society Bulletin*, vol. 79, no. 9, pp. 57-62, 2000.
- [56] R. Chen, M. Yu, R. P. Sahu, I. K. Puri, and I. Zhitomirsky, "The Development of Pseudocapacitor Electrodes and Devices with High Active Mass Loading," *Advanced Energy Materials*, vol. 10, no. 20, p. 1903848, 2020.
- [57] K. Shi and I. Zhitomirsky, "Asymmetric Supercapacitors Based on Activated-Carbon-Coated Carbon Nanotubes," *ChemElectroChem*, vol. 2, no. 3, pp. 396-403, 2015.
- [58] K. Shi and I. Zhitomirsky, "Fabrication of Polypyrrole-Coated Carbon Nanotubes Using Oxidant-Surfactant Nanocrystals for Supercapacitor Electrodes with High Mass Loading and Enhanced Performance," *ACS Applied Materials & Interfaces*, vol. 5, no. 24, pp. 13161-13170, 2013/12/26 2013.
- [59] M. Ata, Y. Liu, and I. Zhitomirsky, "A review of new methods of surface chemical modification, dispersion and electrophoretic deposition of metal oxide particles," *Rsc Advances*, vol. 4, no. 43, pp. 22716-22732, 2014.

- [60] H. Lee, B. P. Lee, and P. B. Messersmith, "A reversible wet/dry adhesive inspired by mussels and geckos," *Nature*, vol. 448, no. 7151, pp. 338-341, 2007.
- [61] B. P. Lee, P. B. Messersmith, J. N. Israelachvili, and J. H. Waite, "Mussel-inspired adhesives and coatings," *Annual review of materials research*, vol. 41, pp. 99-132, 2011.
- [62] R. K. Selvan, C. Augustin, L. J. Berchmans, and R. Saraswathi, "Combustion synthesis of CuFe_2O_4 ," *Materials Research Bulletin*, vol. 38, no. 1, pp. 41-54, 2003.
- [63] R. B. Jimaa, Z. H. Mahmoud, and F. K. Ali, "Evaluation the efficiency of CuFe_2O_4 prepared photolysis by OSD and photo degradation," *Entomol. Appl. Sci. Lett*, vol. 5, no. 2, pp. 91-100, 2018.
- [64] L. Yesappa *et al.*, "Optical properties and ionic conductivity studies of an 8 MeV electron beam irradiated poly (vinylidene fluoride-co-hexafluoropropylene)/ LiClO_4 electrolyte film for opto-electronic applications," *RSC Advances*, vol. 8, no. 28, pp. 15297-15309, 2018.
- [65] P. Tuhania *et al.*, "PVDF-HFP and 1-ethyl-3-methylimidazolium thiocyanate-doped polymer electrolyte for efficient supercapacitors," *High Performance Polymers*, vol. 30, no. 8, pp. 911-917, 2018.
- [66] S. Mahendrakar, M. Anna, and J. Reddy, "Structural, morphological and FTIR of PVDF-HFP and lithium tetrafluoroborate salt as polymer electrolyte membrane in lithium ion batteries," *Int. J. Chem. Technol. Res.*, vol. 8, pp. 319-328, 2015.
- [67] S. A. Soomro, I. H. Gul, H. Naseer, S. Marwat, and M. Mujahid, "Improved performance of $\text{CuFe}_2\text{O}_4/\text{rGO}$ nanohybrid as an anode material for lithium-ion batteries prepared via facile one-step method," *Current Nanoscience*, vol. 15, no. 4, pp. 420-429, 2019.

Chapter 10 Conclusions and Future Works

In general, the overall objective of developing biomimetic strategies for the electrophoretic deposition of polymers and composites was primarily achieved. High quality polytetrafluoroethylene (PTFE), polyvinylidene fluoride (PVDF) and poly(vinylidene fluoride-co-hexafluoropropylene) (PVDF-HFP) polymer coatings and their composites with multifunctional properties were successfully fabricated using catecholate-type and bile acid-type biosurfactants by EPD for promising applications in corrosion protection, biomedical devices, biosensors, and energy storage devices, amongst other things. The adhesion strength of the polymer films prepared in this investigation corresponded to the highest 5B classification, measured according to ASTM test method D3359. This investigation resulted in the development of new families of advanced biosurfactants. The analysis of the influence of surfactant structure and functional groups on dispersion and EPD efficiency of different materials provides an insight into the design of advanced surfactants for colloidal processing of materials of different types. The approaches developed in this research pave the way for the EPD of other chemically inert, electrically neutral polymers and co-depositing them with inorganic materials to create novel nanocomposites with advanced functionality. Specifically, the major findings can be summarized as follows:

1. DChNa is a versatile, charged dispersant and coating-forming molecule which allows for the EPD of PTFE, diamond, and CDs from aqueous solutions. Adsorbed DCh⁻

species on PTFE offered negative charge and electrostatic dispersion of PTFE particles, and anaphoretic transport of PTFE to the anodic substrate, forming deposition by protonation to water insoluble DChH. Potentiodynamic testing showed that PTFE films provide protection against corrosion for steel. Conceptual new strategy for fabricating chemical inert polymer composite films by EPD was demonstrated by using of DChNa as co-dispersant, which also paved the ways for the utilization of other bile acids or salts as biosurfactants for EPD technique.

2. LCA is a promising natural co-surfactant for the EPD of corrosion protective PTFE films and PTFE-diamond composites with reduced porosity and a high deposition yield in an ethanol solvent, which eliminated the gas evolution during aqueous EPD.
3. BAs allowed for controlled EPD of hydrophobic and inert PVDF at high deposition rates in an ethanol suspension, resulting in PVDF having a deposition yield that increased in the order of LCA<CDCA<DCA<UDCA<ChA. The number, position, and orientation of OH groups on the structures of BAs showed great influence on their dispersing efficiency and the deposition yield of PVDF particles. ChA was discovered as a promising co-surfactant for the EPD of PVDF-diamond and PVDF-silica composites with controlled composition.
4. Catecholate-type molecules CA and CV showed unique adsorption capabilities on different materials, making them choice co-dispersants for the EPD of organic-inorganic nanocomposites. It was found that CA and CV adsorbed on PVDF particles through hydrophobic interactions and on the metal oxides of TiO₂, MnO₂, and NiFe₂O₄ through catecholate-type bonding. Tafel and EIS data showed that deposited PVDF

- films provide corrosion protection properties. Co-deposited PVDF-NiFe₂O₄ nanocomposites showed superparamagnetic properties.
5. CA was used for fabricating micrometer level PVDF-HFP particles from large pellets (5 mm in diameter), which facilitated the EPD of dense PVDF-HFP films exhibiting corrosion protection properties. Importantly, the use of CA as a biosurfactant allowed for the co-EPD of PVDF-HFP composites mixed with ferrimagnetic spinel oxides, such as NiFe₂O₄ and CuFe₂O₄. The compositions, microstructures, and magnetic properties of the composite films can be easily tuned by controlling the deposition parameters. PVDF-HFP-CuFe₂O₄ composite films showed ferrimagnetic properties and could potentially exhibit magnetocapacitive properties due to the redox-active properties of CuFe₂O₄ in the negative potential range. The method developed in this investigation provides a simple and versatile strategy for the fabrication of composite films, combining ferrimagnetic properties of spinel oxides with multifunctional properties of ferroelectric polymers.

The biomimetic approaches developed in this research allowed for the development of new strategies for the surface modification of chemically inert PTFE, PVDF and PVDF-HFP fluoropolymers and the deposition of functional polymer films and composites by EPD from colloidal suspensions. Looking ahead, these approaches will pave the way for the EPD of other chemically inert, electrically neutral fluoropolymers or other advanced polymers from other polymer classes. These investigations also provide simple and versatile methods for making composite films that boast multifunctional properties. The use of catecholic and

steroid molecules as co-surfactants provides a basis for a breakthrough in EPD technology for co-depositing different types of materials. It is expected that other catecholate type molecules and BAs/BSs molecules, their derivatives, and other natural biosurfactants can also address the challenges to EPD and be used for the EPD of functional materials for various applications. The new strategies developed during this investigation are promising for the development of electrophoretic nanotechnology of advanced composite films for applications in supercapacitors, batteries, solar cells, biomedical implants and sensors, corrosion protection, and ferroelectric, piezoelectric, and magnetic devices.